# Gasification of waste for hydrogen production

**Phuet Prasertcharoensuk**

Thesis submitted for the Degree of Doctor of Philosophy

Supervisors:

Dr. Anh N. Phan

Prof. Steve J. Bull

School of Engineering, Newcastle University, United Kingdom

October 2019

# Abstract

The transportation sector relies heavily on fossil fuels and contributes up to one third of greenhouse gas emissions. Among available renewable resources, only biomass contains the carbon and hydrogen that can be converted into multiple energy vectors (i.e. heat, electricity, biofuels and chemicals) to reduce the heavy dependency upon fossil fuels and their associated environmental impacts. Advanced thermochemical technologies, i.e. pyrolysis and gasification are considered as potential approaches to convert biomass into fuels for the transportation sector and chemical industry. Although, coal gasification is well developed, gasification of biomass has not been widely commercialised due to a number of challenges including low $H_2$/CO ratios (less than 1), low $H_2$ content (40-60 mol%), low biomass conversion (80-85%), low process efficiency (70-80%), high $CO_2$ content (20-30 mol%) and high tar formation (30-80 g/$Nm^3$). The aim of this study was to develop a modular gasification system to produce $H_2$ from waste biomass/residues to be used as an energy carrier or converted further into synthetic liquid fuels (diesel fuel and gasoline) and valuable chemicals (i.e. methanol, ethanol and alcohol).

Gasification of waste biomass was carried out in a two-stage gasification process in which feedstock was decomposed into intermediate products and subsequently gasified using steam. The effect of operating conditions in the pyrolysis and gasification steps on maximising the $H_2$ production and quality of synthetic gas (known as syngas) as well as process efficiency was studied. The synergistic effect of $CO_2$ environment and catalyst (Ni/MRM, Ni/$Al_2O_3$ and Ni/HZSM-5) on the gas properties and tar formation was evaluated. A small-scale air-blown throat downdraft gasifier was optimised using Computational Fluid Dynamics (CFD) to obtain high quality syngas/$H_2$ production and validated using experimental and literature data.

The pyrolysis temperature has a strong effect on char morphology and the volatiles produced, which in turn affected the syngas properties. Increasing pyrolysis temperature from 600 $^oC$ to 900 $^oC$, resulted in an increase in $H_2$ (from 54 mol% to 66 mol%) and CO (from 5 mol% to 10 mol%) and a reduction in $CO_2$ (from 37 mol% to 22 mol%), $CH_4$ (from 5 mol% to 2 mol%) and tar content (from 39 g/$Nm^3$ to 24 g/$Nm^3$) in the gas stream after gasification.

Around 67 mol% $H_2$ together with high carbon conversion (94%) and low tar formation (21 g/$Nm^3$) were observed under $N_2$/steam gasification at a pyrolysis temperature of 900 $^oC$ and gasification temperature of 1000 $^oC$ with steam to carbon in feedstock molar ratio of 5.7. A process efficiency of 84% was achieved in this case. Combining $CO_2$ and steam in the gasification stage produced up to 78 mol% $H_2$ with a low $CH_4$ (0.9 mol%) and tar content (9 g/$Nm^3$) with process efficiency ≤ 97% at a pyrolysis temperature of 900 $^oC$ and gasification

temperature of 1000 $^{o}$C with steam to carbon in feedstock molar ratio of 3.4. Less than 10 mol% $CO_2$ was generated from $CO_2$/steam gasification compared to 20-30 mol% in $N_2$/steam gasification. Therefore, the use of $CO_2$ in a gasification process could be route to utilise waste $CO_2$ for $H_2$ production from biomass/waste, contributing significantly to the environmental footprint and sustainability of the process. Adding a Ni-based catalyst in the process had no effect on the syngas properties, but reduced by 2-3 times, the amount of tar (particularly heavy PAH compounds). The use of the Ni/MRM catalyst (waste product of bauxite processing) proved to be successful for the removal of naphthalene constituents (58%), the main component in tar, compared to only 50% reduction for the commercial Ni-based catalysts (Ni/$Al_2O_3$ and Ni/HZSM-5).

For a small-scale air-blown throat downdraft gasifier, a throat to gasifier diameter ratio of 0.4 and the position of the air inlet nozzles at 10 cm above the throat provided high quality syngas/$H_2$ production. The modelling can be used to predict the syngas compositions under the various operating conditions and provides an operating window for the development of a simple, highly efficient and robust gasification unit that can be used for $H_2$ production without major downstream processing to remove impurities.

# List of publications

**List of publications from this thesis:**

1. Prasertcharoensuk, P., Hernandez, D.A., Bull, S.J. and Phan, A.N. (2018) "Optimisation of a throat downdraft gasifier for hydrogen production", Biomass and Bioenergy, 116, pp. 216-226.

2. Prasertcharoensuk, P., Bull, S.J. and Phan, A.N. (2019) "Gasification of waste biomass for hydrogen production: Effects of pyrolysis parameters", Renewable Energy, 143, pp. 112-120.

3. Duong, L.T., Prasertcharoensuk, P. and Phan, A.N. (2019) "Biofuel production from lignocellulosic feedstock via thermochemical routes", in Singh, L.K. and Chaudhary, G. (eds.) Liquid Biofuel Production. Massachusetts: Scrivener Publishing LLC, pp. 89-166.

4. Prasertcharoensuk, P., Bull, S.J. and Phan, A.N. "$CO_2$ and catalytic gasification for hydrogen production from waste biomass", Applied Energy (in preparation).

5. Prasertcharoensuk, P., Bull, S.J. and Phan, A.N. "Cold plasma assisted conversion of tar derived from waste biomass gasification", Applied Energy (in preparation).

**List of conference poster and oral presentations from this thesis:**

1. Poster presentation titled "CFD modelling of a throat downdraft gasifier for hydrogen production" at International Research Conference on Sustainable Energy, Engineering, Material and Environment (IRCSEEME), Northumbria University, UK, 26-28 July 2017.

2. Oral presentation titled "High pyrolysis temperature of waste wood for hydrogen production and characterisation" at 3rd International Conference on Hydrogen Energy (AEM2017), University of Surrey, UK, 11-13 September 2017.

3. Oral presentation titled "High pyrolysis temperature of waste wood for energy production" at 14th AIChE Spring Metting: Biomass Conversion to Valuable Products II, Florida, USA, 22-26 April 2018.

4. Oral presentation titled "Gasification of waste wood for Hydrogen production" at NEPIC Technology Showcase Event 2019, The curve, Teesside University, UK, 14 February 2019.

**To my parents**

# Acknowledgements

I would like to express my deepest gratitude to my supervisor Dr. Anh N. Phan for her intensive guidance, encouragement and support in the development of this work. I am also extremely grateful to Prof. Steve J. Bull for co-advising me and spending his valuable time on giving invaluable advices throughout my research. I also express my gratitude to:

- Dr. David A. Hernandez for his guidance and support in the Computational Fluid Dynamics (CFD) modelling.
- Sustainable Campus Newcastle University: Matthew Dunlop for providing the waste wood material.
- Department of Chemistry, University of Glasgow; Prof. Justin Hargreaves for providing the red mud material.
- Mechanical Workshop Technician, Newcastle University: Iain Strong, Iain Ditchburn and Michael Percival for every modification and suggestion you made to the systems.
- Advanced Chemical and Materials Analysis (ACMA), Newcastle University: Maggie White for XRD analysis and Dr. Isabel Arce Garcia for SEM images and EDX analysis.
- Department of Chemistry, Sheffield University: Dr. Jenifer C. Louth for CHN analysis and Simon Thorpe for GC-MS analysis.
- Laboratory Technician, Newcastle University: Rob Dixon and Paul Sterling for lab consumables.
- Process Intensificatiion Group (PIG) members, Newcastle University for their useful contributions and shared knowledge.
- School of Engineering technical, IT, and administrative members of staff.

I am greatly indebted to my parents Vichai and Thanomwan Prasertcharoensuk for all their invaluable help and support throughout the past four years. Lastly, I would also like to thank all my friends and loved one for supporting and encouraging.

# Table of contents

# List of Figures

# List of Tables

# Glossary

## Greek Symbols

| | |
|---|---|
| α | Alpha |
| Ø | Diameter |
| Δ | Delta |
| ε | Epsilon |

## Acronyms/Abbreviations

| | |
|---|---|
| $Al_2O_3$ | Aluminium oxide/Alumina |
| AAEM | Alkali and alkaline earth metallic |
| AOAC | Association of Official Analytical Chemists |
| BS | British Standard |
| BFB | Bubbling fluidized bed |
| BET | Brunauer–Emmett-Teller |
| C | Carbon |
| CO | Carbon monoxide |
| $CO_2$ | Carbon dioxide |
| $CH_4$ | Methane |
| CFB | Circulating fluidized bed |
| CFD | Computational Fluid Dynamics |
| CCE | Carbon conversion efficiency |
| D | Dimensional |
| DSC | Differential scanning calorimetry |
| ESEM | Environmental scanning electron microscopy |
| EDXS | Energy-dispersive X-ray spectroscopy |
| EI | Electron ionisation |
| ER | Equivalence ratio |
| FT | Fischer-Tropsch |
| FB | Fluidized bed |
| FID | Flame ionisation detector |
| FTIR | Fourier-transform infrared spectroscopy |
| GIB | Green Investment Bank |

| | |
|---|---|
| GC | Gas chromatography |
| GC-MS | Gas chromatography-Mass Spectrometry |
| H* | Height |
| $H/H_2$ | Hydrogen |
| $H_2O$ | Water/steam |
| HHV | Higher heating value |
| HZSM-5 | Zeolite ($SiO_2/Al_2O_3$ = 312) |
| IC | Internal combustion |
| ISO | International Standards Organization |
| IEA | International Energy Agency |
| ICP-MS | Inductively coupled plasma mass spectrometry |
| LHV | Lower heating value |
| MSD | Mass selective detector |
| MSW | Municipal solid waste |
| MRM | Modified red mud |
| $Nm^3$ | Normal cubic meter (Temperature: 0 $^oC$ and Pressure: 1 atm) |
| $N/N_2$ | Nitrogen |
| Ni | Nikel |
| $NO_x$ | Nitrogen oxide |
| NIST | National Institute of Standards and Technology |
| Ni/MRM | Nikel on modified red mud supported |
| $Ni/Al_2O_3$ | Nickel on alumina supported |
| Ni/HZSM-5 | Nikel on zeolite ($SiO_2/Al_2O_3$ = 312) supported |
| $O/O_2$ | Oxygen |
| PAH | Polycyclic aromatic hydrocarbon |
| RM | Red mud |
| $SO_x$ | Sulphur oxide |
| S/B | Steam to biomass ratio |
| S/C | Steam to carbon in feedstock molar ratio |
| TGA | Thermogravimetric analysis |
| TCD | Thermal conductivity detector |
| VOC | Volatile organic compound |
| XRD | X-ray diffraction |

# Chapter 1 Introduction

## 1.1 Background

Increasing concerns over greenhouse gas emissions associated with fossil fuel usage that have negative impacts on climate change, insecurity in energy supplies, depletion of natural resources have led to enormous attention towards renewable and sustainable sources (Cazenave and Cozannet, 2014). Alongside other renewable resources such as solar, wind, hydro, geothermal and nuclear, lignocellulosic material such as biomass/waste residues have been considered as potential resources to produce biofuels that can replace petroleum-based products in the transportation sector, which currently relies mainly on fossil fuel (above 90%) and contributes up to 33% of greenhouse gas emissions (International Energy, 2018). Valorisation of biomass/waste will benefit both environmental and energy aspects by converting a significant amount of waste and other residues (2 billion tonnes/year are produced globally and over 100 million tonnes/year in the UK) into transportation fuels/energy (GIB, 2014; Kaza et al., 2018). Many countries have set ambitious goals of using biomass/waste for partially replacing fossil fuels, e.g. increasing the biofuel consumption to 36 billion gallons by 2022 in the USA (Hochman et al., 2017) and the UK setting 15% of its total energy from renewable energy sources, with one-third of this coming from waste and other residues by 2020 (Beurskens LWM, 2018).

Biomass contains cellulose (25-50 wt%), hemicellulose (15-40 wt%), lignin (10-40 wt%), extractives (0-15 wt%) and a small amount of inorganic mineral matter (Kan et al., 2016). It can be converted into chemicals and biofuels via biochemical (anaerobic digestion, fermentation and transesterification) or thermochemical (combustion, pyrolysis and gasification) approaches. In biochemical processes, only cellulose and hemicellulose components can be utilised by conversion into alcohols (ethanol or butanol) (Chakraborty et al., 2012) or hydrocarbons, i.e. alkanes/alkenes (Peralta-Yahya et al., 2012) in the presence of enzymes and/or other microorganisms. In contrast, thermochemical processes, i.e. gasification can transfer all components in the biomass feedstock into $H_2$ or synthetic gas (syngas) which can be then converted into liquid fuels or chemicals (Chaudhari et al., 2001; Balat et al., 2009b; Yung et al., 2009). Gasification is considered the most cost-effective and efficient method for biomass conversion to multiple energy/fuel vectors (i.e. heat, electricity, $H_2$, biofuels and chemicals) (de Lasa et al., 2011; Sikarwar et al., 2016). In addition, it produces low air pollutants (i.e. $SO_x$, $NO_x$ and particulates) (Basu, 2010a; Paula. G. Peres et al., 2013) compared to pyrolysis and combustion processes.

Gasification is a partial oxidation process to convert the feedstock into syngas, which is a mixture of mainly $H_2$ (25-30 mol%) and CO (30-60 mol%) together with small amounts of $CH_4$, $CO_2$, char, ash and tar, at a temperature range of 900-1500 $^oC$ (Ruiz et al., 2013). The proportion of components in the syngas product is strongly influenced by types of gasifier and operating conditions (temperature, gasifying agent and the ratio of gasifying agent to feedstock) as well as properties of the feedstock (Puig-Arnavat et al., 2010; Radwan, 2012; Kumar, 2015). Over the last decades, gasification of biomass/waste has been intensively studied in terms of experimental optimisation of operating conditions (Lv et al., 2004; Luo et al., 2009; Emami Taba et al., 2012; Hernández et al., 2012; Mayerhofer et al., 2012; Pandey et al., 2012; Sanchez-Hernandez et al., 2018), theoretical analysis (Mahishi and Goswami, 2007; Lee et al., 2009; Renganathan et al., 2012; Sircar et al., 2014; Kuo and Wu, 2015; Sharma and Sheth, 2016; Ravi and Kohli, 2018; Sharma et al., 2018) and gasifier design (Henriksen et al., 2006; Fryda et al., 2008a; Abuadala and Dincer, 2010; Song et al., 2012; Gómez-Barea et al., 2013a; Janajreh et al., 2013; Heidenreich and Foscolo, 2015). Nonetheless, gasification of biomass still encounters a number of challenges such as low $H_2$ to CO ratios (less than 1), low $H_2$ content (40-60 mol%), low process efficiency (70-80%) and high tar formation (30-80 g/$Nm^3$). With the low ratio of $H_2$/CO, the syngas needs to be upgraded to obtain the high molar ratio of $H_2$/CO, i.e. above 2 for chemical (i.e. methanol, ethanol and alcohol) and liquid fuel (diesel fuel and gasoline) synthesis via the Fischer-Tropsch method (Chaudhari et al., 2001; Yung et al., 2009). Moreover, the syngas needs to be cleaned to remove tar before it can be used in internal combustion engines (< 0.1 g/$Nm^3$ tar) and gas turbines (< 0.005 g/$Nm^3$) for heat and electricity generation (Woolcock and Brown, 2013; Sikarwar et al., 2016; Li et al., 2018) or to 0.001 g/$Nm^3$ for liquid fuels or chemicals synthesis (Milne et al., 1998; Demirbas, 2006). Tar is the term used for high molecular weight compounds (i.e. polycyclic aromatic hydrocarbons), that condense into sticky substances when the producer gas is cooled down below 60 $^oC$ (Li and Suzuki, 2009) causing operational difficulties for the downstream process (e.g. corrosion, clogging and fouling of installations) (Milne et al., 1998; Zhang et al., 2010) as well as it affected the quality of syngas and the process efficiency (Han and Kim, 2008; Li and Suzuki, 2009; Ruiz et al., 2013).

Tar formation can be minimized either by optimization of operating conditions or adding catalytic bed materials (i.e. dolomite, olivine, char, clay minerals, alkali metal-based and Ni-based catalysts) (Devi et al., 2003; Anis and Zainal, 2011). Catalytic reforming has recently received attention as an effective and efficient method for tar removal, avoiding costly downstream processing (Bridgwater, 1994; Abu El-Rub et al., 2004). Commercial Ni-based catalysts (i.e. Ni/$Al_2O_3$, Ni/HZSM-5, Ni/MgO, Ni/$SiO_2$ and Ni/$K_2O$) have proved to be the most successful catalyst for tar removal in biomass gasification due to high hydrocarbon reforming

activity (Baker et al., 1987; Sutton et al., 2001; Ni et al., 2006) as well as enhancing the formation of $H_2$ (Torres et al., 2007; Chan and Tanksale, 2014; Ashok et al., 2018), but are prone to rapid deactivation caused by coke deposition and crystallite agglomeration (Sikarwar et al., 2016). Therefore, development of different types of catalyst, which have exhibited high catalytic activity for tar removal, high thermal stability, suppression of coke deposition and low cost is required. Red mud is a waste product of bauxite processing; an estimated around 70 million tonnes/year are generated globally (Vangelatos et al., 2009). Red mud management is one of the main challenges in the aluminium industry, with disposal costs of ~ $3 per tonnes of alumina produced (Li, 2001; Vangelatos et al., 2009). The main components of red mud are $Fe_2O_3$, $Al_2O_3$, $SiO_2$, $TiO_2$ and a range of alkali and alkaline earth metals such as CaO and $Na_2O$ (Gräfe et al., 2011; Liu and Zhang, 2011; Evans, 2016) which could be potentially used as an alternative metal oxide catalyst/supporting material. There have been numerous successful studies using red mud as a catalyst for various applications such as hydrocarbon and volatile organic compounds (VOC) cracking (Paredes et al., 2004; Balakrishnan et al., 2009; Rosmaninho et al., 2012), hydrodechlorination (Ordóñez et al., 2001; Halász et al., 2005), coal liquefaction (Yokoyama et al., 1989; Klopries et al., 1990), carbon synthesis (Dunens et al., 2010; Oliveira et al., 2011; Gu et al., 2016) and pyrolysis oil upgrading (Karimi et al., 2012; Kastner et al., 2015). However, the use of red mud for catalytic cracking of tar in biomass gasification has not been assessed. If red mud can be successfully used as a catalyst for gasification of biomass/waste residues, it would contribute significantly to the environmental footprint and sustainability aspects of the process.

Modification of the gasification reactor (known as gasifier) is one of the approaches to minimize tar formation as well as improve the biomass gasification process in terms of process efficiency and syngas quality (Devi et al., 2003; Han and Kim, 2008). Computational Fluid Dynamics (CFD) modelling has been widely used to predict the behaviour of biomass gasification (Zainal et al., 2002; Gerun et al., 2008; Meenaroch et al., 2015) to optimize operating conditions of an existing gasifier, i.e. temperature, air inlet velocity, gasifying agents and gasifying agent to biomass ratios for syngas production (Wu et al., 2013; Lan et al., 2014; Couto et al., 2015; Chaurasia, 2016). However, there are only a few workers that have applied CFD models for designing and optimizing a new configuration of biomass gasifier that can be used for $H_2$/syngas production without major downstream processing to remove impurities (tar in particular).

## 1.2 Aim and objectives

The aim of this PhD thesis was to develop a simple and flexible gasification system to produce $H_2$ and high quality syngas (high $H_2$/CO ratio) from biomass/waste residues. To achieve the aim several objectives were set:

- Determine the effect of temperature, vapour residence time and particle size on the properties of volatiles and char in pyrolysis process.
- Determine the interaction between pyrolysis operating conditions and the gasification step in terms of quality syngas and tar formation.
- Determine the effect of operating conditions in the gasification step: temperature and steam to carbon in feedstock (S/C) molar ratios on $H_2$ production, syngas properties, tar formation and process efficiency.
- Determine the synergistic effect of $CO_2$ environment and catalyst ($Ni/Al_2O_3$ and Ni/HZSM-5) on the syngas properties and process efficiency.
- Investigate the feasibility of red mud (waste product of bauxite processing) as a catalyst for tar removal.
- Optimise a small-scale air-blown throat downdraft gasifier for high quality syngas/$H_2$ production using the Computational Fluid Dynamics (CFD), ANSYS FLUENT 16.1 including model validation using experimental and available literature data.

## 1.3 Layout of the thesis

The thesis is divided into seven chapters. **Chapter 1** is the introduction, providing an overview of biomass conversion routes for transportation fuels/energy applications and the significance of the research together with aims and objectives. **Chapter 2** contains an extensive literature review on biomass gasification technologies, parameters affecting gasification and tar formation and reduction. A review of Computational Fluid Dynamics (CFD) modelling for designing and optimizing of a biomass gasification process is also included. **Chapter 3** covers all the materials used in this research, as well as detailed discussion of experimental set-ups and analytical techniques. Results and discussion are divided into chapters 4, 5 and 6. **Chapter 4** focuses on the pyrolysis process in $N_2$ and $CO_2$ environments. The interactions between pyrolysis conditions and gasification in terms of syngas properties and tar formation is discussed. **Chapter 5** presents the effect of gasification operating parameters such as temperature, steam to carbon in feedstock (S/C) molar ratio and gasifying agent on $H_2$

production. The synergetic effect of gasifying agent ($CO_2$) and catalyst ($Ni/Al_2O_3$ and Ni/HZSM-5 and Ni/MRM) on the $H_2$ production, product properties, tar formation and process efficiency is evaluated. **Chapter 6** presents a mathematical model for optimising the design of a small-scale air-blown throat downdraft gasifier to obtain high quality syngas/$H_2$ production. Finally, conclusions and recommendations are included in **Chapter 7**.

# Chapter 2 Literature review

This chapter explains the rationale and background and reviews the state-of-the-art of biomass gasification including the types of gasifier, influence of operating parameters (i.e. temperature, gasifying agent and gasifying agent to feedstock ratio) on syngas/$H_2$ production, tar formation and tar reduction/removal approaches. A review of Computational Fluid Dynamics (CFD) modelling for designing and optimizing of a biomass gasification process is also included.

## 2.1 Biomass

Lignocellulosic biomass (woody material, agricultural residues and waste) is mainly composed of cellulose, hemicellulose, lignin and others (e.g. extractives), depending upon feedstock as shown in Table 2.1. Cellulose (Figure 2.1) is a long chain linear polymer of glucopyranose units (Fushimi et al., 2009) in a rigid crystalline or amorphous structure that makes up plant cell walls (Pérez et al., 2002). Hemicellulose (Figure 2.1) is a short, highly branched hetero-polymer composed of d-xylose, d-glucose, d-galactose, l-arabinose, 4-O-methyl-glucuronic, d-galacturonic and d-mannose, depending upon the predominant types of sugar present in the polymer (Pérez et al., 2002; Qin et al., 2015). Lignin (Figure 2.1) is the most complex and highly branched of aromatic polymers, i.e. p-hydroxyphenyl, syringyl and guaiacyl (Alén et al., 1996; Singhvi et al., 2014). It provides mechanical strength to biomass cell walls (secondary cell walls) and acts as a cementing agent (Jaya Shakar et al., 2010; Acharya et al., 2012), protecting the cell structure against thermal and chemical degradation (Diebold and Bridgwater, 1997). Extractives are non-structural and non-chemically bound components in biomass, i.e. protein, sucrose, fats, fatty acids, waxes, monoterpenes, phenolic and monosaccharides and their derivatives (Jianjun et al., 2015).

The lignocellulosic composition in biomass feedstock is an important parameter in both biochemical and thermochemical processes as it affects the product properties and conversion and process efficiency. For example, biomass with a high lignin content potentially leads to the formation of phenolic compounds, which are precursors of multiple aromatic ring species in tar in the gasification process (Hosoya et al., 2008; Yu et al., 2014). Moreover, the lignocellulosic compounds also influence the characterisation of products and the decomposition rate in the pyrolysis step, which in turn had a strong influence the quality of syngas and performance of the gasification system (Jiang et al., 2010; Kan et al., 2016; Trubetskaya et al., 2017). In biochemical processes using biomass feedstock containing high lignin content leads to a reduction in process efficiency, due to the enzymes and other microorganisms only being able

to convert the cellulose and hemicellulose content in the biomass feedstock to sugars (Gomez et al., 2008; Gaurav et al., 2017). Therefore, pre-treatment methods, i.e. biological (enzymatic pre-treatment) and/or physico-chemical (steam/ammonia explosion, torrefaction, alkaline hydrolysis, acid hydrolysis and ionic liquids) methods are necessary to remove lignin content in order to achieve the optimum conversion in gasification, thereby contributing to a significantly increasing overall cost and energy consumption of the process as well as an environmental concern for handling and disposal of residual chemicals (Kan et al., 2016; Hosseini Koupaie et al., 2018).

Table 2.1: Examples lignocellulosic compositions of different types of biomass (McKendry, 2002; Isikgor and Becer, 2015; Bajpai, 2016).

| Biomass | wt% (dry basis) | | |
|---|---|---|---|
| | Cellulose | Hemicellulose | Lignin |
| Softwood | 42-50 | 24-27 | 20-27 |
| Hardwood | 51-53 | 26-29 | 15-16 |
| Wheat straw | 35-39 | 23-30 | 12-16 |
| Rice straw | 29-35 | 23-26 | 17-19 |
| Rice husk | 29-36 | 12-29 | 15-20 |
| Corn cobs | 34-41 | 32-36 | 6-16 |
| Switchgrass | 35-40 | 25-30 | 15-20 |
| Bagasse | 25-45 | 28-32 | 15-25 |

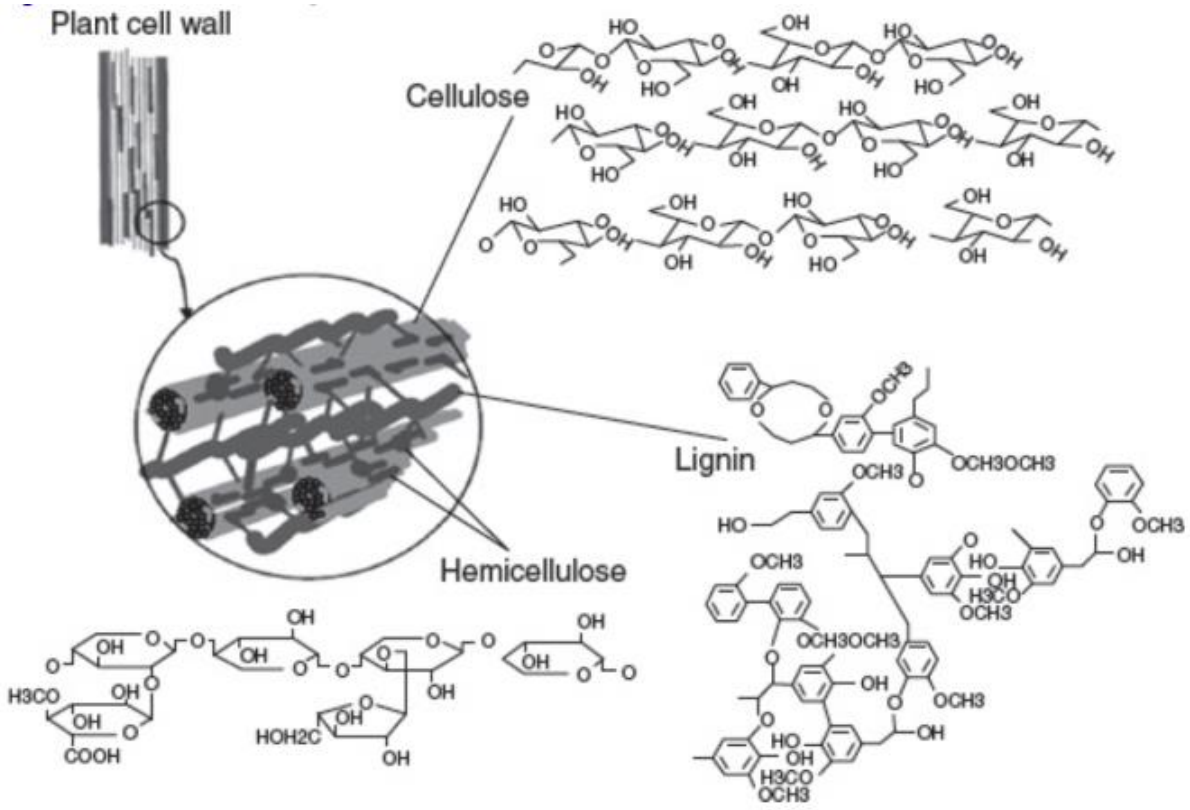


Figure 2.1: Structure of lignocellulose (Rodriguez et al., 2017).

## 2.2 Biomass conversion approaches

The two major pathways to convert lignocellulosic into chemical feedstocks and biofuels include biochemical (anaerobic digestion, fermentation and transesterification) or thermochemical (combustion, pyrolysis and gasification) approaches are shown in Figure 2.2. The choice of the conversion route depends on biomass type, its availability and the form of energy desired (Goyal et al., 2008). In biochemical processes only cellulose and hemicellulose components in the biomass feedstock can be converted into sugars that can be then fermented into either alcohols (ethanol or butanol) (Chakraborty et al., 2012), hydrocarbons i.e. alkanes/alkenes (Peralta-Yahya et al., 2012) in the presence of enzymes and other microorganisms or methane-enriched gas production through anaerobic digestion (Gaurav et al., 2017). These products can be used either as a fuels for transportation or heat and electricity generating using turbines/internal combustion engines (Elshahed, 2010; Hassan and Kalam, 2013). However, there are a number of technical challenges in biochemical processes, i.e. high viscosity substrate, high enzyme cost, enzyme lifetime, process efficiency and long reaction time (up to a week) (Lin and Tanaka, 2006; Stephanopoulos, 2007).

Thermochemical processes involve thermal decomposition of biomass in an oxidizing agent (i.e. air, $O_2$, or steam), inert atmosphere ($N_2$) or their mixture (Bridgwater, 2012). Compared to biochemical processes, thermochemical processes can utilise all three components (cellulose,

hemicellulose and lignin) in the biomass feedstock via a much shorter reaction time (a few hours or a day) and produced multiple products, i.e. solid, liquid and gaseous fuels (Tanger et al., 2013; Voloshin et al., 2016). Furthermore, thermochemical processes have higher conversion and process efficiency, greater versatility and more flexibility to a wide range of biomass feedstock compared to biochemical processes (Chew and Doshi, 2011). Among advanced thermochemical process, gasification is considered as the most cost-effective and efficient method (70-80%) to convert biomass into energy/fuels compared to 15-30% for combustion (Bridgwater, 2003) and 65-75% for pyrolysis processes (Balat et al., 2009a; Bridgwater, 2018) as well as it produces low concentrations of air pollutants (i.e. $SO_x$, $NO_x$ and particulates) (Basu, 2010a; Paula. G. Peres et al., 2013). As shown in Figure 2.2, the synthetic gas (known as syngas) derived from the gasification process can not only be used for heat and electricity generation but also can be further processed to produce liquid fuels (diesel fuel and gasoline) for the transportation sector or valuable chemicals (i.e. methanol, ethanol and alcohol) (de Lasa et al., 2011; Rauch et al., 2014; Sikarwar et al., 2016). Therefore, this study focuses on the gasification process.

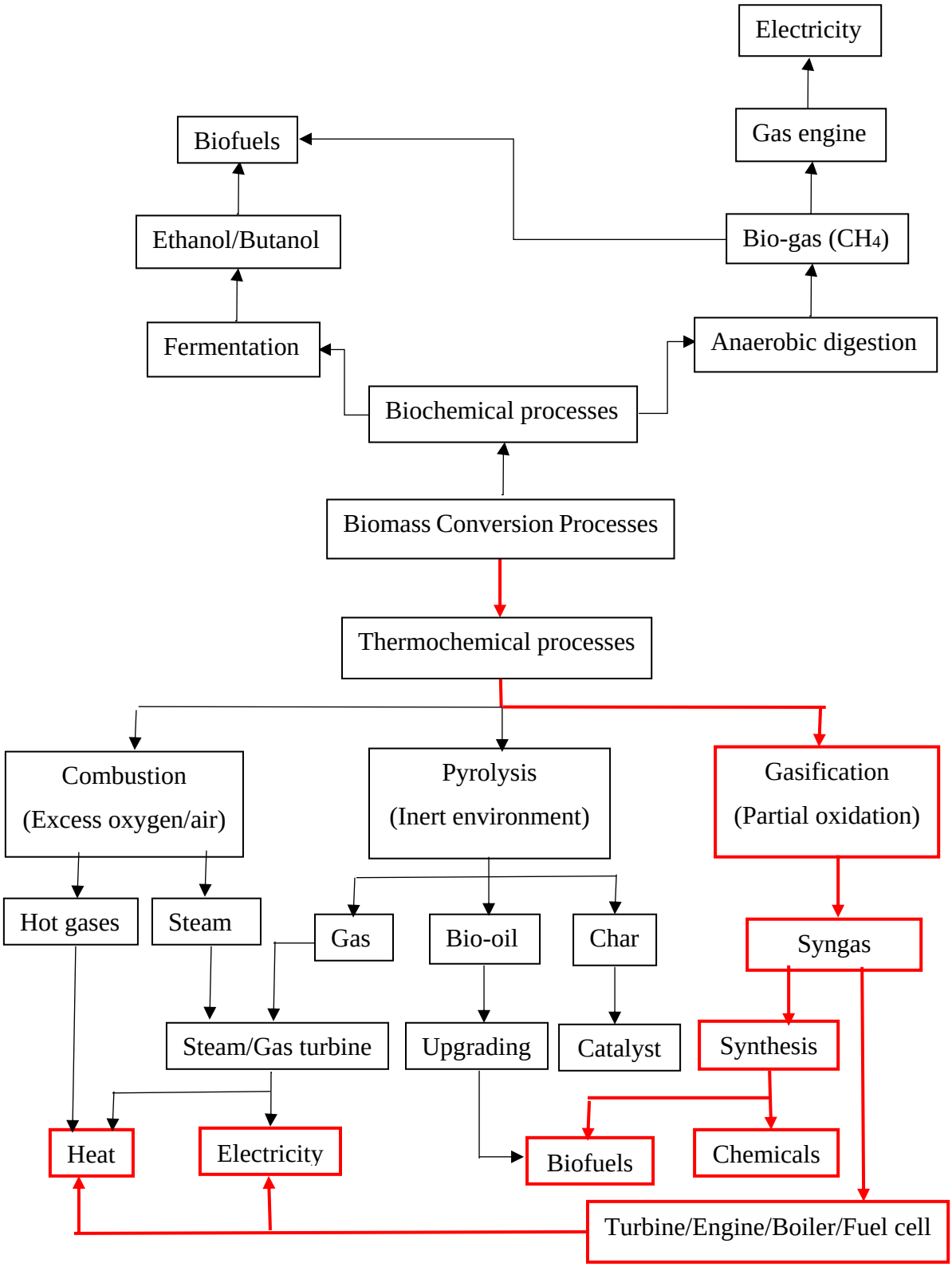


Figure 2.2: Biomass conversion processes and their end products (Bridgwater, 2003; Akhtari et al., 2014).

### 2.3 Gasification process

Gasification is a partial oxidation process to produce gas (known as synthetic gas or syngas) mainly of $H_2$ and CO in a temperature range of 900-1500 $^oC$ (Balat et al., 2009b; Valderrama

Rios et al., 2018). The syngas composition is strongly influenced by the type of gasifier and the operating conditions such as temperature, gasifying agents ($O_2$, $CO_2$, air, steam or their mixture), the ratio of gasifying agent to feedstock, particle size of biomass feedstock and nature of feedstock (Wang et al., 2008; Ruiz et al., 2013). There are four stages in gasification including drying, pyrolysis, oxidation and reduction, which can overlap depending on the type of gasifier.

### 2.3.1 Drying

The drying step occurs at temperatures range ≤ 200 $^{o}$C. For the gasification process, biomass feedstock with the moisture content less than 25 wt% is required to achieve high process efficiency (Wu et al., 2009; Plis and Wilk, 2011; Molino et al., 2016). Drying is energy intensive, i.e. up to 2260 kJ/$kg_{water}$ to remove water from biomass feedstock (Monarca et al., 2012).

### 2.3.2 Pyrolysis

Pyrolysis occurs over a temperature range of 250-800 $^{o}$C in the absence of oxygen/air to form three fractions: a solid (bio-char), liquid (bio-oil) and gaseous fraction (Equation 2.1) with their proportion and properties strongly depending upon the nature of feedstock, particle size, heating rate and temperature (Demirbaş, 2001; Akhtar and Saidina Amin, 2012; Isahak et al., 2012). Pyrolysis plays an important role in biomass gasification because there is a high content of volatile matter (75-85 wt%) in biomass feedstock compared to that in coal (20-30 wt%) (Gabra et al., 2001). Large amounts of volatiles in biomass are released rapidly (20-25 wt%/min) (Seo et al., 2010), leading to a reduction of volatile vapour residence time in the hot zone for reacting with the char, gasifying agent or other gas via heterogeneous and homogeneous reactions, resulting in an incomplete gasification followed by high tar formation and reduced process efficiency (Gil et al., 1997; Zhou et al., 2009; Hernández et al., 2010). Moreover, the properties of volatiles and char derived from the pyrolysis step (feedstock for oxidation and reduction steps) also in turn, affect the syngas properties and tar formation in the gasification process (Prasertcharoensuk et al., 2019).

$$\text{Biomass} \xrightarrow{\text{Heat}} \text{Char} + \text{Volatiles (non} - \text{condensable and condensable gases)} \qquad (2.1)$$

### 2.3.3 Oxidation

The oxidation zone is where the reactions between solid char and volatiles derived from the pyrolysis stage and gasifying agents, i.e. oxygen in air, occurs to form CO, $CO_2$ and $H_2O$ (Equations 2.2-2.9) at temperatures of 1200-1500 $^oC$. The oxidation zone is highly exothermic, providing the heat to sustain the pyrolysis and reduction zones in the gasification process (Molino et al., 2016).

$$CO + \frac{1}{2}O_2 \rightarrow CO_2 \ (\Delta H = -284 \text{ kJ/mol}) \quad (2.2)$$

$$C + \frac{1}{2}O_2 \rightarrow CO \ (\Delta H = -110 \text{ kJ/mol}) \quad (2.3)$$

$$C + O_2 \rightarrow CO_2 \ (\Delta H = -394 \text{ kJ/mol}) \quad (2.4)$$

$$H_2 + \frac{1}{2}O_2 \rightarrow H_2O \ (\Delta H = -242 \text{ kJ/mol}) \quad (2.5)$$

$$CH_4 + 2O_2 \rightarrow CO_2 + 2H_2O \ (\Delta H = -803 \text{ kJ/mol}) \quad (2.6)$$

$$CH_4 + \frac{1}{2}O_2 \rightarrow CO + 2H_2 \ (\Delta H = -36 \text{ kJ/mol}) \quad (2.7)$$

$$C_xH_y + \frac{x}{2}O_2 \rightarrow xCO + \left(\frac{y}{2}\right)H_2 \ (\Delta H = -715 \text{ kJ/mol}) \quad (2.8)$$

$$C_6H_{6.2}O_{1.2} + 4.45O_2 \rightarrow 6CO + 3.1H_2O \ (\Delta H = -80 \text{ kJ/mol}) \quad (2.9)$$

where $C_6H_{6.2}O_{1.2}$ represents unspecific high molecular weight compounds, i.e. tar (Han et al., 2017).

### 2.3.4 Reduction

In the reduction zone the unreacted volatiles and solid char derived from oxidation and pyrolysis zones are further oxidised. The Boudouard (Equation 2.10) and water gas (Equation 2.11) reactions are mainly heterogeneous reactions between the char and $CO_2$ and steam forming $H_2$ and CO, which are dominant at temperatures above 900 $^oC$ (Kwon et al., 2012; Liu et al., 2018). Steam reforming (Equations 2.15 and 2.16), $CO_2$ reforming (Equations 2.17 and 2.18) and the water gas shift (Equation 2.19) reactions are the principal homogeneous reactions in the reduction zone and influence $H_2$ production and the properties of the syngas, i.e. $H_2$/CO ratio

and calorific value (Ratnadhariya and Channiwala, 2009; Puig-Arnavat et al., 2010). In these, forward reactions are more important at high temperatures (i.e. > 700 $^{o}$C) promoting $H_2$ formation (Demirel and Ayas, 2017; Liu et al., 2018).

- Heterogeneous reactions

$$C + CO_2 \leftrightarrow 2CO \ (\Delta H = +173 \text{ kJ/mol}) \quad (2.10)$$

$$C + H_2O \leftrightarrow CO + H_2 \ (\Delta H = +131 \text{ kJ/mol}) \quad (2.11)$$

$$C + 2H_2 \leftrightarrow CH_4 \ (\Delta H = -75 \text{ kJ/mol}) \quad (2.12)$$

- Homogeneous reactions

$$CO_2 + 4H_2 \leftrightarrow CH_4 + 2H_2O \ (\Delta H = -165 \text{ kJ/mol}) \quad (2.13)$$

$$C_xH_y + \left(2x - \frac{y}{2}\right) H_2 \leftrightarrow xCH_4 \ (\Delta H = -498 \text{ kJ/mol}) \quad (2.14)$$

$$CH_4 + H_2O \leftrightarrow CO + 3H_2 \ (\Delta H = +206 \text{ kJ/mol}) \quad (2.15)$$

$$C_xH_y + xH_2O \leftrightarrow \left(\frac{y}{2} + x\right) H_2 + xCO \ (\Delta H = +740 \text{ kJ/mol}) \quad (2.16)$$

$$CO_2 + CH_4 \leftrightarrow 2H_2 + 2CO \ (\Delta H = +247 \text{ kJ/mol}) \quad (2.17)$$

$$C_xH_y + xCO_2 \leftrightarrow 2xCO + \left(\frac{y}{2}\right) H_2 \ (\Delta H = +980 \text{ kJ/mol}) \quad (2.18)$$

$$CO + H_2O \leftrightarrow CO_2 + H_2 \ (\Delta H = -41 \text{ kJ/mol}) \quad (2.19)$$

### 2.4 Types of gasifier

Gasifier design has significant impact on yield and quality of the product gas and tar formation. There are several types of gasifier: fixed-bed gasifiers (updraft or downdraft), fluidized bed gasifiers (bubbling or circulating) and entrained flow gasifiers. Fixed-bed gasifiers are the most common technology for small and medium scale biomass gasification (150 kW to 10 MW) due to their simplicity of construction and relatively low investment cost compared to fluidized bed and entrained flow gasifiers (Bridgwater, 1995; Puig-Arnavat et al., 2010).

### 2.4.1 Fixed-bed gasifier

A fixed-bed gasifier can be classified into two types: updraft gasifier (counter-current) and downdraft gasifier (co-current), depending upon the direction of flow of gasifying agent and product gas.

#### Updraft gasifier

An updraft gasifier (Figure 2.3) can be operated in a temperature range of 900-1000 $^{o}$C with high moisture content feedstock (up to 60 wt%). Therefore, it can be used for, i.e. sewage sludge, animal waste and waste water products (Basu, 2010b; Watson et al., 2018). Feedstock is fed from the top of the gasifier, whereas the preheated gasifying agent enters the gasifier via a perforated/distributed grate at the bottom. Ash and unreacted char are collected through the grate at the bottom of the gasifier. The product gas exits from the top of the gasifier at a temperature range of 200-300 $^{o}$C (Basu, 2010b). The gas composition derived from an updraft gasifier consists of 18-23 mol% $CO_2$, 43-44 mol% CO, 29-31 mol% $H_2$ and 6-7 mol% $CH_4$ (Gordillo et al., 2009) with high tar (high molecular weight compounds) content (10-20 wt% or 30-150 g/Nm$^3$), due to the product gas passing through cool zones before exiting (Basu, 2010b; Fabry et al., 2013). Therefore, the product gas needs to be cleaned, so that it can be used in heat and electricity applications (Radwan, 2012; Asadullah, 2014).

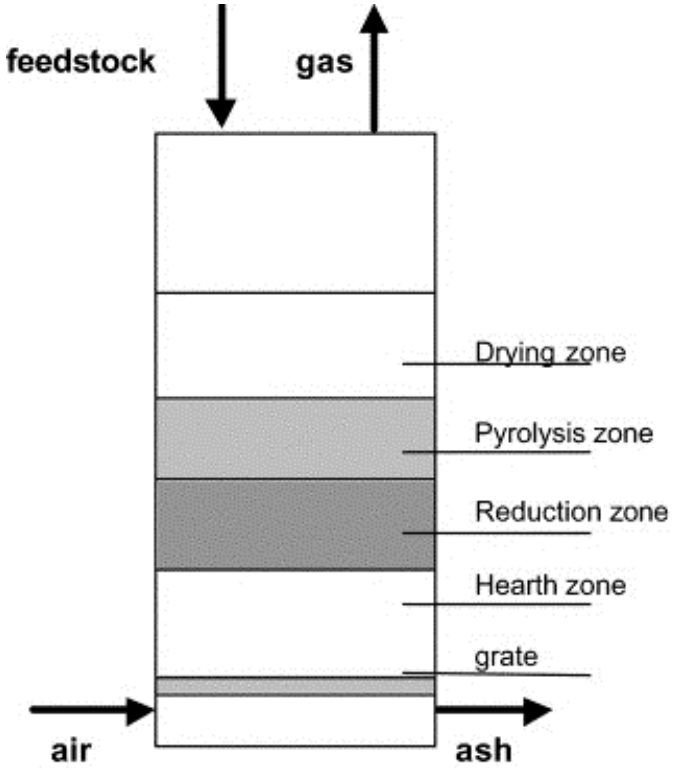


Figure 2.3: Stages of updraft gasifier (Quaak et al., 1999).

**Downdraft gasifier**

A downdraft gasifier (Figure 2.4) can be operated at a temperature range of 1000-1400 $^{o}$C (Asadullah, 2014). Volatiles and char derived from the pyrolysis step move in the same direction as the gasifying agent (downward) through the oxidation and reduction zones. The gasifying agent is introduced into the gasifier through nozzles at the oxidation zone, which is located at the middle part of the reactor. The product gas exits at the bottom of the gasifier at a temperature range of 700-800 $^{o}$C (Bhavanam and Sastry, 2011; Asadullah, 2014), therefore the producer gas need to be cooled down via heat recovery systems before being used in downstream applications (Watson et al., 2018). The gas composition derived from a downdraft gasifier consists of 21-30 mol% $CO_2$, 27-36 mol% CO, 34-41 mol% $H_2$ and 3-8 mol% $CH_4$. A downdraft gasifier produces the gas with low tar content (0.1 wt% or 0.015-3 g/Nm$^3$) (Arena, 2012; Fabry et al., 2013; Ud Din and Zainal, 2016) which can be directly used in internal combustion engines for heat and electricity generation (Watson et al., 2018). However, biomass feedstock must have a particle size in the range of 40-50 mm and moisture content below 20 wt% to obtain uniform temperature across the oxidation zone and minimize mass and heat transfer limitations inside the particles (Bhavanam, 2011; de Lasa et al., 2011; Sikarwar et al., 2016).

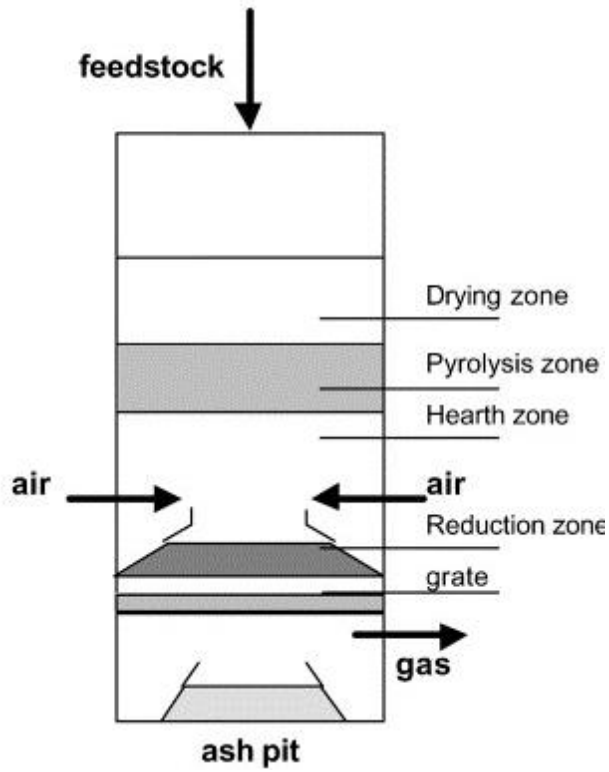


Figure 2.4: Stage of downdraft gasifier (Quaak et al., 1999).

### 2.4.2 Fluidized bed gasifier

A fluidized bed (FB) gasifier is widely used for large scale biomass gasification processing (2-100 MW) (Buragohain et al., 2010) due to (i) high heat and mass transfer, leading to uniform temperature and high reaction rates, (ii) high carbon conversion and (iii) high tolerance to a wide range of biomass feedstocks (Cui and Grace, 2007; Ahmed et al., 2012). Unlike fixed-bed gasifiers, a fluidized bed gasifier is operated under isothermal conditions, therefore all the chemical reactions/zones occur simultaneously (Ruiz et al., 2013). However, there are disadvantages in the fluidized bed gasifiers, i.e. pressure drop, contamination of particulates and/or bed material in the product gas, corrosion, clogging and fouling caused by bed materials, high investment cost and complex construction compared to the fixed-bed gasifiers (Puig-Arnavat et al., 2010; Sun et al., 2013). Moreover, homogeneous properties of the biomass feedstock with a uniform particle size distribution in the range between 6 mm and 30 mm with moisture content below than 55 wt% is required (Basu, 2010a). Depending on the velocity of the gasifying agent, the fluidized bed gasifiers can be classified into bubbling fluidized bed gasifiers (Figure 2.5) and circulating fluidized bed gasifiers (Figure 2.6).

#### Bubbling fluidized bed gasifier

A bubbling fluidized bed (BFB) gasifier is operated at 650-800 $^{o}$C. Biomass fed at one side of the gasifier reacts with gasifying agent (oxygen or oxygen-enriched air) introduced via a distributed grate at the bottom of the gasifier at a velocity in the range of 1-3 m/s (McKendry, 2002; Molino et al., 2016). This velocity range is just above the minimum speed for fluidization of the bed material (typically silica or olivine) and the formation of bubbles (Radwan, 2012). The product gas exits from the top of the gasifier at temperature range of 450-600 $^{o}$C, whereas ash and unreacted char are removed through the grate at the bottom of the gasifier (Farzad et al., 2016; Basu, 2018). The tar content in the producer gas in the range of 4-16 wt% or 4-62 g/Nm$^3$ (McKendry, 2002; Buragohain et al., 2010), which was comparable to that in a updraft gasifier. However, the $H_2$/CO ratio derived from bubbling fluidized bed gasifier (0.5-0.8) (Warnecke, 2000; Kim et al., 2013b) is much lower than the required ratios for syngas applications, i.e. heat and electricity generation via gas turbines or internal combustion engines ($H_2$/CO $\geq$ 1) (Demırbas, 2016) and chemical (i.e. methanol, ethanol and alcohol) and liquid fuels (diesel fuel and gasoline) production via Fischer-Tropsch synthesis which require $H_2$/CO $\geq$ 2 (Chaudhari et al., 2001; Yung et al., 2009). Therefore, the product gas from a bubbling fluidized bed gasifier needs to be upgraded via steam reforming to obtain a high molar ratio of $H_2$/CO before it can be used.

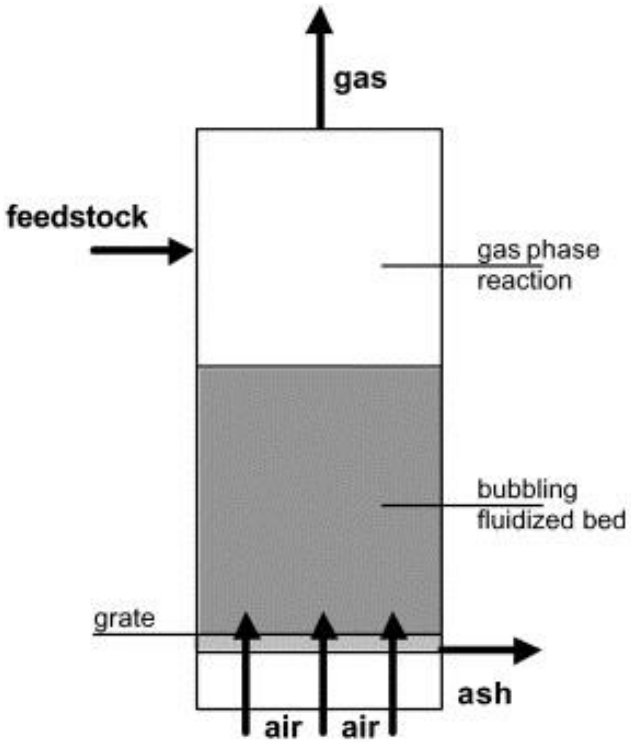


Figure 2.5: Stage of bubbling fluidized bed gasifier (Belgiorno et al., 2003).

**Circulating fluidized bed gasifier**

A circulating fluidized bed (CFB) gasifier is operated at temperatures below 900 $^{o}$C at high velocities of gasifying agent (3.5-5.5 m/s), which is above the transport velocity of the fluidized bed materials (McKendry, 2002). Therefore, all solid particles (ash, char and bed material) are carried out with the product gas exiting at the top of the gasifier and removed from the product gas via cyclone separators (Belgiorno et al., 2003). The bed material is returned to the system at the bottom of the gasifier. A circulating fluidized bed gasifier is particularly suitable for the cases where the size and shape of feedstock is difficult to control as well as for high volatile content feedstock (Kumar et al., 2009). A circulating fluidized bed gasifier produces the product gas with tar content in the range 5-10 wt% or 4-20 g/Nm$^3$ (Basu, 2010a; Puig-Arnavat et al., 2010). The syngas composition consists of 27-30 mol% $H_2$, 31-41 mol% $CO_2$, 2-7 mol% $CH_4$ and 30-33 mol% CO, which is similar to that obtained from a bubbling fluidized bed gasifier (Arena, 2012; Liu et al., 2013).

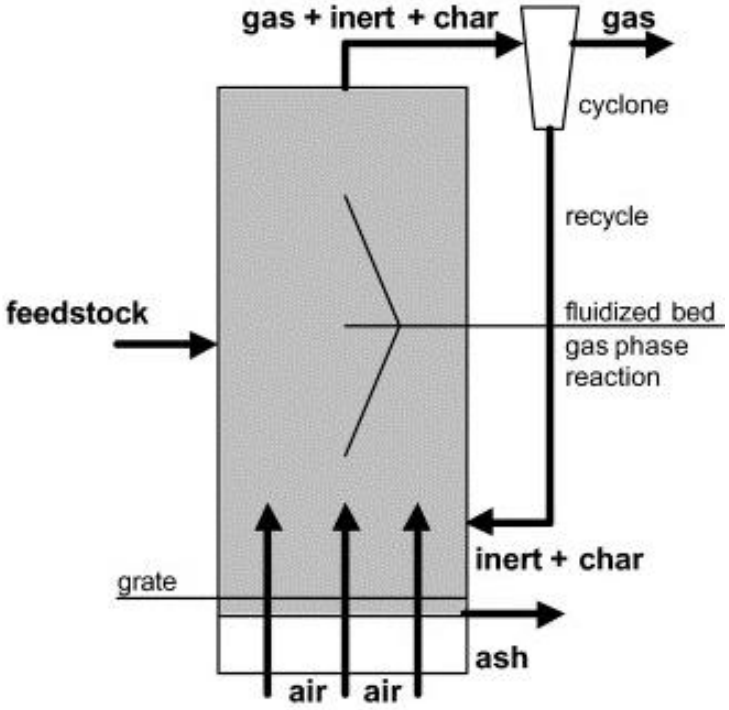


Figure 2.6: Stage of circulating fluidized bed gasifier (Belgiorno et al., 2003).

### 2.4.3 Entrained flow gasifier

An entrained bed gasifier (Figure 2.7) is operated at high temperatures (1300-1500 $^{o}$C) with high pressures (20-70 bar) (Molino et al., 2016). Biomass feedstock with fine particle sizes (< 1 mm) (Ruiz et al., 2013; Farzad et al., 2016) is fed together with the gasifying agent, i.e. pure oxygen either from the top or the side of the gasifier and the product gas exits from the bottom of the gasifier at temperature around 1260 $^{o}$C (Puig-Arnavat et al., 2010). Due to the high pressure, feedstock and water can be well-mixed, therefore it is suitable for wet organic material with moisture content up to 40-60% (i.e. sewage sludge, animal waste and waste water products) (Kirkels and Verbong, 2011; Molino et al., 2016). The entrained flow gasifier can produce syngas consisting of 15-20 mol% $H_2$, 10-15 mol% $CO_2$, 40-60 mol% CO and less than 2 mol% of $CH_4$ with low tar content (0.1 wt% or 0.01-4 g/Nm$^3$) in the gas stream (Zhou et al., 2009; Basu, 2010a; Ruiz et al., 2013). However, there are some disadvantages such as (i) high operating temperatures and pressures, leading to an increase in capital costs (special materials for the system), (ii) high operating costs due to high purity oxygen required for high carbon conversion (close to 100%) and (iii) physical pre-treatment such as milling and grinding of biomass feedstock to obtain particle size in the range of 0.15-1 mm is required (Zhou et al., 2009; Zhang et al., 2010; Zhao et al., 2010).

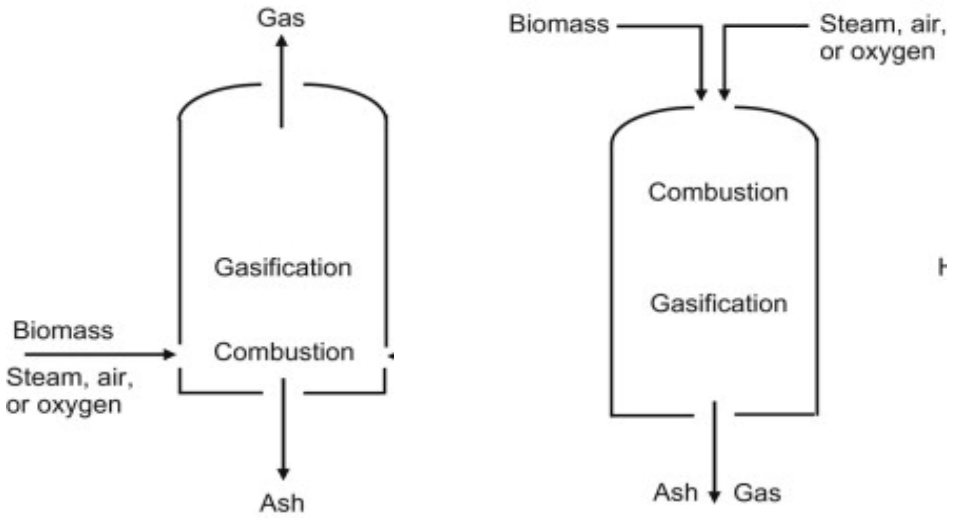


Figure 2.7: Stage of entrained flow gasifier (a) side-fed and (b) top-fed (Basu, 2010a).

### 2.4.4 Two-stage gasifier

Two-stage gasification (Figure 2.8) was developed by the Danish Technical University, Denmark (Henriksen et al., 2006) and the Karlsruhe Institute of Technology, Germany (Trippe et al., 2011) where the pyrolysis and char gasification take place in two separate reactors, in which feedstock was decomposed into intermediate products, i.e. solid (char) and volatiles (non-condensable and condensable gases) via the pyrolysis step (1$^{st}$ reactor) and subsequently gasified in the gasification step (2$^{nd}$ reactor). The two distinct zones allow an independent control and optimized operating conditions for each individual step to obtain high quality syngas/$H_2$ production and minimize tar formation in the gas stream in the biomass gasification (Materazzi et al., 2013) as well as avoiding mixing of produced volatiles and char; consequently adverse impacts on the reactivity and gasification of char are eradicated (Sikarwar et al., 2016). Compared to an existing gasifiers (as described previously), a two-stage gasification process can be used for a wide range of feedstock particularly low-value feedstock such as multiple solid waste (MSW) and plastics with minimum pre-treatment and is scale/load independent (Galindo et al., 2014; Bambang et al., 2018). Moreover, it can produce high $H_2$ content (45-55 mol%) and $H_2$/CO ratio (around 2) with a high calorific value of syngas around 7-11 MJ/Nm$^3$ and process efficiency ≥ 90% compared to 15-41 mol% $H_2$ ($H_2$/CO ratios less than 1) and the syngas heating value of 4-6 MJ/Nm$^3$ generated from existing gasifier designs with process efficiency ≤ 80% (Jaojaruek et al., 2011; Ma et al., 2012; Pei et al., 2018). A two-stage gasifier produces the syngas with much lower tar content (< 0.015 g/Nm$^3$) (Brandt et al., 2000; Šulc et al., 2012; Kosov and Zaichenko, 2016) than updraft (30-150 g/Nm$^3$), downdraft (0.015-3

g/Nm$^3$), fluidized bed (4-62 g/Nm$^3$) and entrained flow (0.01-4 g/Nm$^3$) gasifiers, which can be directly used either in internal combustion engines for heat and electricity generation or converted further into synthetic liquid fuels (diesel fuel and gasoline) and valuable chemicals (i.e. methanol, ethanol and alcohol). Low amount of tar is attributed to the partial combustion of the pyrolytic gases as well as the catalytic effect of the charcoal bed (Brandt et al., 2000; Gómez-Barea et al., 2013b). Therefore, a two-stage gasifier was selected for this study.

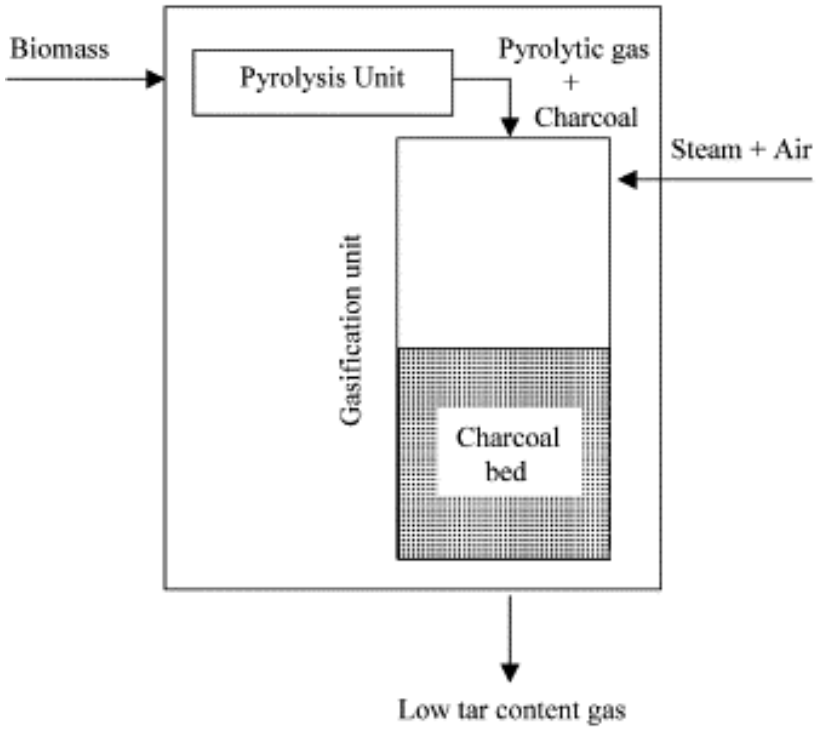


Figure 2.8: Two-stage gasification process (Henriksen et al., 2006).

## 2.5 Parameters affecting gasification process

### 2.5.1 Pyrolysis operating conditions

As soon as lignocellulosic material is heated up to 250-800 $^oC$, it decomposes into volatiles (non-condensable and condensable fraction) and solid char and the product properties strongly depend upon the temperature, heating rate, carrier gas flow rate, nature and particle size of the biomass feedstock (Demirbaş, 2001; Akhtar and Saidina Amin, 2012). The properties of volatiles and char significantly affect the quality of syngas from gasification (Prasertcharoensuk et al., 2019). For example, a high surface area of char will promote mass transfer among the gas, gasifying agent and char particles, accelerating heterogeneous solid-gas reactions occuring in the gasification process, i.e. the Boudouard (Equation 2.10) and water gas (Equation 2.11) reactions, leading to a formation of $H_2$ and CO with minimum unburnt carbon in the ash residues (Ren et al., 2014; Shen, 2015). Moreover, the high specific surface area of the char also enhances the

cracking/reforming of high molecular compounds (tar) in the gasification step (Paethanom and Yoshikawa, 2012; Shen and Fu, 2018). A reduction in liquid fraction (bio-oil) and phenolic compounds (precursors of multiple aromatic ring species in tar) in the pyrolysis step could help to minimize tar formation in biomass gasification (Yu et al., 1997; Demirbas, 2007). High CO concentration in the gas stream derived from the pyrolysis step promotes a significant reaction, i.e. the water gas shift reaction (Equation 2.19) to generate $H_2$ in the gas stream in the gasification process (Kwon et al., 2012).

**Temperature**

Pyrolysis temperature plays an important role in the process, affecting product yields and properties. Low temperatures (< 400 $^{o}$C) favour solid (bio-char) production whereas high temperatures (≥ 400 $^{o}$C) promote liquid production (Figure 2.9) (Huynh et al., 2016). However, a further increase in pyrolysis temperature above 600 $^{o}$C, enhances the formation of gas (Figure 2.9) due to the secondary cracking of volatiles and char (Akhtar and Saidina Amin, 2012; Bridgwater, 2012; Adams et al., 2018).

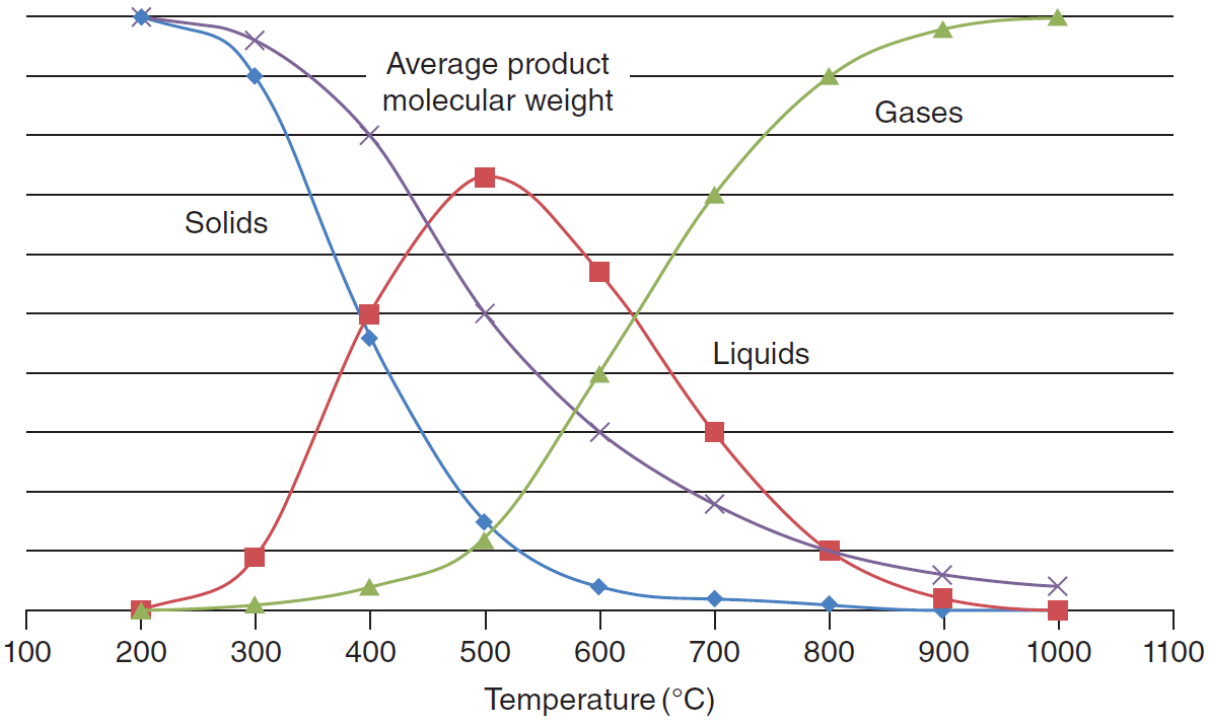


Figure 2.9: Relationship between product distribution and reaction temperature in pyrolysis of lignocellulosic materials (Huynh et al., 2016).

The pyrolysis temperature affects char, liquid and gas properties. For example, the carbon content in char derived from straw increased from 45.6 wt% to 59.2 wt%, whereas oxygen and

hydrogen decreased from 38.5 wt% to 11.0 wt% and from 5.8 wt% to 1.5 wt% when the pyrolysis temperature increased from 200-600 $^{o}$C, due to an increases in the level of carbonization in the process (Zhang et al., 2015). Table 2.2 summarises the effect of pyrolysis temperature on the chemical composition of char for various feedstocks.

Table 2.2: The elemental composition of char derived from different biomass feedstocks and pyrolysis temperature.

| Biomass feedstock | Temperature ($^{o}$C) | C | H | O* | N |
|---|---|---|---|---|---|
| | | wt% (dry basis and ash free) | | | |
| Douglas fir wood (Suliman et al., 2016) | 350 | 70.1 | 5.8 | 23.9 | 0.2 |
| | 400 | 74.8 | 5.2 | 19.8 | 0.2 |
| | 450 | 75.3 | 4.7 | 19.7 | 0.3 |
| | 500 | 76.7 | 4.2 | 18.8 | 0.3 |
| | 550 | 82.4 | 4.1 | 13.2 | 0.3 |
| | 600 | 85.6 | 3.7 | 10.4 | 0.3 |
| Wood (Ronsse et al., 2013) | 300 | 54.1 | 5.9 | 39.4 | 0.6 |
| | 450 | 82.5 | 3.8 | 13.2 | 0.5 |
| | 600 | 90.0 | 2.6 | 6.8 | 0.6 |
| | 750 | 92.5 | 1.4 | 5.4 | 0.7 |
| Wood (Brendova et al., 2012) | 450 | 76.2 | 2.4 | 20.2 | 1.2 |
| | 500 | 77.7 | 2.2 | 19.0 | 1.1 |
| | 550 | 78.7 | 2.0 | 18.3 | 1.0 |
| Rice straw (Fu et al., 2011) | 600 | 82.7 | 0.6 | 15.4 | 1.3 |
| | 700 | 83.9 | 0.5 | 14.3 | 1.3 |
| | 800 | 87.7 | 0.5 | 10.4 | 1.4 |
| | 900 | 92.0 | 0.5 | 6.1 | 1.4 |
| | 1000 | 95.8 | 0.5 | 2.2 | 1.5 |

* By difference

Increasing pyrolysis temperature accelerated the rate of decomposition (Ertaş and Hakkı Alma, 2010; Abdel-Fattah et al., 2015; Pradhan et al., 2016), resulting in an increase in the release of volatiles which in turn causes the formation of small pores on the surface of a biomass particle, thereby increasing the surface area and pore volume of char (Ahmad et al., 2012; Kim et al., 2013a). The surface area of apple tree branch char was increased from 2.4 $m^2/g$ to 108.6 $m^2/g$ and the total pore volume from $2.6\times10^{-3}$ $cm^3/g$ to $58.5\times10^{-3}$ $cm^3/g$ when increasing pyrolysis temperature from 300-600 $^oC$ (Zhao et al., 2017). Increasing pyrolysis temperature from 300-700 $^oC$ increased surface area of soybean stover char from 5.6 $m^2/g$ to 420.3 $m^2/g$ and pore volume up to 19.0 $\times10^{-2}$ $cm^3/g$ at pyrolysis temperature of 700 $^oC$ (Ahmad et al., 2012). However, higher pyrolysis temperatures, i.e. above 900 $^oC$ cause a reduction in surface area (from 66.5 $m^2/g$ at 900 $^oC$ to 49.8 $m^2/g$ at 1000 $^oC$) and pore volume (from $30.6\times10^{-3}$ $cm^3/g$ at 900 $^oC$ to $23.0\times10^{-3}$ $cm^3/g$ at 1000 $^oC$) of cotton straw char (Fu et al., 2011). This is due to shrinkage, cracking and rupture of char at high temperature.

The effect of pyrolysis temperature on the liquid (bio-oil) yield is well understood. However, there is no clear correlation between the pyrolysis temperature and the liquid properties (Lehto et al., 2013). However, there are suggestions that the concentration of chemical components in the liquid product, i.e. acids, ketones, esters, alcohols, aldehydes, furans and sugars and their derivatives, which derived from decomposition of cellulose and hemicellulose in the biomass feedstock, gradually decreased with increasing pyrolysis temperature (Chen et al., 2012; Chen et al., 2016b). High temperatures promoted the formation of phenolic compounds (lignin decomposition), which are precursors of multiple aromatic ring species in tar due to Diels-Alder reactions which are favoured at high temperature (i.e. above 500 $^oC$) (Cypres, 1987; Heo et al., 2010; Jiang et al., 2010). Water content in the liquid also increased with temperature, e.g. water content in liquid derived from miscanthus increased from 30.8 wt% at 350 $^oC$ to 34.5 wt% at 450 $^oC$ and up to 65 wt% at 550 $^oC$ (Heo et al., 2010). This is due to secondary reactions (i.e. dehydration), which occur at high pyrolysis temperatures. A similar trend was found in other studies on coconut shells, the water content in the liquid increased from 40.3 wt% at 350 $^oC$ to 45.3 wt% and 50.3 wt% at pyrolysis temperatures of 450 $^oC$ and 575 $^oC$ respectively (Gao et al., 2016b). However, a decrease from 64.1 wt% to 58.8 wt% in water content of the liquid product from poplar wood was observed when the pyrolysis temperature increase from 400-600 $^oC$ (Chen et al., 2016b), which agreed very well with other findings on cotton stalk (from 70.5 wt% to 67.5 wt%) (Chen et al., 2012) and pine nut shells (from 61.6 wt% to 55.6 wt%) (Chen et al., 2016a) at the same temperature range.

Table 2.3: Effect of pyrolysis temperature on the composition of pyrolysis gases from different biomass feedstocks (Fu et al., 2011).

| Biomass feedstock | Temperature (°C) | $H_2$ | $CO_2$ | CO | $CH_4$ | $C_2$-$C_6$ |
|---|---|---|---|---|---|---|
| | | mol% | | | | |
| Mize stalk | 600 | 3.4 | 31.1 | 45.3 | 15.0 | 5.2 |
| | 700 | 3.7 | 26.4 | 52.1 | 12.7 | 5.1 |
| | 900 | 6.7 | 15.8 | 56.9 | 18.7 | 1.9 |
| | 1000 | 4.8 | 13.2 | 61.0 | 20.0 | 1.0 |
| Rice straw | 600 | 5.3 | 36.2 | 43.3 | 6.8 | 8.4 |
| | 700 | 9.1 | 28.6 | 45.0 | 11.1 | 6.2 |
| | 900 | 5.4 | 25.4 | 50.1 | 18.0 | 1.1 |
| | 1000 | 7.1 | 19.7 | 51.7 | 20.4 | 1.1 |
| Cotton straw | 600 | 4.6 | 29.6 | 45.0 | 14.1 | 6.7 |
| | 700 | 4.2 | 22.2 | 53.8 | 14.8 | 5.0 |
| | 900 | 5.5 | 18.3 | 56.9 | 18.0 | 1.3 |
| | 1000 | 3.5 | 17.0 | 57.1 | 21.4 | 1.0 |
| Rich husk | 600 | 5.0 | 29.3 | 45.6 | 15.1 | 5.0 |
| | 700 | 5.9 | 22.9 | 51.2 | 15.3 | 4.7 |
| | 900 | 4.9 | 16.4 | 56.6 | 20.7 | 1.4 |
| | 1000 | 1.6 | 14.2 | 59.9 | 23.0 | 1.3 |

Increasing the pyrolysis temperature of pterocarpus indicus from 450 °C to 700 °C caused an increase in CO (from 49.2 mol% to 62.1 mol%) and $CH_4$ (from 1.0 to 12.7 mol%) formation, whereas the $CO_2$ concentration gradually decreased from 48.5 mol% at 450 °C to 22.2 mol% at 700 °C (Luo et al., 2004). This is because when the $CO_2$ releasing from inner layers of a particle (decarboxylation reactions) it reacts with a hot char layer via the Boudouard reaction (Equation 2.10), which is dominant at temperatures above 900 °C, leading to the formation of CO (Kwon et al., 2012; Leal et al., 2016; Liu et al., 2018). Moreover, $CO_2$ will react with other hydrocarbons ($C_2$-$C_6$) via the dry reforming reaction (Equation 2.18) to form $CH_4$, CO or $H_2$ at

temperatures above 700 °C (Kwon et al., 2012; Leal et al., 2016). Table 2.3 summarise the effect of temperature on the gas derived from pyrolysis for various feedstocks.

**Heating rate**

Heating rate affects product yields as it related to the heat transfer rate from the reactor to the feedstock and the extent of the secondary reactions for volatiles and char. High heating rates cause a reduction of volatile vapour residence time in the hot zone and minimize the secondary reactions, leading to formation of a liquid product (Şensöz and Can, 2002). Increasing the heating rate during moso bamboo pyrolysis, i.e. from 5 °C/min to 30 °C/min at a pyrolysis temperature of 700 °C, increased the gas yield from 29.7 wt% at 5 °C/min to 42.9 wt% at 30 °C/min and liquid yield from 34.6 wt% to 39.2 wt% at the expense of char (from 31.1 wt% to 22.5 wt%) fraction (Chen et al., 2014). This is due to the fact that a high heating rate leads to a fast decomposition of the biomass material to the primary volatiles (both condensable and non-condensation fractions). Table 2.4 summarises the effect of heating rate on product yields for various feedstocks. However, increasing heating rate from 10-50 °C/min in pyrolysis had little effect on the properties of pyrolysis products (Chen et al., 2014; Chen et al., 2016b).

Table 2.4: Effect of heating rate on product distribution from different biomass feedstocks at pyrolysis temperature of 600 °C.

| Biomass feedstock | Heating rate (°C/min) | Char | Liquid | Gas* |
|---|---|---|---|---|
| | | wt% | | |
| Ferula orientalis L. (Aysu and Küçük, 2014) | 15 | 26.3 | 41.0 | 32.7 |
| | 30 | 24.9 | 41.8 | 33.3 |
| | 50 | 23.4 | 42.4 | 34.2 |
| Poplar wood (Chen et al., 2016b) | 10 | 31.9 | 37.9 | 30.2 |
| | 30 | 25.0 | 39.1 | 35.9 |
| | 50 | 21.7 | 39.9 | 38.4 |
| Paulownai wood (Yorgun and Yıldız, 2015) | 10 | 25.5 | 45.0 | 29.5 |
| | 50 | 20.2 | 48.9 | 30.9 |

* By difference

**Carrier gas flow rate**

The carrier gas flow rate, e.g. nitrogen flow rate, determines the hot vapour residence time in the pyrolysis step (Akhtar and Saidina Amin, 2012). Short hot vapour residence times (< 2 s) favour liquid production because they minimize further decomposition of desirable products (Bridgwater, 2012). The liquid yield of saccharina japonica increased from 31.2 wt% to 37.2 wt%, while gas (from 37.0 wt% to 28.5 wt%) and char (from 31.9 wt% to 37.2 wt%) decreased when increasing the $N_2$ flow rate from 100 ml/min to 500 ml/min at a fixed pyrolysis temperature of 550 $^oC$ (Ly et al., 2016). This is because the increasing nitrogen flow rate caused the reduction of volatiles vapour residence time in the hot zone, which in turn minimized secondary reactions (i.e. thermal cracking and secondary reactions) that crack condensable vapours into gaseous products (Pütün et al., 2004; Şensöz and Angın, 2008).

Table 2.5: Effect of nitrogen flow rate on pyrolysis product yield from different biomass feedstocks.

| Biomass feedstock | $N_2$ flow rate (ml/min) | Char | Liquid | Gas* |
|---|---|---|---|---|
| | | wt% | | |
| Cynara cardunculus L. (Encinar et al., 2000) | 100 | 19.0 | 43.8 | 37.2 |
| | 200 | 18.8 | 43.8 | 37.4 |
| | 300 | 18.7 | 44.0 | 37.3 |
| Corncob (Demiral et al., 2012) | 50 | 25.2 | 35.0 | 39.8 |
| | 100 | 23.6 | 35.8 | 40.6 |
| | 150 | 24.4 | 37.6 | 38.0 |
| | 200 | 24.2 | 38.2 | 37.6 |
| Sunflower pressed (Gerçel, 2002) | 25 | 26.5 | 29.3 | 44.2 |
| | 50 | 24.8 | 30.6 | 44.6 |
| | 100 | 21.6 | 31.5 | 46.9 |
| | 200 | 21.6 | 31.3 | 47.1 |
| | 400 | 21.0 | 31.0 | 48.0 |

* By difference

Increasing the carrier gas ($N_2$) flow rate from 50-250 ml/min in the pyrolysis of jute dust at a temperature of 500 $^oC$, decreased char yield from 34.3 wt% to 28.7 wt% and increased gas yield from 16.9 wt% to 33.7 wt%, while the liquid yield was maximized at 150 ml/min (31.1 wt%) (Choudhury et al., 2014). Within a carrier gas ($N_2$) flow rate range of 50-200 ml/min at a fixed pyrolysis temperature of 500 $^oC$, the liquid and gas yield from pyrolysis of olive bagasse increased from 35.2 wt% to 37.7 wt% and from 4.1 wt% to 6.9 wt% respectively, whereas the char yield remained unchanged (around 32 wt%) with increasing carrier gas flow rate (Şensöz et al., 2006). A similar observation was reported (Encinar et al., 2000; Gerçel, 2002; Demiral et al., 2012) at nitrogen flow rates of 25-300 ml/min (Table 2.5). However, carrier gas flow rates of 50-300 ml/min (corresponding to residence times of 1-3 s) has no influence on the pyrolysis product properties (Encinar et al., 2000; Acıkgoz et al., 2004; Demiral and Şensöz, 2006; Ly et al., 2016).

**Particle size**

The particle size is another parameter that affects the pyrolysis product properties because the particle size influences the heat and mass transfer rates (Yorgun and Yıldız, 2015). Small particles are preferred for liquid and gas production (more volatiles released) due to no heat transfer limitation inside the particle (Heo et al., 2010; Akhtar and Saidina Amin, 2012). Increasing the particle size of safflower seed and rapeseed from 0.4 mm to 1.8 mm increased char yield (from 20.2 wt% to 24.7 wt%) but decreased the liquid (from 44.7 wt% to 34.3 wt%) and gas yield (from 27.8 wt% to 25.2 wt%) at a pyrolysis temperature of 500 $^oC$ (Beis et al., 2002). The liquid yield derived from miscanthus was maximised (62.6 wt%) at particle size of 0.3-0.7 mm at a pyrolysis temperature of 450 $^oC$ and started to decrease to around 53.8 wt% with increasing particle size to 1.3 mm, while the char yield increased from 20.2 wt% to 26.4 wt% (Heo et al., 2010). This is due to larger particles having a greater temperature gradient within them, which reduces the average temperature and decomposition rate, therefore minimizing liquid and gas yields and maximizing the char fraction (Bennadji et al., 2014). A reduction in liquid yield from 61.1 wt% to 52.2 wt% was also observed by increasing particle size of sugarcane bagasse from 0.1 mm to 0.5 mm at pyrolysis temperature of 800 $^oC$ (Sohaib et al., 2017). When the particle size of Ferula orientalis L. increased from 0.2 mm to 0.9 mm, the liquid yield decreased from 45.0 wt% to 43.3 wt% and gas yield from 28.8 wt% to 27.5 wt%, while char yield increased from 26.2 wt% to 29.2 wt% at a pyrolysis temperature of 500 $^oC$ (Aysu and Küçük, 2014). In comparison, numerous studies (Encinar et al., 2000; Yorgun, 2003; Demiral and Şensöz, 2006; Septien et al., 2012; Yorgun and Yıldız, 2015; Varma and

Mondal, 2017) showed that the particle size had no significant effect on the pyrolysis product properties.

### 2.5.2 Gasification operating conditions

#### Gasifying agents

Gasifying agents (air, steam, oxygen or their mixtures) significantly influence the syngas composition and its calorific values (Table 2.6). Therefore, the choice of a gasifying agent used strongly depends upon the requirements of the product gas application and the economic feasibility (Matas Güell et al., 2012). Air is the cheapest and is widely used as the gasifying agent for biomass gasification, while it produces syngas with low calorific value (4-6 $MJ/Nm^3$), which is only suitable for small-scale power engines (< 2 MW) (Kalinci et al., 2009; Yung et al., 2009). This is because $O_2$ in the air promotes undergoes combustion reactions of the char and volatiles derived from the pyrolysis step to form $CO_2$ instead of the fuel gas (i.e. $H_2$, CO and $CH_4$), resulting in a low calorific value of the product gas (Niu et al., 2014). Moreover, the syngas produced from air gasification contains up to 60 mol% of $N_2$ in the gas product, which requires a $N_2$ separation process (i.e. pressure swing adsorption or membrane separation) to extract $N_2$ from the gas stream to improve the quality of syngas in terms of calorific value as well as minimizing $NO_x$ formation during downstream operations, leading to an increase in capital and operational costs of the process (Navarro et al., 2007; Thamavithya and Dutta, 2008).

Table 2.6: The characterisation of syngas obtained from different gasifying agents in biomass gasification (Herguido et al., 1992; La Villetta et al., 2017; Shayan et al., 2018).

| Gasifying agent | Air | Oxygen | Oxygen-enriched air | Steam |
|---|---|---|---|---|
| Cost | Low | High | Medium | Medium |
| Calorific value ($MJ/Nm^3$) | 4-6 | 10-15 | 6-9 | 15-20 |
| $H_2$ (mol%) | 15-21 | 32-37 | 26-28 | 44-49 |
| CO (mol%) | 19-23 | 42-48 | 28-32 | 23-35 |
| $CH_4$ (mol%) | 1-3 | 2-3 | 1-2 | < 1 |
| $CO_2$ (mol%) | 8-16 | 12-15 | 8-10 | 5-10 |

Oxygen as a gasifying agent produces a medium calorific value syngas (10-15 MJ/$Nm^3$), which can be readily used for liquid fuel production or chemical synthesis (Shayan et al., 2018). However, the drawback of oxygen gasification is the cost of high purity oxygen (≥ 99.5%) generation (Saxena et al., 2008; Kirkels and Verbong, 2011). An alternative way for using oxygen as a gasifying agent in the gasification process is oxygen-enriched air (30-40 mol% $O_2$), which is cheaper and also improves the quality of syngas (Hosseini et al., 2012; Kumar, 2015) in terms of $H_2$ content, $H_2$/CO ratio and the calorific value of syngas compared to air gasification (Table 2.6). Steam can produce high calorific value syngas (15-20 MJ/$Nm^3$) with high $H_2$ concentration (44-49 mol%) (Table 2.6) due to the additional of hydrogen from the water gas (Equation 2.11), steam reforming (Equations 2.15 and 2.16) and water gas shift (Equation 2.19) reactions (Hulteberg and Karlsson, 2009; James et al., 2014). However, the main disadvantage of using steam as a gasifying agent is the energy required for steam production causing a reduction in process efficiency (Ruiz et al., 2013; Asadullah, 2014). Recently, $CO_2$ has been considered as an oxidizing agent for biomass gasification to obtain high quality syngas/$H_2$ production without major downstream processing to remove impurities (tar in particular) (Gao et al., 2016a; Sadhwani et al., 2016). This is because, in theory, $CO_2$ has the ability to react with char (Equation 2.10) and volatiles (Equations 2.17 and 2.18) derived from the pyrolysis step to form $H_2$ and CO with minimum unburnt carbon in the ash residues and minimum tar formation (Guizani et al., 2015b; Prabowo et al., 2015; Valin et al., 2016). Moreover, the use of $CO_2$ in a gasification process also contributes significantly to improving the environmental footprint and sustainability of the process. Extensive research focused on the effect of $CO_2$ either in the pyrolysis step (Borrego et al., 2009; Kwon et al., 2012; Chen et al., 2013; Guizani et al., 2014; Farrow et al., 2015; Liu et al., 2018) or char gasification (Di Blasi, 2009; Van de steene et al., 2011; Guizani et al., 2013; Nilsson et al., 2014; Guizani et al., 2015a; Guizani et al., 2016; Sadhwani et al., 2016) on product yields and properties and process efficiency. However, there is a lack of systematic studies on the effects of $CO_2$ with different feedstocks and the interactions between $CO_2$ and steam on $H_2$/syngas production, syngas properties, tar formation and process efficiency in the entire biomass gasification process.

**Steam to biomass ratio**

A steam to biomass (S/B) ratio refers to the ratio of mass of steam per mass of feedstock. The S/B ratio affects $H_2$ content, syngas properties and tar formation as well as the process efficiency (Kuo and Wu, 2015; Tursun et al., 2016). Increasing the S/B ratio is expected to produce high $H_2$ and $CO_2$ content with a small amount of $CH_4$, CO and tar formation in the gas stream as a result of the water gas (Equation 2.11), steam reforming (Equations 2.15 and 2.16)

and water gas shift (Equation 2.19) reactions, which are promoted by steam (Watson et al., 2018). Figure 2.10 shows the typical effect of S/B ratio (0-4.5) on the syngas composition from steam gasification of biowaste feedstocks such as pine sawdust (Luo et al., 2009; Tursun et al., 2016), waste wood (Wu et al., 2006b), legume straw and pine sawdust (Wei et al., 2007), dealcoholized marc of grape (Hernández et al., 2012), rice husk (Ge et al., 2016), sewage sludge (Gai et al., 2016) and multiple solid waste (MSW) (Luo et al., 2012).

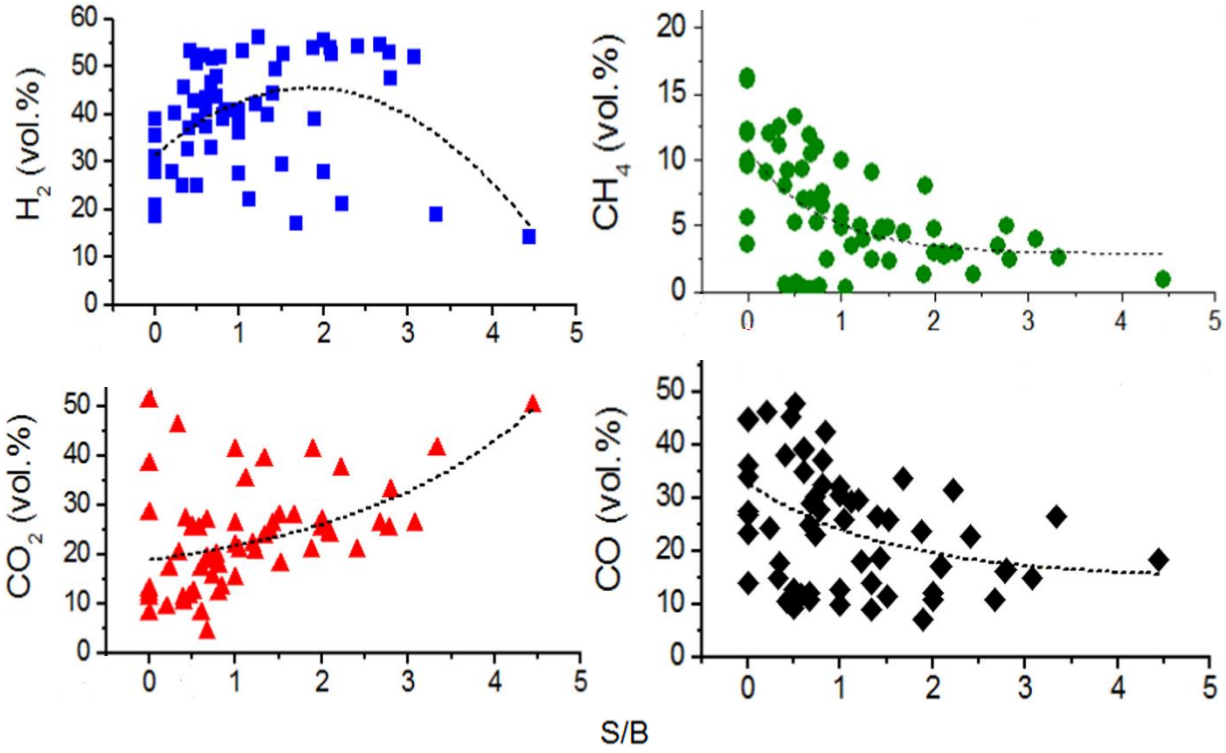


Figure 2.10: Effect of steam to biomass (S/B) ratio on the gas composition from steam gasification of lignocellulosic materials (Watson et al., 2018).

The $H_2$ content maximized (45 mol%) at the S/B ratio of 2.0 and decreased with a further increase in S/B ratio (from 45 mol% at S/B ratio of 2.0 to 40 mol% and 25 mol% at an S/B ratio of 3.0 and 4.0 respectively) as shown in Figure 2.10. This is due to the excessive amount of steam causing a reduction of gasification temperature, which affects the chemical reactions leading to $H_2$ production (i.e. the water gas reaction, the water gas shift reaction and the steam and $CO_2$ reforming reactions) (Yan et al., 2010; Ran and Li, 2012; Zhai et al., 2017). Moreover, increasing the S/B ratio decreases the volatile vapour residence time in the hot zone for reacting with char, steam or other gases, resulting in an incomplete gasification. It was suggested (Gil et al., 1997; Zhou et al., 2009; Hernández et al., 2010) that a sufficient vapour residence time for biomass gasification was between 3 seconds and 4 seconds. Figure 2.10 shows the $CO_2$ content in the gas stream from lignocellulosic steam gasification increased when increasing the

S/B ratio, i.e. from 20 mol% at no steam injection to 50 mol% at a S/B ratio of 4.5, whereas a reduction of $CH_4$ (from 12 mol% to 3 mol%) and CO (from 35 mol% to 20 mol%) was observed when increasing the S/B ratio from 0 to 4.5. It was reported (Yan et al., 2010) that the heating value of producer gas decreased from 9.2 MJ/$Nm^3$ to 8.1 MJ/$Nm^3$ when the S/B ratio was increased from 0.04 to 0.4 for steam gasification of pine sawdust, due to a reduction in CO (from 22.5 mol% to 12.8 mol%) and $CH_4$ (from 5.2 mol% to 2.4 mol%). The gas yield increased from 0.7 $Nm^3$/kg to 2.2 $Nm^3$/kg at the expense of tar and solid fractions. The carbon conversion was 98.8% with around 1.2 wt% carbon remaining in the residues (ash) at a S/B ratio of 0.3. A similar observation was also found in multiple solid waste (MSW) steam gasification, increasing the S/B ratio from 0.5 to 2.4, increased the gas yield from 90.6 wt% to 99.7 wt% at the expense of tar (from 1.16 wt% to 0 wt%) and solid (from 14.5 wt% to 9.5 wt%) fractions, therefore increasing carbon conversion (from 50.4% to 84.9%) (Luo et al., 2012). However, the S/B ratio is not an accurate indicator to optimize $H_2$/syngas production and process efficiency in the steam biomass gasification because the performance of the gasification process is strongly dependent upon the nature of the feedstock, i.e. carbon content, which is the main component in the biomass feedstock (40-55 wt%). Therefore, it would be better if the optimum steam required for the gasification is determined as a ratio of steam and carbon content in biomass feedstock (S/C) as this can be adjusted according to the initial carbon content in any type of biomass feedstock to achieve the best carbon conversion and thermal efficiency of the process.

**Temperature**

The temperature is a crucial parameter in biomass gasification because it influences the thermodynamic behaviour of reactions occurring in the gasification process particularly in the reduction zone, where both endothermic and exothermic reactions occur simultaneously (Emami Taba et al., 2012; Alipour Moghadam Esfahani et al., 2017). It was reported (Nipattummakul et al., 2010) that increasing the gasification temperature of sewage sludge from 700 $^oC$ to 1000 $^oC$, increased the $H_2$ (from 48.2 mol% to 57.7 mol%) and the CO (from 10.0 mol% to 19.8 mol%) content in the gas stream, while the $CH_4$ and $CO_2$ concentration decreased. This is because the endothermic reactions, i.e. the Boudouard reaction (Equation 2.9), water gas reaction (Equation 2.10), steam and dry reforming reactions (Equations 2.15-2.18) in the reduction zone accelerate at high temperatures (i.e. above 700 $^oC$) to form $H_2$ and CO (Kalinci et al., 2009; Farzad et al., 2016). A similar behaviour was also reported on steam gasification of architectural salvage (Wu et al., 2006b), multiple solid waste (MSW) (Luo et al., 2012), rice husk (Loha et al., 2011), waste wood (Mayerhofer et al., 2012), almond shells (Rapagnà et al.,

2000) and cotton stalk chip (Yang et al., 2019) in the temperature range 650-1000 $^{o}$C. Gasification temperature affects not only the syngas composition but also the carbon and tar conversion (Devi et al., 2003). The carbon conversion efficiency of pine sawdust steam gasification significantly increased (from 61.5% up to 99.9%), whereas the tar content in the gas stream decreased from 3.9 wt% to 0.4 wt% when increasing the gasification temperature from 600 $^{o}$C to 900 $^{o}$C (Luo et al., 2009). Increasing the gasification temperature of legume and pine sawdust in steam gasification from 750 $^{o}$C to 850 $^{o}$C, altered the gas yield from 71.2 wt% to 98.7 wt% at the expense of char (from 7.9 wt% to 1.2 wt%) and tar (from 5.3 wt% to 1.2 wt%) fractions (Wei et al., 2007), which agreed very well with other findings on steam gasification of different biomass feedstocks such as pine sawdust (Luo et al., 2009; Yan et al., 2010; Tursun et al., 2016), wood pellets (Mayerhofer et al., 2012), almond shells (Rapagnà et al., 2000) and multiple solid waste (MSW) (Guan et al., 2009; He et al., 2009).

## 2.6 Tar formation, properties and removal

### 2.6.1 Tar

Tar is a complex mixture of high molecular weight compounds (Table 2.7) which condense into sticky substances when the gas is cooled down below 60 $^{o}$C (Devi et al., 2003) causing operational difficulties for the downstream process (corrosion, clogging and fouling of installations) (Milne et al., 1998; Zhang et al., 2010) as well as it affecting the quality of syngas and the process efficiency (Li and Suzuki, 2009; Ruiz et al., 2013). The process temperature has a significant influence on tar properties (Figure 2.11). This phenomenon can be explained due to an increase in process temperature enhancing the secondary reactions (i.e. Diels-Alder reactions) to convert the oxygenated compounds (primary tar) derived from the decomposition of the cellulose, hemicellulose and lignin content in the biomass feedstock via the pyrolysis step into light aromatic hydrocarbons, phenolics and olefins compounds (secondary tar) in the temperature range of 700-850 $^{o}$C (Devi et al., 2005), which then subsequently form tertiary tar (polycyclic aromatic hydrocarbons; PAH) with a further increase in gasification temperature (above 900 $^{o}$C) (Wolfesberger-Schwabl et al., 2012; Guan et al., 2016). It was reported (Basu, 2010a) that the order of tar formation in biomass gasification as a function of the type of gasifier was entrained flow (~ 0.4 g/Nm$^3$) < downdraft (~ 1 g/Nm$^3$) < fluidized bed (~ 10 g/Nm$^3$) < updraft (~ 50 g/Nm$^3$). Nonetheless, the tar content in the syngas derived from biomass gasification is much higher than the contaminant limits for a various syngas applications, i.e. heat and electricity generation using IC engines/gas turbines (< 0.1 g/Nm$^3$) and chemical and

liquid fuel synthesis via Fischer-Tropsch (< 0.001 g/Nm$^3$) (Sikarwar et al., 2016). Therefore, the removal of tar is considered to be the key challenge in the biomass gasification process.

Table 2.7: Classification of tar compounds (Li and Suzuki, 2009; Guan et al., 2016).

| Class name | Property | Representative compounds | Concentration (wt%) |
|---|---|---|---|
| GC-undetectable | Very heavy tar, can not be detected by GC-FID or GC-MS | Determined by subtracting the gas chromatography-detectable tar fraction from the total gravimetric tar | 2 |
| Heterocyclic aromatics | Tar containing hetero atoms and highly water soluble compounds | Pyridine, Phenol, cresols, Quinoline, Isoquinoline and Dibenzophenol | 17 |
| Light aromatic | Usually light hydrocarbons with single ring; do not pose a problem regarding condensability and solubility | Toluene, Ethylbenzene, Xylenes and Styrene | 46 |
| Light PAH compounds | 2 and 3 rings compounds; condense at low temperature even at very low concentration | Naphthalene, Methylnaphthalene, Biphenyl, Acenaphthalene, Phenanthrene and Anthracene | 34 |
| Heavy PAH compounds | Larger than 3 rings, these components condense at high temperatures at low concentrations | Fluoranthene, Pyrene, Chrysene, Perylene and Coronene | 1 |

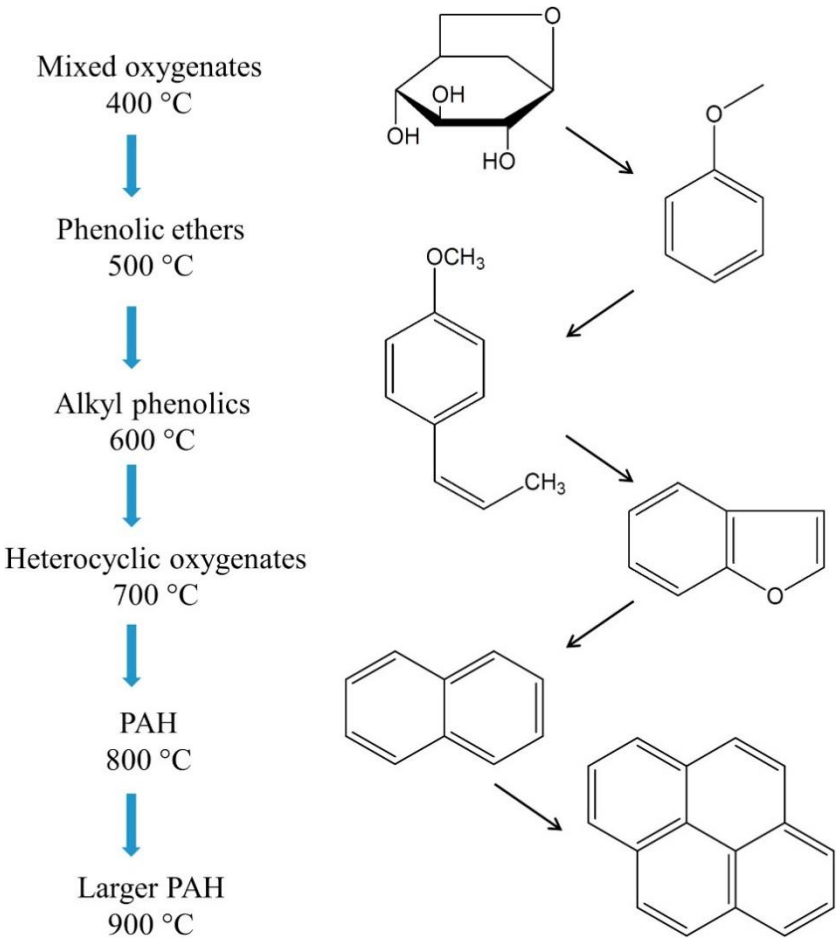


Figure 2.11: Tar formation scheme as a function of temperature (Elliott, 1988).

### 2.6.2 Tar removal techniques

Tar formation in biomass gasification can be minimized via primary or second methods (Zhao et al., 2010; Arena, 2012). The primary methods (Figure 2.12a) are employed in the gasifier itself such as (i) optimization of operating conditions (temperature, gasifying agent and the ratio of gasifying agent to feedstock), (ii) adding catalysts and/or additives in the bed and (iii) modification of the gasifier (Pereira et al., 2012). However, the secondary methods (Figure 2.12b) require using separate equipment in a downstream process such as cyclones, barrier filters, rotating particle separators, electrostatic precipitators, absorbers, wet scrubbers, venturi scrubbers and catalyst bed cracking systems (Hasler and Nussbaumer, 1999; Pereira et al., 2012). The secondary methods are more effective in removal of tar and particulates from the syngas (> 90%) compared to 60-70% in the primary methods, however they are not always economically viable, since downstream gas cleaning equipment adds greatly to the capital investment of the overall processes (Devi et al., 2003; Wang et al., 2008; Anis and Zainal, 2011).

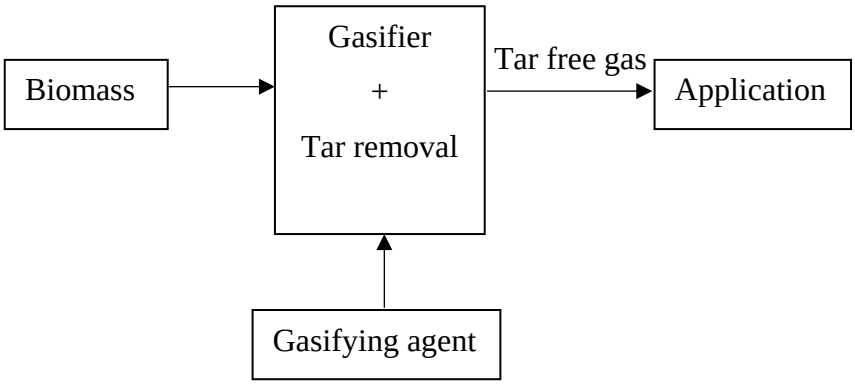


(a)

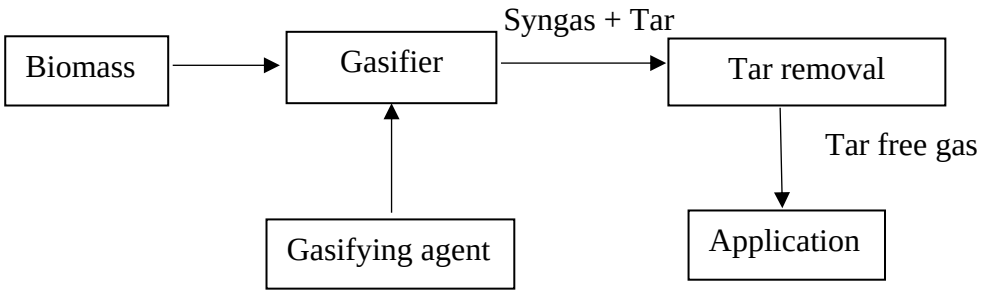


(b)

Figure 2.12: Tar reduction techniques (a) primary methods and (b) secondary methods (Devi et al., 2003).

Recently, catalytic reforming has received considerable attention and is considered as an effective and efficient method for tar removal, avoiding costly downstream processing (Bridgwater, 1994; Abu El-Rub et al., 2004). Common catalysts are dolomite, olivine, clay minerals, alkali metal-based and Ni-based catalysts (Devi et al., 2003; Anis and Zainal, 2011). However, a Ni-based catalysts has proved to be the most successful catalyst for tar removal (> 95%) in biomass gasification compared to only 60-85% reduction for conventional catalysts due to high hydrocarbon reforming activity (Baker et al., 1987; Sutton et al., 2001; Ni et al., 2006). Moreover, the Ni-based catalyst also promotes the water gas shift reaction (Equation 2.19) (Torres et al., 2007; Chan and Tanksale, 2014; Ashok et al., 2018). The activity of the Ni-based catalyst ($Ni/Al_2O_3$) was compared to that of other conventional catalysts (i.e. sand, olivine and stabilized alumina) in the gasification of maple wood chips (Ammendola et al., 2010). It was found that the $Ni/Al_2O_3$ catalyst exhibited better tar removal (78%) compared to 35% for sand, 56% for olivine and 61% for stabilized alumina. A similar observation has been made in other studies (Simell and Bredenberg, 1990) on the tar conversion activity of different catalysts; the order was $Ni/Al_2O_3$ > dolomite > activated $Al_2O_3$ > $SiO_2/Al_2O_3$ > SiC. A $Ni/Al_2O_3$ catalyst

proved to be a promising catalyst for removal of tar; as it can remove up to 99.8% of the tar in the syngas (from 9.5 g/$Nm^3$ to 0.02 g/$Nm^3$) from wood chip gasification (Pfeifer and Hofbauer, 2008). It was reported (Wu et al., 2006b) that using a $Ni/Al_2O_3$ catalyst in waste wood gasification increased the $H_2$ content up to 52 mol% at 750 $^oC$ (similar to non-catalytic gasification at 950 $^oC$) with a tar content of 8.3 g/$Nm^3$ (compared to 27.3 g/$Nm^3$ in non-catalytic condition). The tar concentration from gasification of cedar wood was significantly decreased from 23.7 wt% in non-catalytic condition to 2.1 wt% in the presence of $Ni/Al_2O_3$ (Kimura et al., 2006). The $H_2$/CO ratio increased from 0.4 (non-catalytic condition) to around 2.1-2.5 for Ni-based catalysts. A Ni/HZSM-5 was also proved to be effective in eliminating tar (99% destruction efficiency) and produced a slightly higher $H_2$ concentration in gasification of obsolete seed corn than $Ni/Al_2O_3$ catalyst at identical operating conditions (Zhang et al., 2004), these results are similar to those reported elsewhere (Velegol et al., 1997; Dou et al., 2003; Corma et al., 2007; Buchireddy et al., 2010). However, the main disadvantage of the Ni-based catalyst is rapid catalyst deactivation caused by coke deposition and crystallite agglomeration during the gasification process (Srinakruang et al., 2006; Sikarwar et al., 2016). Therefore, the development of different types of catalyst that exhibit high catalytic activity for tar removal, high thermal stability, suppression of coke deposition and low costs is required.

Around 70 million tonnes/year of red mud, a waste product of bauxite processing, is generated globally (Vangelatos et al., 2009). Red mud management is one of the main challenges in the aluminium industry, as disposal cost are around $3 per tonnes of alumina produced (Li, 2001; Vangelatos et al., 2009). The main components of red mud are $Fe_2O_3$, $Al_2O_3$, $SiO_2$, $TiO_2$ and a range of alkali and alkaline earth metal oxides, such as CaO and $Na_2O$ (Gräfe et al., 2011; Liu and Zhang, 2011; Evans, 2016) and thus red mud could be potentially used as an alternative metal oxide catalyst/support material. A number of studies were carried using red mud as a catalyst for various applications such as hydrocarbon and volatile organic compounds (VOC) cracking (Paredes et al., 2004; Balakrishnan et al., 2009; Rosmaninho et al., 2012), hydrodechlorination (Ordóñez et al., 2001; Halász et al., 2005), coal liquefaction (Yokoyama et al., 1989; Klopries et al., 1990), carbon synthesis (Dunens et al., 2010; Oliveira et al., 2011; Gu et al., 2016) and pyrolysis oil upgrading (Karimi et al., 2012; Kastner et al., 2015). However, the use of red mud for catalytic cracking of tar in biomass gasification has not yet been assessed. If red mud can be successfully used as a catalyst for gasification of biomass, it would contribute significantly to the environmental footprint and sustainability aspects of the process.

## 2.7 Modelling of gasifier

Modification of a gasifier is one of the approaches to minimize tar formation (as described in section 2.6.2) as well as improving and developing the biomass gasification process in terms of process efficiency and syngas quality (Zainal et al., 2002). Computational Fluid Dynamics (CFD) modelling is considered as an efficient design tool to predict the behaviour of biomass gasification to optimize operating conditions of an existing gasifier or design and optimize a new gasifier. It can be used to predict scale-up behaviour therefore reduce engineering cost (Gerun et al., 2008; Meenaroch et al., 2015). To design and optimize a gasifier either an Eulerian-Lagrange or Eulerian-Eulerian approaches could be used to model gas and solid phases depending on the purpose of the study, together with the conservation equations (momentum, mass and energy) and the standard k-ε turbulence model for the gas phase. In the Eulerian-Lagrange approach each particle inside the system is individually tracked, so it is suitable to study particle size distributions, interactions of particles, mass and heat transfer between particles and transient forces acting at the particle level (Gerber et al., 2010; Fan et al., 2016). Therefore, this approach is suited for the modelling of fluidized bed gasifiers due to the interactions between particles and the bed materials across the gasifier, hence tracking of those particles is necessary to give a better understanding of the system. However, the main disadvantage of the Eulerian-Lagrange approach is it is very computation time intensive when tracking a large number of particle collisions coupled with chemical reactions (Wang et al., 2009). In contrast, the Eulerian-Eulerian approach, assume both solid and gas phases are treated as a second continuous phase (Feng et al., 2012). This method is used to predict the macroscopic characteristics of a system with relatively low computational time and it has been used for modelling of fixed-bed gasifiers for many years (Ku et al., 2015; Lu et al., 2016). However, the Eulerian-Eulerian approach has limitations, as it does not recognize the characteristics of particles across the system (Bhutani et al., 2016).

Most CFD studies have focused on the effect of operating conditions (i.e. biomass feedstock, air inlet velocity, gasifying agent, temperature, air/steam ratio and gasifying agent to biomass ratios) on the temperature profile, syngas composition and flow patterns of an existing design of a downdraft gasifier (Rogel and Aguillón, 2006; Gerun et al., 2008; Siva Kumar et al., 2008; Wu et al., 2013; Zhao et al., 2013; Dejtrakulwong and Patumsawad, 2014; Meenaroch et al., 2015; Chaurasia, 2016) using the Eulerian-Eulerian approach. A fixed-bed throat downdraft gasifier is preferable in those studies because it is known to produce high quality syngas, with low tar content (0.015–3 g/Nm$^3$) in the gas stream compared to that in a updraft gasifier (30-150 g/Nm$^3$) (Basu, 2010a) as well as its simplicity to construct and relatively low investment cost compared to fluidized bed and entrained flow gasifiers (Bridgwater, 1995; Puig-Arnavat et

al., 2010). The effect of air flow rate on the temperature profile along the axis of the gasifier and the syngas composition at the gasifier outlet of a 10 kg/hr throat downdraft gasifier was investigated using the ANSYS FLUENT CFD modelling code (Meenaroch et al., 2015). The influence of air inlet velocity and air to fuel ratio on the flow pattern, temperature profile, hot vapour residence time and tar conversion in throat downdraft gasifier was also found in other studies (Gerun et al., 2008; Zhao et al., 2013). Moreover, the effects of the initial air inlet temperature, air flow rate and mole fraction of $O_2$ in the primary air on product properties ($H_2$, CO, $CO_2$, $CH_4$ and tar) in a throat downdraft gasifier has been studied using the COMSOL Multiphysics CFD software (Chaurasia, 2016). The operating parameters that affect the throat downdraft gasifier performance, i.e. particle size of biomass feedstock, moisture content and air inlet temperature was optimized in terms of process efficiency and syngas/$H_2$ production (Siva Kumar et al., 2008). CFD has also been used to simulate the effect of moisture content in the biomass feedstock and air to fuel ratio (Dejtrakulwong and Patumsawad, 2014), air inlet temperature, steam to air ratio (Wu et al., 2013) and biomass feedstock composition (Rogel and Aguillón, 2006) on the gasification temperature profile, tar formation, syngas properties and process efficiency in throat downdraft gasifier. However, only a few workers have been applied CFD model for studying interactions between various design aspects of a gasifier and operating conditions to propose an optimized configuration of a throat downdraft gasifier for high quality $H_2$/syngas production. For example, ANSYS FLUENT with the standard k-ε model was applied to investigate the effect of the number and angle of air inlet nozzles on the performance of a throat downdraft gasifier, its temperature distribution and the properties of the product gas (Zhao et al., 2013; Dzulfansyah et al., 2014; Ravi Kumar et al., 2016). The influence of throat angle and nozzle inclination on the performance of a throat downdraft gasifier was also reported (Jayah et al., 2003; Siva Kumar et al., 2008; Dejtrakulwong and Patumsawad, 2014). However, the effect of the ratio of throat to gasifier body diameter and the position of the air inlet nozzles above the throat on performance of a throat downdraft gasifier has not been examined elsewhere in literature.

### 2.8 Summary

Over last decades, gasification of lignocellulosic materials has been intensively studied focusing on the design and the optimum operating conditions to obtain high quality syngas. However, gasification of biomass still encounters a number of challenges such as low $H_2$/CO ratios (less than 1), low $H_2$ content (40-60 mol%), low process efficiency (70-80%) and high tar formation and $CO_2$ in the gas stream. Steam is a promising gasification agent that produces a high content of $H_2$ and high calorific value of the produced gas compared with air, oxygen

and oxygen-enriched air. However, an excessive amount of steam could cause a negative effect on $H_2$ content, syngas properties and tar formation as well as the process efficiency. The use of $CO_2$ as an oxidizing agent in biomass gasification could help to improve the gasification process in terms of conversion, energy efficiency and tar removal. Although, the effect of $CO_2$ on product yield and properties either in the pyrolysis step or char gasification has been examined, there is a lack of comprehensive studies on the interactions between $CO_2$ and steam and how these would affect $H_2$ production, syngas properties, tar formation and the process efficiency of the entire biomass gasification process. Tar formation in biomass gasification can be minimized by in-situ adding catalysts. Ni-based catalysts such as $Ni/Al_2O_3$ and Ni/HZSM-5 are commonly used for tar removal in biomass gasification due to their high hydrocarbon reforming activity as well as enhancing the formation of $H_2$. However, the main disadvantage of the Ni-based catalyst is a rapid catalyst deactivation caused by coke deposition and crystallite agglomeration during the gasification process. Therefore, developing different types of catalysts that exhibit high catalytic activity for tar removal, high thermal stability, suppression of coke deposition and low cost are required. Red mud a waste of bauxite processing has been used as a catalyst for various applications such as hydrocarbon and volatile organic compound (VOC) cracking, coal liquefaction and pyrolysis oil upgrading with promising results. However, the use of red mud for catalytic cracking of tar in biomass gasification has not yet been studied. Computational Fluid Dynamics (CFD) modelling has been widely used to predict the behaviour of biomass gasification process for scale-up and to optimize operating conditions of an existing gasifier. Little research has focused on using CFD for designing and optimizing a new configuration of biomass gasifier that can be used for $H_2$/syngas production without major downstream processing to remove impurities (tar in particular).

# Chapter 3 Materials and Methods

This chapter describes the characterisation of all the materials, i.e. waste wood and catalysts used in this research. The detailed description of experimental set-ups and operating conditions: conventional pyrolysis ($N_2$ environment), $CO_2$ pyrolysis, $N_2$/steam gasification, $CO_2$/steam gasification and catalytic gasification are described below. The technical specifications of the equipment used for product analysis: solid residues, liquid fraction and gas are mentioned in this chapter.

## 3.1 Materials

Waste wood collected at Sustainable Campus Newcastle University consisted of branch cedar, beech, birch, ash, willow, pine and olive. The waste wood was ground and sieved to 850 µm using Endecotts laboratory test sieves (BS 410/1986) (Figure 3.1a) for characterisation of the waste wood, i.e. proximate and ultimate analysis, energy content and inorganic compound identification. Samples were also saw cut into various size of 0.5, 1 or 2 $cm^3$ cube for experimental pyrolysis and gasification tests (Figure 3.1b) to study the effect of particle size on thermochemical processes.

(a)

(b)

Figure 3.1: Examples of waste wood samples used for (a) characterisation and (b) pyrolysis and gasification experiments.

### 3.1.1 Characterisation

#### Proximate analysis

The proximate analysis of the waste wood was carried out based on British Standard (BS ISO 11722:2013), and includes measurement of the moisture content, volatile matter content, ash content and fixed carbon as a percentage of the original weight of the fuel (1.0 ± 0.1 g). Details of the analysis can be found in Appendix A.1. The analysis was repeated three times to test reproducibility and scatter in the data. As shown in Table 3.1, the waste wood had a very high volatile matter (84.1 wt%) and low ash content (< 1 wt%) compared to coal (20-35 wt% volatile and 10-20 wt% ash). The high volatile matter of lignocellulosic material poses a number of challenges in the gasification process compared to coal gasification, i.e. if the rapid released of volatiles and if the gasifying agent is not well-mixed and/or the temperature of the gasifier (the oxidation zone in particular) is not high enough for the cracking of volatiles, this leads to a considerable amount of large molecular weight species (known as tar), which are difficult to breakdown in the later process stages and end up in the gas stream (Li and Suzuki, 2009; Arena, 2012; Cheng, 2017), causing operational difficulties for the downstream processes (i.e. corrosion, clogging and fouling of installations) (Milne et al., 1998; Balat et al., 2009b).

Table 3.1: Proximate and ultimate analysis of waste wood.

| Proximate analysis (wt%, dry basis) | Values |
|---|---|
| Volatile matter | 84.1 ± 1.4 |
| Fixed carbon | 15.6 ± 2.1 |
| Ash content | 0.3 ± 1.1 |
| Ultimate analysis (wt%, dry basis and ash free) | Values |
| C | 41.8 ± 0.3 |
| H | 6.4 ± 0.3 |
| O* | 51.5 ± 0.5 |
| N | 0.3 ± 0.3 |
| HHV (MJ/kg) | 17.7 ± 2.4 |
| Empirical formula of waste wood | $C_6H_{11}O_{5.5}N_{0.04}$ |

*By difference

**Ultimate analysis**

The ultimate analysis is used for determination of the elemental composition (C, H, N and O) of the fuel. The elemental analysis was carried out using a Carlo Erba 1108 elemental analyser controlled with CE Eager 200. The samples weighed of 1.0 ± 0.1 mg were subjected to complete and instantaneous oxidation (flash combustion) at 1020 $^{o}$C, which converts all organic substances into combustion products ($H_2O$, $CO_2$ and $NO_x$). The products then passed over elemental copper (Porapak (PQS) column) at 860 $^{o}$C to remove excess oxygen and nitrogen oxide to their elemental form, i.e. $CO_2$, $N_2$ and $H_2$. The elemental compositions were quantified by a thermal conductivity detector (TCD). The experiment was repeated three times. The H/C and O/C ratios are simple parameters to characterise hydrocarbons fuels, in which the O/C ratio of biomass (0.4-0.8) was around 2-4 times greater than that of standard coal (0.2), since the biomass consists mainly of oxygen (51 wt%) (Table 3.1) compared to around 7-10 wt% in coal, resulting in a low heating value of fuels. From the ultimate analysis shown in Table 3.1 the empirical formula for waste wood is $C_6H_{11}O_{5.5}N_{0.04}$.

**Energy content**

High heating value (HHV) was determined by using a CAL2K ECO Bomb calorimeter. Each sample was weighed to approximately 1.0 ± 0.1 g and placed into a stainless steel crucible. The crucible was introduced into the vessel and placed into direct contact with a cotton wire, attached to a firing wire and two electrodes for ignition. The sample was ignited and combusted in the pressurised vessel (filled with pure oxygen, at 3MPa). The procedure was repeated three times for error analysis. The HHV of the waste wood in this study was around 17.7 MJ/kg (Table 3.1), which agreed well with the HHV of typical woody biomass (18-25 MJ/kg) (Jenkins et al., 1998; Begum et al., 2013). However, the HHV of waste wood was around 50% of that of coal (30 MJ/kg), this is due to the high oxygen and moisture content in the sample compare to that in coal.

**Inorganic compounds**

Acid digestion of waste wood was carried out in a microwave acid digester according to the British Standard (BS EN ISO 16967:2015) with some modification. Details of the analysis can be found in Appendix A.2. The acid solutions were analysed using inductively coupled plasma mass spectrometry (ICP-MS); (Thermo Scientific X-series2) to determine inorganic compounds in the waste wood. Inductively coupled plasma (RF plasma) was used to produce ions (ionization) for the elements present in the fuel and then the concentration of trace elements

was analysed by a quadrupole mass spectrometer (Elan 6000). The experiment was repeated three times. The waste wood consists mainly of (ppb): Ca 9039, K 2975, Mg 1226, P 244, B 195, Fe 182, Mn 85 and Al 83 (Table 3.2). The presence of inert species (i.e. K, Ca, Si, Mg and Na) in the fuel could act as a catalyst in the cracking/reforming of tar (Anis and Zainal, 2011; Paethanom and Yoshikawa, 2012; Liu et al., 2016; Shen and Fu, 2018). However, the inorganic species are transformed in the gasification condition into more stable compounds, i.e. NaO, $Al_2O_3$, $P_2O_5$, $K_2O$, $K_2CO_3$, KCl, $SiO_2$, $Fe_2O_3$, $CaCO_3$, CaO and MgO as crystalline phases in the ash (Vassilev et al., 2013; Benedetti et al., 2018), causing fouling, erosion and corrosion of installations as well as slagging and agglomeration in the fuel bed (Wei et al., 2005; Sonwane et al., 2006).

Table 3.2: Inorganic compounds in waste wood.

| Inorganic elements | Concentration (ppb) |
|---|---|
| B | 195.2 ± 9.0 |
| Mg | 1226.0 ± 10.1 |
| Al | 83.7 ± 2.2 |
| P | 244.7 ± 15.0 |
| K | 2975.1 ± 73.1 |
| Ca | 9039.2 ± 468.3 |
| Ti | 5.6 ± 0.4 |
| Mn | 85.2 ± 6.1 |
| Fe | 182.4 ± 11.7 |
| Cu | 25.9 ± 2.2 |
| Zn | 48.2 ± 0.1 |
| Sr | 29.8 ± 1.6 |
| Ba | 50.8 ± 2.5 |
| Pb | 21.8 ± 0.1 |

**Lignocellulose composition**

The lignocellulosic composition of the fuel (cellulose, hemicellulose and lignin) was determined using the Van Soest Method (AOAC 2002.04:2002) (Van Soest et al., 1991). Details of the analysis can be found in Appendix A.3. The same procedure was repeated three times. The cellulose and lignin content in the biomass feedstock are critical parameters for evaluation of the characteristics of pyrolysis, since the relative amount of cellulose and lignin influence the decomposition rate of the biomass, char formation, liquid composition and the quality of syngas (Gani and Naruse, 2007). Lignocellulosic biomass containing cellulose (25-50 wt%), hemicellulose (15-40 wt%), lignin (10-40 wt%), extractives (0-15 wt%) and a small amount of inorganic mineral matter can be used as feedstock to produce biofuels via biological/chemical, combination (biochemical) or thermochemical approaches (Vassilev et al., 2012; Kan et al., 2016). The lignocellulosic composition of waste wood in this study was cellulose (45.4 wt%), hemicellulose (29.1 wt%), lignin (24.6 wt%) and extractives (0.9 wt%). Therefore, the waste wood has potential as a fuel for thermochemical processes such as pyrolysis and gasification.

**Differential scanning calorimetry**

Differential scanning calorimetry (DSC) was used for determination of the decomposition temperature and thermal behaviour of the lignocellulose composition (cellulose, hemicellulose, lignin and extractives) in waste wood, and was carried out in a TA instrument DSC Q20. Approximately 50.0 ± 0.1 mg of sample were placed into an aluminium crucible (Tzero aluminium pan) and sealed with a pierced lid. Analysis was carried out between 30 $^{o}$C and 500 $^{o}$C at a heating rate of 20 $^{o}$C/min, with a $N_2$ flow rate of 50 ml/min. The experiment was repeated three times. As shown in Figure 3.2, there are three major peaks appearing from the waste wood sample: (i) peak between 90 $^{o}$C and 125 $^{o}$C, caused by moisture evaporation, (ii) peak at a temperature of 290 $^{o}$C representing the decomposition of hemicellulose and (iii) cellulose decomposition at around 360 $^{o}$C. Another peak at a temperature of 225 $^{o}$C could corresponded to the decomposition of extractives such as protein, sucrose, fats, fatty acids, waxes and monoterpenes in the waste wood. This agrees very well with other findings (Hosoya et al., 2007; Yang et al., 2007) showing that decomposition of hemicellulose and cellulose initiates at 220 $^{o}$C and 250 $^{o}$C and completes at around 320 $^{o}$C and 400 $^{o}$C respectively. The lignin decomposition starts at temperature range of 200-400 $^{o}$C and is completed at around 900 $^{o}$C (Gani and Naruse, 2007; Yang et al., 2007; Lv et al., 2010). However, the DSC instrument used

in this study was limited to a maximum operating temperature of 500 ºC, therefore the thermal behaviour of lignin in the waste wood could not be examined.

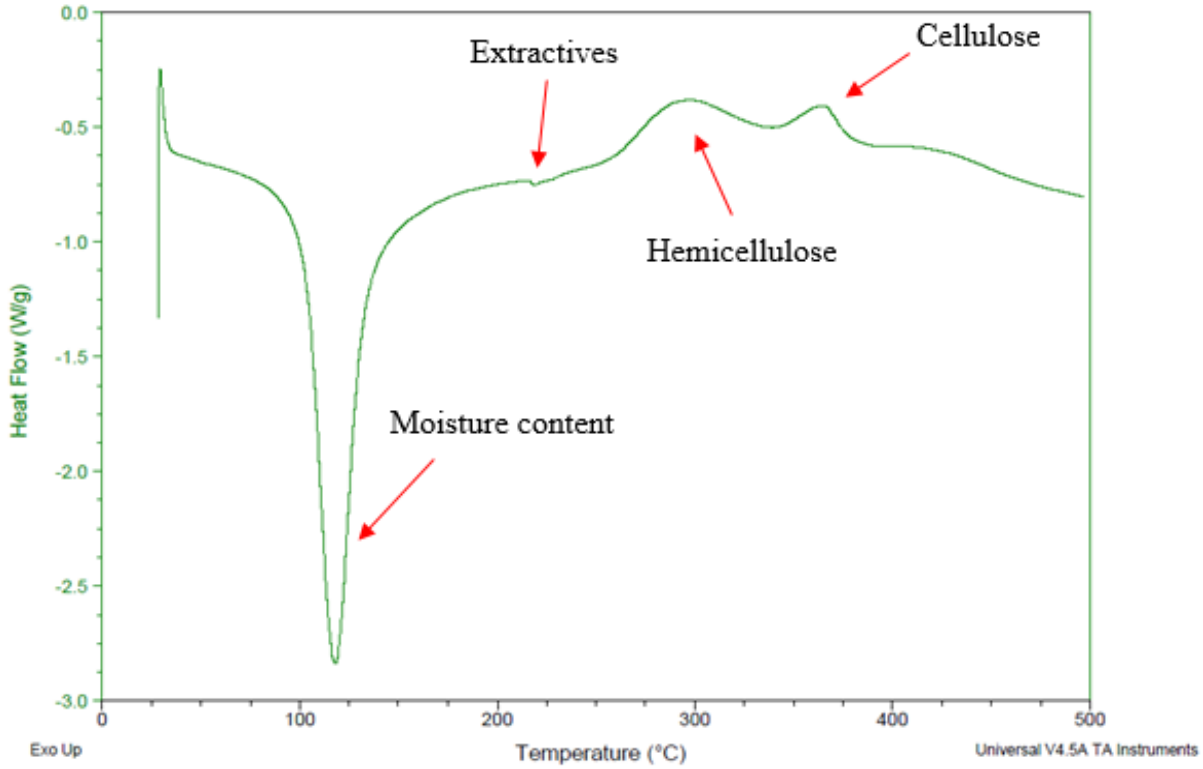


Figure 3.2: DSC curve of waste wood at heating rate of 20 ºC/min and a nitrogen flow of 50 ml/min.

**Thermogravimetric analysis**

Thermogravimetric analysis (TGA) of the waste wood was undertaken using a Perkin Elmer STA 6000 to assess thermal degradation, volatilisation rate, moisture content, volatile matter content and solid residues of fuel by measurement of weight loss as a function of temperature and time under a controlled atmosphere ($N_2$). This procedure was repeated three times for reproducibility. The waste wood samples weighing approximately 15.0 ± 0.1 mg were placed in an aluminium crucible on the balance of the TGA analyser. Prior to the experiments, the system was continuously purged with $N_2$ (20 minutes) to allow the TGA balance to stabilise. The samples were heated from 25 ºC to 900 ºC (based on the temperature range of pyrolysis experiments) at various heating rates of 10, 20, 30 or 40 ºC/min under a $N_2$ atmosphere (30 ml/min) to assess the effect of heating rate on thermal behaviour. The weight loss versus time/temperature was recorded on-line by the STA 6000 software as shown in Figure 3.3. Up to 13% weight loss was observed at temperature below 100 ºC due to the release of moisture content. At temperatures of 220-400 ºC a rapid decreases weight (around 70 wt%) was observed

due to the volatilisation of the hemicellulose and cellulose at the rate: 7 %/min (10 $^{o}$C/min), 13 %/min (20 $^{o}$C/min), 21 %/min (30 $^{o}$C/min) and 25 %/min for 40 $^{o}$C/min. At higher temperature (≥ 400 $^{o}$C), the rate of weight loss was much lower (1-4 %/min) for a further 17% weight loss for all tested heating rate. The results obtained from TGA analysis (Figure 3.3) corresponded well with data obtained from the proximate analysis (Table 3.1). Figure 3.3 shows the decomposition temperature of waste wood was shifted to higher temperatures when increasing the heating rate, i.e. 220 $^{o}$C at 10 $^{o}$C/min to nearly 300 $^{o}$C at 40 $^{o}$C/min, results in reducing the decomposition time of the fuel, i.e. from 68 minutes (10 $^{o}$C/min) to 17 minutes (40 $^{o}$C/min). A fully decomposed waste wood at the final temperature of 900 $^{o}$C was observed at the heating rate of 10-20 $^{o}$C/min (0 wt% solid residues) as it provide sufficient time for fuels to decompose compared to about 8-10 wt% residue remaining at higher heating rate (> 20 $^{o}$C/min) (Figure 3.3).

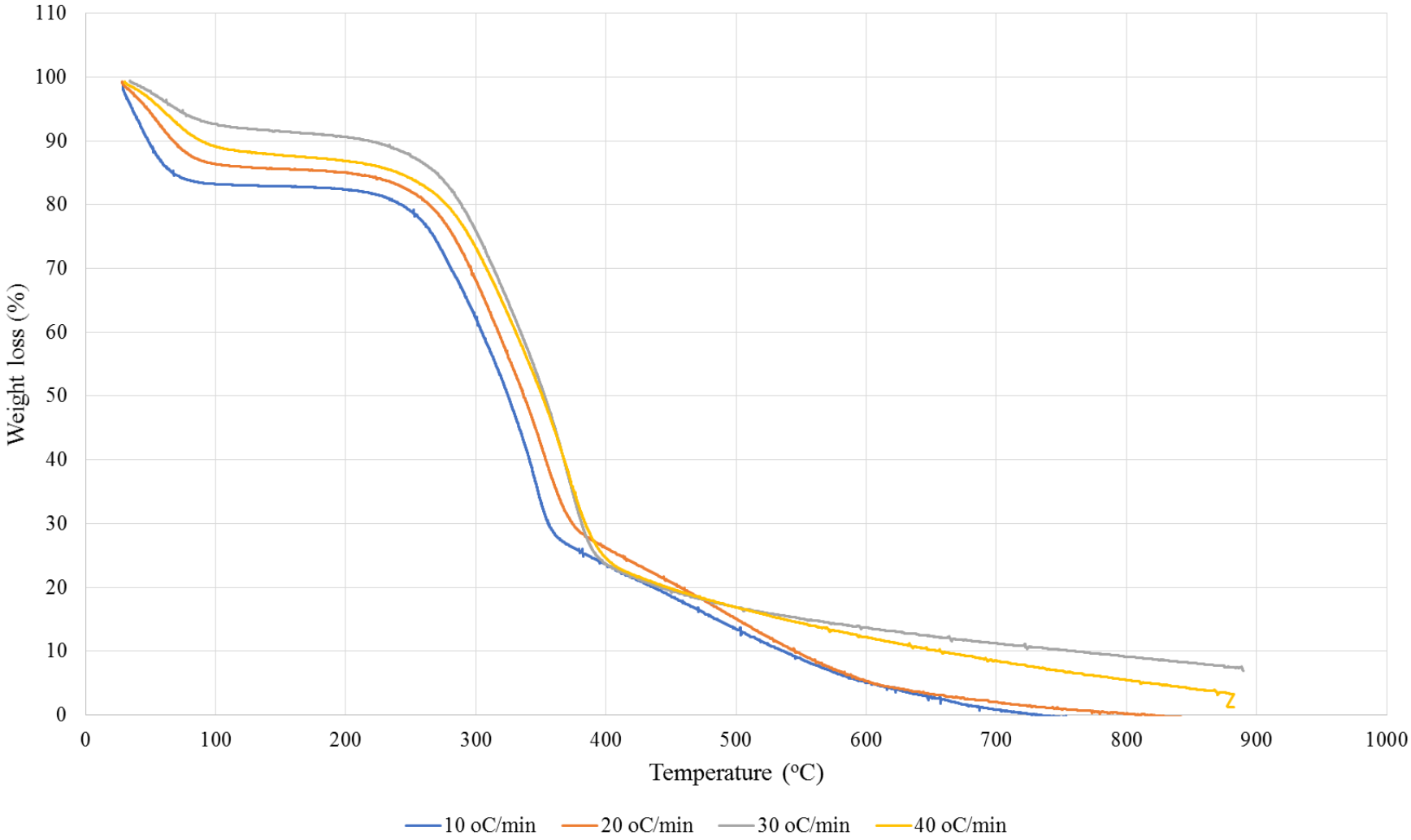


Figure 3.3: Weight loss of waste wood sample from thermogravimetric analysis (TGA) at the heating rate of 10, 20, 30 and 40 °C/min and nitrogen flow rate of 30 ml/min.

### 3.2 Catalysts

#### 3.2.1 Preparation methods

Red mud (RM) was used and compared with a commercial $Al_2O_3$ and zeolite (HZSM-5) catalyst in terms of $H_2$ production, catalytic cracking (of tar in particular) and their reusability in biomass gasification. The RM was selected for this study because: (i) it is a waste product of bauxite processing, (ii) it is a relatively low cost and abundant resource, (iii) it is a rich metal oxide catalyst, (iv) it is resistant to sintering and poisoning and (v) limited research is available on the viability of RM as a catalytic cracking for biomass gasification. The raw red mud (RM) that was collected from a site in Southern India in 2006 was kindly supplied by the Department of Chemistry, University of Glasgow.

Table 3.3: The elemental composition of RM and MRM.

| Elemental composition | wt% (dry basis) | |
|---|---|---|
| | RM | MRM |
| $SiO_2$ | 16.5 ± 2.1 | 19.7 ± 1.0 |
| $Al_2O_3$ | 25.4 ± 1.0 | 30.6 ± 2.1 |
| $Fe_2O_3$ | 38.7 ± 2.2 | 42.9 ± 2.3 |
| $TiO_2$ | 2.6 ± 1.7 | 2.5 ± 1.1 |
| CaO | 3.1 ± 1.1 | 0.7 ± 0.4 |
| MgO | 2.0 ± 1.0 | 1.4 ± 0.6 |
| $Na_2O$ | 8.0 ± 2.4 | 1.1 ± 1.7 |
| $P_2O_5$ | 2.1 ± 0.1 | 0.4 ± 0.1 |
| MnO | 2.0 ± 0.2 | 0.5 ± 0.3 |

Red mud (MRM) was modified based on previous studies (Cao et al., 2014; Fang et al., 2016; Liu et al., 2017). Approximately 25.0 ± 0.1 g of RM sample was mixed with 100 ml deionized water and 150 ml 6 M HCl (Sigma-Aldrich) in a 500 ml beaker. The sample was vigorously stirred at 80-85 $^oC$ for 2 hours. The pH of the mixed solution was adjusted until pH ~8 using 1 M $NH_4OH$ (Sigma-Aldrich). After 1 hour ageing at 70-80 $^oC$, the solution was washed until pH ~7 using deionized water and anhydrous ethanol (99.8% purity, Sigma Aldrich) to (i) maintain

the structure of the colloid, (ii) improve the surface area and pore size of the sample and (iii) remove chloride ions. The solution was filtered and dried in an oven at 110 $^{o}$C for 12 hours and then calcined in air at 600 $^{o}$C for 4 hours for analysis. The elemental composition of RM and MRM was determined from three random ground samples taken from a bulk catalyst sample using ICP-MS (as described previously) and is shown in Table 3.3. The contents of CaO and $Na_2O$ in the MRM were much lower than those in RM, suggesting that most of Ca and Na were removed during catalyst preparation (Cao et al., 2014). However, the content of other components gradually increased. This could be due to several effects: (i) dissolution (HCl) of the main minerals such as bayerite ($Al(OH)_3$), iron oxide hydroxide (FeOOH), cancrinite ($Na_6CaAl_6Si_6(CO_3)O_{24}\cdot 2H_2O$), perovskite ($CaTiO_3$), hydrogarnet ($3CaO\cdot Al_2O_3\cdot SiO_2\cdot 4H_2O$), calcite ($CaCO_3$) and gibbsite ($\gamma$-$Al(OH)_3$), (ii) decomposition during the calcination step and (iii) conversion into amorphous form, i.e. $Fe_2O_3$, $Al_2O_3$, $SiO_2$ and $TiO_2$ during the precipitation process (Table 3.3). A commercial zeolite, HZSM-5 ($SiO_2/Al_2O_3$ of 312) and $Al_2O_3$ nanopowder (< 50 nm) were purchased from Sigma-Aldrich. The 20 wt% Ni on the supporting material: MRM, HZSM-5 and $Al_2O_3$ catalysts was synthesized using an impregnation method (Cao et al., 2014). Approximately 3.0 ± 0.1 g of $Ni(NO_3)_2\cdot 6H_2O$ (99.9% purity, Sigma Aldrich) was mixed with 2.4 ± 0.1 g of MRM, HZSM-5 or $Al_2O_3$ and then dissolved in 15 ml of anhydrous ethanol (99.8% purity, Sigma Aldrich) in 40 ml beaker. The mixture was vigorously stirred at 60 $^{o}$C for 1 hour and then dried in an oven at 80 $^{o}$C overnight to evaporate ethanol followed by calcination at 600 $^{o}$C for 4 hours in air. The catalysts precursors were then ground to powder form (< 50 µm) for catalytic gasification experiments. Finally, the catalysts were treated in $H_2$ at 600 $^{o}$C to reduce NiO to Ni overnight, before carrying out the experiments.

### 3.2.2 Characterisation

#### Scanning Electron Microscopy-Energy Dispersive X-ray (SEM-EDX) analysis

The physical morphology, elemental composition and distribution of catalyst was examined from three random regions by Environmental Scanning Electron Microscopy (ESEM) using a Hitachi TM 3030 ESEM equipped with an EDAX SiLi energy dispersive X-ray detector (EDX). The ESEM was operated at a 15 kV accelerating voltage and 500x-3500x magnification, without a conductive coating to examine the samples in their natural state. SEM images of Ni/MRM (Figure 3.4) that were processed using ImageJ software to quantify particle size showed around 90% of the catalyst particles were between 4.2 nm and 13.0 nm with an average particle size of 5.9-7.4 nm. The EDXS mapping using spot technology (Figure 3.4c) showed the main elements in the chemical composition in Ni/MRM are Al (13.3 wt%), Fe (27.4 wt%),

Si (8.7 wt%), O (29.4 wt%) and Ni (19.9 wt%) with a small amount of Cl (0.5 wt%) and Ti (0.8 wt%), which agrees very well with the results obtained from ICP-MS analysis as described previously.

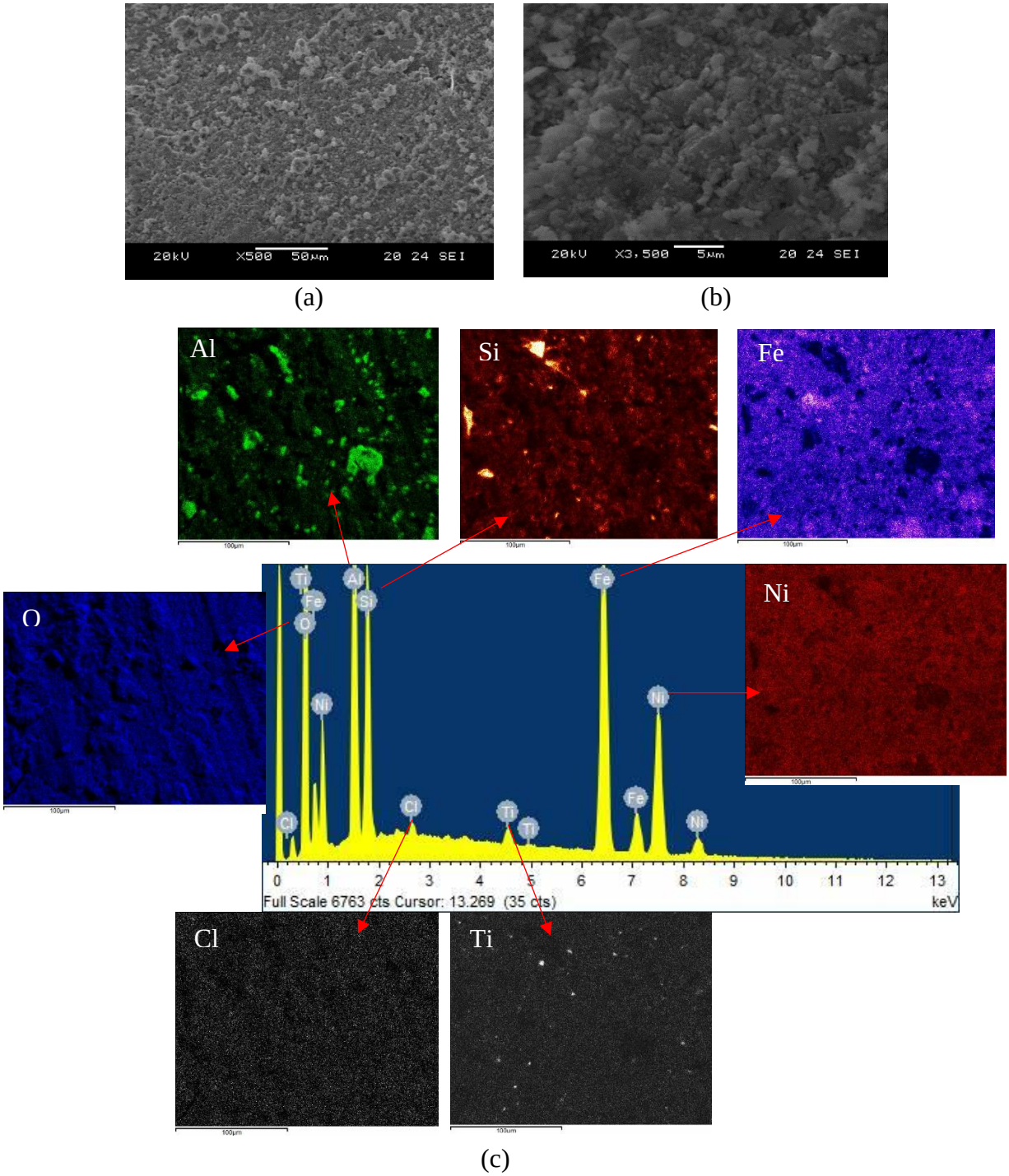


Figure 3.4: SEM images of Ni/MRM catalyst at magnification of (a) 500x and (b) 3500x and (c) EDXS mapping.

The SEM images (Figure 3.5) showed the majority of $Ni/Al_2O_3$ (70%) particles were between 7.1 nm and 12.7 nm in size. About 15% ranged between 12.7 nm and 14.2 nm, 10% between 14.2 nm and 16.6 nm and the remaining 5% was distributed between 16.6 nm and 17.9 nm. Figure 3.5c shows that the $Ni/Al_2O_3$ catalyst comprised of 35.2 wt% O, 44.6 wt% Al and 20.2 wt% Ni. Figures 3.6a and b shows SEM images of the Ni-HZSM-5 catalyst with a fairly uniform particle distribution in the size range between 4.4 nm and 9.7 nm in size (over 90%) and the remaining 10% was distributed between 9.7 nm and 12.0 nm. EDXS mapping results (Figure 3.6c) showed that the chemical composition in Ni-HZSM-5 are O (27.2 wt%), Si (30.0 wt%), Ni (21.6 wt%) and Al (21.2 wt%) corresponding to Si/Al ratio of 4.2. The results obtained from EDXS mapping of Ni/MRM (Figure 3.4c), $Ni/Al_2O_3$ (Figure 3.5c) and Ni/HZSM-5 (Figure 3.6c) catalysts showed all the Ni particles were uniformly distributed on the surface of supporting materials: MRM, $Al_2O_3$ and HZSM-5 catalysts.

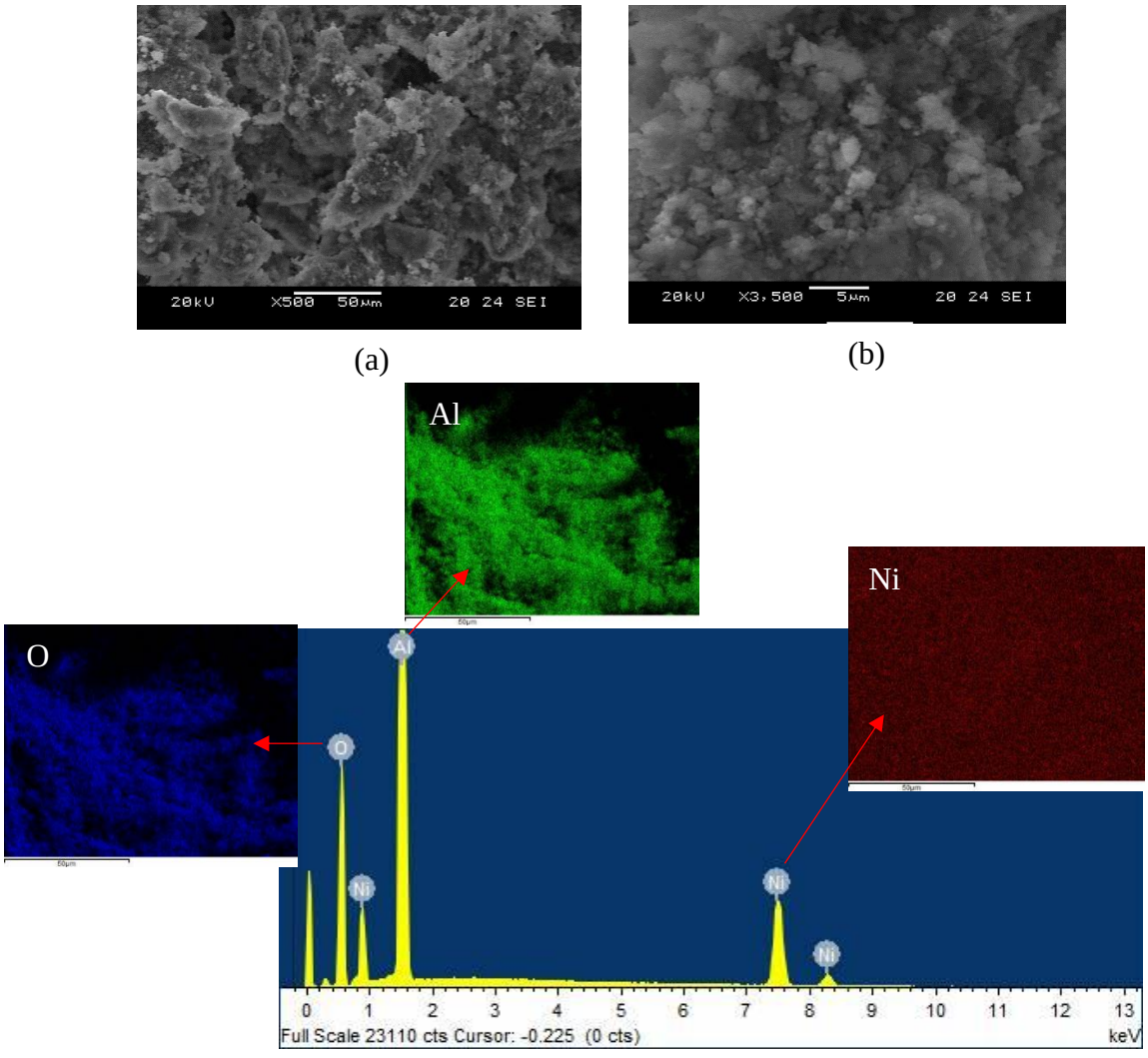


Figure 3.5: SEM images of $Ni/Al_2O_3$ catalyst at magnification of (a) 500x and (b) 3500x and (c) EDXS mapping.

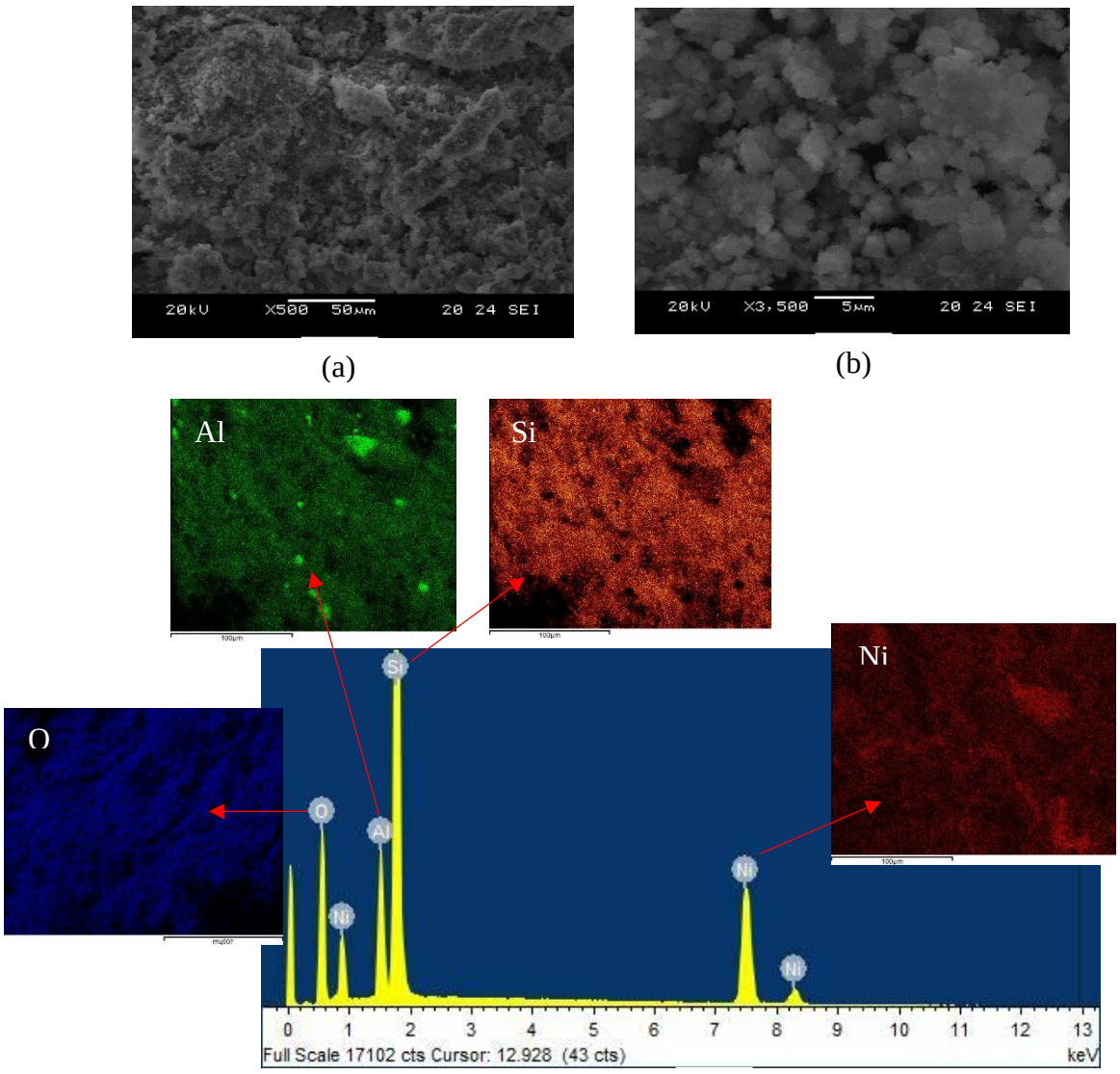


Figure 3.6: SEM images of Ni/HZSM-5 catalyst at magnification of (a) 500x and (b) 3500x and (c) EDXS mapping.

**Surface area and pore characterisation**

Catalyst surface area, total pore volume and pore size distribution were determined from three random ground samples taken from a bulk catalyst sample using the Brunauer Emmett Teller (BET) nitrogen physisorption isotherms conducted at 77 K using a Thermo Scientific Surfer Gas Adsorption Porosimeter. Approximately 100.0 ± 0.1 mg of sample was loaded into a burette and then outgassed at 120 $^{o}$C overnight in high vacuum (10 Torr) to remove any physisorbed materials (moisture in particular) and create a clean catalyst surface. The volume of $N_2$ adsorbed was measured and plotted to construct the catalyst isotherm which was further processed with the Surfer software.

Table 3.4: Properties of fresh and Ni-based catalysts.

| Catalysts | Specific surface area ($m^2/g$) | Total pore volume ($cm^3/g$) | Pore size (nm) |
|---|---|---|---|
| Raw red mud (RM) | 14.5 ± 1.4 | 0.2 | 6.2-18.6 |
| Modified red mud (MRM) | 180.5 ± 8.6 | 0.1 | 3.3-9.9 |
| Ni/MRM | 114.8 ± 5.2 | 0.1 | 1.7-3.1 |
| Raw HZSM-5 | 216.0 ± 10.9 | 0.2 | 4.1-12.4 |
| Ni/HZSM-5 | 170.6 ± 8.2 | 0.2 | 2.9-6.7 |
| Raw $Al_2O_3$ | 192.5 ± 9.6 | 0.1 | 2.0-11.2 |
| Ni/$Al_2O_3$ | 158.3 ± 7.4 | 0.1 | 1.2-8.0 |

As shown in Table 3.4, the specific surface area of RM had significantly increased from 14.5 $m^2/g$ to 180.5 $m^2/g$ after modified due to the catalyst preparation techniques (as described previously). A fresh commercial HZSM-5 and $Al_2O_3$ nanopowder catalysts had a specific surface area of 216 $m^2/g$ and 192.5 $m^2/g$ respectively. The BET results of the Ni-based catalysts (Table 3.4) show a decrease in surface area (around 18-36%), pore volume and size compared to that in the fresh catalysts supports, i.e. from 180.5 $m^2/g$ (MRM) to 114.8 $m^2/g$ in Ni/MRM, this because the Ni particles were distributed on the surface of supporting materials and remove the local microroughness. Ni/HZSM-5 presented the highest high surface area (170.6 $m^2/g$) followed by Ni/$Al_2O_3$ (158.3 $m^2/g$) and Ni/MRM (114.8 $m^2/g$).

**X-ray diffraction (XRD) analysis**

The crystalline phases present in catalysts were analysed by Panalytical X'Pert Pro multipurpose diffractometer (MPD) equipped with an X'Celerator and a secondary monochromator (Cu-Kα radiation), operated at 40 kV, 40 mA and wavelength ($K_{\alpha 1}$) of 0.15 nm. The scanning was performed over a 2θ range of 5°-85° with a step size of 0.03°. The same procedure was repeated three times. Only Ni/MRM was analysed by XRD, since MRM contained a variety of metal oxides (confirmed by the results obtained from ICP-MS) compared to that in a commercial catalyst, i.e. Ni/HZSM-5 and Ni/$Al_2O_3$ only NiO, $Al_2O_3$ and $SiO_2$ were presence in crystalline phases. Ni/MRM XRD spectrum (Figure 3.7) consists mainly of MgO,

$CaCO_3$, $Al_2O_3$, $Fe_2O_3$, CaO and $SiO_2$ with small amount of NiO, corresponding well with data obtained from ICP-MS analysis (Table 3.3) and EDXS mapping (Figure 3.4c).

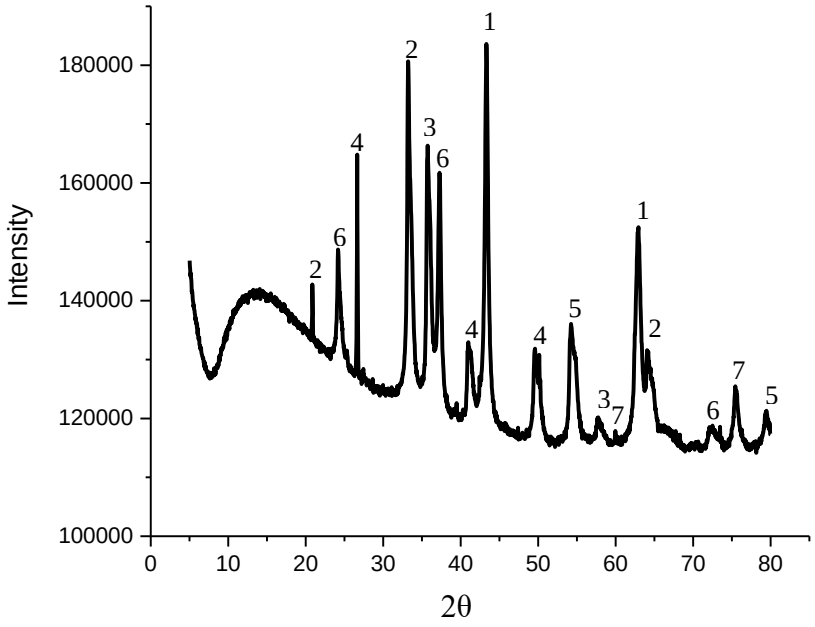


Figure 3.7: XRD spectrum of Ni/MRM catalyst (1: Periclase (MgO), 2: Calcite ($CaCO_3$), 3: Alumina ($Al_2O_3$), 4: Hematite ($Fe_2O_3$), 5: Lime (CaO), 6: Sand ($SiO_2$) and 7: Cubic nickel (NiO)).

### 3.3 Experimental set-ups

#### 3.3.1 Pyrolysis

Approximately 25.0 ± 0.1 g of the waste wood (0.5, 1 or 2 $cm^3$ cube) was placed in the centre of a 33 mm diameter and 830 mm long Inconel 600 fixed-bed (Figure 3.8). Prior to the experiments, the reactor was continuously purged with $N_2$. As soon as the system was air-free (confirmed by gas chromatography), the $N_2$ was adjusted to a fixed flow rate of 30 or 120 ml/min to study the effect of hot vapour residence time (1-3 seconds) on product yields and properties in the pyrolysis step. The heating system was then switched on at a fixed heating rate of 20 $^oC$/min based on TGA results (Figure 3.3) and preliminary trials in this study shows that there was no significant effect of the heating rate on product yields and characterisation of products between 10 $^oC$/min and 20 $^oC$/min. As soon as the set temperature was reached, i.e. 600, 700, 800 or 900 $^oC$, the system was held for a further 15 minutes before it being switched off to ensure full decomposition of the volatiles released. The volatiles released from the pyrolysis were cooled down in two condensers, kept in an ice bath (0 $^oC$), whereas the non-condensable gas was collected in a 500 ml tedlar sample bag for gas analysis. The solid residues

and condensable liquid were collected and weighted for their yields and stored in glass bottles for further analysis when the reactor temperature was below 50 $^{o}$C. A similar procedure was applied for $CO_2$ pyrolysis at a pyrolysis temperature of 900 $^{o}$C and particle size of 1 $cm^3$ cube (Table 3.5).

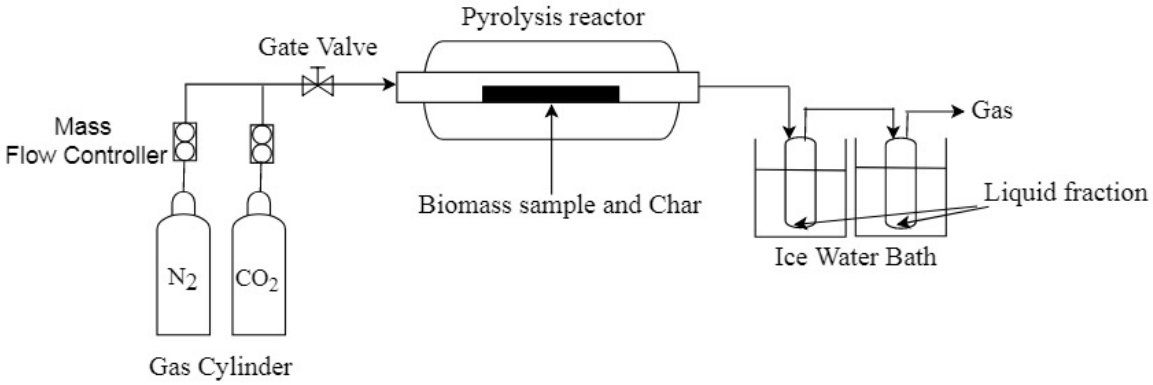


Figure 3.8: Schematic of the pyrolysis experimental.

Table 3.5: Operating conditions in pyrolysis experiments.

| Operating conditions | Particle size ($cm^3$ cube) | Operating temperature ($^{o}$C) | Carrier gas (ml/min) | |
|---|---|---|---|---|
| $N_2$ pyrolysis | 0.5, 1, 2 | 600, 700, 800, 900 | $N_2$: 30-120 | |
| $CO_2$ pyrolysis | 1 | 900 | $CO_2$ | $N_2$ |
| | | | 120 | 0 |
| | | | 100 | 20 |
| | | | 60 | 60 |
| | | | 40 | 80 |
| | | | 20 | 100 |
| | | | 0 | 100 |

The experimental set-up to examine the effect of pyrolysis product properties on the gasification stage is illustrated in Figure 3.9. Approximately 25.0 ± 0.1 g of waste wood (1 $cm^3$ cube) was placed in the centre of a 33 mm diameter and 830 mm long Inconel fixed-bed pyrolysis reactor (1$^{st}$ reactor) and 5.0 ± 0.1 g of char derived from conventional ($N_2$) and $CO_2$ pyrolysis at temperature of 600-900 $^{o}$C and particle size of 1 $cm^3$ cube (Table 3.5) was placed at the centre

of 33 mm diameter and 1100 mm long Inconel fixed-bed gasification reactor (2nd reactor). The electric furnace heater was then turned on to heat the gasification reactor (2nd reactor) to a desired temperature of 1000 °C with a fixed required carrier gas ($N_2$ or $CO_2$) flow rate of 120 ml/min (Table 3.5) to create the desired atmospheric conditions. As soon as the system was stabilised (15 minutes), the electric furnace of the pyrolysis reactor (1st reactor) was switched on to ramp up to 600-900 °C at a fixed heating rate of 20 °C/min. Once the volatiles are released from the pyrolysis stage (around 280-290 °C), deionized water was pumped to the heating vessel at constant flow rate of 1.8 g/min corresponding to a steam to carbon in biomass feedstock (S/C) molar ratio of 3.4. As soon as the temperature reached the set point the system was held for a further 15 minutes to allow the gas composition to stabilise before both furnaces were switched off. The products collection and analysis procedure were similar to those in the pyrolysis experiment.

### 3.3.2 Two-stage gasification

A two-stage gasification set-up is shown in Figure 3.9. Approximately 25.0 ± 0.1 g of waste wood was placed at the centre of a 33 mm diameter and 830 mm long Inconel fixed-bed pyrolysis reactor (1st reactor) and around 5.0 ± 0.1 g of char derived from pyrolysis at an $N_2$ flow rate of 120 ml/min (Table 3.5) was placed in the centre of a 33 mm diameter and 1100 mm long Inconel fixed-bed gasification reactor (2nd reactor). Prior to the experiments, the reactor was continuously purged with $N_2$. As soon as the system was air-free, the electric furnace heater was then turned on to heat the 2nd reactor (gasification) to a desired temperature of 600, 800, 900, 1000 or 1100 °C. Once the temperature of the 2nd reactor reached the set point, the 1st reactor (pyrolysis) was heated up to 900 °C at a heating rate of 20 °C/min (based on the pyrolysis experiment). The system was held for a further 15 minutes when the set temperature of the 1st reactor was reached to allow the gas composition to stabilise before both furnaces were switched off. The volatiles at the outlet of the 2nd reactor were cooled down in two condensers, kept in an ice bath (0 °C). The non-condensable gas was collected in a 500 ml tedlar sample bag for gas analysis. The solid residues from both reactors (pyrolysis and gasification) and condensable liquid were collected and weighted for their yields and stored in glass bottles for further analysis when the reactor temperature was below 50 °C. For the experiments with the additional of steam, when the temperature of the 1st reactor reached 280-290 °C (the waste wood started to decompose), the steam was injected at T-mixer before going into the 2nd reactor at a flow rate of 1.8, 3.0, 4.0 and 5.0 g/min corresponding to S/C molar ratios of 3.4, 5.7, 7.7 and 9.6. For $CO_2$ gasification, a similar procedure was also applied. The temperature of the

pyrolysis and gasification reactors was fixed at 900 ºC and 1000 ºC and the S/C molar ratio of 1.0, 2.7, 3.4 and 5.7.

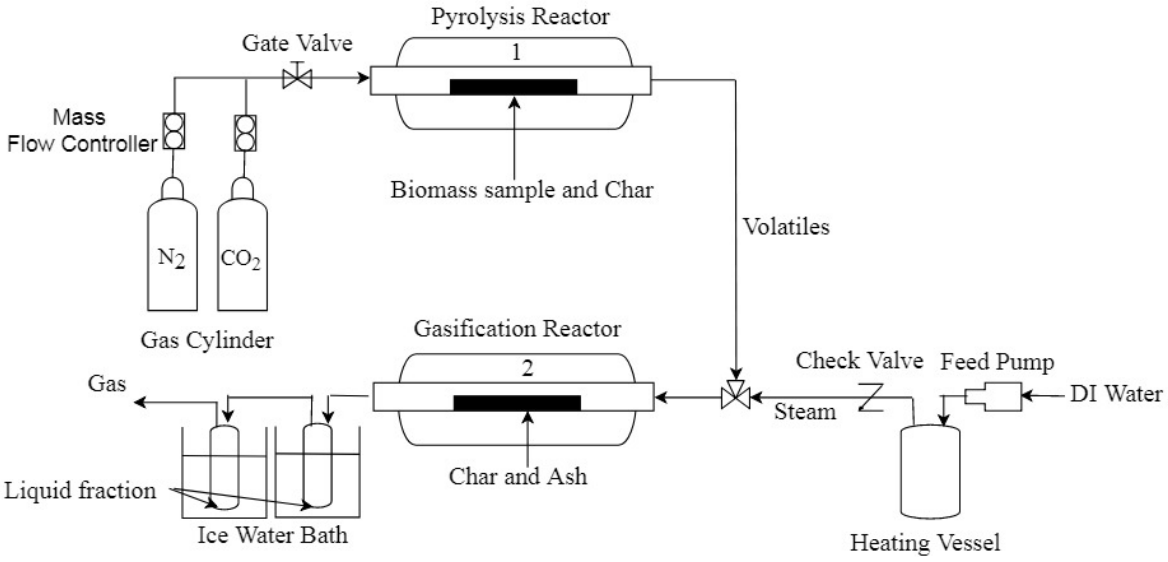


Figure 3.9: Schematic of two-stage gasification experimental.

The catalytic gasification set-up is illustrated in Figure 3.10 and is run with a similar procedure to that described previously. Approximately 0.3 ± 0.1 g of catalyst (prepared in section 3.2.1) was placed next to the char bed in the 2nd reactor (gasification reactor) as shown in Figure 3.10. The S/C molar ratio was fixed at 5.7 for the $N_2$ environment and 3.4 for the $CO_2$ atmosphere and pyrolysis and gasification temperature of 900 ºC and 1000 ºC. These values are based on the operating conditions in the two-stage gasification system for the highest hydrogen production.

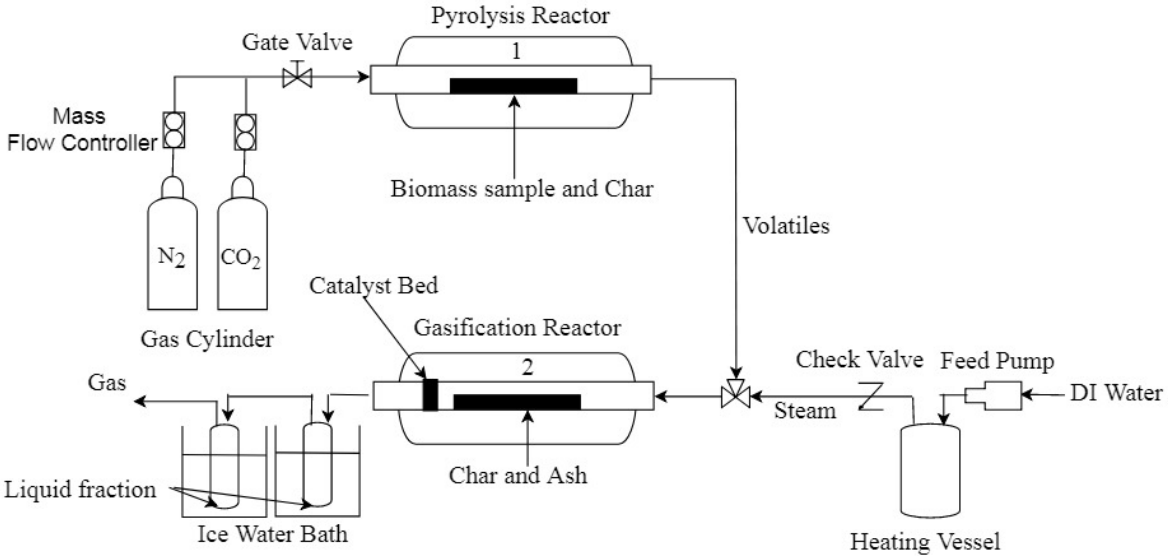


Figure 3.10: Schematic of catalytic two-stage gasification experimental.

### 3.4 Product analysis

#### 3.4.1 Gas composition

Non-condensable gas from all experiments was analysed using a Varian 450-GC gas chromatograph (GC) equipped with 5 columns and 3 detectors (1 TCD and 2 FID) with argon as carrier gas at a flow rate of 1 ml/min. A Molecularsieve ultimate 13X column (1.5 m × 1/8" × 2.0 mm) was used to detect the permanent gases ($CO_2$, CO, $H_2$, $N_2$ and $CH_4$). A Hayesep T and Q ultimetal column (0.5 m × 1/8" × 2.0 mm) was used to detect $CO_2$, C2s (acetylene, ethylene and ethane) and hydrocarbon gases. A CP-SIL 5CB capillary column (25 m × 0.25 mm × 0.4 µm) was used with a FID to determine hydrocarbons. A CP-WAX 52CB capillary column (25 m × 0.32 mm × 1.2 µm) equipped with another FID was used to detect light oxygenated compounds. The temperature program for the GC oven was as follows: the initial temperature was 40 $^oC$, 2 minutes hold time followed by a ramp to 50 $^oC$ (4 $^oC$/min) held for 0.5 minutes, then ramped to 100 $^oC$ at the rate of 8 $^oC$/min and final temperature of 120 $^oC$ (10 $^oC$/min). The TCD and FID detector temperatures were set at 175 $^oC$ and 255 $^oC$ respectively. Before carrying out the experiments the GC was calibrated using a standard gas mixture (15 mol% $H_2$, 10 mol% $CO_2$, 2 mol% $O_2$, 49 mol% $N_2$, 3 mol% $CH_4$, and 20 mol% CO), which was purchased from Scientific and Technical gases Ltd.

#### 3.4.2 Solid residues

**Physicochemical properties**

The char derived from pyrolysis experiments and solid residues after gasification (ash) were examined by: proximate analysis (moisture content, volatile matter content, ash content and fixed carbon), ultimate analysis (C, H, N and O), energy content (calorific value; HHV), SEM-EDX analysis (physical morphology, elemental composition and distribution), BET analysis (specific surface area and pore size distribution) and XRD analysis (crystalline phases). The analytical procedure was performed as described in sections 3.1.1 and 3.2.2.

**Fourier-transform infrared (FTIR) spectroscopy**

The Fourier-transform infrared spectroscopy (FTIR) was used for determination of functional groups (C-C, C=C, C-O, C=O, O-H and C-H) in char samples derived from pyrolysis experiments using an Agilent Cary 630 FTIR spectrometer with KBr as a background reference. Scanning was performed over the range 600-4000 $cm^{-1}$. The same procedure was repeated three times on each sample for reproducibility.

### 3.4.3 Liquid fraction

#### Physicochemical properties

The liquid fractions derived from pyrolysis and gasification experiments were examined by ultimate analysis (C, H, N and O) and energy content (calorific value; HHV). The procedure was the same as the one explained in section 3.1.1.

#### Water content

The water content (wt%) in the liquid sample were measured using a Volumetric Karl-Fischer titration (915 KF Ti-Touch). The Hydranal Composite 5K (purchased from Sigma Aldrich) used as the titration reagent and 1:3 methanol:chloroform (v/v) as the titration solvent. Approximately 100.0 ± 0.1 mg of liquid sample and 45 ml of titration solvent were added to the titration cell, then stirring by magnetic stirrer to extract water. The titration end point is automatic determined the amount of water in the sample. The procedure was repeated three times on each sample.

#### Chemical composition

The chemical compounds in the liquid samples were identified and quantified using a 7200 Accurate-Mass Q-TOF GC-MS and gas chromatography Flame ionization detector (GC-FID) equipped with a 60 m × 250 µm × 0.25 µm capillary column (14%-cyanopropyl-phenly-methylpolysiloxane, Restek Rtx-1707) with helium as carrier gas at a flow rate of 1 ml/min. The 1 µL of liquid sample was injected in the split mode with a split ratio of 30:1 at a constant temperature of 250 $^{o}$C. The temperature program for GC oven was as follows: the initial oven temperature set to 45 $^{o}$C, 10 minutes hold time then ramped up to 250 $^{o}$C at the rate of 3 $^{o}$C/min and held at 250 $^{o}$C for 5 minutes. The MSD transfer line was operated at 280 $^{o}$C in the electron ionization (EI) mode at 70 eV, with mass scan range of 29-600 m/z. The ion source and quad temperature were set at 230 $^{o}$C and 150 $^{o}$C respectively. Identification of chemical composition was done using the National Institute of Standards and Technology (NIST) spectral library and the MassBank high resolution mass database. The major compounds that have relatively high content (based on the %area) in liquid samples were quantified by the external standard method. The standard chemicals used to quantify the amount of a component in the liquid samples can be found in Appendix B.

### 3.5 Data processing

The yield of products is determined based on initial mass of feedstock:

$$\text{Solid yield (wt\%)} = \frac{M_{solid}}{M_{feedstock}} \quad (3.1)$$

$$\text{Liquid yield (wt\%)} = \frac{M_{liquid}}{M_{feedstock}} \quad (3.2)$$

$$\text{Gas yield (wt\%)} = 100 - (\%\text{solid yield} + \%\text{liquid yield}) \quad (3.3)$$

where $M_{liquid}$ and $M_{solid}$ are the mass of liquid (g) and solid residues (g) after each experiment and $M_{feedstock}$ is the initial mass of the feedstock (g).

The low heating value (LHV) of the product gas is estimated using Equation 3.4 (Shen et al., 2017):

$$LHV_{syngas}\left(\frac{MJ}{Nm^3}\right) = 10.8[H_2] + 12.6[CO] + 35.8[CH_4] \quad (3.4)$$

where $[H_2]$, $[CO]$ and $[CH_4]$ are component mole fraction in the product gas.

The tar formation in the gas stream can be determined by:

$$\frac{T}{V} = \frac{M_{liquid}}{V_{syngas}} \quad (3.5)$$

where $M_{liquid}$ is the mass of liquid after each experiment (g) and $V_{syngas}$ is total volume of the producer gas ($Nm^3$).

The cold gas efficiency (CGE) is defined as follows:

$$\mathrm{CGE}\ (\%) = \frac{\mathrm{LHV_{syngas}} \times \mathrm{Y_{syngas}}}{\mathrm{LHV_{feedstock}}} \tag{3.6}$$

where $\mathrm{LHV_{syngas}}$ is the low heating value of the product gas (MJ/Nm$^3$); $\mathrm{Y_{syngas}}$ is dry gas yield (Nm$^3$/kg) and $\mathrm{LHV_{feedstock}}$ is the low heating value of the feedstock (MJ/kg).

The process efficiency (PE) is defined as:

$$\mathrm{PE}\ (\%) = \frac{\mathrm{LHV_{syngas}} \times \mathrm{Y_{syngas}}}{\mathrm{LHV_{feedstock}} + \mathrm{E_{heating}} + \mathrm{E_{steam}}} \tag{3.7}$$

where $\mathrm{LHV_{syngas}}$ is the low heating value of the product gas (MJ/Nm$^3$); $\mathrm{Y_{syngas}}$ is dry gas yield (Nm$^3$/kg); $\mathrm{LHV_{feedstock}}$ is the low heating value of the feedstock (MJ/kg); $\mathrm{E_{heating}}$ is energy required to heat feedstock (MJ/kg) and $\mathrm{E_{steam}}$ is energy required to generate steam (MJ/kg).

The carbon conversion efficiency (CCE) is defined by:

$$\mathrm{CCE}\ (\%) = \frac{\mathrm{M_{c,in}} - \mathrm{M_{c,out}}}{\mathrm{M_{c,in}}} \tag{3.8}$$

where $\mathrm{M_{c,in}}$ is mass of carbon in feedstock (g) and $\mathrm{M_{c,out}}$ is unreacted carbon after each experiment (g).

# Chapter 4 Pyrolysis of waste wood

This chapter focuses on studying the effects of operating conditions on the properties of products derived from pyrolysis (feedstock for the gasification process) to understand the behaviour of pyrolysis and to optimize operating conditions in pyrolysis of high volatile containing materials, i.e. waste wood for high quality syngas/hydrogen production via a gasification process. This chapter starts with an investigation of the effect of operating parameters, i.e. temperature, particle size and inert gas ($N_2$) flow rate (corresponding to hot vapour residence time) on the properties of volatiles and char. The synergistic effect of $CO_2$ assisted pyrolysis is also explored and compared with conventional pyrolysis ($N_2$ environment) in terms of product yields and properties. Moreover, the effect of pyrolysis conditions in both $N_2$ and $CO_2$ environment on the gasification process in terms of quality of synthetic gas (syngas) and tar formation were investigated. The content of this chapter has been previously published in "Gasification of waste for hydrogen production: effects of pyrolysis parameters", Renewable Energy Journal (Prasertcharoensuk et al., 2019).

## 4.1 Conventional pyrolysis ($N_2$ environment)

### 4.1.1 The effect of pyrolysis temperature on product yields and properties

Table 4.1 shows that pyrolysis operating temperatures of 600-700 $^oC$ had a little effect on product yields. A further increase in temperature to 700-800 $^oC$ resulted in a 23% increase in gas yield mainly at the expense of the liquid. This is because the decomposition of the feedstock almost ceased at temperatures above 700 $^oC$ and volatiles were deeply cracked at high temperatures to form gases. This was evidenced by the amount of fixed carbon and the char carbon content remained constant at 93-94 wt% and 87 wt% as shown in Table 4.2. Although, there is a small amount of volatiles (around 3-4 wt%) present in the char, they are tightly bonded or locked in stable structures and could not be released at the tested operating conditions (Liu et al., 2015; Chen et al., 2016c). The carrier gas flow rate in a range of 30-120 ml/min (hot vapour residence time around 1-3 seconds) had little effect on the product yields (Table 4.1). This could be because the residence time was insufficient to promote significant cracking of the volatiles. However, a small increase in the extent of cracking (around 4%) has been reported by others at temperatures of 550 $^oC$ when the hot vapour residence time is between 5 seconds and 6 seconds (Gerçel, 2002; Aysu and Küçük, 2014; Moralı and Şensöz, 2015; Moralı et al., 2016; Varma and Mondal, 2017).

Table 4.1: Pyrolysis product yields over various pyrolysis temperature and nitrogen flow rates at particle size of 1 $cm^3$ cube.

| Pyrolysis temperature (°C)/$N_2$ flow rate (ml/min) | Char (wt%) | Liquid (wt%) | Gas* (wt%) |
|---|---|---|---|
| 600/30 | 25.1 ± 1.2 | 50.5 ± 0.7 | 24.4 ± 0.2 |
| 600/120 | 25.3 ± 0.7 | 51.1 ± 0.4 | 23.6 ± 1.3 |
| 700/30 | 23.7 ± 0.6 | 50.5 ± 2.1 | 25.8 ± 0.2 |
| 700/120 | 23.7 ± 1.0 | 50.7 ± 1.1 | 25.6 ± 1.2 |
| 800/30 | 22.5 ± 0.7 | 47.7 ± 0.3 | 29.8 ± 1.7 |
| 800/120 | 22.5 ± 0.3 | 47.6 ± 0.4 | 29.9 ± 1.6 |
| 900/30 | 22.0 ± 1.0 | 46.9 ± 2.0 | 31.1 ± 0.9 |
| 900/120 | 22.2 ± 1.1 | 47.4 ± 1.4 | 30.4 ± 0.8 |

*By difference

As seen in the IR spectrum (Figure 4.1), hydroxyl groups (OH) at ~3300 $cm^{-1}$ and the aliphatic C-H stretching vibration at ~2900 $cm^{-1}$ in the raw material (Figure 4.1a) disappeared at temperatures, i.e. 600 °C (Figure 4.1b) whereas other functional groups, i.e. C=O (stretching vibration at ~1700 $cm^{-1}$), aromatic C-C/C=C (vibration at ~1600 $cm^{-1}$), C-O (stretching peak at ~1100 $cm^{-1}$) and the aromatic C-H (stretching vibration between 700 $cm^{-1}$ and 900 $cm^{-1}$), decreased their intensities with increasing pyrolysis temperatures and completely disappeared at temperatures above 700 °C (Figures 4.1c-e). The results obtained from this study (Figure 4.1) agree very well with other findings (Kim et al., 2013a; Gai et al., 2014; Elmay et al., 2015; Liu et al., 2015; Chen et al., 2016c), where the functional groups on the char surface started to decrease at pyrolysis temperatures above 550 °C. Removal of functional groups at high temperature provides char with a high stability and degree of condensation (Enders et al., 2012; Song and Guo, 2012; Jindo et al., 2014; Rafiq et al., 2016; Figueredo et al., 2017). Experimental results show that the energy content of the biomass feedstock was mainly stored in the liquid and char fractions (Table 4.2). The energy yield (which is defined as calorific value of product × product yield/calorific value of raw material × mass of feedstock) was around 42-47% in the liquid fraction and 39-46% in the char over the tested range of temperatures.

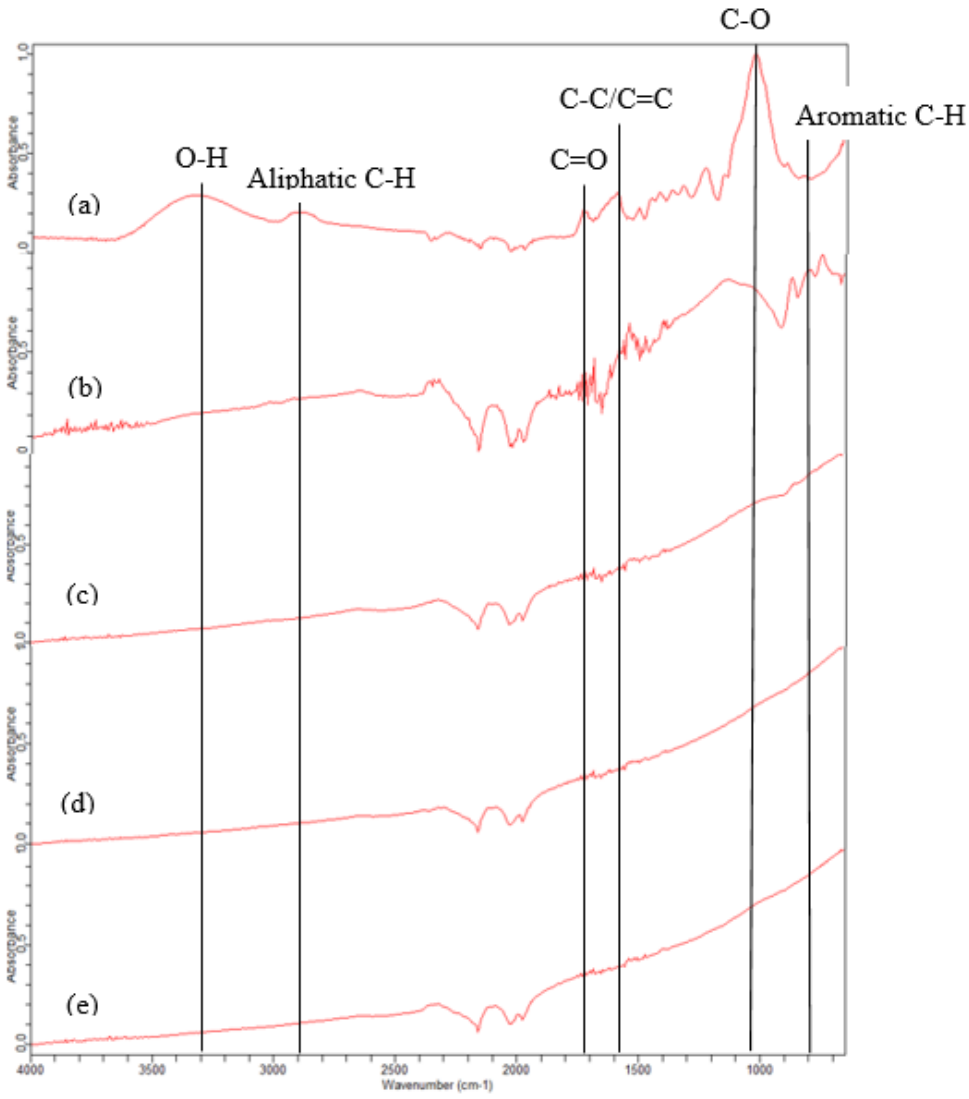


Figure 4.1: FTIR spectra of (a) biomass feedstock (waste wood) and char obtained from pyrolysis at a temperature of (b) 600 °C, (c) 700 °C, (d) 800 °C and (e) 900 °C at a fixed nitrogen flow rate of 120 ml/min and particle size of 1 $cm^3$ cube.

Table 4.2: Properties of pyrolysis products from pyrolysis of waste wood at 600, 700, 800 and 900 °C at a fixed nitrogen flow rate of 120 ml/min and particle size of 1 $cm^3$ cube.

| Pyrolysis temperature (°C) | 600 | 700 | 800 | 900 |
|---|---|---|---|---|
| Char properties (dry basis) | | | | |
| Volatile matter (wt%) | 10.1 ± 2.2 | 7.2 ± 1.7 | 4.6 ± 1.4 | 3.6 ± 1.9 |
| Fixed carbon (wt%) | 87.5 ± 1.3 | 90.2 ± 2.1 | 92.7 ± 1.0 | 93.6 ± 1.0 |
| Ash content (wt%) | 2.4 ± 1.1 | 2.6 ± 0.7 | 2.7 ± 0.7 | 2.8 ± 0.3 |

| | | | | |
|---|---|---|---|---|
| C ± 0.3 (wt%) | 85.8 | 87.0 | 87.3 | 87.6 |
| H ± 0.3 (wt%) | 2.4 | 1.9 | 1.7 | 1.5 |
| O ± 0.5* (wt%) | 11.4 | 10.6 | 10.5 | 10.3 |
| N ± 0.3 (wt%) | 0.4 | 0.5 | 0.5 | 0.6 |
| The empirical formula | $C_6H_2O_{0.6}N_{0.02}$ | $C_6H_{1.6}O_{0.5}N_{0.03}$ | $C_6H_{1.4}O_{0.5}N_{0.03}$ | $C_6H_{1.2}O_{0.5}N_{0.04}$ |
| HHV (MJ/kg) | 32.5 ± 3.4 | 33.0 ± 2.1 | 33.5 ± 2.2 | 33.6 ± 1.4 |
| Surface area ($m^2/g$) | 38.6 ± 1.7 | 78.9 ± 3.9 | 82.0 ± 4.2 | 98.4 ± 4.6 |
| Liquid properties (wet basis) | | | | |
| C ± 0.3 (wt%) | 44.7 | 44.2 | 44.5 | 44.7 |
| H ± 0.3 (wt%) | 7.5 | 7.6 | 7.7 | 7.4 |
| O ± 0.5* (wt%) | 47.7 | 48.0 | 47.7 | 47.8 |
| N ± 0.3 (wt%) | 0.1 | 0.2 | 0.1 | 0.1 |
| The empirical formula | $CH_2O_{0.8}N_{0.002}$ | $CH_{2.1}O_{0.8}N_{0.003}$ | $CH_{2.1}O_{0.8}N_{0.002}$ | $CH_2O_{0.8}N_{0.002}$ |
| Water content in liquid fraction (wt%) | 43.9 ± 1.4 | 44.1 ± 1.8 | 44.6 ± 1.5 | 43.7 ± 1.8 |
| pH | 2.3 ± 0.2 | 2.3 ± 0.1 | 2.4 ± 0.2 | 2.4 ± 0.3 |
| HHV (MJ/kg) | 17.3 ± 2.4 | 16.5 ± 1.3 | 17.5 ± 2.4 | 17.2 ± 2.2 |
| Gas composition | | | | |
| $H_2$ (mol%) | 12.5 ± 2.1 | 16.3 ± 1.3 | 18.3 ± 1.2 | 22.3 ± 1.3 |
| CO (mol%) | 38.5 ± 0.9 | 42.7 ± 1.1 | 45.4 ± 3.1 | 47.6 ± 0.8 |
| $CO_2$ (mol%) | 32.8 ± 2.1 | 27.5 ± 0.7 | 23.1 ± 0.4 | 15.1 ± 1.1 |
| $CH_4$ (mol%) | 9.6 ± 1.3 | 11.3 ± 0.8 | 11.7 ± 0.3 | 13.4 ± 2.2 |
| $C_2$-$C_5$ (mol%) | 6.6 ± 0.7 | 2.2 ± 0.3 | 1.5 ± 0.6 | 1.6 ± 0.2 |
| $H_2$/CO | 0.3 | 0.4 | 0.4 | 0.5 |

*By difference

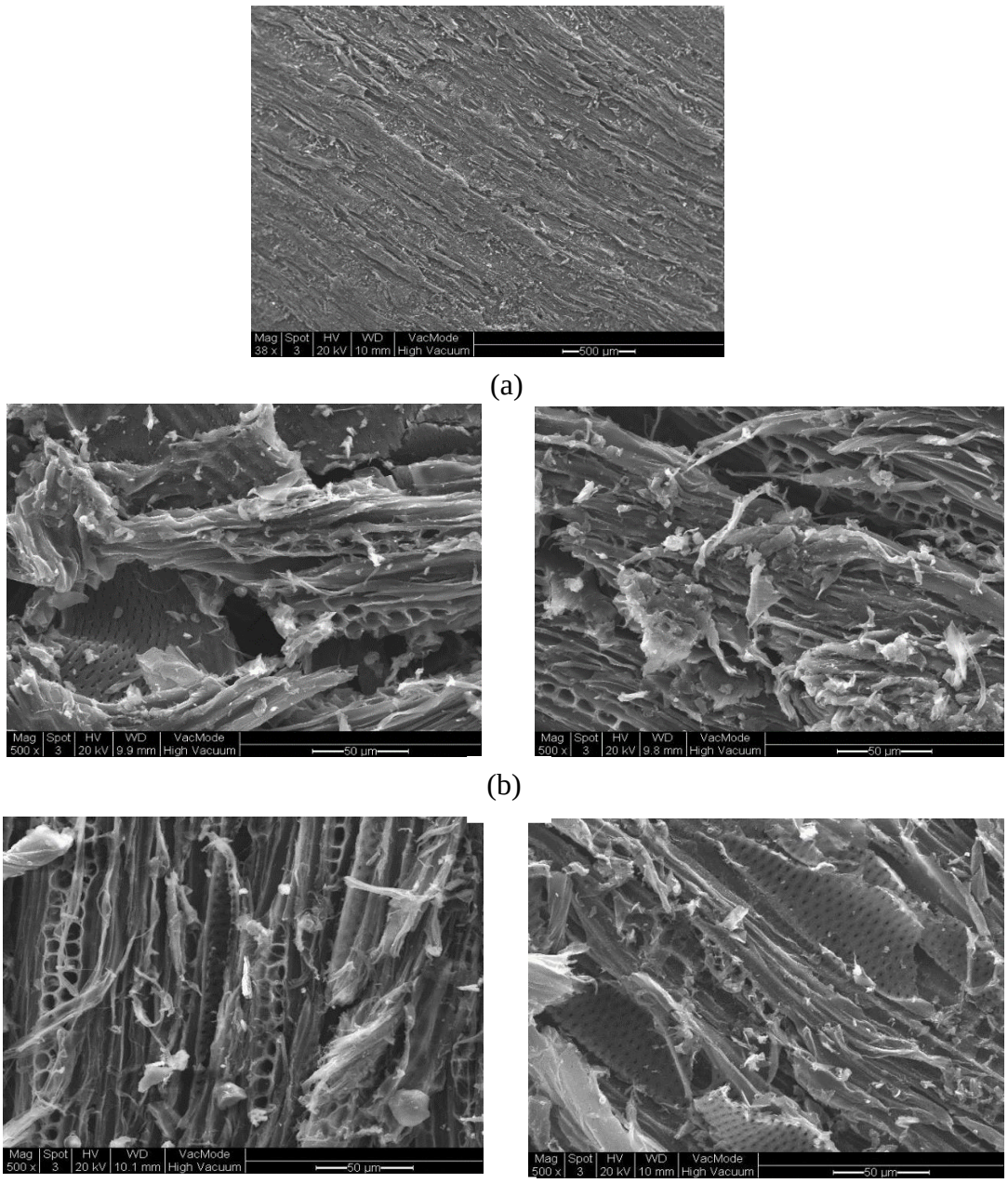


Figure 4.2: SEM images of (a) waste wood raw material (at a magnification of 38x) and char (at a magnification of 500x) obtained from pyrolysis at a temperature of (b) 600 $^{o}$C and (c) 900 $^{o}$C at a fixed nitrogen flow rate of 120 ml/min and particle size of 1 $cm^3$ cube.

Figure 4.2 shows the change in the char morphology with pyrolysis temperature. At a fixed particle size of 1 $cm^3$ cube, increasing temperature accelerated the rate of decomposition (Ertaş and Hakkı Alma, 2010; Abdel-Fattah et al., 2015; Pradhan et al., 2016), resulting in the formation of small pores on the surface of the char (due to the released volatiles) from the smooth solid cells of the raw material (Figure 4.2a). The specific surface area of char increased from 38.6 $m^2/g$ at 600 $^{o}$C to 98.4 $m^2/g$ at 900 $^{o}$C (Table 4.2). A significant increase in the total pore volume from $21.7 \times 10^{-3}$ $cm^3/g$ to $52.1 \times 10^{-3}$ $cm^3/g$ and micropore (2-30 nm) volume from

$13.1 \times 10^{-3}$ $cm^3/g$ to $34.4 \times 10^{-3}$ $cm^3/g$ was observed when increasing the pyrolysis temperature from 600 ºC to 900 ºC. The average pore diameter of the char surface was found to be in the range of 7-12 µm, suggesting a sufficient pore size to accommodate the volatiles from biomass, i.e. aromatic and polycyclic aromatic hydrocarbons (PAH) (< 2 µm) (Yang et al., 2005; Wu et al., 2006a; Ladji et al., 2014). The high specific surface area and pore volume from char derived at high pyrolysis temperature (Table 4.2) will promote the mass transfer between the gas and char particles, accelerating heterogeneous solid-gas reactions in the later stages of processing, thereby reducing unburnt carbon in the ash residues (Arenas and Chejne, 2004; Rehrah et al., 2016).

Table 4.2 shows the $CO_2$ concentration gradually decreased from 32.8 mol% to 15.1 mol%, whereas CO formation increased from 38.5 mol% to 47.6 mol% when increasing the pyrolysis temperature from 600 ºC to 900 ºC. This is because when $CO_2$ was released from inner layers of a particles, it can react with a hot char layer via the Boudouard reaction ($C + CO_2 \rightarrow 2CO$), which is dominant at temperatures above 700 ºC, leading to the formation of CO (Kwon et al., 2012). Moreover, $CO_2$ could also react with other hydrocarbons ($C_1$-$C_5$) via the dry reforming reaction ($C_xH_y + xCO_2 \leftrightarrow 2xCO + \left(\frac{y}{2}\right)H_2$) to form $H_2$ and CO at temperatures above 640 ºC (Kwon et al., 2012; Leal et al., 2016). The $H_2$/CO ratio increased when increasing temperature, i.e. from 0.3 at 600 ºC to 0.5 at 900 ºC, with an increase in both $H_2$ and CO concentration (Table 4.2), however it is still much lower than the required ratios for syngas applications, i.e. chemical production and transportation fuel which require $H_2/CO \geq 2$ (Chaudhari et al., 2001; Torres et al., 2007; Yang et al., 2007).

The liquid product was highly acidic with pH of 2.3-2.4 containing a large amount of water, around 44 wt% (based on liquid fraction) or 22 wt% based on feedstock (Table 4.2). This causes corrosion, clogging and fouling of installations and difficulties in ignition due to low calorific value, thereby reducing the local combustion temperature (Aubin and Roy, 1990; Balat et al., 2009b; Göransson et al., 2011; Sikarwar et al., 2016). The liquid product had much higher H/C (~ 2.0) and O/C (~ 0.8) ratios than those in heavy fossil-based oil (H/C ~ 1.5 and almost zero oxygen) (Oasmaa and Czernik, 1999; Zhang et al., 2013). If all water is removed, the liquid product would have a H/C ratio in the range of 1.3-1.4 and O/C of 0.4-0.5, which is still higher than the required ratios for transport fuel applications compared to petroleum-based fuels. In addition, the liquid derived from pyrolysis not only thermal unstable caused by high oxygen (35-40 wt%) and water content (30-45 wt%), but also shows chemical instability due to containing more than 300 chemical compounds; oxygen-containing compounds in particular (i.e. hydroxyacetaldehyde, 5-hydroxymethylfurfural, acetol, phenol and derivatives, levoglucosan and anhydrosugars) (Oasmaa et al., 1997; Lehto et al., 2013; Alvarez et al., 2014)

are present in the liquid product. As shown in Table 4.3 fully decomposed unstable compounds (i.e. sugars and their derivatives) were observed at pyrolysis temperatures above 700 $^{o}$C, while the concentration of other compounds derived from decomposition of cellulose and hemicellulose, i.e. acids, ketones, aldehydes and furans and its derivatives gradually decreased with increasing temperature. However, phenol and its derivatives increased with pyrolysis temperature due to Diels-Alder reactions which are favoured at high temperatures (Cypres, 1987). At all tested temperatures, the liquid consisted mainly of furan and its derivatives and phenolic compounds (around 60%). This indicates that high temperature alone can not decompose aromatics compounds into gaseous products.

Table 4.3: Chemical compositions in liquid derived from pyrolysis of waste wood (based on feedstock) over various pyrolysis temperature at a fixed nitrogen flow rate of 120 ml/min and particle size of 1 cm$^3$ cube.

| Function groups | wt% (dry basis) | | | |
|---|---|---|---|---|
| | 600 $^{o}$C | 700 $^{o}$C | 800 $^{o}$C | 900 $^{o}$C |
| Acids | 2.1 | 1.3 | 0.8 | 0.7 |
| Esters | 1.4 | 1.6 | 0.5 | 0.6 |
| Ketones | 2.9 | 2.6 | 0.9 | 1.0 |
| Alcohols | 1.1 | 1.1 | 0.8 | 0.7 |
| Aldehydes | 1.1 | 1.1 | 0.6 | 0.6 |
| Furan and its derivatives | 4.9 | 4.4 | 4.9 | 3.7 |
| Sugars | 1.5 | 0.3 | - | - |
| Phenol and its derivatives | 12.7 | 15.4 | 16.7 | 18.1 |
| Unknown | 1.0 | 0.6 | 1.1 | 1.3 |

### 4.1.2 The effect of particle size on product yields and properties

Decreasing particle size from 2 cm$^3$ to 0.5 cm$^3$ cube had a significant effect on the char and gas yields, i.e. an approximately 31% decrease in the char yield and 29% increase in the gas yield (Table 4.4). This is due to heat transfer limitation in larger particles, causing higher temperature gradients inside the particles. From experimental results it took around 46 minutes for the middle of a 0.5 cm$^3$ particle to reach the set temperature of 900 $^{o}$C but 52 minutes for 1 cm$^3$ and

up to 62 minutes for 2 $cm^3$ particle (Figure 4.3a). The outer char layer could act as a hard shell hindering the release of volatiles (Hanson et al., 2002; Bennadji et al., 2014), resulting in increasing the char yield from 19.8 wt% for 0.5 $cm^3$ to 28.7 wt% for 2 $cm^3$ particle and the volatile content in char (6.5 wt% for 2 $cm^3$ but only 2.3 wt% for 0.5 $cm^3$ particle) as shown in Table 4.4. A similar effect occurs in a continuous gasification process where feedstock is continuously fed and heated up in a hot zone. Thus, understanding the temperature profile of single particle could help in designing a gasifier that provides sufficient time for decomposed of fuels. Figure 4.3b shows that a particle size of 0.5 $cm^3$ cube needs to stay in the pyrolysis zone around 20 seconds to reach a temperature of 900 $^oC$, compared to approximately 32 and 50 seconds for a 1 $cm^3$ and 2 $cm^3$ particle respectively. It was found in this study that in isothermal conditions at a temperature of 900 $^oC$, the liquid yield was slightly higher than batch conditions (around 13-17%) at the expense of gas and char yields for all tested particle sizes. However, there is no significant difference in the characterisation of pyrolysis products (gas, char and liquid fraction) between isothermal and batch conditions.

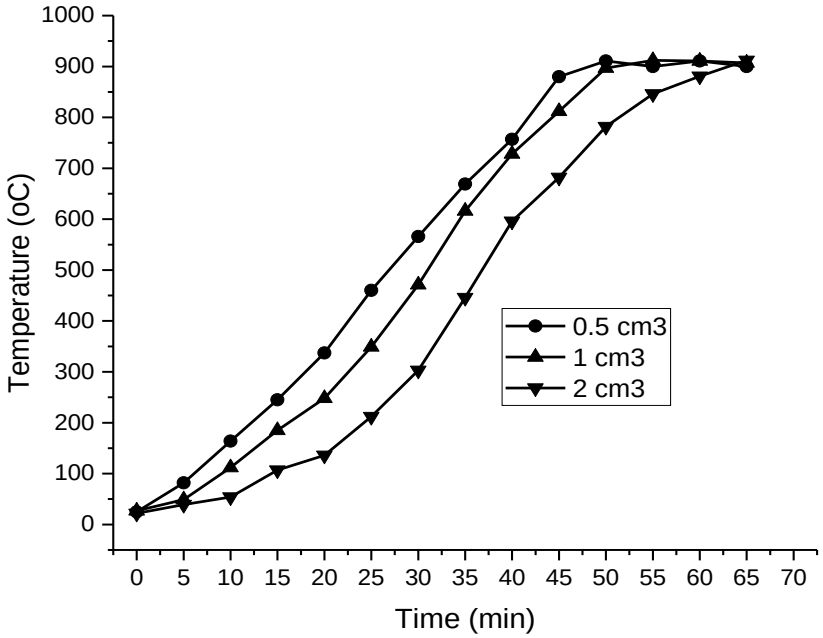


(a)

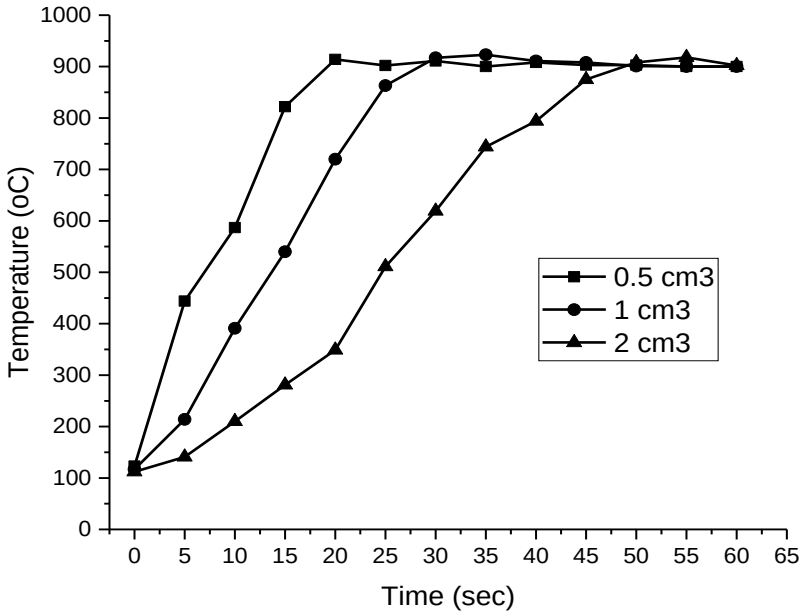


(b)

Figure 4.3: Temperature profiles at the middle of different particle sizes of waste wood feedstock (0.5, 1 and 2 $cm^3$ cube) (a) batch condition and (b) isothermal condition at a fixed the temperature of 900 $^oC$ and nitrogen flow rate of 120 $cm^3$/min.

Although, there was a little variation in C, H, O content (Table 4.4), the specific surface area of char was significantly enhanced up to 124.5 $m^2$/g at 0.5 $cm^3$ from 73.0 $m^2$/g at 2 $cm^3$ cube. The small variation in the repeated measurements (5%) was because different char samples derived from different waste wood feedstock pieces were chosen when determining specific surface

area. Decreasing particle sizes from 2 $cm^3$ to 0.5 $cm^3$ cube led to increases the total pore volume from 39.1 × $10^{-3}$ $cm^3/g$ to 66.3 × $10^{-3}$ $cm^3/g$ and the micropore volume from 23.1 × $10^{-3}$ $cm^3/g$ to 42.9 × $10^{-3}$ $cm^3/g$. This was confirmed via SEM images (Figure 4.4); the presence of cracking and development of the pore structure (micropores and macropores) was observed for the small particle size due to the rapid release of volatiles.

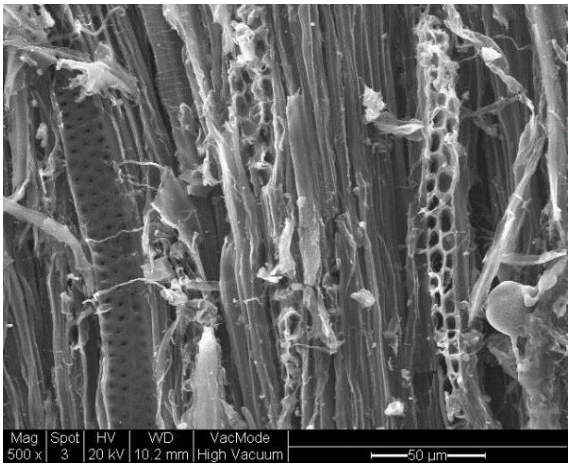


(a)

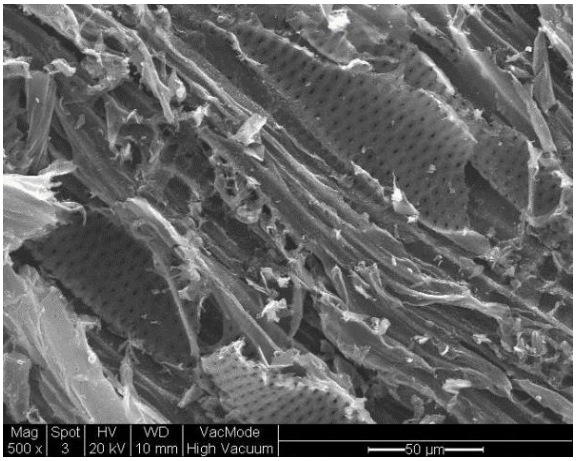


(b)

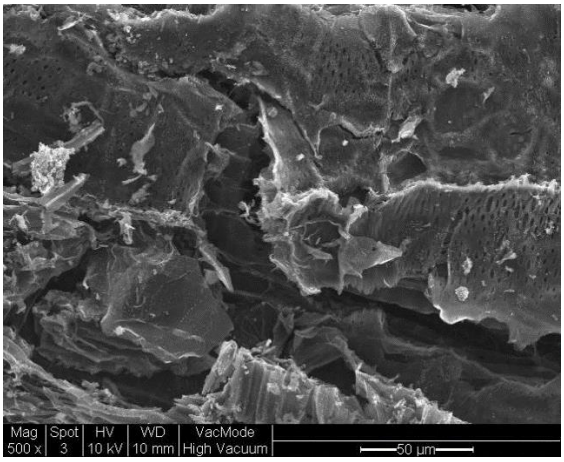


(c)

Figure 4.4: SEM images at a magnification of 500x of char obtained from pyrolysis batch condition (a) 0.5 $cm^3$ cube, (b) 1 $cm^3$ cube and (c) 2 $cm^3$ cube at pyrolysis temperature of 900 $^oC$ and nitrogen flow rate of 120 ml/min.

Due to the significant difference in temperature observed for large particles, an increase of $CO_2$ from 11.0 mol% to 20.5 mol% and light hydrocarbon ($C_2$-$C_5$) from 0.8 mol% to 3.8 mol% occurs whereas other gas concentrations gradually decrease with increasing particle size from 0.5 $cm^3$ to 2 $cm^3$ cube. As shown in Table 4.4, reducing particle size to 0.5 $cm^3$ cube had little effect on the ratio of $H_2$/CO (around 0.5).

Table 4.4: Product yields and properties obtained from pyrolysis batch condition at different particle size 0.5, 1 and 2 $cm^3$ cube at pyrolysis temperature of 900 $^oC$ and nitrogen flow rate of 120 ml/min.

| Particle size ($cm^3$ cube) | 0.5 | 1 | 2 |
|---|---|---|---|
| Product yields | | | |
| Char (wt%) | 19.8 ± 2.2 | 22.2 ± 1.1 | 28.7 ± 1.1 |
| Liquid (wt%) | 47.6 ± 0.7 | 47.4 ± 1.4 | 46.0 ± 0.4 |
| Gas* (wt%) | 32.6 ± 1.4 | 30.4 ± 0.8 | 25.3 ± 0.5 |
| Char properties (dry basis) | | | |
| Volatile matter (wt%) | 2.3 ± 1.0 | 3.6 ± 1.9 | 6.5 ± 1.4 |
| Fixed carbon (wt%) | 95.6 ± 2.2 | 93.6 ± 1.0 | 91.1 ± 1.9 |
| Ash content (wt%) | 2.1 ± 1.1 | 2.8 ± 0.3 | 2.4 ± 0.7 |
| C ± 0.3 (wt%) | 87.9 | 87.6 | 87.4 |
| H ± 0.3 (wt%) | 1.4 | 1.5 | 1.7 |
| O ± 0.5* (wt%) | 10.1 | 10.3 | 10.4 |
| N ± 0.3 (wt%) | 0.6 | 0.6 | 0.5 |
| The empirical formula | $C_6H_{1.1}O_{0.5}N_{0.04}$ | $C_6H_{1.2}O_{0.5}N_{0.04}$ | $C_6H_{1.4}O_{0.5}N_{0.03}$ |
| HHV (MJ/kg) | 34.0 ± 4.4 | 33.6 ± 3.3 | 33.3 ± 3.5 |
| Surface area ($m^2/g$) | 124.5 ± 5.3 | 98.4 ± 4.6 | 73.00 ± 3.2 |
| Liquid properties (wet basis) | | | |
| C ± 0.3 (wt%) | 46.4 | 44.7 | 41.5 |
| H ± 0.3 (wt%) | 7.4 | 7.4 | 7.1 |
| O ± 0.5* (wt%) | 46.0 | 47.8 | 51.3 |
| N ± 0.3 (wt%) | 0.2 | 0.1 | 0.1 |
| The empirical formula | $CH_{1.9}O_{0.7}N_{0.003}$ | $CH_2O_{0.8}N_{0.002}$ | $CH_2O_{0.9}N_{0.002}$ |

| | | | |
|---|---|---|---|
| Water content in liquid fraction (wt%) | 43.6 ± 2.4 | 43.7 ± 1.8 | 46.2 ± 1.4 |
| pH | 2.4 ± 0.2 | 2.4 ± 0.3 | 2.3 ± 0.3 |
| HHV (MJ/kg) | 18.0 ± 1.4 | 17.2 ± 2.2 | 14.9 ± 2.7 |
| Gas composition | | | |
| $H_2$ (mol%) | 24.4 ± 1.2 | 22.3 ± 2.3 | 18.2 ± 0.9 |
| CO (mol%) | 49.4 ± 0.4 | 47.6 ± 2.2 | 47.1 ± 2.3 |
| $CO_2$ (mol%) | 11.0 ± 1.7 | 15.1 ± 1.1 | 20.5 ± 1.7 |
| $CH_4$ (mol%) | 14.4 ± 0.6 | 13.4 ± 1.7 | 10.4 ± 1.6 |
| $C_2$-$C_5$ (mol%) | 0.8 ± 0.2 | 1.6 ± 1.3 | 3.8 ± 1.6 |
| $H_2$/CO | 0.5 | 0.5 | 0.4 |

*By difference

Increasing particle size slightly decreased the carbon content in the liquid (from 46.4 wt% for 0.5 $cm^3$ to 41.5 wt% for 2 $cm^3$ cube) whereas the water content in liquid fraction increased slightly to around 6% (Table 4.4). This could be due to the rapid release of volatile matter, minimizing secondary reactions (i.e. dehydration) in small particles (Bai et al., 2013; Ronsse et al., 2013; Aysu and Küçük, 2014; Tan et al., 2017). The calorific values (HHV) of the liquid decreased from 18.0 MJ/kg at 0.5 $cm^3$ to 14.9 MJ/kg at 2 $cm^3$ cube (Table 4.4). Phenol and its derivatives decreased from 18.6 wt% at 0.5 $cm^3$ to 13.7 wt% at 2 $cm^3$ cube (Table 4.5). This could be due to the incomplete decomposition of lignin in the feedstock at the tested temperatures (Cypres, 1987; Branca et al., 2003; Alvarez et al., 2014). However, the concentration of other compounds in liquid fraction gradually increased with increasing particle size as shown in Table 4.5.

Table 4.5: Chemical compositions in liquid derived from pyrolysis batch condition (based on feedstock) over a range of particle size (0.5, 1 and 2 $cm^3$ cube) at pyrolysis temperature of 900 $^oC$ and nitrogen flow rate of 120 ml/min.

| Functional groups | wt% (dry basis) | | |
|---|---|---|---|
| | 0.5 $cm^3$ cube | 1 $cm^3$ cube | 2 $cm^3$ cube |
| Acids | 0.7 | 0.7 | 0.9 |
| Esters | 1.6 | 0.6 | 1.1 |
| Ketones | 0.8 | 1.0 | 2.2 |
| Alcohols | 1.0 | 0.7 | 1.3 |
| Aldehydes | 0.6 | 0.6 | 1.0 |
| Furan and its derivative | 2.8 | 3.7 | 4.3 |
| Phenol and its derivatives | 18.6 | 18.1 | 13.7 |
| Unknown | 0.8 | 1.3 | 0.3 |

### 4.2 $CO_2$ pyrolysis

Table 4.6 shows that using 100% $CO_2$ as a carrier gas in the pyrolysis process alters the gas yield (from 30.4 wt% to 48.7 wt%) at the expense of the liquid (from 47.4 wt% to 35.4 wt%) and char (from 22.2 wt% to 15.9 wt%) fractions compared to that in the $N_2$ environment. This is because $CO_2$ reacts with (i) volatiles (i.e. hydrocarbons and oxygenated compounds) at temperatures above 640 $^oC$ and (ii) char according to the Boudouard reaction ($C + CO_2 \rightarrow 2CO$) at temperatures above 700 $^oC$ (Kwon et al., 2012; Leal et al., 2016; Liu et al., 2018), thereby reducing the liquid and char fractions. Thus, $CO_2$ pyrolysis is not suitable for solid fuel production compared to the $N_2$ condition. The char properties derived from $CO_2$ differed to those derived from the $N_2$ atmosphere in terms of carbon content and the specific surface area as shown in Table 4.6. Using 100% $CO_2$ as a carrier gas in the pyrolysis process produced a char having a high carbon content (93 wt%) and specific area of 618.6 $m^2/g$ compared to 87.6 wt% of carbon and 98.4 $m^2/g$ in $N_2$ environment at the pyrolysis temperature of 900 $^oC$ and particle size of 1 $cm^3$ cube (Table 4.6), which was slightly higher than those reported in literature (91 wt% of carbon and ~ 500 $m^2/g$) at identical operating conditions (González et al., 2009; Klinghoffer et al., 2012; Liu et al., 2018). This is because $CO_2$ reacts with the char leading to a collapse of the structure which was confirmed by SEM images showing highly porous char

in the $CO_2$ environment (Figure 4.5), which is consistent with previous studies (Cho et al., 2016; Lee et al., 2017). Therefore, char derived from $CO_2$ pyrolysis has potential use as adsorbent for waste water treatment. When 100% $CO_2$ as a carrier gas in the pyrolysis process, the gas mixture contained mainly CO (55.4 mol%) and 27.8 mol% $H_2$ compared to 47.6 mol% CO and 22.3 mol% $H_2$ obtained in the $N_2$ environment (Table 4.6). This is because $CO_2$ promotes char reactions ($C + CO_2 \rightarrow 2CO$) and $CO_2$ reforming reactions ($C_xH_y + xCO_2 \leftrightarrow 2xCO + \left(\frac{y}{2}\right)H_2$) in the process, leading to an increase $H_2$ and CO concentration in the gas stream. This was evidenced by a reduction of $CO_2$ and $CH_4$ in the gas stream and both the char and liquid fractions under $CO_2$ pyrolysis conditions (Table 4.6). The concentration of light hydrocarbons ($C_2$-$C_5$) in the gas phase was slightly increased from 1.6 mol% ($N_2$ atmosphere) to 2.2 mol% in $CO_2$, due to the cracking of high molecular weight compounds ($C_{5+}$) into lighter hydrocarbons or gaseous products (i.e. $H_2$ and $CH_4$).

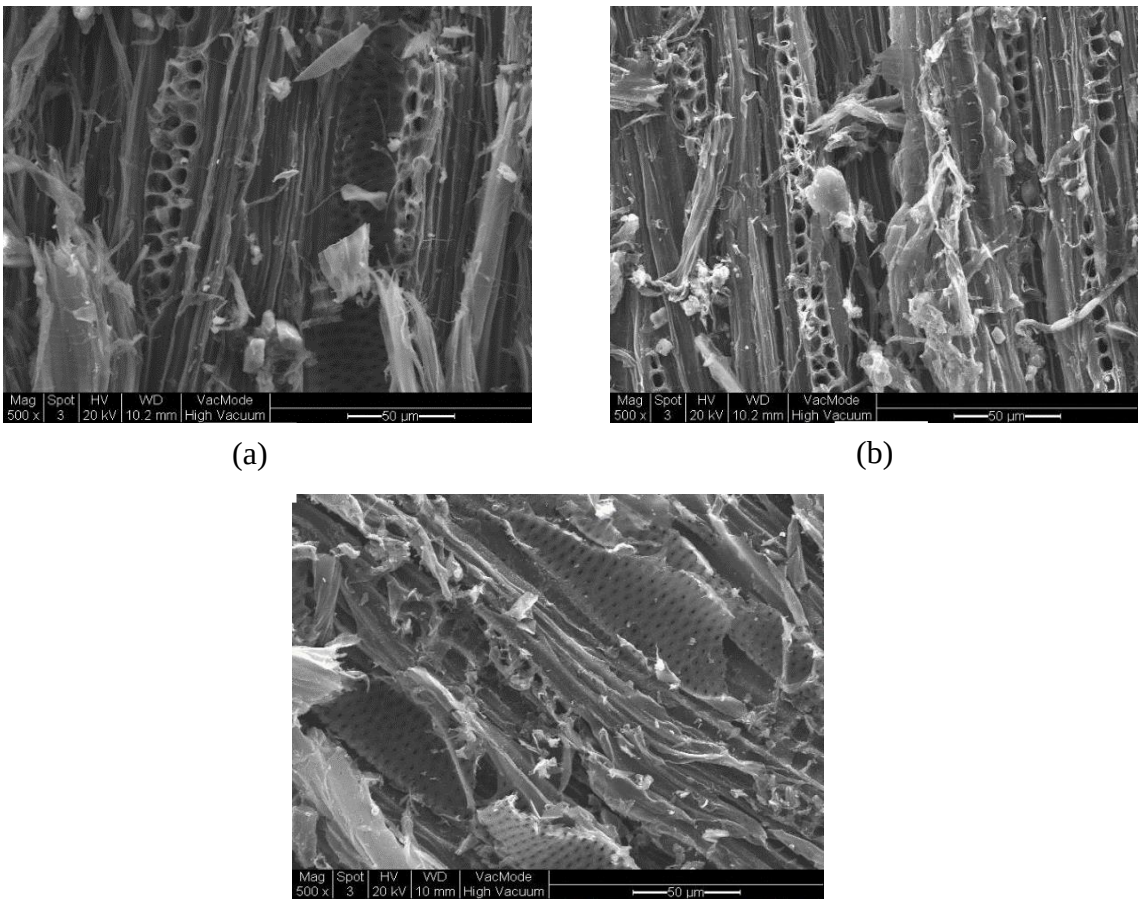


Figure 4.5: SEM images at a magnification of 500x of char obtained from (a) $CO_2$ (120 ml/min), (b) $CO_2/N_2$ ratio of 1/1 (60/60 ml/min) and (c) $N_2$ (120 ml/min) at pyrolysis temperature of 900 $^oC$ and particle size of 1 $cm^3$ cube.

Table 4.6: Yield and properties of pyrolysis products from pyrolysis of waste wood at various $CO_2$ concentration at a fixed pyrolysis temperature of 900 $^oC$ and particle size of 1 $cm^3$ cube.

| Operating condition | $CO_2/N_2$ (ml/min) | | | | | |
|---|---|---|---|---|---|---|
| | 120/0 | 100/20 | 60/60 | 40/80 | 20/100 | 0/120 |
| Char (wt%) | 15.9 ± 2.3 | 17.6 ± 1.7 | 17.9 ± 1.1 | 18.2 ± 0.7 | 20.0 ± 0.1 | 22.2 ± 1.1 |
| Liquid (wt%) | 35.4 ± 1.1 | 38.9 ± 0.6 | 44.4 ± 2.0 | 45.9 ± 0.8 | 47.7 ± 0.6 | 47.4 ± 1.4 |
| Gas* (wt%) | 48.7 ± 0.7 | 43.5 ± 1.1 | 37.7 ± 0.9 | 35.9 ± 1.4 | 32.3 ± 0.4 | 30.4 ± 0.8 |
| Char properties (dry basis) | | | | | | |
| Volatile matter (wt%) | 3.1 ± 2.4 | 3.4 ± 1.7 | 3.4 ± 1.9 | 3.3 ± 3.2 | 3.6 ± 1.1 | 3.6 ± 2.0 |
| Fixed carbon (wt%) | 92.5 ± 1.6 | 93.9 ± 1.1 | 93.2 ± 1.4 | 93.4 ± 2.1 | 93.5 ± 2.2 | 93.6 ± 1.3 |
| Ash (wt%) | 4.4 ± 0.7 | 2.7 ± 1.1 | 3.4 ± 0.3 | 3.3 ± 0.2 | 2.9 ± 1.0 | 2.8 ± 0.8 |
| C ± 0.3 (wt%) | 93.1 | 91.9 | 91.1 | 90.2 | 88.9 | 87.6 |
| H ± 0.3 (wt%) | 1.7 | 1.5 | 1.6 | 1.4 | 1.6 | 1.5 |
| O ± 0.5* (wt%) | 4.8 | 6.0 | 6.8 | 7.9 | 9.0 | 10.3 |
| N ± 0.3 (wt%) | 0.4 | 0.6 | 0.5 | 0.5 | 0.5 | 0.6 |
| HHV (MJ/kg) | 28.2 ± 2.1 | 28.9 ± 2.2 | 30.2 ± 1.4 | 30.6 ± 1.7 | 31.8 ± 1.1 | 33.6 ± 2.4 |

| | | | | | | |
|---|---|---|---|---|---|---|
| Surface area ($m^2/g$) | 618.6 ± 14.7 | 473.6 ± 16.1 | 376.1 ± 10.8 | 301.2 ± 14.5 | 297.9 ± 13.8 | 98.4 ± 4.6 |
| Liquid properties (wet basis) | | | | | | |
| C ± 0.3 (wt%) | 41.1 | 43.6 | 42.2 | 44.4 | 43.0 | 44.7 |
| H ± 0.3 (wt%) | 18.6 | 16.0 | 14.6 | 10.5 | 11.4 | 7.4 |
| O ± 0.5* (wt%) | 40.1 | 40.2 | 43.0 | 45.0 | 45.4 | 47.7 |
| N ± 0.3 (wt%) | 0.2 | 0.2 | 0.2 | 0.1 | 0.2 | 0.1 |
| Water content in liquid fraction (wt%) | 42.6 ± 2.2 | 41.5 ± 1.2 | 42.9 ± 1.5 | 43.0 ± 1.6 | 44.9 ± 0.7 | 43.7 ± 1.8 |
| HHV (MJ/kg) | 21.7 ± 3.3 | 19.7 ± 2.1 | 19.4 ± 1.4 | 17.1 ± 1.2 | 16.9 ± 1.8 | 17.2 ± 2.2 |
| Gas composition | | | | | | |
| $H_2$ (mol%) | 27.8 ± 2.2 | 27.3 ± 1.4 | 23.9 ± 2.3 | 22.2 ± 1.1 | 22.4 ± 1.6 | 22.3 ± 1.3 |
| CO (mol%) | 55.4 ± 0.7 | 57.7 ± 0.6 | 51.9 ± 1.5 | 53.7 ± 1.2 | 52.7 ± 2.4 | 47.6 ± 0.8 |
| $CO_2$ (mol%) | 4.0 ± 1.3 | 6.0 ± 1.1 | 15.0 ± 0.7 | 14.80 ± 2.3 | 14.4 ± 2.4 | 15.1 ± 1.1 |
| $CH_4$ (mol%) | 10.6 ± 0.4 | 6.1 ± 0.7 | 7.5 ± 1.3 | 7.3 ± 0.7 | 8.7 ± 1.1 | 13.4 ± 2.2 |
| $C_2$-$C_5$ (mol%) | 2.2 ± 0.3 | 2.9 ± 0.4 | 1.7 ± 0.1 | 2.0 ± 0.1 | 1.8 ± 0.4 | 1.6 ± 0.2 |

*By difference

The liquid product fraction derived from $CO_2$ pyrolysis still containing large amount of water, around 42 wt% (based on liquid fraction) compared to 44 wt% in $N_2$ environment (Table 4.6). However, the oxygen content in liquid decreased from 47.7 wt% in $N_2$ atmosphere to 40.1 wt% in $CO_2$ environment, leading to an increase in calorific value (HHV) from 17.2 MJ/kg to 21.7 MJ/kg (Table 4.6). The liquid fraction derived from $CO_2$ pyrolysis had a heating value of 21.7 MJ/kg, however it is still much lower than that of petroleum-based fuel oil (42-47 MJ/kg). As shown in Table 4.7 the $CO_2$ atmosphere resulted in increasing acid product yield (acetic acid in particular) from 0.7 wt% under $N_2$ to 1.8 wt% under $CO_2$, while phenol and its derivatives decreased by 35% (from 18.1 wt% $N_2$ to 11.7 wt% $CO_2$). It can be concluded that $CO_2$ pyrolysis could suppress the formation of benzene derivatives and polycyclic aromatic hydrocarbon (PAH) in the later stage of processing (Kwon and Castaldi, 2012; Kwon et al., 2015; Cho et al., 2016; Lee et al., 2017; Shen et al., 2017).

Table 4.7: Compositions in liquid from pyrolysis of waste wood (based on feedstock) at various $CO_2$ concentration at a fixed pyrolysis temperature of 900 $^oC$ and particle size of 1 $cm^3$ cube.

| Function groups | $CO_2/N_2$ (ml/min) | | | |
|---|---|---|---|---|
| | 120/0 | 100/20 | 40/80 | 0/120 |
| | wt% (dry basis) | | | |
| Acids | 1.8 | 1.5 | 1.4 | 0.7 |
| Esters | 1.3 | 1.1 | 0.8 | 0.6 |
| Ketones | 1.1 | 0.9 | 1.0 | 1.0 |
| Alcohols | 0.2 | 0.2 | 0.6 | 0.7 |
| Aldehydes | 0.7 | 0.9 | 1.1 | 0.6 |
| Furan and its derivatives | 3.0 | 3.6 | 4.2 | 3.7 |
| Phenol and its derivatives | 11.7 | 14.1 | 16.6 | 18.1 |
| Unknown | 0.4 | 0.3 | 0.5 | 1.3 |

### 4.3 The effect of pyrolysis conditions on the gasification process

The pyrolysis products derived from three different pyrolysis temperature (i.e. 600, 800 and 900 $^oC$) at a fixed particle size of 1 $cm^3$ cube and the selected carrier gas ($N_2$ or $CO_2$) flow rate of 120 ml/min were used to examine the effect of pyrolysis conditions on the gasification

process in terms of quality of synthetic gas (syngas) and tar formation via a two-stage gasification. Gasification was fixed at a temperature of 1000 °C and a steam to carbon in feedstock (S/C) molar ratio of 3.4. Table 4.8 shows in the $N_2$ environment the tar formation in the gas stream decreased from 38.9 g/Nm$^3$ (products derived at 600 °C pyrolysis) to 24.2 g/Nm$^3$ (products derived at 900 °C pyrolysis) corresponding to around 38% tar removal. This could be because high specific surface area and pore volume from char derived at high pyrolysis temperature (Table 4.2) promotes cracking/reforming of tar by adsorbed along the porosity distributed at the surface of char (Anis and Zainal, 2011; Paethanom and Yoshikawa, 2012; Liu et al., 2016; Shen and Fu, 2018).

Table 4.8: The effect of pyrolysis conditions on a two-stage gasification at a fixed particle size of 1 cm$^3$ cube, gasification temperature of 1000 °C and steam to carbon in feedstock (S/C) molar ratio of 3.4.

| Carrier gas | $N_2$ | | | $CO_2$ |
|---|---|---|---|---|
| Pyrolysis temperature (°C) | 600 | 800 | 900 | 900 |
| Gas yield* (wt%) | 86.1 ± 3.4 | 89.0 ± 2.1 | 94.8 ± 1.7 | 97.4 ± 1.8 |
| Solid residues (wt%) | 7.2 ± 1.4 | 3.1 ± 0.7 | 0.8 ± 1.1 | 0.2 ± 1.0 |
| Tar yield (wt%) | 6.7 ± 1.1 | 7.9 ± 1.4 | 4.4 ± 0.8 | 2.4 ± 0.8 |
| Tar in gas stream (g/Nm$^3$) | 38.9 | 32.1 | 24.2 | 9.1 |
| $CO_2$ (mol%) | 37.0 ± 2.3 | 31.9 ± 1.2 | 22.2 ± 1.2 | 5.6 ± 2.7 |
| $H_2$ (mol%) | 53.8 ± 1.3 | 58.8 ± 1.2 | 65.8 ± 1.0 | 77.7 ± 1.2 |
| $CH_4$ (mol%) | 4.7 ± 0.7 | 3.1 ± 1.2 | 2.2 ± 0.8 | 0.9 ± 2.1 |
| CO (mol%) | 4.5 ± 0.8 | 6.2 ± 1.1 | 9.8 ± 1.9 | 15.8 ± 2.1 |

*By difference

Moreover, high porosity of char also enhances accessing gasifying agent ($O_2$, $CO_2$ or steam) to form $H_2$ and CO via the heterogeneous solid-gas reactions occurs in the gasification process, i.e. the Boudouard reaction ($C + CO_2 \rightarrow 2CO$) and the water gas reaction ($C + H_2O \rightarrow 2CO + H_2$) (Menéndez et al., 2007; Ren et al., 2014). The $H_2$ and CO in the product gas increased from 53.8 mol% to 65.8 mol% and 4.5 mol% to 9.8 mol% with the products derived from pyrolysis temperature of 600 °C and 900 °C respectively in the $N_2$ environment (Table 4.8). Increasing

the pyrolysis temperature from 600 °C to 900 °C alters the gas yield (from 86.1 wt% to 94.8 wt%) at the expense of solid residues (ash) (from 7.2 wt% to 0.8 wt%) and unburnt carbon in the ash residues (< 0.01 wt%) at a fixed gasification temperature of 1000 °C and a steam to carbon in feedstock (S/C) molar ratio of 3.4 (Table 4.8). Using 100% $CO_2$ as a carrier gas in pyrolysis process could further decreased tar formation in the gas stream from 24.2 g/Nm$^3$ in $N_2$ environment to 9.1 g/Nm$^3$ in $CO_2$ environment corresponding to around 63% tar removal (Table 4.8). This is because the combination of $CO_2$ and steam promotes tar cracking reactions, i.e. the dry reforming reaction ($C_xH_y + xCO_2 \leftrightarrow 2xCO + \left(\frac{y}{2}\right)H_2$) and steam reforming reactions ($C_xH_y + xH_2O \leftrightarrow \left(\frac{y}{2} + x\right)H_2 + xCO$) occurs in the gasification process. An enhancement in gas properties (high CO concentration (55.4 mol%)) and improved the properties of char (high porosity (618.6 m$^2$/g)) and liquid fraction (low phenolic compounds (11.7 wt%)), results from the presence of $CO_2$ in the pyrolysis compared to 47.6 mol% CO in the gas stream, char surface area of 98.4 m$^2$/g and 18.1 wt% of phenolic compounds in the liquid product derived from the $N_2$ atmosphere at a temperature of 900 °C (Tables 4.6 and 4.7). Therefore, it promotes a significant reactions in the oxidation and reduction steps in the gasification process, i.e. the Boudouard reaction ($C + CO_2 \rightarrow 2CO$), the water gas reaction ($C + H_2O \rightarrow 2CO + H_2$), the water gas shift reaction ($CO + H_2O \leftrightarrow CO_2 + H_2$) and $CO_2$ reforming reactions ($C_xH_y + xCO_2 \leftrightarrow 2xCO + \left(\frac{y}{2}\right)H_2$), leading to the formation of $H_2$ (77.7 mol%) and CO (15.8 mol%) in the producer gas and increase in the gas yield up to 97.4 wt% at the expense of solid residues (ash) (0.2 wt%) (Table 4.8).

### 4.4 Summary

Pyrolysis in the range 600-900 °C has significantly influence on the char properties, i.e. increasing surface area and total pore size up to 2-3 times (from 38.6 m$^2$/g to 98.4 m$^2$/g) when increasing temperature, accelerating the heterogeneous solid-gas reactions. Increasing the pyrolysis temperature increased the $H_2$ content, i.e. from 12.5 mol% (600 °C) to around 22 mol% (900 °C), whilst decreasing hydrocarbons ($C_2$-$C_5$) and $CO_2$ in the gas stream. Pyrolysis temperatures above 700 °C fully decomposed unstable compounds, i.e. levoglucosan and their derivatives in the liquid fraction, but promoted the formation of phenolic compounds which are precursors for multi-ring aromatic species in the later stages of processing. A 41% reduction in surface area and total pore volume of the char was observed when increasing particle size from 0.5 cm$^3$ to 2 cm$^3$ cube. Nonetheless, only decreasing size to 0.5 cm$^3$ cube and applying a high temperature in pyrolysis would not be sufficient to produce the high $H_2$/CO ratio required for syngas applications (only 0.4-0.5 achieved). Using $CO_2$ as a carrier gas in pyrolysis alters the

gas yield (60%) at the expense of liquid (from 47.4 wt% to 35.4 wt%) and char (from 22.2 wt% to 15.9 wt%) fractions compared to that in a $N_2$ atmosphere at a temperature of 900 $^oC$. An enhancement in char properties with high carbon content (93 wt%) and surface area (618.6 $m^2/g$), results from the presence of $CO_2$ in the pyrolysis. The gas mixture under $CO_2$ pyrolysis contained mainly CO (55.4 mol%) and 27.8 mol% $H_2$ compared to CO (47.6 mol%) and $H_2$ (22.3 mol%) in a $N_2$ environment with similar $H_2$/CO ratio (0.5). Moreover, $CO_2$ improved the properties of liquid in terms of calorific value (21.7 MJ/kg) composition, which are closer to that needed for conversion to transportation fuel. Therefore, the use of $CO_2$ in pyrolysis could be a promising approach for utilisation of waste $CO_2$ and for energy production (i.e. $H_2$ and liquid fuel); it would therefore contribute significantly to the environmental and sustainability aspects of the process. In addition, $CO_2$ enhances the pyrolysis product properties (i.e. char with high porosity, high CO concentration in the gas stream and low phenolic compounds in the liquid product) that are required for high quality syngas/hydrogen production via a gasification process.

# Chapter 5 Gasification of waste wood

This chapter focuses on studying the effect of gasification operating parameters, i.e. temperature and steam to carbon in feedstock (S/C) molar ratio to maximise the $H_2$ production via the gasification process at a optimum the pyrolysis temperature of 900 $^oC$ and particle size of 1 $cm^3$ cube (based on the optimum conditions in the pyrolysis step observed in Chapter 4). The synergistic effect of $CO_2$ as gasifying agent and catalysts (Ni/MRM, $Ni/Al_2O_3$ and Ni/HZSM-5) was investigated and compared with the conventional steam gasification (i.e. in $N_2$) in terms of $H_2$ production, quality of synthetic gas (syngas), tar formation and process efficiency.

## 5.1 $N_2$/steam gasification

### 5.1.1 The effect of gasification temperature on product yields and properties

Table 5.1 shows that increasing gasification temperature significantly increased the gas yield, i.e. from 81.8 wt% (600 $^oC$) to 96.3 wt% (1000 $^oC$), which is higher than reported in literature (84-92 wt%) on steam biomass gasification at a temperatures range of 800-1200 $^oC$ (Chaudhari et al., 2001; Yan et al., 2010; Niu et al., 2017). The change in the gas yield was negligible when gasification temperature above 1000 $^oC$. The solid residue (ash) rapidly decreased from 14.3 wt% at 600 $^oC$ to 0.2 wt% at gasification temperature of 1000-1100 $^oC$ (Table 5.1). This was because the water gas reaction ($C + H_2O \rightarrow 2CO + H_2$) and Boudouard reaction ($C + CO_2 \rightarrow 2CO$), which are dominant at temperatures above 900 $^oC$ (Kwon et al., 2012; Liu et al., 2018) promoting $H_2$ and CO formation and increasing the carbon conversion in the process (Table 5.1). For every 100 $^oC$ increase in gasification step, the $H_2$ and CO concentration gradually increased by 6 mol% $H_2$ (from 48.8 mol% to 68.5 mol%) and 2 mol% CO (from 4.5 mol% to 13.7 mol%) while the concentrations of $CO_2$ and $CH_4$ decreased at the rates of 5 mol% $CO_2$ (from 39.9 mol% to 17.7 mol%) and 2 mol% for $CH_4$ (from 6.8 mol% to 0.1 mol%). This is because of the chemical reactions occurring in the gasification to generate $H_2$ and CO, i.e. steam reforming ($C_xH_y + xH_2O \leftrightarrow \left(\frac{y}{2} + x\right)H_2 + xCO$) and $CO_2$ reforming ($C_xH_y + xCO_2 \leftrightarrow 2xCO + \left(\frac{y}{2}\right)H_2$) favours forward reactions at high temperatures (i.e. > 700 $^oC$) (Nikoo and Amin, 2011; Demirel and Ayas, 2017; Liu et al., 2018). However, the tar yield remained around 3-4 wt% at all tested gasification temperature (Table 5.1), indicating that high temperature alone can not decompose the polycyclic aromatic hydrocarbon (PAH) compounds.

Table 5.1: Effect of gasification temperature on product yields and properties at a fixed particle size of 1 $cm^3$ cube, pyrolysis temperature of 900 $^oC$ and S/C molar ratio of 5.7 under $N_2$ atmosphere.

| Gasification temperature ($^oC$) | 600 | 800 | 900 | 1000 | 1100 |
|---|---|---|---|---|---|
| Solid residues (wt%) | 14.3 ± 1.2 | 10.8 ± 0.7 | 7.1 ± 1.1 | 0.2 ± 0.4 | 0.2 ± 0.5 |
| Gas yield* (wt%) | 81.8 ± 0.8 | 85.0 ± 1.6 | 89.1 ± 1.6 | 96.3 ± 1.0 | 96.7 ± 1.5 |
| Tar yield (wt%) | 3.9 ± 0.2 | 4.2 ± 0.4 | 3.8 ± 0.1 | 3.5 ± 0.3 | 3.1 ± 0.1 |
| Carbon conversion (%) | 59.8 ± 0.8 | 68.9 ± 1.3 | 76.6 ± 1.0 | 94.4 ± 0.9 | 95.1 ± 0.8 |
| $H_2$ (mol%) | 48.8 ± 2.4 | 53.8 ± 1.7 | 60.6 ± 2.7 | 67.2 ± 2.2 | 68.5 ± 2.0 |
| CO (mol%) | 4.5 ± 1.1 | 5.1 ± 1.3 | 6.7 ± 0.4 | 8.8 ± 1.2 | 13.7 ± 1.0 |
| $CO_2$ (mol%) | 39.9 ± 1.4 | 36.4 ± 2.4 | 29.8 ± 1.7 | 22.5 ± 2.6 | 17.7 ± 2.2 |
| $CH_4$ (mol%) | 6.8 ± 1.3 | 4.7 ± 0.7 | 2.9 ± 1.0 | 1.5 ± 1.0 | 0.1 ± 0.4 |
| $LHV_{syngas}$ ($MJ/Nm^3$) | 9.5 ± 1.8 | 9.6 ± 1.7 | 9.7 ± 2.1 | 10.3 ± 1.6 | 10.5 ± 1.3 |
| Cold gas efficiency (%) | 50.0 ± 1.0 | 59.1 ± 1.4 | 69.8 ± 1.2 | 95.6 ± 1.1 | 97.0 ± 1.0 |
| Process efficiency (%) | 42.4 ± 2.2 | 49.3 ± 1.7 | 57.8 ± 1.5 | 83.5 ± 1.4 | 85.6 ± 2.0 |

* By difference

As shown in Table 5.1 high $H_2$/CO ratios (5.0-10.8) in the syngas were obtained from all tested gasification temperatures compared to $H_2/CO \leq 1$ in air gasification (Lv et al., 2004; Leibbrandt et al., 2013; Rauch et al., 2014; Zeng et al., 2016). The calorific values of syngas ($LHV_{syngas}$) varied between 9.5 $MJ/Nm^3$ and 10.5 $MJ/Nm^3$ (Table 5.1), which is 2-3 times higher than for air gasification (3-6 $MJ/Nm^3$) (Dogru et al., 2002; Kalinci et al., 2009; Hernández et al., 2012; Kwiatkowski et al., 2013). This is because $O_2$ in air promoting undergoes combustion reactions of char and volatiles derived from the pyrolysis step to form $CO_2$ (30-40 mol%) (Atnaw et al., 2013; Kim et al., 2013b) instead of the fuel gas (i.e. $H_2$, CO and $CH_4$) compared to around 20-30 mol% $CO_2$ derived from steam gasification (Niu et al., 2017; Zhai et al., 2017; Shayan et al., 2018), resulting in a low calorific value of product gas. Increasing gasification temperature increased heating value of the syngas ($LHV_{syngas}$), thereby increase the cold gas efficiency (the ratio of heating value of syngas ($LHV_{syngas}$) to that of the feedstock), i.e. from 50% (600 $^oC$) to

96-97% at gasification temperature of 1000-1100 $^{o}$C (Table 5.1). If taking into account the total energy required to generate steam (0.05 MJ at S/C molar ratio of 5.7) and to heat feedstock, i.e. 0.02 MJ at 600 $^{o}$C and 0.05 MJ at 1100 $^{o}$C. The process efficiency was significantly increased up to 84-86% at a gasification temperature of 1000-1100 $^{o}$C from 42% at 600 $^{o}$C (Table 5.1) which is around 5-10% higher than reported in literature (Chaudhari et al., 2001; Ptasinski et al., 2007; Yan et al., 2010; Leibbrandt et al., 2013; Niu et al., 2017) on the efficiency of steam biomass gasification process.

Table 5.2: The composition of tar (based on feedstock) at various gasification temperatures at a fixed particle size of 1 cm$^3$ cube, pyrolysis temperature of 900 $^{o}$C and S/C molar ratio of 5.7 under $N_2$ atmosphere.

| Gasification temperature ($^{o}$C) | 600 | 800 | 900 | 1000 | 1100 |
|---|---|---|---|---|---|
| Tar in gas stream (g/Nm$^3$) | 42.9 | 38.1 | 30.5 | 21.2 | 17.7 |
| Heterocyclic aromatic (wt%) | 0.2 | 0.4 | 0.4 | 0.5 | 1.0 |
| Light PAH compounds (2-3 rings) (wt%) | 3.0 | 3.0 | 2.6 | 2.1 | 0.9 |
| Heavy PAH compounds (4-7 rings) (wt%) | 0.9 | 0.8 | 0.8 | 0.9 | 1.2 |
| Naphthalene and its derivatives in tar (wt%) | 1.1 | 1.2 | 1.2 | 1.2 | 0.2 |

As shown in Table 5.2, tar content in the product gas was significantly decreased from 42.9 g/Nm$^3$ to 17.7 g/Nm$^3$ (59% tar removal) when increasing gasification temperature from 600 $^{o}$C to 1100 $^{o}$C. The tar content in this study was lower than that obtained from steam biomass fixed-bed downdraft gasifier (30-80 g/Nm$^3$ or 10-27 wt% based on biomass feedstock) (Torres et al., 2007; Liu et al., 2012; Rauch et al., 2014), but higher than that in air biomass gasification (1-16 g/Nm$^3$) (Milne et al., 1998; Gil et al., 1999; Zhang et al., 2004). This is because the high molecular weight volatiles derived from the pyrolysis step are partially oxidised by $O_2$ in air, resulting in a reduction of tar in the producer gas (Gilbert et al., 2009; Weston et al., 2014). Nonetheless, the tar content in the syngas derived from both air and steam biomass gasification is still higher than the contaminant limits for a various syngas applications, i.e. heat and electricity generation using IC engines/gas turbines (< 0.1 g/Nm$^3$) and chemical synthesis, i.e.

methanol and liquid fuel via Fischer-Tropsch synthesis (< 0.001 g/Nm$^3$) (Tijmensen et al., 2002; Hamelinck et al., 2004; Leibold et al., 2008; Woolcock and Brown, 2013; Sikarwar et al., 2016; Li et al., 2018). The majority components in tar derived from biomass gasification were the light polycyclic aromatic hydrocarbons, consisting mainly of naphthalene constituents (Table 5.2), which is similar to others observations (Devi et al., 2003; Furusawa and Tsutsumi, 2005; Devi et al., 2006; Wolfesberger et al., 2009). Table 5.2 shows that gasification temperatures above 1000 $^o$C promotes the cracking of light PAH from 2.1 wt% at 1000 $^o$C to 0.9 wt% at 1100 $^o$C and naphthalene from 1.2 wt% to 0.2 wt%. However, the heavy PAH compounds (4-7 rings) remained around 0.9-1.2 wt% at all tested gasification temperatures (Table 5.2) due to their thermal stability (Myrén et al., 2002; Feng et al., 2017; Valderrama Rios et al., 2018). A similar finding was reported (Kinoshita et al., 1994; Brage et al., 2000; Feng et al., 2017) that an increasing gasification temperature above 900 $^o$C; it promotes the cracking of tar toward one-ring aromatics products (i.e. benzene, toluene and styrene), while the concentration of heavy PAH compounds (4-7 rings) remained constant over the tested range of gasification temperatures (500-1100 $^o$C). This indicates that even the combination of high temperature and steam could not decompose the heavy PAH compounds in tar derived from biomass gasification into lighter hydrocarbons or gaseous products.

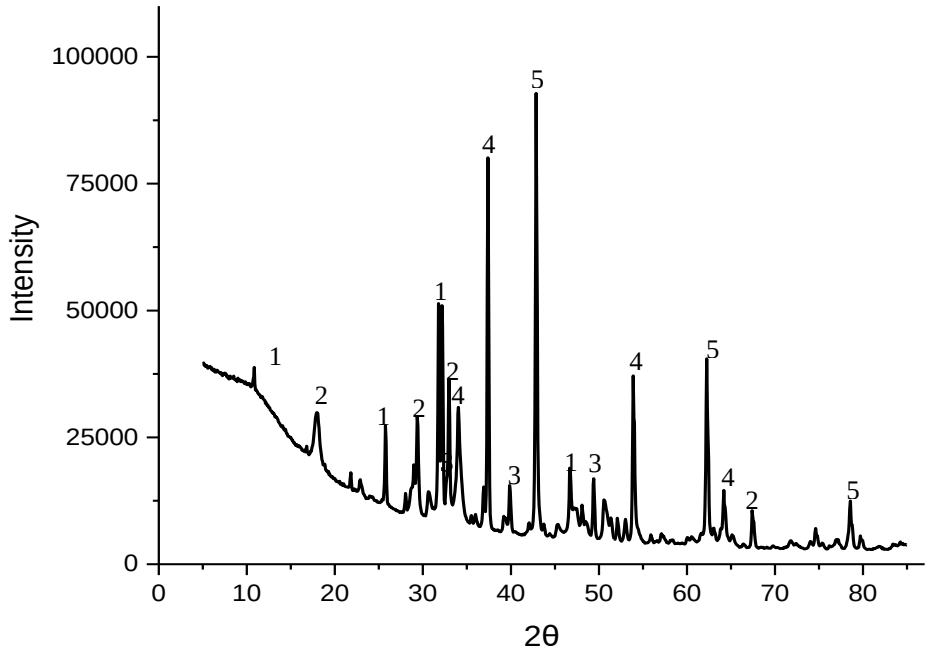


Figure 5.1: XRD spectrum of ash derived from gasification temperatures of 1000 $^o$C at a fixed particle size of 1 cm$^3$ cube, pyrolysis temperature of 900 $^o$C and S/C molar ratio of 5.7 under $N_2$ atmosphere (1: Hydroxylapatite ($Ca_5(PO_4)_3(OH)$), 2: Calcite ($CaCO_3$), 3: Takedaite ($Ca_3(BO_3)_2$), 4: Lime (CaO) and 5: Periclase (MgO)).

Solid residue (ash) contained the alkali and alkaline earth metals (AAEM) in the biomass feedstock consisting mainly of Si, Al, Fe, Ca, K, P, B and Mn, which transform into more stable species (crystalline phases) during the gasification process. It was reported (Liu et al., 2016; Shen and Fu, 2018) that these metals could act as catalysts for cracking/reforming of tar in the gasification process. However, these inorganic species could cause a number of challenges such as fouling, erosion and corrosion of installations as well as slagging and agglomeration when the gasification temperatures above 1200 $^{o}$C (melting point) (Fryda et al., 2008b; Werkelin et al., 2010). The gasification temperature in this study was in a range of 600-1100 $^{o}$C, which only just enough to transfer these metals into stable forms (crystalline phases), i.e. hydroxylapatite ($Ca_5(PO_4)_3(OH)$), calcite ($CaCO_3$), takedaite ($Ca_3(BO_3)_2$), lime (CaO) and periclase (MgO) (Figure 5.1). Little variation in the mineral phase composition was observed over the tested range gasification temperatures (600-1100 $^{o}$C).

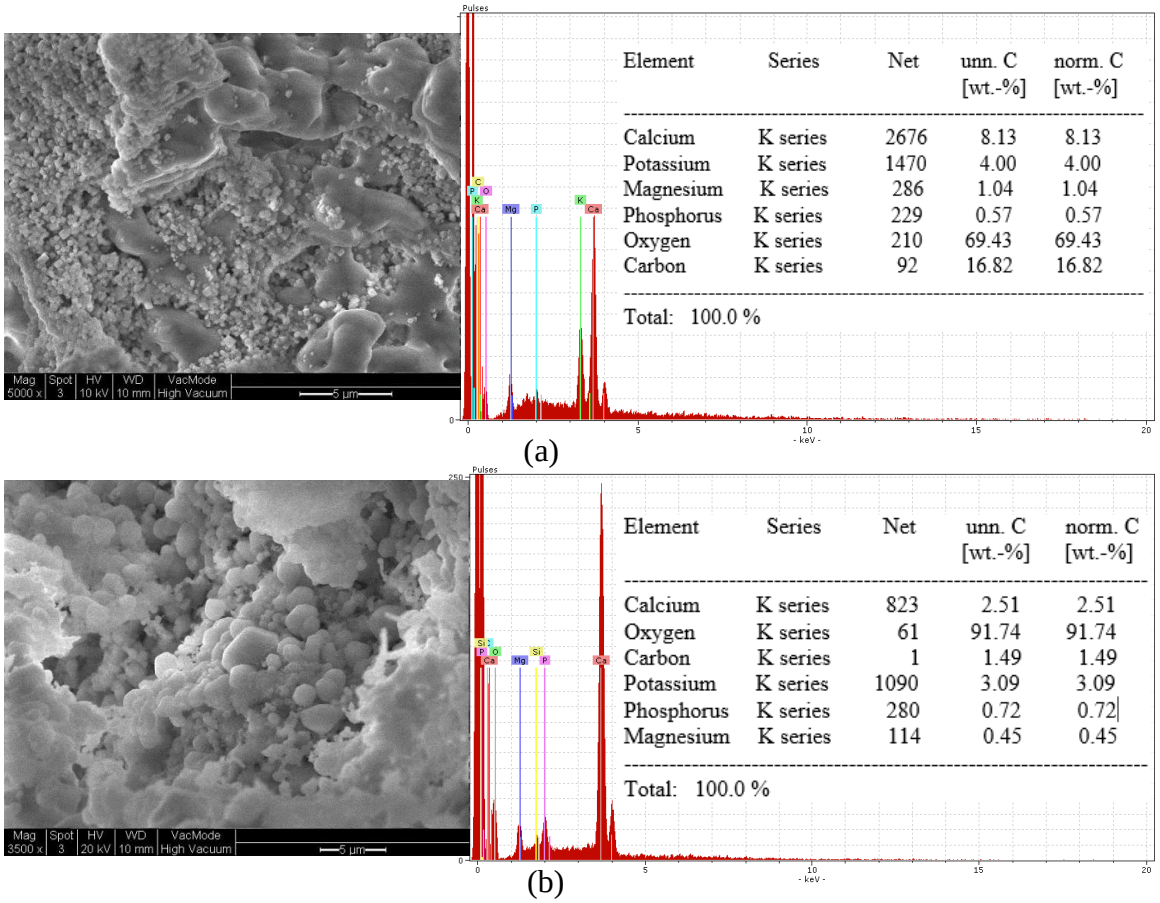


Figure 5.2: SEM images (magnification of 3500x) and elemental compositions of ash obtained at gasification temperature of (a) 600 $^{o}$C and (b) 1000 $^{o}$C at a fixed particle size of 1 $cm^3$ cube, pyrolysis temperature of 900 $^{o}$C and S/C molar ratio of 5.7 under $N_2$ atmosphere.

The EDXS results (Figure 5.2) shows the carbon remaining in the ash significantly decreased from 16.8 wt% at gasification temperature of 600 $^{o}$C (Figure 5.2a) to 1.5 wt% at gasification temperature of 1000 $^{o}$C (Figure 5.2b) with similar hydrogen content (< 1 wt%) remaining compared to 41.8 wt% carbon and 6.4 wt% hydrogen in waste wood sample (as described in Chapter 3). This indicates that most of the carbon and hydrogen in the feedstock is converted at gasification temperatures of 1000-1100 $^{o}$C, corresponded to around 94-95% carbon conversion efficiency (Table 5.1), which is higher than reported in literature (85-90%) on carbon conversion efficiency of steam biomass gasification process (Yan et al., 2010; Leibbrandt et al., 2013; Niu et al., 2017).

### 5.1.2 The effect of steam to carbon in feedstock (S/C) molar ratio on product yields and properties

The steam to carbon in feedstock (S/C) molar ratio is also an important parameter which has a strong influence in both the product yields and concentration of $H_2$ as well as the energy efficiency of the process. Applying steam in the gasification process resulted in a significant decrease in the solid residues, i.e. from 12.3 wt% with no steam injection to 0.2 wt% at a S/C molar ratio of 5.7-9.6 (Table 5.3). This is because steam promotes char reactions at a temperature range of 1000-1100 $^{o}$C (Kalinci et al., 2009), leading to a formation of gas products (from 84 wt% to 97 wt%) and increasing the carbon conversion (from 73% to 96%) in the gasification process (Table 5.3). However, the tar remained at around 3-4 wt% over the tested range S/C molar ratios (Table 5.3). Increasing S/C molar ratios increased $H_2$ and $CO_2$ concentration in the gas stream, i.e. from 51.0 mol% $H_2$ and 14.2 mol% $CO_2$ at no steam injection to 67.2 mol% $H_2$ and 22.5 mol% $CO_2$ at S/C molar ratios of 5.7, whereas the CO concentration gradually decreased from 28.8 mol% to 8.8 mol% (Table 5.3). This is due to steam promoting the water gas shift reaction at the gasification temperature range of 790-1050 $^{o}$C (Bustamante et al., 2002; Choi and Stenger, 2003; Demirel and Ayas, 2017). However, a further increase in S/C molar ratios above 5.7 caused a slight reduction in $H_2$ content from 67.2 mol% at S/C molar ratio of 5.7 to 62.0 mol% at S/C molar ratio of 9.6 (Table 5.3). This could be because increasing S/C molar ratio leads to a reduction of volatiles vapour residence time in the hot zone for reacting with char, steam or other gas, i.e. from 4 seconds at a S/C molar ratio of 5.7 to 1-2 seconds at S/C molar ratio of 9.6. A sufficient vapour residence time for biomass gasification was between 3 seconds and 4 seconds (Gil et al., 1997; Zhou et al., 2009; Hernández et al., 2010). Moreover, excessive amount of steam could cause a reduction of gasification temperature, which affects the chemical reactions toward $H_2$ production (i.e. water

gas reaction, water gas shift reaction and steam and $CO_2$ reforming reactions) (Yan et al., 2010; Ran and Li, 2012; Zhai et al., 2017). A similar observation was found in this study that the gasification temperature decreased from 1000 $^oC$ to around 912 $^oC$ and 880 $^oC$ when increasing S/C molar ratio to 7.7 and 9.6 respectively, whereas a difference was negligible at S/C molar ratio of 3.4 and 5.7. Thus, a tight control of S/C molar ratio is a crucial parameter in steam biomass gasification to maximise the $H_2$ production.

Table 5.3: The effect of S/C molar ratio on product yields and properties at a fixed particle size of 1 $cm^3$ cube, pyrolysis and gasification temperature of 900 $^oC$ and 1000 $^oC$ under $N_2$ atmosphere.

| S/C molar ratio | 0 | 3.4 | 5.7 | 7.7 | 9.6 |
|---|---|---|---|---|---|
| Solid residues (wt%) | 12.3 ± 0.3 | 0.8 ± 1.1 | 0.2 ± 0.4 | 0.2 ± 0.2 | 0.2 ± 0.3 |
| Gas yield* (wt%) | 83.5 ± 1.3 | 94.8 ± 1.7 | 96.3 ± 1.0 | 96.7 ± 0.8 | 96.9 ± 0.3 |
| Tar yield (wt%) | 4.2 ± 0.4 | 4.4 ± 0.5 | 3.5 ± 0.3 | 3.1 ± 0.3 | 2.9 ± 0.5 |
| Carbon conversion (%) | 72.7 ± 1.3 | 91.0 ± 1.4 | 94.4 ± 0.9 | 96.3 ± 1.0 | 96.2 ± 0.8 |
| $H_2$ (mol%) | 51.0 ± 1.7 | 65.8 ± 1.0 | 67.2 ± 2.2 | 64.9 ± 1.4 | 62.0 ± 1.1 |
| CO (mol%) | 28.8 ± 1.7 | 9.8 ± 0.9 | 8.8 ± 1.2 | 7.7 ± 1.2 | 7.1 ± 1.3 |
| $CO_2$ (mol%) | 14.2 ± 2.2 | 22.2 ± 1.2 | 22.5 ± 2.6 | 26.0 ± 1.7 | 29.6 ± 2.2 |
| $CH_4$ (mol%) | 6.0 ± 1.1 | 2.2 ± 0.8 | 1.5 ± 1.0 | 1.4 ± 1.6 | 1.3 ± 1.1 |
| $LHV_{syngas}$ ($MJ/Nm^3$) | 12.5 ± 1.2 | 11.7 ± 1.3 | 10.3 ± 1.6 | 8.7 ± 0.5 | 7.2 ± 0.4 |
| Cold gas efficiency (%) | 86.4 ± 0.8 | 95.1 ± 1.1 | 95.6 ± 1.1 | 84.2 ± 1.0 | 74.0 ± 1.8 |
| Process efficiency (%) | 77.0 ± 1.6 | 81.4 ± 1.4 | 83.5 ± 1.4 | 66.9 ± 1.5 | 56.9 ± 1.1 |

*By difference

Increasing S/C molar ratio had a negative effect on the heating value of the producer gas (Table 5.3), which is similar to results reported in literature (Udomsirichakorn and Salam, 2014; Zhai et al., 2017; Shayan et al., 2018). This is due to an increase of $CO_2$ concentration in the gas stream and decrease of CO and $CH_4$ when increasing S/C molar ratios (Table 5.3). The cold gas efficiency increased from 86.4% with no steam to 96% at a S/C molar ratio range of 3.4-5.7 and then decreased to 74% with a further increase in a S/C molar ratio to 9.6 (Table 5.3). This can be explained due to a reduction of $LHV_{syngas}$ at higher S/C molar ratios (Table 5.3). The

process efficiency decreased by 30% (from 81% to 57%) when increasing the S/C molar ratio from 3.4 to 9.6 (Table 5.3). This is due to energy required for steam production from 0.03 MJ to 0.1 MJ when increasing the S/C molar ratio from 3.4 to 9.6. The calculated process efficiency in this study does not take into account the energy required for separation of water out of the product gas via the downstream process of condensation, therefore the difference could be higher than what is reported here. Thus, controlling the amount of steam injection to achieve the best thermal efficiency is required in steam biomass gasification.

Table 5.4: The composition of tar (based on feedstock) obtained at various S/C molar ratio at a fixed particle size of 1 $cm^3$ cube, pyrolysis and gasification temperature of 900 $^oC$ and 1000 $^oC$ under $N_2$ atmosphere.

| S/C molar ratios | 0 | 3.4 | 5.7 | 7.7 | 9.6 |
|---|---|---|---|---|---|
| Tar in gas stream ($g/Nm^3$) | 34.7 | 24.2 | 21.2 | 20.8 | 20.6 |
| Heterocyclic aromatic (wt%) | 1.4 | 0.4 | 0.5 | 0.7 | 0.3 |
| Light PAH compounds (2-3 rings) (wt%) | 2.5 | 2.4 | 2.1 | 2.0 | 1.8 |
| Heavy PAH compounds (4-7 rings) (wt%) | 0.3 | 1.0 | 0.9 | 0.4 | 0.8 |
| Naphthalene and its derivatives in tar (wt%) | 1.6 | 1.4 | 1.2 | 1.1 | 0.9 |

Combining a high gasification temperature (1000 $^oC$) and steam enhancing the decomposition of tar content in the gas stream from 34.7 $g/Nm^3$ at no steam injection to 21 $g/Nm^3$ at S/C molar ratios of 5.7-9.6, corresponding to around 40% reduction (Table 5.4). This is because steam enhances the cracking of heavy hydrocarbon at temperature above 700 $^oC$ (Gilbert et al., 2009; Mayerhofer et al., 2012) evidenced by the increase in gas yield with increasing S/C molar ratios (Table 5.3). Increasing the S/C molar ratio led to a significantly decreased concentration of light PAH compounds, particularly naphthalene constituents, i.e. from 1.6 wt% at no steam injection to 0.9 wt% at a S/C molar ratio of 9.6 (Table 5.4). However, the heavy PAH compounds in tar was slightly increased from 0.3 wt% to 0.8 wt% in the gas stream when increasing S/C molar ratios (Table 5.4). This could be due to the recombination of the primary tar (i.e. phenol, benzene and toluene) via dimerization and cyclisation (H-abstraction-$C_2H_2$-addition sequence)

reactions in the presence of steam (Ledesma et al., 2000; Feng et al., 2017). As shown in Tables 5.2 and 5.4, increasing the gasification temperature exhibited a better tar removal (59%) than increasing S/C molar ratios (41%).

### 5.2 $CO_2$/steam gasification

As shown in Table 5.5, without steam injection, 100% $CO_2$ as the gasifying agent produced the gas containing mainly CO (81.3 mol%) followed by 18.0 mol% $H_2$ without $CO_2$ compared to 28.8 mol% CO, 51.0 mol% of $H_2$ and 14.2 mol% $CO_2$ in a $N_2$ environment. However, combining $CO_2$ and steam at a S/C molar ratio of 3.4 increased 4 times $H_2$ in the gas stream, i.e. from 18.0 mol% up to 77.7 mol% compared to 65.8 mol% $H_2$ in a $N_2$ atmosphere at identical operating conditions (Table 5.5). This is because steam and $CO_2$ promote char reactions and steam and dry reforming reactions of volatiles derived from the pyrolysis step at temperature above 700 $^oC$, enhancing the formation of $H_2$ and CO (Shen et al., 2017; Detchusananard et al., 2018). However, a further increase in S/C molar ratio above 3.4 in $CO_2$/steam gasification caused a slight reduction in $H_2$ (from 77.7 mol% to 68.1 mol%) but an increase in CO concentration (from 15.8 mol% to 24.0 mol%) (Table 5.5). This could be due to the reverse water gas shift reaction (Bustamante et al., 2002). As shown in Table 5.5, the producer gas contained a very small amount of $CO_2$ (maximum 7.0 mol% at S/C molar ratio of 5.7) when using 100% $CO_2$ as gasifying agent. When combining 100% $CO_2$ as gasifying agent with steam at a S/C molar ratio of 1.0, no $CO_2$ in the gas stream was observed (Table 5.5), suggesting all the $CO_2$ was reacted with char and volatiles derived from the pyrolysis step (Kwon et al., 2012; Leal et al., 2016). The carbon conversion efficiency (CCE) of $CO_2$/steam gasification increasing from 83.2% (no steam added) up to 96.9% at a S/C molar ratio of 3.4, which was comparable to a $N_2$/steam gasification (94.4%) at a S/C molar ratio of 5.7 (Table 5.5). Thus, 100% $CO_2$ as gasifying agent would be the desirable operating conditions for steam gasification process to convert biomass into fuels (i.e. $H_2$) as it required less steam than in a $N_2$/steam gasification to obtain high carbon conversion. Although, increasing the S/C molar ratios had no significant effect on the syngas heating value ($LHV_{syngas}$) derived from both $N_2$ and $CO_2$ steam gasification (Table 5.5) which is also observed in literature (Chaiwatanodom et al., 2014; Pohořelý et al., 2014). The cold gas efficiency increased with increasing S/C molar ratio, i.e. from 70.3% at no steam injection to 97.6% at a S/C molar ratio of 3.4 under $CO_2$ environment (Table 5.5). This is due to a significant increase in gas yield from 86.1 wt% (no steam injection) to 97.4 wt% at a S/C molar ratio of 3.4 at the expense of solid (from 11.2 wt% to 0.2 wt%) and tar (from 2.7 wt% to 2.5 wt%) fractions (Table 5.5). A further increase in a S/C molar ratio above 3.4 caused a reduction in the cold gas efficiency due to the decrease in $H_2$ content (Table 5.5). If taking

into account the energy required to heat biomass from 25 $^{o}$C to 1000 $^{o}$C (0.05 MJ) and for steam production, i.e. 0.01 MJ at a S/C molar ratio of 1.0 and 0.03 MJ at S/C molar ratio of 3.4. The process efficiency of $CO_2$/steam gasification was low (around 64%) at no steam injection but increased up to 97.3% at a S/C molar ratio of 3.4 and decreased to 84.8% with a further increase in a S/C molar ratio (Table 5.5). The process efficiency at all tested S/C molar ratio in $CO_2$/steam gasification (Table 5.5) was higher than that in a $N_2$/steam gasification observed in this study (81-84%) and in literature (70-80%) (Yan et al., 2010; Leibbrandt et al., 2013; Niu et al., 2017). Therefore, the use of 100% $CO_2$ as a carrier gas in steam gasification could be a promising way for utilisation of waste $CO_2$ for energy/$H_2$ production as well as improve the gasification process in terms of conversion and energy efficiency.

Table 5.5: Product yields and properties in $N_2$ and $CO_2$ steam gasification at various S/C molar ratio at a fixed particle size of 1 $cm^3$ cube and pyrolysis and gasification temperature of 900 $^oC$ and 1000 $^oC$.

| Operating conditions | $N_2$ | | | $CO_2$ | | | | |
|---|---|---|---|---|---|---|---|---|
| | S/C molar ratio | | | | | | | |
| | 0 | 3.4 | 5.7 | 0 | 1.0 | 2.7 | 3.4 | 5.7 |
| Solid residues (wt%) | 12.3 ± 0.3 | 0.8 ± 1.1 | 0.2 ± 0.4 | 11.2 ± 1.3 | 4.2 ± 2.0 | 0.3 ± 1.7 | 0.2 ± 1.0 | 0.1 ± 0.8 |
| Gas yield* (wt%) | 83.5 ± 1.3 | 94.8 ± 1.7 | 96.3 ± 1.0 | 86.1 ± 1.8 | 93.1 ± 1.1 | 97.2 ± 2.4 | 97.4 ± 1.8 | 97.5 ± 1.0 |
| Tar yield (wt%) | 4.2 ± 0.4 | 4.4 ± 0.5 | 3.5 ± 0.3 | 2.7 ± 1.3 | 2.7 ± 0.8 | 2.5 ± 1.0 | 2.5 ± 0.9 | 2.4 ± 0.2 |
| Carbon conversion (%) | 72.7 ± 1.3 | 91.0 ± 1.4 | 94.4 ± 0.9 | 83.2 ± 1.1 | 91.0 ± 0.3 | 96.0 ± 0.7 | 96.9 ± 0.4 | 96.3 ± 0.6 |
| $H_2$ (mol%) | 51.0 ± 1.7 | 65.8 ± 1.0 | 67.2 ± 2.2 | 18.0 ± 2.5 | 69.1 ± 1.9 | 77.4 ± 1.7 | 77.7 ± 1.3 | 68.1 ± 1.5 |
| CO (mol%) | 28.8 ± 1.7 | 9.8 ± 0.9 | 8.8 ± 1.2 | 81.3 ± 2.5 | 29.9 ± 2.7 | 16.8 ± 0.5 | 15.8 ± 0.6 | 24.0 ± 1.6 |
| $CO_2$ (mol%) | 14.2 ± 2.2 | 22.2 ± 1.2 | 22.5 ± 2.6 | 0 | 0 | 4.9 ± 1.2 | 5.6 ± 1.8 | 7.0 ± 1.0 |
| $CH_4$ (mol%) | 6.0 ± 1.1 | 2.2 ± 0.8 | 1.5 ± 1.0 | 0.7 ± 0.2 | 1.0 ± 0.7 | 0.9 ± 0.1 | 0.9 ± 0.5 | 0.9 ± 0.2 |
| $LHV_{syngas}$ ($MJ/Nm^3$) | 12.5 ± 1.2 | 11.7 ± 1.3 | 10.3 ± 1.6 | 13.2 ± 1.0 | 12.8 ± 0.4 | 12.4 ± 0.4 | 12.3 ± 0.3 | 12.1 ± 0.1 |
| Cold gas efficiency (%) | 86.4 ± 0.8 | 95.1 ± 1.1 | 95.6 ± 1.1 | 70.3 ± 1.1 | 87.1 ± 1.0 | 94.4 ± 0.3 | 97.6 ± 0.5 | 88.7 ± 0.8 |
| Process efficiency (%) | 77.0 ± 1.6 | 81.4 ± 1.4 | 83.5 ± 1.4 | 64.2 ± 1.3 | 86.4 ± 0.9 | 93.0 ± 1.6 | 97.3 ± 0.4 | 84.8 ± 1.1 |

*By difference

Increasing $CO_2$ percentage from 16% ($CO_2/N_2$ ratio of 20/100) to 100% $CO_2$ in the carrier gas increased CO (from 7.2 mol% to 15.8 mol%) and $H_2$ (from 72.3 mol% to 77.7 mol%) compared to 9.8 mol% CO and 65.8 mol% $H_2$ in the $N_2$ atmosphere at a fixed S/C molar ratio of 3.4 (Table 5.6). $CO_2$ concentration in the carrier gas promotes the reactions between $CO_2$ and char and other hydrocarbons/oxygenated compounds at temperature above 700 $^oC$ (Gilbert et al., 2009; Mayerhofer et al., 2012), leading to a formation of $H_2$ and CO. This was evidenced by the gas yield increased from 94.8 wt% in a $N_2$ atmosphere to 96.2 wt% at 16% $CO_2$ ($CO_2/N_2$ ratio of 20/100) and 97.4 wt% at 100% $CO_2$ in the carrier gas at the expense of solid (from 0.8 wt% in a $N_2$ to 0.2 wt% in a $CO_2$) and tar (from 4.4 wt% in a $N_2$ to 2.5 wt% in a $CO_2$) fractions (Table 5.6). As shown in Table 5.6, the $CO_2$ concentration in the gas products (outlet) derived from all tested $CO_2$ gasifying conditions at a fixed S/C molar ratio of 3.4 (i.e. 15.2 mol% at 33% $CO_2$ ($CO_2/N_2$ ratio of 40/80) and 5.6 mol% at 100% $CO_2$ in the carrier gas) was much lower than in a $N_2$/steam gasification in this study (22.2 mol%) and in literature (20-30 mol%) (Chaudhari et al., 2001; Udomsirichakorn and Salam, 2014; Zhai et al., 2017; Shayan et al., 2018). The $CH_4$ concentration decreased from 1.8 mol% to 0.9 mol% when increasing $CO_2$ concentration in a carrier gas (Table 5.6), due to the dry reforming reaction promoted by $CO_2$ (Chaiwatanodom et al., 2014; Sadhwani et al., 2016). The gasification process efficiency was significantly increased by 20% (from 81.4% in a $N_2$ atmosphere to 97.3% in a $CO_2$ atmosphere) at a fixed S/C molar ratio of 3.4 (Table 5.6). The calculated process efficiency in this study does not take into account the energy required for $N_2$ separation in the case of using $N_2$ or air as a carrier gas in gasification process, therefore the difference could be higher than what is reported here. If using the flue gas produced from a typical power plant, i.e. a coal-fired plant (10-16 mol% $CO_2$) (Sass et al., 2005; Lee et al., 2008; Songolzadeh et al., 2014) as gasifying agent in the gasification process for $H_2$ production, the case is almost equivalent to the $CO_2/N_2$ ratio of 20/100 (16% $CO_2$) in this study with results shown in Table 5.6, up to 72.3 mol% $H_2$ can be produced at a S/C molar ratio of 3.4, compared to only 65.8 mol% $H_2$ generated from $N_2$/steam gasification at identical conditions (Table 5.6). Therefore, the direct use of flue gas as a carrier gas in steam gasification process of biomass/waste residues will be a promising approach to utilise waste $CO_2$ to increase the sustainability in terms of both environmental and economical drivers for an industrial process.

Table 5.6: Effect of $CO_2$ concentration in the carrier gas on product yields and properties in steam gasification process at a fixed particle size of 1 $cm^3$ cube, pyrolysis and gasification temperature of 900 $^oC$ and 1000 $^oC$ and S/C molar ratio of 3.4.

| Operating conditions | $CO_2/N_2$ (ml/min) | | | | | |
|---|---|---|---|---|---|---|
| | 0/120 | 20/100 | 40/80 | 60/60 | 100/20 | 120/0 |
| Solid residues (wt%) | 0.8 ± 1.1 | 0.3 ± 1.2 | 0.3 ± 0.4 | 0.2 ± 1.1 | 0.2 ± 0.7 | 0.2 ± 1.0 |
| Gas yield* (wt%) | 94.8 ± 1.7 | 96.2 ± 2.3 | 96.4 ± 1.1 | 97.0 ± 0.7 | 97.1 ± 1.9 | 97.4 ± 1.8 |
| Tar yield (wt%) | 4.4 ± 0.5 | 3.5 ± 0.9 | 3.3 ± 0.2 | 2.8 ± 0.4 | 2.7 ± 0.7 | 2.5 ± 0.9 |
| Carbon conversion (%) | 91.0 ± 1.4 | 93.1 ± 1.1 | 94.0 ± 0.3 | 94.7 ± 0.6 | 96.6 ± 0.3 | 96.9 ± 0.4 |
| $H_2$ (mol%) | 65.8 ± 1.0 | 72.3 ± 2.0 | 72.5 ± 1.4 | 73.9 ± 1.2 | 74.5 ± 2.2 | 77.7 ± 1.3 |
| CO (mol%) | 9.8 ± 0.9 | 7.2 ± 0.4 | 10.5 ± 1.6 | 13.2 ± 1.3 | 14.8 ± 0.8 | 15.8 ± 0.6 |
| $CO_2$ (mol%) | 22.2 ± 1.2 | 18.7 ± 0.2 | 15.2 ± 0.6 | 11.1 ± 1.2 | 9.8 ± 0.8 | 5.6 ± 1.8 |
| $CH_4$ (mol%) | 2.2 ± 0.8 | 1.8 ± 0.3 | 1.8 ± 0.3 | 1.8 ± 0.4 | 0.9 ± 0.1 | 0.9 ± 0.5 |
| $LHV_{syngas}$ (MJ/ $Nm^3$) | 11.7 ± 1.3 | 11.5 ± 0.3 | 11.8 ± 0.7 | 11.8 ± 0.4 | 12.1 ± 0.1 | 12.3 ± 0.3 |
| Cold gas efficiency (%) | 95.1 ± 1.1 | 95.4 ± 1.0 | 96.0 ± 0.7 | 96.9 ± 1.3 | 97.6 ± 0.2 | 97.6 ± 0.5 |
| Process efficiency (%) | 81.4 ± 1.4 | 89.3 ± 2.0 | 93.7 ± 1.4 | 94.9 ± 0.7 | 96.1 ± 0.4 | 97.3 ± 0.4 |

* By difference

Table 5.7: The composition of tar (based on feedstock) under various gasification conditions at a fixed particle size of 1 $cm^3$ cube and pyrolysis and gasification temperature of 900 $^oC$ and 1000 $^oC$.

| Operating conditions | $N_2$ | | $CO_2$ | | | $CO_2/N_2$ (ml/min) | | | |
|---|---|---|---|---|---|---|---|---|---|
| | | | | | | 100/20 | 60/60 | 40/80 | 20/100 |
| | S/C molar ratios | | | | | | | | |
| | 0 | 3.4 | 0 | 2.7 | 3.4 | | | | |
| Tar in gas stream ($g/Nm^3$) | 34.7 | 24.2 | 27.5 | 9.4 | 9.1 | 11.9 | 12.6 | 16.4 | 18.3 |
| Heterocyclic aromatic (wt%) | 1.4 | 0.4 | 0.4 | 0.3 | 0.2 | 0.2 | 0.2 | 0.3 | 0.1 |
| Light PAH compounds (2-3 rings) (wt%) | 2.5 | 2.4 | 1.7 | 1.5 | 1.3 | 1.6 | 1.9 | 2.3 | 2.7 |
| Heavy PAH compounds (4-7 rings) (wt%) | 0.3 | 1.0 | 0.6 | 0.7 | 0.9 | 0.9 | 0.7 | 0.7 | 0.7 |
| Naphthalene and its derivatives in tar (wt%) | 1.6 | 1.4 | 2.1 | 1.9 | 0.7 | 1.3 | 1.2 | 1.5 | 1.7 |

Table 5.7 shows using 100% $CO_2$ as gasifying agent up to 21% reduction in tar in the gas stream (from 34.7 g/Nm$^3$ in a $N_2$ atmosphere to 27.5 g/Nm$^3$ in a $CO_2$ atmosphere) at no steam injection condition. When combining $CO_2$ and steam remove up to 67% tar in the gas stream (from 27.5 g/Nm$^3$ at no steam injection to 9.1 g/Nm$^3$ at S/C molar ratio of 3.4). The tar content in $CO_2$/steam gasification was much lower than $N_2$/steam gasification (24.2 g/Nm$^3$) at identical conditions in this study and other (30-80 g/Nm$^3$) (Torres et al., 2007; Liu et al., 2012; Rauch et al., 2014). This is due to the combination of $CO_2$ and steam promoting the cracking of tar via steam and dry reforming reactions (Nikoo and Amin, 2011; Demirel and Ayas, 2017; Liu et al., 2018). Moreover, an enhancement in char properties (high porosity; 618 m$^2$/g) results from the presence of $CO_2$ in the pyrolysis compared to 98.4 m$^2$/g in a $N_2$ atmosphere (as described in Chapter 4) also promotes the tar cracking/reforming process by adsorbed along the porosity distributed at the surface of char (Anis and Zainal, 2011; Paethanom and Yoshikawa, 2012; Liu et al., 2016; Shen and Fu, 2018). At a fixed S/C molar ratio of 3.4, the tar gradually decreased with increasing $CO_2$ percentage in the carrier gas, i.e. from 18.3 g/Nm$^3$ at 16% $CO_2$ ($CO_2$/$N_2$ ratio of 20/100) to 12.6 g/Nm$^3$ at 50% $CO_2$ ($CO_2$/$N_2$ ratio of 60/60) and 11.9 g/Nm$^3$ at 83% $CO_2$ ($CO_2$/$N_2$ ratio of 100/20) respectively (Table 5.7) which is similar to what is reported in literature by others (Renganathan et al., 2012; Feng et al., 2017). As shown in Table 5.7 a low $CO_2$ concentration than 50% ($CO_2$/$N_2$ ratio of 60/60) in the carrier gas had no significant effect on the tar compositions compared to $N_2$/steam gasification at a fixed S/C molar ratio of 3.4. However, a significantly decreased of light PAH compounds; particularly naphthalene constituents was observed when increasing S/C molar ratio, i.e. 2.1 wt% at no steam injection to 1.9 wt% at a S/C molar ratio of 2.7 and 0.7 wt% at a S/C molar ratio of 3.4 in $CO_2$/steam gasification (Table 5.7). Although, the heavy PAH compounds (4-7 rings) remained around 0.6-0.9 wt% at all tested $CO_2$ conditions.

### 5.3 Catalytic steam gasification

Three different types of Ni-based catalysts, namely Ni/MRM, Ni/HZSM-5 and Ni/$Al_2O_3$ were chosen in this study, which was placed at the end of char bed in the gasification reactor (as described in section 3.3.2). The effect of catalysts on the quality of syngas and tar formation was tested in both $N_2$ and $CO_2$ steam gasification at a fixed pyrolysis and gasification temperature of 900 $^o$C and 1000 $^o$C. The S/C molar ratio was fixed at 5.7 for the $N_2$ environment and 3.4 for the $CO_2$ environment (based on the optimum condition for the highest hydrogen production as described in sections 5.1 and 5.2).

### 5.3.1 The effect of catalyst in $N_2$/steam gasification

Applying catalyst in the gasification process slightly increased the gas yield to 98 wt% from 96 wt% in non-catalytic condition at the expense of tar yield (from 4 wt% to 1 wt%) whereas the solid residue (ash) remained constant at around 0.2-0.3 wt% with all tested catalysts (Table 5.8). This is due to the Ni-based catalyst enhanced the cleavage of C-C and C-H bonds in tar through α-scissions to form lighter hydrocarbons or gaseous products (i.e. $H_2$ and $CH_4$) (Richardson et al., 2010; Xie et al., 2012; Alipour Moghadam Esfahani et al., 2017). Table 5.8 shows that catalysts had little influence on the gas composition. The concentration of $CH_4$ decreased from around 2 mol% in non-catalytic condition to 0.1-0.2 mol% in the presence of Ni-based catalysts, indicating that Ni-based catalysts enhance the methane reforming (Chan and Tanksale, 2014; Baktash et al., 2015). Although, the $H_2$ and $CO_2$ concentrations in the gas stream slightly increased by 5% (from 67 mol% to 70 mol%) and 13% (from 23 mol% to 26 mol%) respectively, while CO content was decreased from 9 mol% to 5 mol% in the presence of Ni-based catalyst (Table 5.8). This phenomenon can be explained due to the water gas shift reaction occurs in steam gasification process promoted by the Ni-based catalyst (Abu El-Rub et al., 2004; Torres et al., 2007; Valderrama Rios et al., 2018).

The tar content in the gas stream significantly decreased from 21.2 g/$Nm^3$ (non-catalytic) to 6.0 g/$Nm^3$ (around 72% tar removal) for all three Ni-based catalysts (Table 5.8). As shown in Table 5.8, all tar components decreased their concentration; particularly the heavy PAH compounds in the presence of Ni-based catalyst agreed very well with other findings (Torres et al., 2007; de Lasa et al., 2011). Therefore, Ni-based catalyst is a promising catalyst for tar removal in biomass gasification as it can remove up to 67% of the heavy PAH compounds in tar from 0.9 wt% in non-catalytic $N_2$/steam gasification to 0.3 wt% in catalytic $N_2$/steam gasification shown in Table 5.8, which can not be removed by changing the operating conditions in $N_2$/steam gasification, i.e. temperatures or S/C molar ratio shown in Tables 5.2 and 5.4. It can be observed that the Ni/MRM catalyst removes up to 58% naphthalene in the product gas (from 1.2 wt% at non-catalytic condition to 0.5 wt%) compared to only 50% reduction for the commercial Ni-based catalyst, i.e. Ni/HZSM-5 and Ni/$Al_2O_3$ (Table 5.8). This is due to a variety of metal oxides, i.e. NiO, $SiO_2$, $Al_2O_3$, $Fe_2O_3$, $TiO_2$, CaO, MgO, $Na_2O$, $P_2O_5$ and MnO in the Ni/MRM (as described in 3.2.2), which enhance tar cracking/reforming (naphthalene in particular) (Madadkhani, 2016; Valderrama Rios et al., 2018).

Table 5.8: Effect of Ni-based catalysts on the products yield and properties at a fixed particle size of 1 $cm^3$ cube, pyrolysis and gasification temperature of 900 $^oC$ and 1000 $^oC$ and S/C molar ratio of 5.7 under $N_2$ atmosphere.

| Catalysts | Non-catalytic | Ni/MRM | $Ni/Al_2O_3$ | Ni/HZSM-5 |
|---|---|---|---|---|
| Solid residues (wt%) | 0.2 ± 0.4 | 0.3 ± 0.4 | 0.3 ± 0.2 | 0.3 ± 0.3 |
| Gas yield* (wt%) | 96.3 ± 1.0 | 98.7 ± 2.2 | 98.7 ± 1.0 | 98.7 ± 1.6 |
| Tar yield (wt%) | 3.5 ± 0.3 | 1.0 ± 0.4 | 1.0 ± 0.1 | 1.0 ± 0.2 |
| Tar in gas stream ($g/Nm^3$) | 21.2 | 5.9 | 5.5 | 5.7 |
| Heterocyclic aromatic (wt%) | 0.5 | 0.2 | 0.3 | 0.1 |
| Light PAH compounds (2-3 rings) (wt%) | 2.1 | 0.5 | 0.4 | 0.7 |
| Heavy PAH compounds (4-7 rings) (wt%) | 0.9 | 0.3 | 0.3 | 0.2 |
| Naphthalene and its derivatives in tar (wt%) | 1.2 | 0.5 | 0.4 | 0.6 |
| $H_2$ (mol%) | 67.2 ± 2.2 | 69.6 ± 1.3 | 70.3 ± 1.0 | 69.3 ± 1.1 |
| CO (mol%) | 8.8 ± 1.2 | 4.4 ± 1.0 | 5.2 ± 1.2 | 5.0 ± 1.1 |
| $CO_2$ (mol%) | 22.5 ± 2.6 | 25.8 ± 1.7 | 24.3 ± 1.4 | 25.5 ± 1.7 |
| $CH_4$ (mol%) | 1.5 ± 1.0 | 0.2 ± 1.1 | 0.1 ± 1.1 | 0.2 ± 1.0 |

*By difference

However, the major problem of using Ni/MRM as a catalyst is the deactivation of catalyst after two gasification cycles compared to $Ni/Al_2O_3$ and Ni/HZSM-5 which are still active after the third cycles (Table 5.9). This was evidenced by the rise in tar yield (from 1 wt% to 4 wt%) at the expense of gas yield (from 98 wt% to 96 wt%) after the second cycle which is equal to the results obtained from non-catalytic conditions (Table 5.9). However, $Ni/Al_2O_3$ and Ni/HZSM-5 catalysts showed almost stable catalytic performance over the third cycle (Table 5.9). Decreasing in the surface area (12.0 $m^2/g$), total pore volume (0.01 $cm^3/g$) and pore size distribution (1.0-2.1 nm) of Ni/MRM was observed after the second cycle compared to that in

fresh catalyst (114.8 $m^2$/g, 0.1 $cm^3$/g and 1.7-3.1 nm) (Table 5.10). This could be because the catalyst pores were clogged/blocked by heavy compounds (tar) and coke deposition during the cracking process over time, corresponding to the loss of catalytic activity (Wang et al., 1998; Sehested, 2006; Serrano et al., 2012; Wang et al., 2014). It was confirmed via SEM images showing in the spent Ni/MRM the circular granules were less prominent (smoother) and more sintered at the surface than in the fresh catalyst (Figure 5.3a). However, for $Ni/Al_2O_3$ and Ni/HZSM-5 catalyst there was no significant change in the catalyst morphology (Figures 5.3b and c) and surface area and pores distribution (Table 5.10).

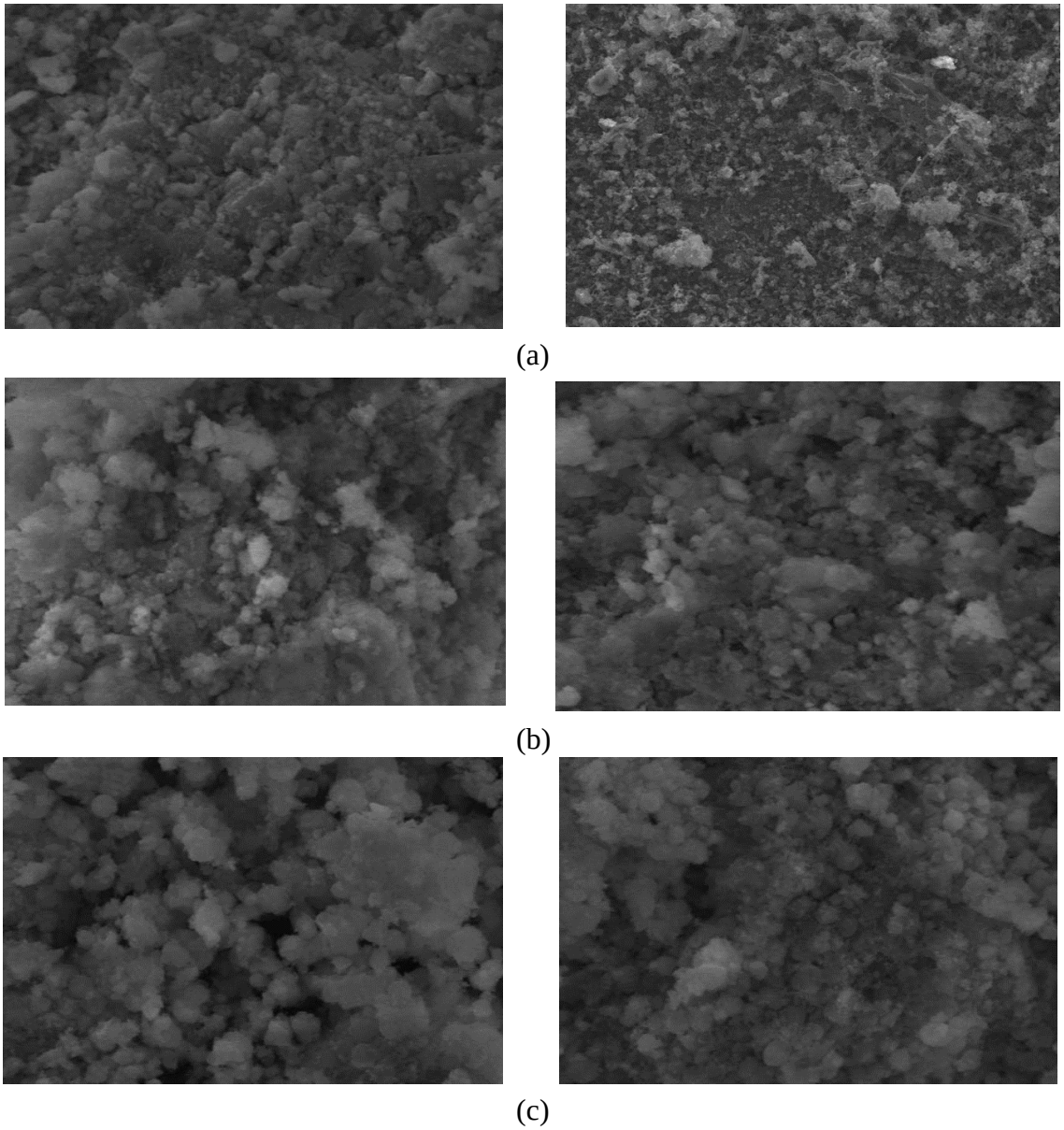

Figure 5.3: SEM image at a magnification of 3500x of fresh (left) and spent (right) Ni-based catalyst after the second cycle at a fixed pyrolysis and gasification temperature of 900 $^oC$ and 1000 $^oC$ and S/C molar ratio of 5.7 under $N_2$ atmosphere: (a) Ni/MRM, (b) $Ni/Al_2O_3$ and (c) Ni/HZSM-5.

Table 5.9: The performance of Ni-based catalyst over the consecutive cycles at a fixed particle size of 1 $cm^3$ cube, pyrolysis and gasification temperature of 900 ºC and 1000 ºC and S/C molar ratio of 5.7 under $N_2$ atmosphere.

| Number of cycles | Non-catalytic | Ni/MRM | | | Ni/$Al_2O_3$ | | | Ni/HZSM-5 | | |
|---|---|---|---|---|---|---|---|---|---|---|
| | 0 | 1 | 2 | 3 | 1 | 2 | 3 | 1 | 2 | 3 |
| Gas yield (wt%) | 96.3 ± 1.0 | 98.6 ± 2.2 | 98.0 ± 2.4 | 95.9 ± 2.3 | 98.7 ± 1.0 | 97.2 ± 0.6 | 98.1 ± 0.4 | 98.7 ± 1.6 | 98.3 ± 1.7 | 98.7 ± 1.1 |
| Tar yield (wt%) | 3.5 ± 0.3 | 1.0 ± 0.4 | 1.4 ± 0.7 | 3.9 ± 0.4 | 1.0 ± 0.1 | 1.1 ± 0.3 | 0.9 ± 0.3 | 1.0 ± 0.2 | 0.9 ± 0.1 | 0.9 ± 0.1 |
| Tar in gas stream ($g/Nm^3$) | 21.2 | 5.9 | 6.2 | 21.8 | 5.5 | 5.6 | 5.2 | 5.7 | 5.3 | 5.3 |
| Heterocyclic aromatic (wt%) | 0.5 | 0.2 | 0.4 | 0.6 | 0.2 | 0.3 | 0.3 | 0.2 | 0.3 | 0.2 |
| Light PAH compounds (2-3 rings) (wt%) | 2.1 | 0.8 | 1.0 | 2.3 | 0.8 | 0.7 | 0.5 | 0.8 | 0.5 | 0.7 |
| Heavy PAH compounds (4-7 rings) (wt%) | 0.9 | 0.03 | 0.05 | 1.0 | 0.05 | 0.1 | 0.07 | 0.03 | 0.07 | 0.04 |
| Naphthalene and its derivatives in tar (wt%) | 1.2 | 0.5 | 0.6 | 1.1 | 0.4 | 0.2 | 0.3 | 0.6 | 0.6 | 0.7 |

Table 5.10: Properties of fresh and spent Ni-based catalyst after the second cycle at a fixed particle size of 1 $cm^3$ cube, pyrolysis and gasification temperature of 900 °C and 1000 °C and S/C molar ratio of 5.7 under $N_2$ atmosphere.

| Number of cycles | Ni/MRM | | Ni/$Al_2O_3$ | | Ni/HZSM-5 | |
|---|---|---|---|---|---|---|
| | Fresh | Spent | Fresh | Spent | Fresh | Spent |
| Specific surface area ($m^2/g$) | 114.8 ± 5.2 | 12.0 ± 1.1 | 158.3 ± 7.4 | 146.7 ± 4.9 | 170.6 ± 8.2 | 166.2 ± 12.1 |
| Total pore volume ($cm^3/g$) | 0.1 | 0.01 | 0.1 | 0.1 | 0.2 | 0.1 |
| Pore size (nm) | 1.7-3.1 | 1.0-2.1 | 1.2-8.0 | 1.7-4.2 | 2.9-6.7 | 2.1-4.4 |

### 5.3.2 The effect of catalyst in $CO_2$/steam gasification

Similarly to $N_2$/steam gasification (described in section 5.3.1), catalyst had little effect on gas yield and composition in $CO_2$/steam gasification (Table 5.11). However, adding a catalyst in a $CO_2$/steam gasification decreased the tar content in the gas stream from 9.1 g/$Nm^3$ (non-catalytic) to 4 g/$Nm^3$ (Table 5.11), which was lower than that in a catalytic $N_2$/steam gasification (6 g/$Nm^3$) (Table 5.8). Up to 97% of the heavy PAH compounds in tar was removed from the gas stream in catalytic $CO_2$/steam gasification (from 0.9 wt% in non-catalytic $CO_2$/steam gasification to 0.04 wt% in catalytic $CO_2$/steam gasification) compared to around 67% reduction in catalytic $N_2$/steam gasification (Table 5.8). The result indicates that all the Ni-based catalysts are more active for tar cracking/reforming under $CO_2$ atmosphere. Therefore, the combination of $CO_2$ and catalyst could eliminate tar formation in the gas stream derived from steam biomass gasification, particularly the heavy PAH compounds. Referring the $N_2$/steam gasification in which Ni/MRM was deactivated after the second cycle (Table 5.9), however all Ni-based catalysts in $CO_2$/steam gasification are still active after the third cycle (Table 5.12). This was evidenced by the gas yield (97-98 wt%) and the tar yield (1 wt%) with their composition remained almost constant over the consecutive cycles (Table 5.12). This is because $CO_2$ reacts with tar and carbon residues (coke) on the surface of the spent catalyst via dry reforming and the Boudouard reactions, enhancing the reduction of the contaminants (i.e. tar, unsaturated hydrocarbon compounds and coke) in the spent catalyst and recovery of their activity (Snoeck et al., 2002; Mahamulkar et al., 2016).

Table 5.11: Effect of Ni-based catalysts on the products yield and properties at a fixed particle size of 1 $cm^3$ cube, pyrolysis and gasification temperature of 900 $^oC$ and 1000 $^oC$ and S/C molar ratio of 3.4 under $CO_2$ atmosphere.

| Catalysts | Non-catalytic | Ni/MRM | $Ni/Al_2O_3$ | Ni/HZSM-5 |
|---|---|---|---|---|
| Solid residues (wt%) | 0.2 ± 1.0 | 0.1 ± 0.8 | 0.1 ± 0.6 | 0.2 ± 0.9 |
| Gas yield* (wt%) | 97.4 ± 1.8 | 98.9 ± 1.7 | 99.0 ± 2.1 | 98.8 ± 2.0 |
| Tar yield (wt%) | 2.5 ± 0.9 | 1.0 ± 0.7 | 0.9 ± 0.7 | 1.0 ± 0.4 |
| Tar in gas stream ($g/Nm^3$) | 9.1 | 3.8 | 3.6 | 4.1 |
| Heterocyclic aromatic (wt%) | 0.2 | 0.1 | 0.1 | 0.2 |
| Light PAH compounds (2-3 rings) (wt%) | 1.3 | 0.8 | 0.7 | 0.8 |
| Heavy PAH compounds (4-7 rings) (wt%) | 0.9 | 0.04 | 0.02 | 0.02 |
| Naphthalene and its derivatives in tar (wt%) | 0.7 | 0.6 | 0.5 | 0.6 |
| $H_2$ (mol%) | 77.7 ± 1.3 | 76.8 ± 1.7 | 78.0 ± 2.4 | 76.2 ± 2.3 |
| CO (mol%) | 15.8 ± 0.6 | 16.6 ± 3.9 | 14.8 ± 1.3 | 16.5 ± 2.2 |
| $CO_2$ (mol%) | 5.6 ± 1.8 | 5.6 ± 2.8 | 6.4 ± 1.3 | 6.6 ± 1.5 |
| $CH_4$ (mol%) | 0.9 ± 0.5 | 1.0 ± 1.0 | 0.8 ± 2.0 | 0.7 ± 1.0 |

*By difference

Table 5.12: The performance of Ni-based catalyst over the consecutive cycles at a fixed particle size of 1 $cm^3$ cube, pyrolysis and gasification temperature of 900 ºC and 1000 ºC and S/C molar ratio of 3.4 under $CO_2$ atmosphere.

| Number of cycles | Non-catalytic | Ni/MRM | | | Ni/$Al_2O_3$ | | | Ni/HZSM-5 | | |
|---|---|---|---|---|---|---|---|---|---|---|
| | 1 | 1 | 2 | 3 | 1 | 2 | 3 | 1 | 2 | 3 |
| Gas yield (wt%) | 97.4 ± 1.8 | 98.9 ± 1.7 | 97.3 ± 2.2 | 97.6 ± 1.1 | 99.0 ± 2.1 | 97.4 ± 1.8 | 98.7 ± 1.0 | 98.8 ± 2.0 | 98.3 ± 1.7 | 97.9 ± 1.5 |
| Tar yield (wt%) | 2.5 ± 0.9 | 1.0 ± 0.7 | 1.2 ± 0.4 | 1.2 ± 0.1 | 0.9 ± 0.7 | 0.6 ± 0.3 | 0.7 ± 0.3 | 1.0 ± 0.4 | 1.1 ± 0.4 | 1.4 ± 0.1 |
| Tar in gas stream ($g/Nm^3$) | 9.1 | 3.8 | 3.9 | 3.9 | 3.6 | 3.1 | 3.2 | 4.1 | 4.1 | 4.1 |
| Heterocyclic aromatic (wt%) | 0.2 | 0.1 | 0.2 | 0.3 | 0.1 | 0.1 | 0.3 | 0.2 | 0.2 | 0.7 |
| Light PAH compounds (2-3 rings) (wt%) | 1.3 | 0.8 | 0.9 | 0.8 | 0.7 | 0.5 | 0.4 | 0.8 | 0.8 | 0.7 |
| Heavy PAH compounds (4-7 rings) (wt%) | 0.9 | 0.04 | 0.06 | 0.05 | 0.02 | 0.01 | 0.04 | 0.02 | 0.05 | 0.04 |
| Naphthalene and its derivatives in tar (wt%) | 0.7 | 0.6 | 0.6 | 0.5 | 0.5 | 0.4 | 0.4 | 0.6 | 0.6 | 0.5 |

## 5.4 Summary

Gasification temperature and steam to carbon in biomass (S/C) molar ratio had strong effects on $H_2$ concentration, gas yield as well as on the process efficiency. Up to 67 mol% $H_2$, 94% carbon conversion efficiency and 84% process efficiency were achieved at a gasification temperature of 1000 $^oC$ and S/C molar ratio of 5.7 in the $N_2$/steam gasification. More than 50% of the tar in the gas stream (from 43 g/$Nm^3$ to 21 g/$Nm^3$) was removed at gasification temperature of 1000-1100 $^oC$ and S/C molar ratio of 5.7 in the $N_2$/steam gasification. When combining $CO_2$ and steam, up to 78 mol% $H_2$ with carbon conversion efficiency and process efficiency of $\leq$ 97% were achieved at gasification temperature of 1000 $^oC$ and S/C molar ratio of 3.4. $CO_2$ concentration in the syngas derived from $CO_2$/steam gasification was around 5-7 mol% which was much lower than in the $N_2$/steam gasification (20-30 mol%). When 100% $CO_2$ was used as a gasifying agent and a S/C molar ratio of 1.0 at gasification temperature of 1000 $^oC$, there was no $CO_2$ in the syngas. The tar content in the gas stream was significantly decreased by 63% from 24 g/$Nm^3$ in the $N_2$/steam gasification to 9 g/$Nm^3$ in the $CO_2$/steam gasification at gasification temperature of 1000 $^oC$ and S/C molar ratio of 3.4. Therefore, the use of $CO_2$ in a gasification process could be an alternative route to utilise waste $CO_2$ and for energy production (i.e. $H_2$) as well as improve the gasification process in terms of conversion, energy efficiency and tar removal; contributes significantly to environmental footprint and sustainability of the process. When a Ni-based catalyst (i.e. Ni/MRM, Ni/HZSM-5 and $Ni/Al_2O_3$) was added, there were little variation in $H_2$ concentration, but around a 2-3 times reduction of tar in the gas stream; particularly the heavy PAH compounds (97% reduction). In addition, the Ni/MRM (waste product of bauxite processing) proved to be a successful/alternative catalyst for removal of naphthalene constituents (58%), the main component in tar compared to only 50% reduction for the commercial Ni-based catalysts ($Ni/Al_2O_3$ and Ni/HZSM-5).

# Chapter 6 Optimisation of air-blown throat downdraft gasifier

This chapter focuses on the synergistic effect of a throat downdraft gasifier design parameters with respect to achieve high quality syngas production, especially for $H_2$ production. A 20 cm diameter throat downdraft gasifier was designed and numerically optimised using Computational Fluid Dynamics (CFD) modelling. The effect of throat diameter and the position of the air inlet nozzles above the throat on the properties of the product gas and the temperature profile in the gasifier were systematically investigated and validated using experimental and literature data. The content of this chapter has been previously published in "Optimisation of a throat downdraft gasifier for hydrogen production", Biomass and Bioenergy Journal (Prasertcharoensuk et al., 2018).

## 6.1 Geometry and mesh construction

A 3D model and the volume discretization of a 20 cm diameter and 55 cm long throat downdraft gasifier (Figure 6.1a) was created and meshed using DesignModeler (Figure 6.1b). The height of the pyrolysis, oxidation and reduction zones were estimated at 15 cm, 10 cm and 30 cm respectively. Throat diameters of 5, 6, 8 and 10 cm were varied to obtain ratios of throat to gasifier diameter of 0.25-0.50 with varying positions of the air inlet nozzles above the throat of 8, 10 or 12 cm. A mesh independence study was carried out at various node and cell counts of 28179, 34708, 44754, 57060 and 60201. It was found that at fixed operating conditions increasing the nodes and cells above 44754 had no effect on the behaviour of the gasifier in terms of gas and temperature profile. Therefore, the model was built at these conditions where the solutions converged (Figure 6.1b).

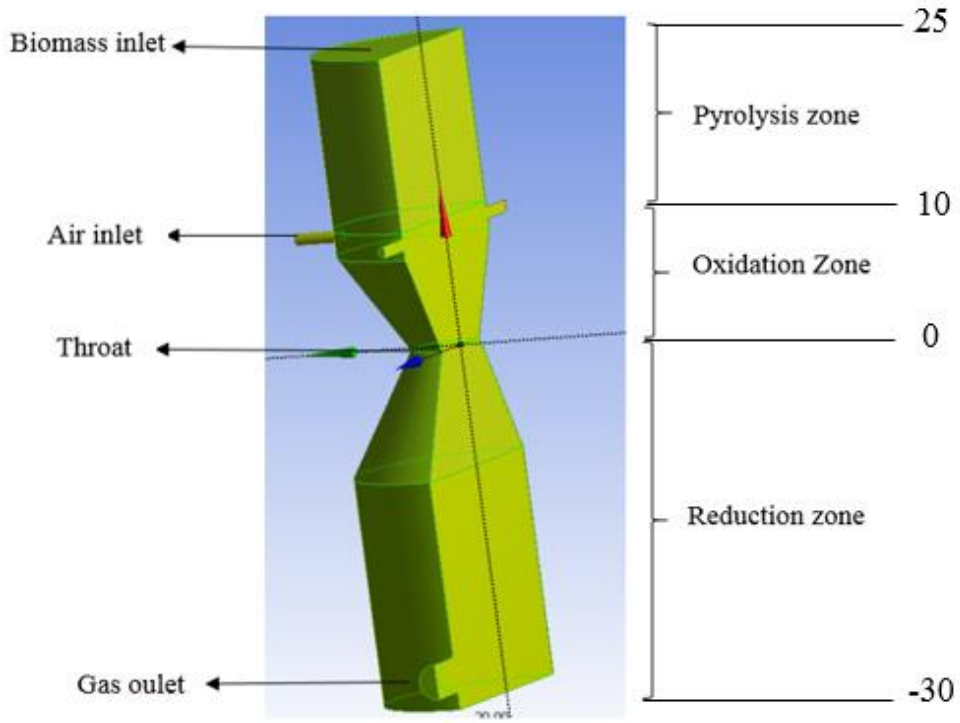


(a)

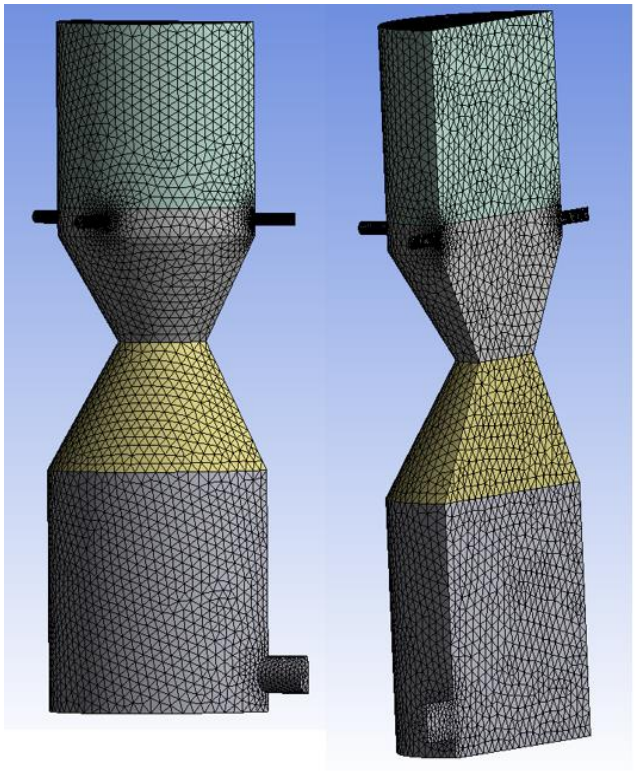

(b)

Figure 6.1: (a) Configuration of the throat downdraft gasifier and (b) Mesh model of the throat downdraft gasifier.

## 6.2 Computational model

Computational Fluid Dynamics (CFD) software, ANSYS FLUENT 16.1 was used for numerical simulation in this study. The main objective of the CFD analysis was to obtain accurate and reliable modelling results in a reasonable computational time to enable design optimisation. The species transport solution is solved by using the pressure-based solver under gravitational acceleration. As this study mainly focused on syngas production from a throat downdraft gasifier instead of characterising the particles, i.e. particle size distributions, interactions of particles, mass and heat transfer between particles and transient forces acting at the particle level. Therefore, the modified Eulerian-Eulerian approach was chosen for this study over the Eulerian-Lagrange approach to solve transport phenomena, with the conservation of momentum, mass and energy equations. The standard k-ε model was used to capture the turbulent flow of the gas phase inside the gasifier with the standard wall functions. The SIMPLE algorithm scheme was used to solve the pressure-velocity coupling and the standard scheme was chosen for the pressure discretization. The second order upwind scheme was implemented to obtained accurate results for other calculated variables.

### 6.2.1 Model assumptions

To simplify the simulation of a throat downdraft gasifier, the following assumptions were made:

- The gasifier configuration of a throat downdraft gasifier included pyrolysis, oxidation and reduction zones.
- The gasifier was operated under steady state conditions at atmospheric pressure.
- The wall was assumed to be insulated perfectly; there was no heat loss through the gasifier wall. A no-slip boundary condition occurred at the wall of the gasifier. The heat flux at the gasifier wall was therefore neglected.
- The dry-wood feed rate was 1 kg/hr at a temperature of 400 K with a moisture content of 5 wt%. These values were based on the experimental results of the feedstock after passing the drying zone.
- The gasifying agent (air) was introduced through nozzles at 293 K.
- The ratio of the actual air/fuel to the stoichiometric air/fuel (ER ratio) was fixed at 0.25. This value was based on a typical value for air gasification reported in literature (Wang et al., 2008; Yaliwal et al., 2014).

### 6.2.2 Governing equations

**The momentum conservation equation**

The momentum equation based on the Newton's laws of motion, relates the sum of the forces acting on a fluid element to its acceleration which is the rate of change of momentum in the direction of the resultant force. The momentum conservation equation can be written in the following form:

$$\frac{\partial}{\partial t}(\rho\vec{v}) + \nabla . (\rho\vec{v}\vec{v}) = -\nabla p + \nabla.(\tau) + \rho\vec{g} + \vec{F} \tag{6.1}$$

where $\rho$ is the static pressure, $\rho\vec{g}$ and $\vec{F}$ are the gravitational body force and external body force respectively. The stress tensor $\tau$ in Equation 6.1 is defined by:

$$\tau = \mu\left[(\nabla\vec{v} + \nabla\vec{v}^{T}) - \frac{2}{3}\nabla.\vec{v}I\right] \tag{6.2}$$

where I is the unity matrix and $\vec{v}^{T}$ is the transpose of $\vec{v}$.

**The mass conservation equation**

The general form of the mass conservation equation, known as the continuity equation is written as follows:

$$\frac{\partial\rho}{\partial t} + \nabla.(\rho\vec{v}) = S_m \tag{6.3}$$

where $S_m$ is the mass added to the continuous phase from the dispersed second phase.

**The energy conservation equation**

The energy conservation is based on the first law of thermodynamics, the internal energy gained by a system must be equal to the heat absorbed by the system minus work done by the system. It can be written in the general form as follows:

$$\frac{\partial}{\partial t}(\rho E) + \nabla.\left(\vec{v}(\rho E + p)\right) = \nabla.\left(k_{eff}\nabla T - \sum_{j=1}^{N} h_j \vec{J}_j + (\tau.\vec{v})\right) + S_h \quad (6.4)$$

where $k_{eff}$ is the effective thermal conductivity ($k + k_t$, where $k_t$ is the turbulent thermal conductivity). The first three terms of the right hand side of the Equation 6.4 represent heat flux due to the conduction according to Fourier's law of conduction, species diffusion and viscous dissipation due to normal shear stresses respectively. The total energy E in Equation 6.4 can be defined by:

$$E = h - \frac{p}{\rho} + \frac{v^2}{2} \quad (6.5)$$

where the enthalpy is defined as:

$$h = \sum_{j=1}^{N} Y_j h_j \quad (6.6)$$

with $Y_j$ being the mass fraction of species j and

$$h_j = \int_{T_{ref}}^{T} c_{p,j}\, dT \quad (6.7)$$

where the value used for $T_{ref}$ in the sensible enthalpy for the pressure-based solver is 298.15 K.

**Transport equation for standard k-epsilon**

The standard k-ε model is one of the most used turbulence models in Computational Fluid Dynamics due to its robustness and reasonable accuracy for a wide range of flows. The k-ε model is a semi empirical model based on transport equations for turbulent kinetic energy k and its dissipation rate ε. In the derivation of the model it is assumed that the flow is fully turbulent and the effects of molecular viscosity are negligible. The transport equations for turbulent kinetic energy and its dissipation rate are defined as follow:

$$\frac{\partial}{\partial t}(\rho k) + \frac{\partial}{\partial x_i}(\rho k u_i) = \frac{\partial}{\partial x_j}\left[\left(\mu + \frac{\mu_t}{\sigma_k}\right)\frac{\partial k}{\partial x_j}\right] + G_k + G_b - \rho\varepsilon - Y_m + S_k \quad (6.8)$$

$$\frac{\partial}{\partial t}(\rho\varepsilon) + \frac{\partial}{\partial x_i}(\rho\varepsilon u_i) = \frac{\partial}{\partial x_j}\left[\left(\mu + \frac{\mu_t}{\sigma_\varepsilon}\right)\frac{\partial \varepsilon}{\partial x_j}\right] + C_{1\varepsilon}\frac{\varepsilon}{k}(G_k + C_{3\varepsilon}G_b) - C_{2\varepsilon}\rho\frac{\varepsilon^2}{k} + S_\varepsilon \quad (6.9)$$

where $S_k$ and $S_\varepsilon$ are the source terms for k and ε respectively and $G_k$ is the term for the production of turbulent kinetic energy due to the mean velocity gradient and the Reynolds stress is defined as:

$$G_k = -\rho\overline{u_i' u_j'}\frac{\partial u_j}{\partial x_i} \quad (6.10)$$

$G_b$ represents the generation of turbulent kinetic energy that arises due to buoyancy and is defined as follows:

$$G_b = \beta g_i \frac{\mu_t}{Pr_t}\frac{\partial T}{\partial x_i} \quad (6.11)$$

$Y_M$ represents the contribution of the fluctuating dilatation in compressible turbulence to the overall dissipation rate and is defined as:

$$Y_M = 2\rho\varepsilon M_t^2 \quad (6.12)$$

The turbulent viscosity ($\mu_t$) is computed by combining the local values of turbulent kinetic energy (k) and dissipation rate (ε) at each point by:

$$\mu_t = \rho C_\mu \frac{k^2}{\varepsilon} \quad (6.13)$$

The values of $C_{1\varepsilon}$, $C_{2\varepsilon}$, $C_{\mu}$, $\sigma_k$ and $\sigma_\varepsilon$ in Equations 6.8 and 6.9 are constants and their values for the standard k-ε model are follows: $C_{1\varepsilon}$=1.44, $C_{2\varepsilon}$= 1.92, $C_{\mu}$= 0.09, $\sigma_k$=1.00 and $\sigma_\varepsilon$=1.30

### 6.2.3 Reactions model

#### The pyrolysis zone

Pyrolysis is the thermochemical decomposition of feedstock to condensable and non-condensable gases and char in the absence of oxygen/air in a temperature range of 673-923 K (Shafie et al., 2012; Ruiz et al., 2013). The overall pyrolysis decomposition is described in Figure 6.2.

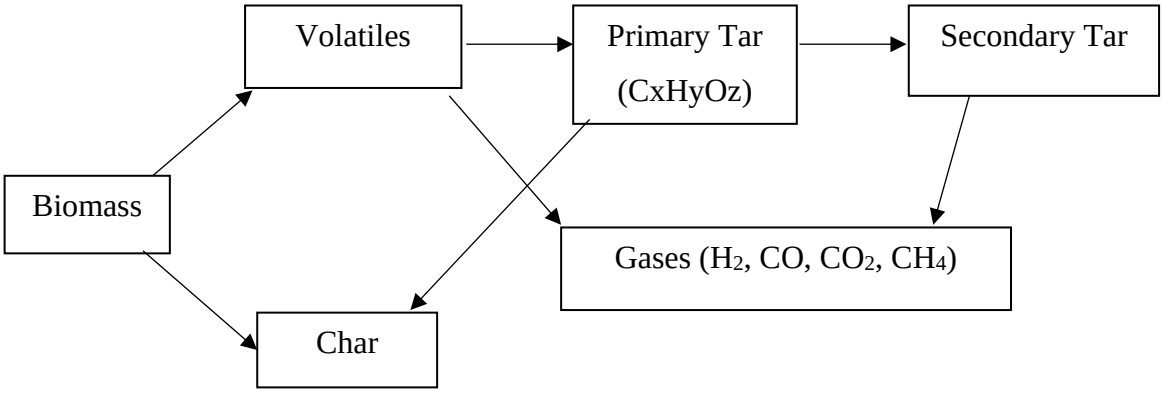


Figure 6.2: Reaction pathways in the pyrolysis zone (Fernando and Narayana, 2016).

However, there is limited kinetic reaction data available in the literature to represent the exact mechanisms of the pyrolysis zone (Figure 6.2). This is mainly due to the large numbers of possible reactions occurring in the pyrolysis zone of which can generate tar. Tar is a complex mixture of condensable hydrocarbons containing single and multiple ring aromatic compounds with or without complex polycyclic aromatic hydrocarbons (PAH) (Mojtahedi et al., 1995; Simell et al., 1996). Therefore, a simple one-step global reaction model is reported in literature (Roberts, 1970; Blasi, 2000; Di Blasi, 2008; Fernando et al., 2015), which has been widely accepted to model the pyrolysis processes reactions. The kinetic reaction rate parameters used in the model are listed in Table 6.1.

#### The oxidation zone

The oxidation zone is where the reactions between char and volatiles from the pyrolysis zone and the gasifying agent (air) occur at a temperature between 1373-1773 K (Basu, 2010a) to generate most of the CO, $H_2O$ and $CO_2$. The main reactions in the oxidation zone as follows and their kinetic reaction rate parameters that are used in the model are listed in Table 6.1.

$$C + \frac{1}{2}O_2 \rightarrow CO \ (\Delta H = -110 \text{ kJ/mol}) \quad (6.14)$$

$$C + O_2 \rightarrow CO_2 \ (\Delta H = -394 \text{ kJ/mol}) \quad (6.15)$$

$$H_2 + \frac{1}{2}O_2 \rightarrow H_2O \ (\Delta H = -242 \text{ kJ/mol}) \quad (6.16)$$

$$CO + \frac{1}{2}O_2 \rightarrow CO_2 \ (\Delta H = -284 \text{ kJ/mol}) \quad (6.17)$$

$$2CO + O_2 \rightarrow 2CO_2 \ (\Delta H = -125 \text{ kJ/mol}) \quad (6.18)$$

$$CH_4 + \frac{1}{2}O_2 \rightarrow CO + 2H_2O \ (\Delta H = -36 \text{ kJ/mol}) \quad (6.19)$$

$$CH_2O_{0.8} + 0.6O_2 \rightarrow CO + H_2O \quad (\Delta H = -80 \text{ kJ/mol}) \quad (6.20)$$

where $CH_2O_{0.8}$ represents unspecific high molecular weight compounds (known as tar) obtained from pyrolysis experiments as described in Chapter 4.

**The reduction zone**

In this zone the remaining residues and gaseous products from the pyrolysis and oxidation zones are converted into non-condensable gases ($H_2$, CO, $CO_2$, $CH_4$) in a temperature range of 973-1273 K (Puig-Arnavat et al., 2010; Ruiz et al., 2013), including both heterogeneous and homogeneous reactions. The main reactions in the reduction zone are as follows and their kinetic reaction rate parameters that are used in the model are listed in Table 6.1.

$$C + CO_2 \leftrightarrow 2CO \ (\Delta H = +173 \text{ kJ/mol}) \quad (6.21)$$

$$C + H_2O \leftrightarrow CO + H_2 \ (\Delta H = +131 \text{ kJ/mol}) \quad (6.22)$$

$$C + 2H_2 \leftrightarrow CH_4 \ (\Delta H = -75 \text{ kJ/mol}) \quad (6.23)$$

$$CO_2 + CH_4 \leftrightarrow 2H_2 + 2CO \ (\Delta H = +247 \text{ kJ/mol}) \quad (6.24)$$

$$CO_2 + H_2 \leftrightarrow H_2O + CO \ (\Delta H = +42 \text{ kJ/mol}) \quad (6.25)$$

$$CH_4 + H_2O \leftrightarrow CO + 3H_2 \ (\Delta H = +206 \text{ kJ/mol}) \quad (6.26)$$

$$CO + H_2O \leftrightarrow CO_2 + H_2 \ (\Delta H = -41 \text{ kJ/mol}) \quad (6.27)$$

### 6.2.4 Boundary conditions and solution methods

The model assumes that the waste wood passes through the drying zone, which is separated by the configuration of the throat downdraft gasifier set-up (Figure 6.1a). This assumption is accepted as, in reality, the feedstock must be dried to a certain moisture content (< 10 wt%) before feeding into the gasifier particularly in a throat downdraft gasifier (Puig-Arnavat et al., 2010; Asadullah, 2014). The waste wood was fed from the top of the gasifier through the pyrolysis zone at a constant rate of 1 kg/hr at temperature of 400 K with the initial moisture content less than 5 wt% (Figure 6.1a). The values were based on the experimental results as described in section 6.2.1. The physicochemical characteristics of the wood was experimentally determined and the kinetic reaction parameters in each zone (i.e. pyrolysis, oxidation and reduction) that used for numerical simulation in this study were adapted from literature values (Table 6.1). The gasifying agent (air) introduced into the gasifier through four inlet nozzles, which are located at the middle part of the gasifier (oxidation zone) (Figure 6.1a) at a fixed ratio of the actual air/fuel to the stoichiometric air/fuel (ER ratio) of 0.25 and air inlet temperature of 293 K. The numerical methods and boundary conditions used in this model are shown in Table 6.1.

Table 6.1: Parameters used for modelling a throat downdraft gasifier.

| Properties of wood | |
|---|---|
| Proximate analysis | wt% (dry basis) |
| Volatile matter | 84.1 |
| Fixed carbon | 15.4 |
| Ash | 0.5 |
| Ultimate analysis | wt% (dry basis, ash free) |
| C | 41.8 |
| H | 6.4 |
| O* | 51.5 |
| N | 0.3 |
| High heating value (MJ/kg) | 17.7 |
| The empirical formula of wood | $C_6H_{11}O_{5.5}N_{0.04}$ |

| Kinetic reaction rates occurred in gasification process | | | |
|---|---|---|---|
| Chemical reactions | Pre-exponential factor ($s^{-1}$) | Activation Energy ($\times 10^2$) (kJ/mol) | Reference |
| Pyrolysis zone | | | |
| Biomass → Char, volatiles ($H_2$, CO, $CO_2$, $CH_4$) and tar | $1.5 \times 10^3$ | 1.1 | (Roberts, 1970) |
| Oxidation zone | | | |
| Equation 6.14 | $7.9 \times 10^4$ | 1.1 | (Groeneveld and van Swaaij, 1980) |
| Equation 6.15 | $5.7 \times 10^9$ | 3.9 | (Kashiwagi and Nambu, 1992) |
| Equation 6.16 | $1.6 \times 10^9$ | 2.4 | (Sharma, 2011; Saleh et al., 2018) |
| Equation 6.17 | $1.3 \times 10^8$ | 2.8 | |
| Equation 6.18 | $3.3 \times 10^7$ | 1.3 | (Hautman et al., 1981; Bryden and Ragland, 1996) |
| Equation 6.19 | $1.6 \times 10^{10}$ | 0.4 | (Bryden and Ragland, 1996; Desroches-Ducarne et al., 1998) |
| Equation 6.20 | $9.2 \times 10^6$ | 0.8 | (Bryden and Ragland, 1996) |
| Reduction zone | | | |
| Equation 6.21 | $1.3 \times 10^{15}$ | 1.7 | (Hobbs et al., 1993; Benguerba et al., 2015) |
| Equation 6.22 | $5.6 \times 10^9$ | 1.3 | |
| Equation 6.23 | $7.0 \times 10^3$ | 0.8 | |
| Equation 6.24 | $1.3 \times 10^6$ | 2.5 | (Benguerba et al., 2015; Shahkarami and Fatemi, 2015) |
| Equation 6.25 | $3.5 \times 10^5$ | 0.4 | |
| Equation 6.26 | $3.0 \times 10^5$ | 2.0 | (Tinaut et al., 2008) |

| | | | |
|---|---|---|---|
| Equation 6.27 | $2.7 \times 10^{-2}$ | 0.4 | (Biba et al., 1978; Yoon et al., 1978) |
| Boundary conditions | Boundary type | Value | Temperature (K) |
| Air inlet | Velocity inlet | 1.7 m/s | 293 |
| Biomass inlet | Mass flow inlet | $2.8 \times 10^{-4}$ kg/s | 400 |
| Gas outlet | Pressure outlet | 0 Pa | - |
| Symmetry | Symmetry | - | - |
| Gasifier wall | Wall | 0 W/m$^2$ | - |
| Solution methods | | | |
| Pressure-Velocity Coupling | | SIMPLE | |
| Gradient | | Least Squares Cell Based | |
| Pressure | | Standard | |
| All other parameters | | Second Order Upwind | |
| Solution Controls | | | |
| Under-Relaxation Factors | | | |
| Pressure | | 0.3 | |
| Density | | 1 | |
| Body Forces | | 1 | |
| Momentum | | 0.7 | |
| Turbulent Kinetic Energy | | 0.8 | |
| Turbulent Dissipation Rate | | 0.8 | |
| Turbulent Viscosity | | 1 | |
| Energy | | 1 | |
| Temperature | | 1 | |
| Mean Mixture Fraction | | 1 | |
| Mixture Fraction Variance | | 0.9 | |

| | |
|---|---|
| Discrete Phase Sources | 0.5 |
| Solution Initialization | |
| Initialization Method | Hybrid Initialization |
| Run Calculation | |
| Number of Iterations | 1500 |

* By difference

### 6.3 The effect of throat to gasifier diameter: modelling results and validation

#### 6.3.1 Syngas composition

The composition of syngas in the throat downdraft gasifier with a throat diameter 5, 6, 8 and 10 cm (or ratios of throat to gasifier diameter of 0.25-0.50) at a fixed position of the air inlet nozzles at 10 cm above the throat is illustrated in Figure 6.3. The results show that the throat diameter had a significant impact on the formation of syngas across the throat downdraft gasifier. The $H_2$ and CO formation was high in the reduction zone (28-31 mol% $H_2$ and 25-32 mol% of CO) compared to that in pyrolysis and oxidation zones (Figure 6.3). This is due to the Boudouard (Equation 6.21), water gas (Equation 6.22), $CO_2$ reforming (Equation 6.24) and steam reforming (Equation 6.26) reactions occurring in this zone, leading to formation of $H_2$ and CO in the gas stream. The $CO_2$ concentration was low in the pyrolysis zone (5-11 mol%) but increased to 21-27 mol% in the oxidation zone. This increase is due to complete combustion (Equation 6.15) and the oxidation of CO in the gas stream (Equations 6.17 and 6.18). A decrease in $CO_2$ in the reduction zone to around 14 mol% could be due to $CO_2$ reacting with char and volatiles (i.e. $CH_4$ and $H_2$), which derived from pyrolysis step via the Boudouard reaction (Equation 6.21) and the $CO_2$ reforming reaction (Equation 6.24). The $CH_4$ concentration was maximised in the pyrolysis zone at 17-18 mol% and further reduced in the oxidation and reductions zones to 3-5 mol%, due to the steam and $CO_2$ reforming reactions (Figure 6.3). A uniform formation of syngas across the throat downdraft gasifier was observed at a ratio of throat diameter to gasifier diameter of 0.40 (Figure 6.3c). This is due to a good proportion of the ratio of throat diameter to gasifier diameter and the air velocity inlet, resulting in well-mixed between volatiles and gasifying agent (air), which results in a uniform formation of product gas across the throat downdraft gasifier.

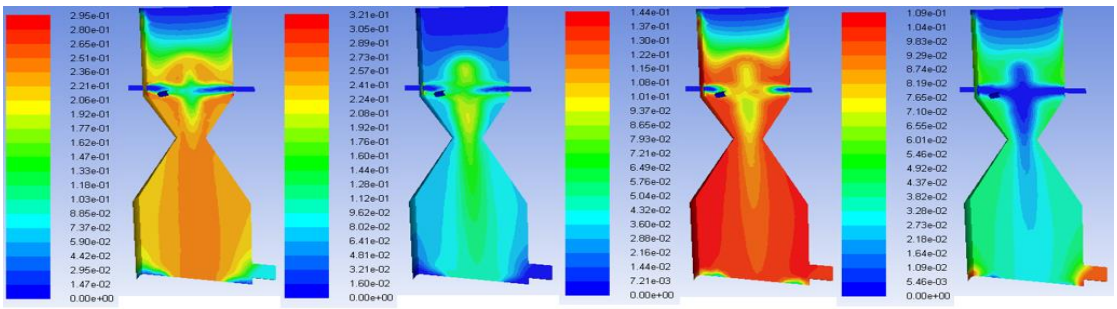


(a)

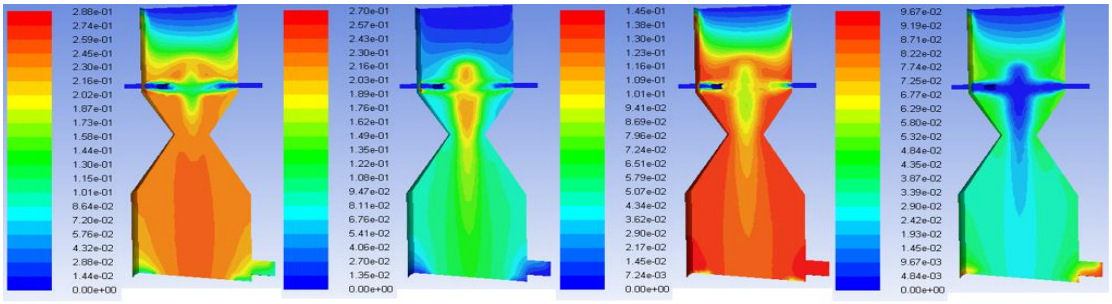


(b)

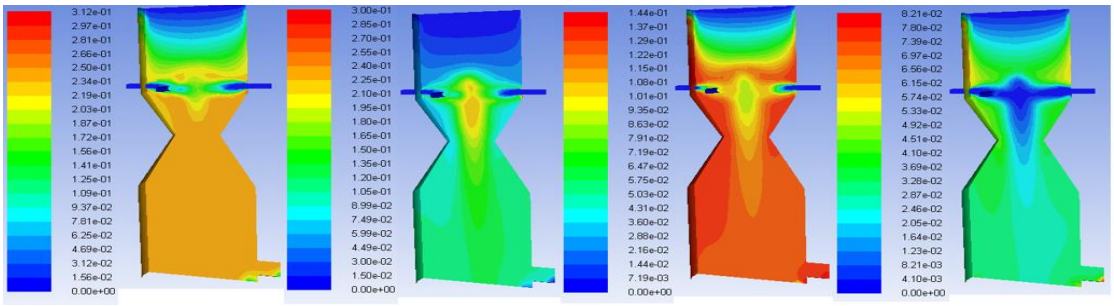


(c)

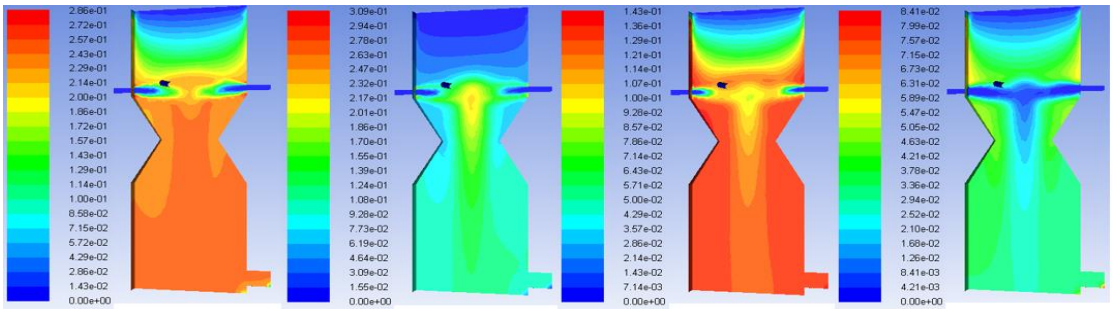


(d)

Figure 6.3: Gas profiles at a ratio of throat to gasifier diameter of (a) 0.25, (b) 0.30, (c) 0.40 and (d) 0.50 at a fixed position of the air inlet nozzles at 10 cm above the throat.

Table 6.2: Gas composition at the outlet over various throat diameters at a fixed position of the air inlet nozzles at 10 cm above the throat.

| Gas composition (mol%) | Throat diameter, cm (ratio of throat to gasifier diameter) | | | |
|---|---|---|---|---|
| | 5 (0.25) | 6 (0.30) | 8 (0.40) | 10 (0.50) |
| $H_2$ | 29.5 | 28.8 | 31.2 | 28.6 |
| CO | 32.1 | 27.0 | 25.0 | 25.9 |
| $CO_2$ | 14.4 | 14.5 | 14.4 | 14.3 |
| $CH_4$ | 5.9 | 4.7 | 3.2 | 3.4 |
| $H_2$/CO | 0.9 | 1.1 | 1.3 | 1.1 |

As shown in Table 6.2 the ratio of throat diameter to the body of gasifier had a considerable effect on the $H_2$/CO ratio and $CH_4$ concentration, but little influence on the $CO_2$ concentration in the gas stream. The $H_2$ concentration at the outlet (31.2 mol%) was maximised at a ratio of throat to gasifier diameter of 0.40 and decreased when increasing the ratio of throat to gasifier diameter, whereas the concentration of $CO_2$ remained almost constant at around 14.4 mol% with all tested throat to gasifier diameter ratios (Table 6.2). The $CH_4$ concentration decreased from 5.9 mol% to 3.4 mol% when increasing the ratio of throat to gasifier diameter from 0.25 to 0.50. The syngas composition obtained from this study (Table 6.2) had a slightly higher than other modelling studies of throat downdraft gasifier (Jayah et al., 2003; Gerun et al., 2008; Janajreh and Al Shrah, 2013; Simone et al., 2013; Wu et al., 2013; Couto et al., 2015; Chaurasia, 2016; Yucel and Hastaoglu, 2016); previous modelling studies of throat downdraft gasifiers have shown that the final syngas composition are in the range of 13-25 mol% $H_2$, 18-38 mol% CO, 8-11 mol% $CO_2$ and 1-3 mol% of $CH_4$. The differences are due to differences in model assumptions, kinetic parameters, the feedstock properties and/or gasifier design.

Table 6.3: The experimental designs and operating parameters of a throat downdraft gasifier.

| Operating conditions | [1] | [2] | [3] | [4] | This study |
|---|---|---|---|---|---|
| Feedstock | Wood | | | | |
| Proximate analysis (wt%, dry basis) | | | | | |
| Volatile matter | 81.3 | 83.7 | 82.2 | 82.2 | 84.1 |
| Fixed carbon | 17.7 | 15.2 | 17.5 | 16.8 | 15.4 |
| Ash | 1.0 | 1.1 | 0.3 | 1.0 | 0.5 |
| Ultimate analysis (wt%, dry basis, ash free) | | | | | |
| C | 50.7 | 47.3 | 50.4 | 48.6 | 41.8 |
| H | 6.2 | 5.8 | 6.0 | 6.2 | 6.4 |
| O* | 41.2 | 46.1 | 43.0 | 44.9 | 51.5 |
| N | 1.9 | 0.8 | 0.6 | 0.3 | 0.3 |
| Biomass feed rate (kg/hr) | 3.5-4.0 | - | 3.1 | 1.0 | 1.0 |
| Particle size (cm) | 1 | 5 | 3-7 | 3 | 1 |
| Gasifier dimensions (H*/Ø) (cm) | 55/28 | 250/60 | 92/22 | 110/39 | 55/20 |
| Throat diameter (cm) | 7 | 20 | 9 | 18 | 5-10 |
| Throat to gasifier diameter ratio | 0.25 | 0.33 | 0.41 | 0.45 | 0.25-0.50 |
| Equivalence ratio (ER) | 0.23 | 0.27 | 0.35 | 0.36 | 0.25 |

* By difference

H*: The height of gasifier and Ø: Gasifier diameter

[1]: (Yucel and Hastaoglu, 2016), [2]: (Zainal et al., 2002), [3]: (Chawdhury and Mahkamov, 2010) and [4]: (Gunarathne et al., 2013).

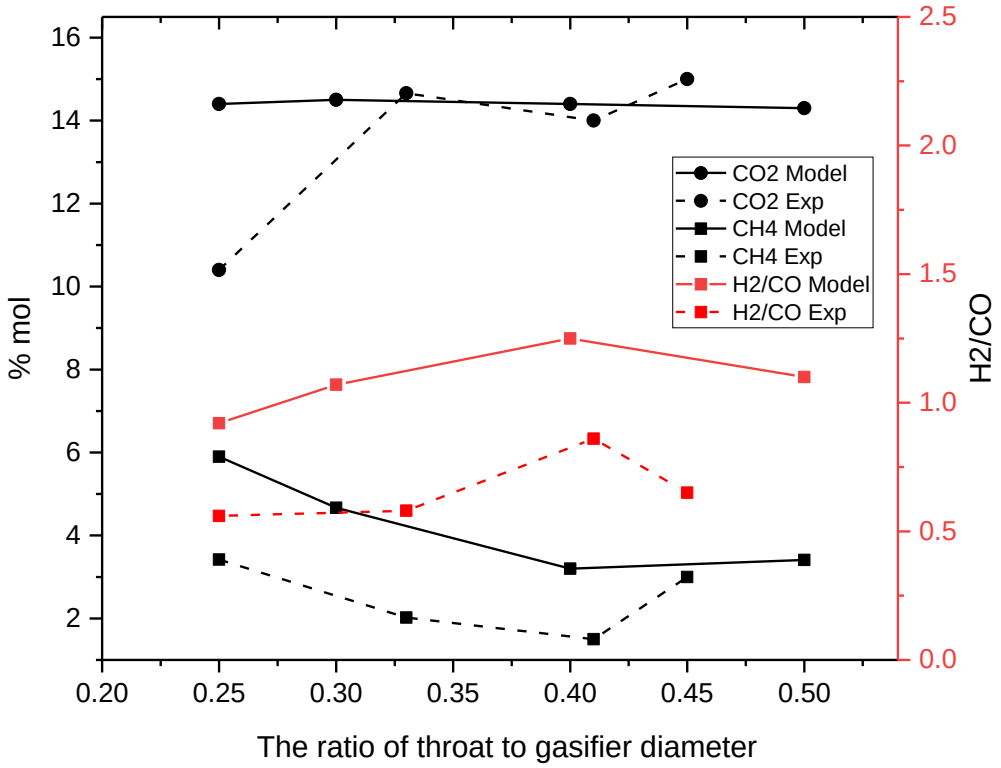


Figure 6.4: Comparison of modelling gas composition obtained from this study and experimental data from literature (Zainal et al., 2002; Chawdhury and Mahkamov, 2010; Gunarathne et al., 2013; Yucel and Hastaoglu, 2016).

Comparisons with experimental data of a small-scale throat downdraft gasifier reported in literature (Zainal et al., 2002; Chawdhury and Mahkamov, 2010; Gunarathne et al., 2013; Yucel and Hastaoglu, 2016) the gasifier designs and operating parameters are shown in Table 6.3. Figure 6.4 shows that the ratio of $H_2$/CO increased from 0.56 to 0.86 when increasing the ratio of throat to gasifier diameter from 0.25 to 0.41 and then decreased to 0.65 with a further increase in the ratio of throat to gasifier diameter to 0.45, which agreed well with modelling results of this study (Table 6.2). All the gas composition obtained in this study (Table 6.2) and the experimental data from the literature show the same trends with approximately 4.6% difference across the range (Figure 6.4). It is also noted that the concentration of syngas from this study was slightly higher than that obtained from the experimental data. This is because (i) the simulation model leads to more effective gasification reactions, in terms of kinetic reaction rates compared to experimental due to the assumption of no heat loss in the system, (ii) a difference in the equivalence ratio (ER) and (iii) the composition of biomass feedstock used, resulting in a difference the proportion of components in the syngas product.

### 6.3.2 Temperature profile

The temperature distributions across the throat downdraft gasifier at various throat diameters of 5, 6, 8 and 10 cm, corresponding to the ratios of throat to gasifier diameter of 0.25-0.50 at a fixed position of the air inlet nozzles of 10 cm above the throat are illustrated in Figure 6.5. It can be observed that between 10 cm and 25 cm, corresponding to the pyrolysis zone (Figure 6.1a) the temperature increased from 400 K to 1100 K. This is due to the heat provided by the radiation from the oxidation zone, which is the hottest part of the throat downdraft gasifier. However, no significant changes in the temperature distribution in the pyrolysis zone were observed under any of the tested throat diameters (Figure 6.5). The oxidation zone occurred at the height of 0 cm to 10 cm in the gasifier (Figure 6.1a). This is important as this is the region where the main reactions occur in the throat downdraft gasifier; in consequence the correlation between throat diameter, gasifier diameter and the position of the air inlet nozzles has an effect on the temperature distribution and the properties of the syngas produced. As shown in Figure 6.5 a high and uniform temperature of 2000 K across the oxidation zone was observed with a ratio of throat to gasifier diameter of 0.40 (Figure 6.5c) compared to that at a ratio of 0.25 and 0.30 at 1800 K and 0.50 at 1600 K. It was suggested (Pfeifer et al., 2004; Kumar et al., 2009) that high and uniform temperature (> 1473 K) in the oxidation zone could minimize tar formation in the gas stream to achieve high quality syngas production in air-blown biomass gasification. The reduction zone at distance of 0 cm to -30 cm (Figure 6.1a), had temperature in the range of 900-1000 K with all tested throat to gasifier diameter ratios (Figure 6.5). The syngas ($H_2$ and CO) is mainly produced in this region via Boudouard (Equation 6.21), water gas (Equation 6.22), $CO_2$ reforming (Equation 6.24), steam reforming (Equation 6.26) and water gas shift (Equation 6.27) reactions. The trend of modelling temperature distribution in three different zones (pyrolysis, oxidation and reduction) agreed very well with experimental data reported in the literature (Zainal et al., 2002; Chawdhury and Mahkamov, 2010; Gunarathne et al., 2013; Yucel and Hastaoglu, 2016). The differences between the modelling temperatures and those obtained from literature was less than 5%. The differences were due to (i) no heat loss in the system, (ii) rates of reactions occurring in the oxidation zone and (iii) the ratio of the actual air/fuel to the stoichiometric air/fuel (ER ratio), i.e. a higher ER ratio leading to an increase in the gasification temperature particularly in the oxidation zone (Kumar et al., 2009; Wu et al., 2009).

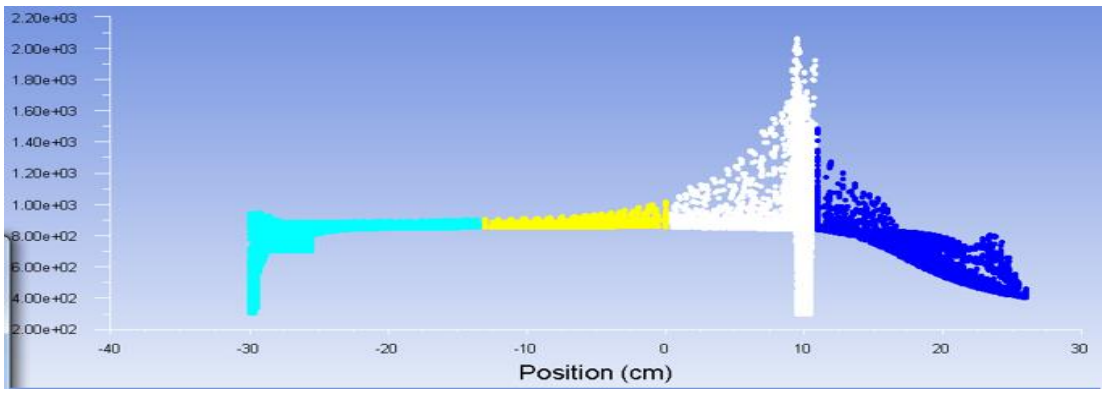


(a)

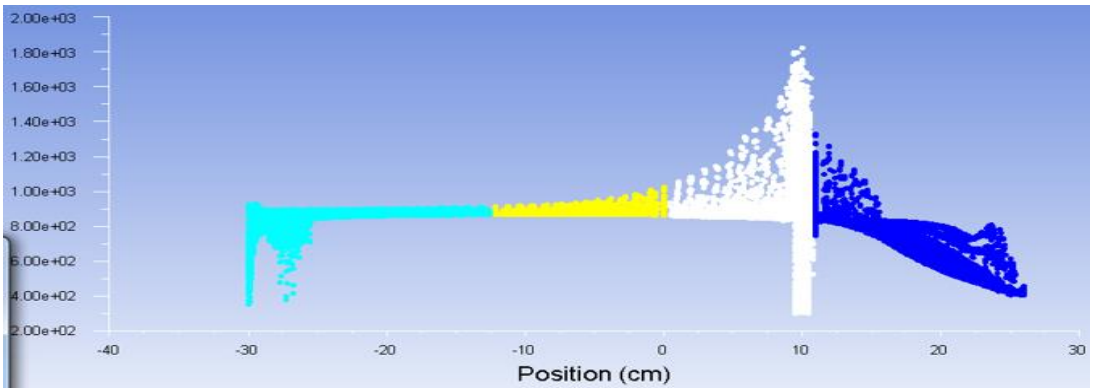


(b)

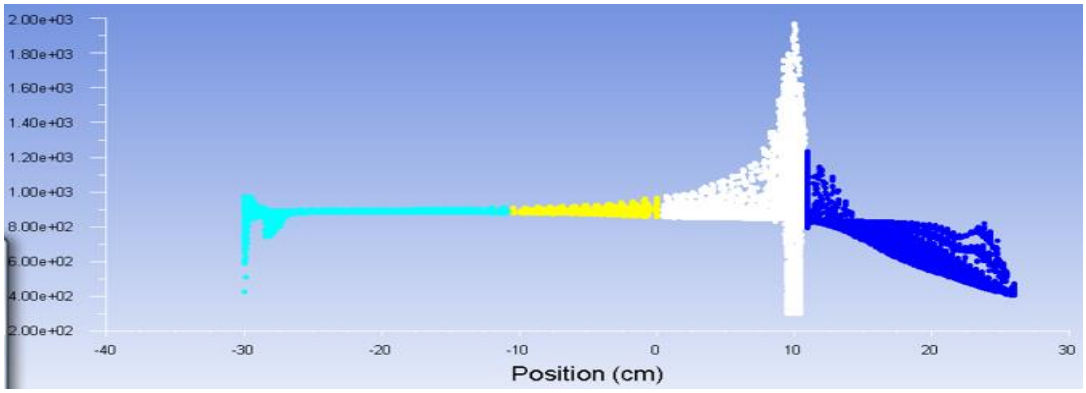


(c)

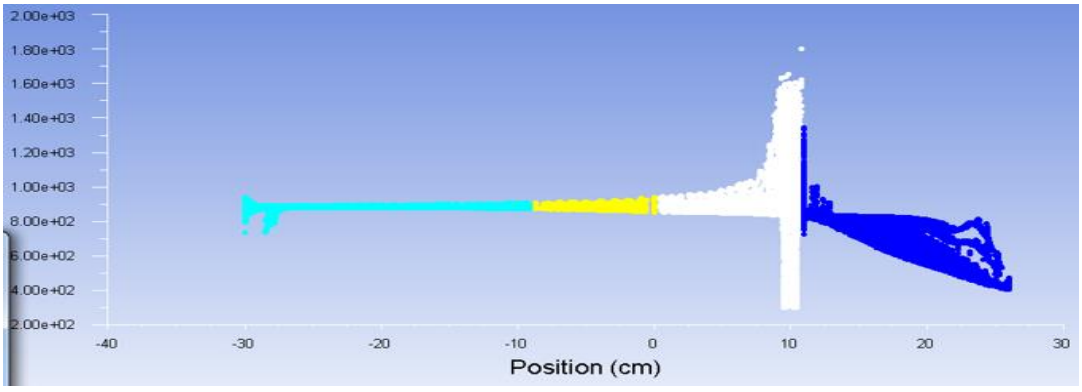


(d)

Figure 6.5: Temperature distribution at a ratio of throat to gasifier diameter of (a) 0.25, (b) 0.30, (c) 0.40 and (d) 0.50 at a fixed position of the air inlet nozzles at 10 cm above the throat.

## 6.4 The effect of the air inlet nozzles position above the throat

### 6.4.1 Syngas composition

The formation of syngas in a throat downdraft gasifier under various air inlet nozzles positions located at 8, 10 and 12 cm above the throat at a fixed throat to gasifier diameter ratio of 0.40 are illustrated in Figure 6.6. $H_2$ and CO concentrations were maximised in the reduction zone in the range of 27-31 mol% $H_2$ and 23-27 mol% of CO. The $CO_2$ concentration was low (6-10 mol%) in the pyrolysis zone and maximised at 23-27 mol% in the oxidation zone followed by a decrease to around 14 mol% after passing through the reduction zone. A similar trend was observed with the $CH_4$ concentration. As shown in Figure 6.6, the formation of syngas was more uniform across the throat downdraft gasifier for the position of the air inlet nozzles at 10 cm (Figure 6.6b) and 12 cm (Figure 6.6c) compared to 8 cm above the throat (Figure 6.6a). When the air inlet nozzles were positioned at 8 cm above the throat, they sat at the beginning of the inclination of the throat, therefore cold spots may occur, resulting in low and non-uniform temperature in the oxidation zone.

Table 6.4: Gas composition at the outlet over various air inlet nozzles positions above the throat at a fixed throat to gasifier diameter ratio of 0.40.

| Gas composition (mol%) | Air inlet nozzles position above the throat (cm) | | |
|---|---|---|---|
| | 8 | 10 | 12 |
| $H_2$ | 27.8 | 31.2 | 27.2 |
| CO | 27.6 | 25.0 | 23.8 |
| $CO_2$ | 14.4 | 14.4 | 14.4 |
| $CH_4$ | 3.8 | 3.2 | 2.6 |
| $H_2$/CO | 1.0 | 1.3 | 1.1 |

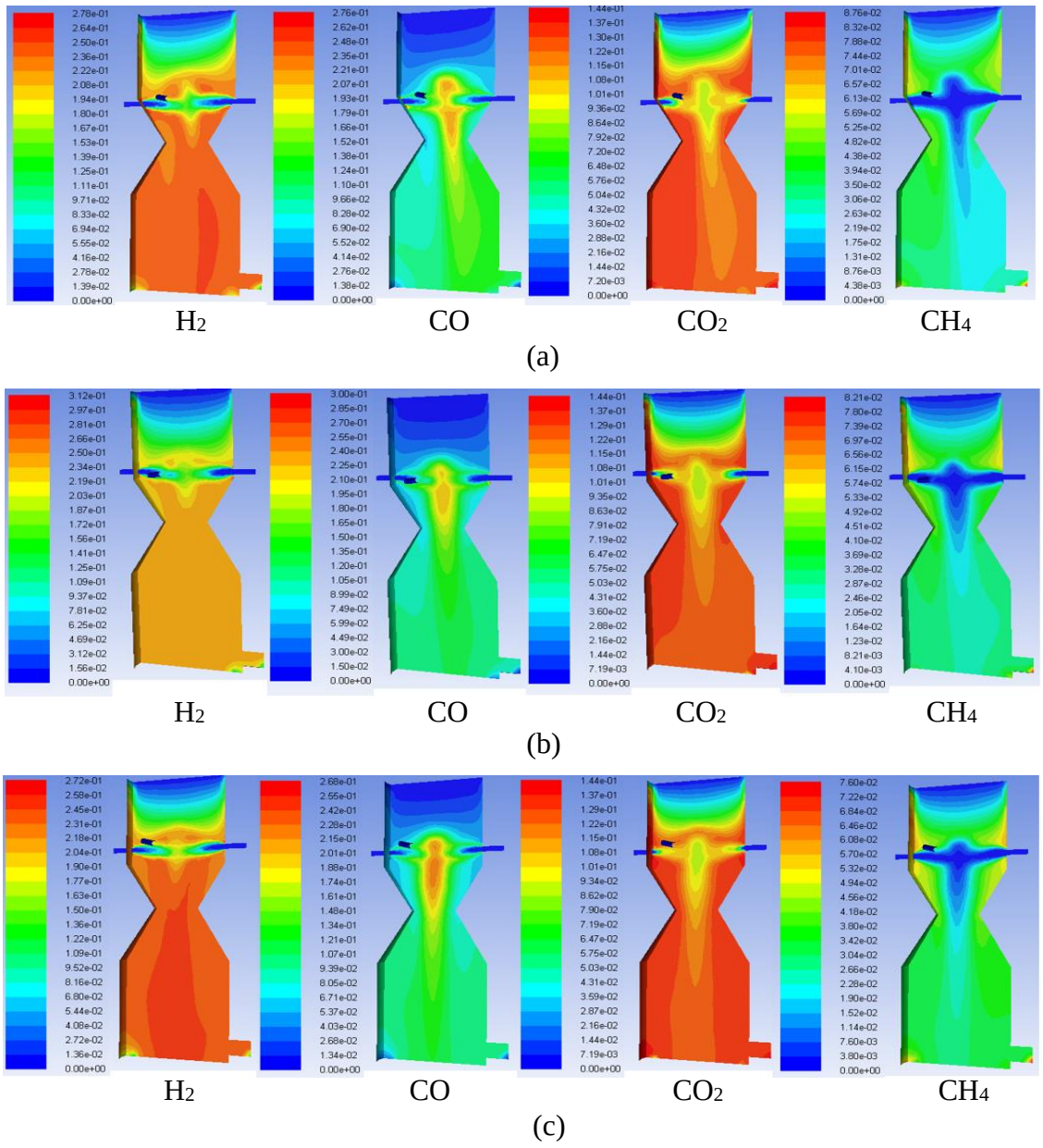


Figure 6.6: Gas profiles at the air inlet nozzles position at (a) 8 cm, (b) 10 cm and (c) 12 cm above the throat at a fixed throat to gasifier diameter ratio of 0.40.

A comparison of the main syngas compositions generated under the various air inlet nozzles positions above the throat at a fixed throat to gasifier diameter ratio is illustrated in Table 6.4. It can be observed that the air inlet position had a significant effect on the concentration of $H_2$, CO and $CH_4$, but no influence on the $CO_2$ concentration. The ratio of $H_2$/CO increased from 1.0 to 1.3 and decreased to 1.1 when increasing the air inlet nozzles distance above the throat from 8 cm to 10 cm and 12 cm respectively (Table 6.4). The concentration of $CH_4$ decreased from 3.8 mol% to 2.6 mol%, with an increase in air inlet position from 8 cm to 12 cm above the throat, while the concentration of $CO_2$ remained constant at 14.4 mol% with all tested air inlet nozzle positions (Table 6.4). These results can be explained because increasing the height

of the air inlet nozzles position above the throat results in a reduction in the length of the pyrolysis zone, therefore the formation of $CH_4$ in this region was decreased. At the same time increasing the length of the reduction zone results in an increase the reaction time in this zone (Equations 6.21-6.27), leading to an increases in concentrations of $H_2$ and CO and a reduction of $CH_4$ concentration in the gas stream (Table 6.4), which is similar to results observed in the literature (Kumararaja and Sethumadhavan, 2013; Liu et al., 2013; Md Isa et al., 2015). The maximum ratio of $H_2$/CO (1.3) obtained in this study (Table 6.4) was in good agreement with experimental data obtained in a small-scale throat downdraft gasifier at a fixed position of the air inlet nozzles at 10 cm above the throat (Zainal et al., 2002; Chawdhury and Mahkamov, 2010; Janajreh and Al Shrah, 2013; Simone et al., 2013). It is known that the ratio of $H_2$/CO in the syngas has significant impact on its utilization, i.e. $H_2/CO \geq 1$ is suitable for heat and electricity generating using turbines/internal combustion engines in a small-scale engines (< 2 MW), whereas the ratio of $H_2/CO \geq 2$ can be used for chemical synthesis, i.e. methanol and liquid fuel via Fischer-Tropsch synthesis (Chaudhari et al., 2001; Cao et al., 2008; Yung et al., 2009; Rauch et al., 2014). From Table 6.4 it can be concluded that high quality syngas with a high ratio of $H_2$/CO at 1.3 and low concentrations of $CO_2$ and $CH_4$ in the gas stream was obtained at the position of the air inlet nozzles at 10 cm above the throat.

### 6.4.2 Temperature profile

The temperature distribution across the throat downdraft gasifier under various air inlet nozzles positions located at 8, 10 and 12 cm above the throat at a fixed throat to gasifier diameter ratio of 0.40 is illustrated in Figure 6.7. The position of the air inlet nozzles had no significant effect on the temperature distribution in the pyrolysis and reduction zones (Figure 6.7). However, the temperature was more uniform across the oxidation zone at a position of 10 cm (Figure 6.7b) and 12 cm (Figure 6.7c) rather than 8 cm above the throat (Figure 6.7a). This is because the position of the air inlet nozzles at 8 cm above the throat was located at the inclination of the throat, causing cold spots in the oxidation zone, therefore resulting in low and non-uniform temperature. Low and non-uniform in the oxidation zone (< 1473 K), leads to a considerable amount of large molecular weight species (tar) in the gas stream (Milne et al., 1998; Gerun et al., 2008; Zhao et al., 2013), which creates operational difficulties for the downstream process, i.e. corrosion, clogging and fouling of the installation (Morf et al., 2002; Zhang et al., 2010; Zhao et al., 2013).

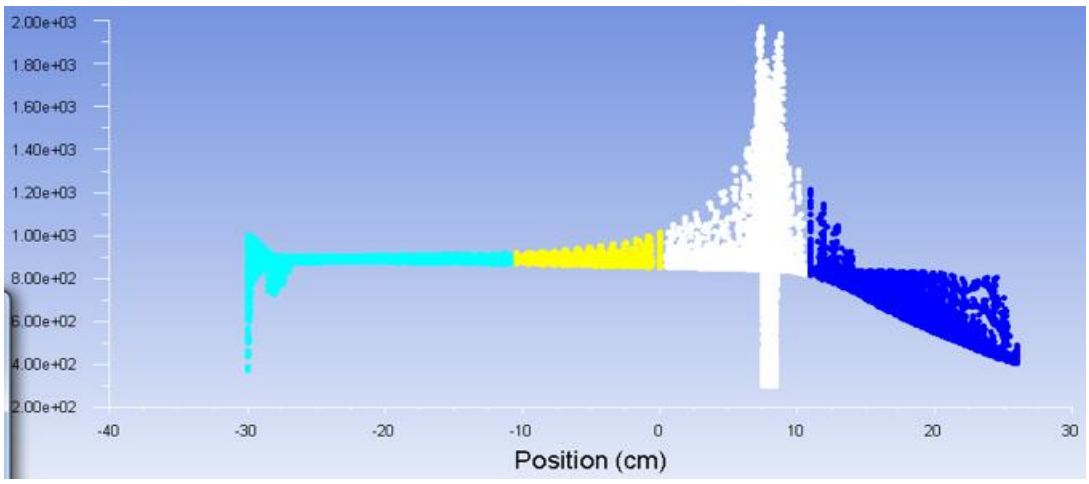


(a)

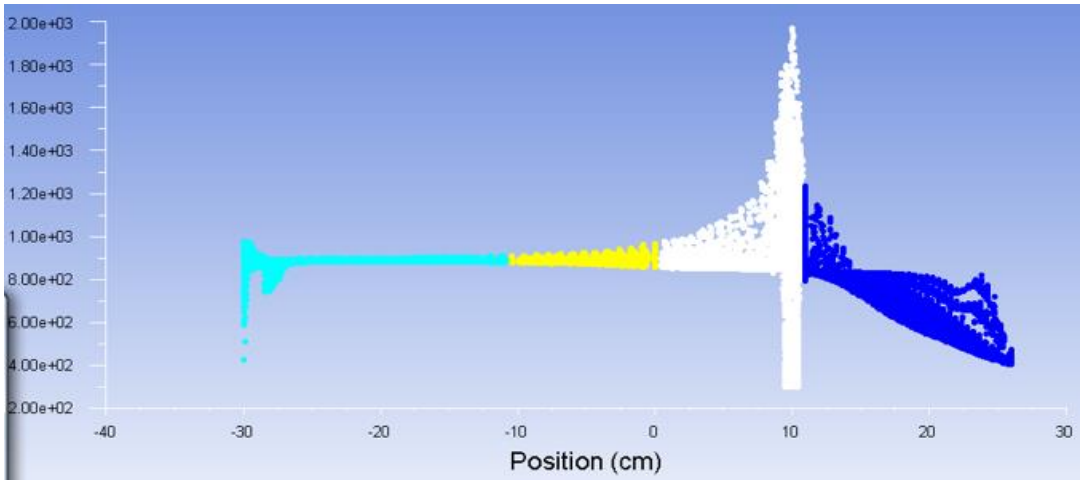


(b)

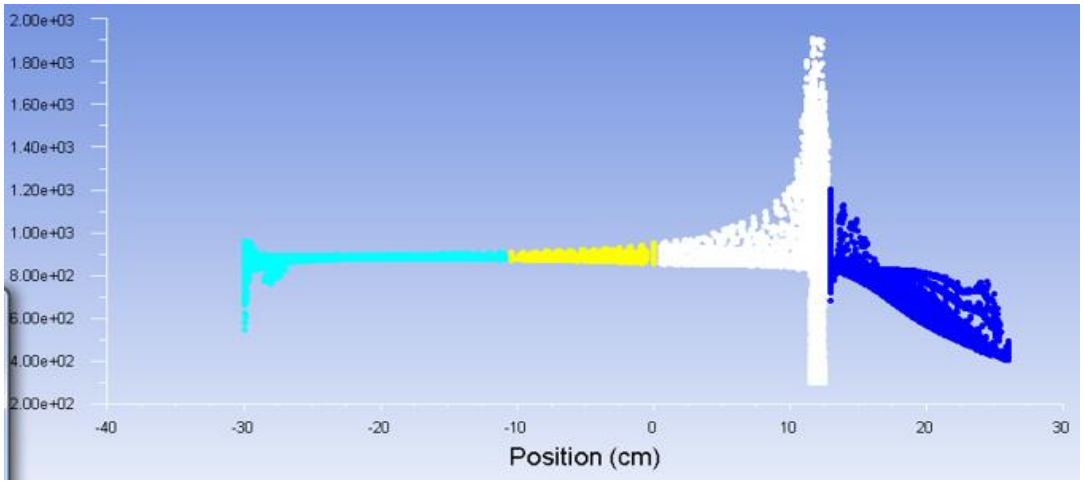


(c)

Figure 6.7: Temperature distribution at the air inlet nozzles position at (a) 8 cm, (b) 10 cm and (c) 12 cm above the throat at a fixed throat to gasifier diameter ratio of 0.40.

The optimal design of throat downdraft gasifier obtained from this study with a throat diameter of 8 cm or ratios of throat to gasifier diameter of 0.40 at a fixed position of the air inlet nozzles at 10 cm above the throat was then used AutoCAD software to create 3D model for laboratory scale throat downdraft gasifier. All details of laboratory scale air-blown throat downdraft gasifier can be found in Appendix C.

### 6.5 Summary

A 20 cm diameter throat downdraft gasifier was designed and numerically optimised using the Computational Fluid Dynamics (CFD), ANSYS FLUENT 16.1. The produced gas composition and temperature distribution across the throat downdraft gasifier were predicted and validated over various ratios of throat to gasifier diameter of 0.25-0.50 and the positions of the air inlet nozzles at 8, 10 and 12 cm above the throat. The modelling results showed that throat to gasifier diameter ratios and the position of the air inlet nozzles had a significant effect on the syngas formation, the properties of the gas and the temperature distribution particularly in the oxidation zone. Increasing the ratio of throat to gasifier diameter decreased $CH_4$ concentration (from 5.9 mol% to 3.4 mol%) but had no effect on $CO_2$ formation (14.4 mol%). The highest concentration of $H_2$ (31.2 mol%) and $H_2$/CO ratio (1.3) was obtained at a throat to gasifier diameter ratio of 0.40. Increasing further the ratio of throat to gasifier diameter caused a reduction in $H_2$ and the ratio of $H_2$/CO. Increasing the air inlet position from 8 cm to 10 cm above the throat increased the ratio of $H_2$/CO from 1.0 to 1.3. A further increase in the air inlet nozzle caused a reduction of $H_2$/CO to 1.1. A 31% reduction in the concentration of $CH_4$ was observed when increasing the air inlet nozzles from 8 cm to 12 cm above the throat. A very good agreement between experimental and modelling data in term of gas composition was observed, with less than 5% difference. The trend in temperature distribution in the gasifier obtained from the modelling was also in good agreement with experimental data. Therefore, the modelling in this study can be used to predict the syngas compositions under the various operating conditions in a fixed throat downdraft gasifier. It can also be used in the scaling up of the gasification process to pilot/industrial scales.

# Chapter 7 Conclusions and recommendations for future work

## 7.1 General conclusions

Increasing concerns over greenhouse gas emissions associated with fossil fuel usage that have negative impacts on climate change, insecurity in energy supplies, depletion of natural resources have led to enormous attention towards renewable and sustainable sources (Cazenave and Cozannet, 2014). Alongside, other renewable resources such as solar, wind, hydro, geothermal and nuclear, lignocellulosic material such as biomass/waste residues have been considered as potential resources to produce biofuels/energy via biochemical or thermochemical approaches that can reduce the heavy dependency upon fossil fuels and their associated environmental impacts (International Energy, 2018). Biomass is the most abundant source of energy in this context after oil, coal and natural gas. A significant amount of biomass/waste residues (2 billion tonnes/year) are produced globally with a combined estimated energy potential of ~ 49 EJ annually, accounting for ~ 14% of total global energy demand (Van de Velden et al., 2010). In the European Union around 400 million tonnes/year of waste wood are generated, contributing energy potential of ~ 10 EJ per year, accounts for ~ 94% of the currently used biomass for energy (Kaza et al., 2018).

Advanced thermochemical technologies, i.e. gasification are considered the most energy efficient and cost-effective solution to convert biomass/waste into multiple energy vectors, i.e. heat, electricity, biofuels and chemicals (Sikarwar et al., 2016). Moreover, gasification is considered as a desirable management technology/alternative with notable advantages over current waste management techniques, e.g. incineration and landfill disposal by avoiding incineration cost (~ $48/tonnes and rising by $8/tonnes per year) and reducing landfill space (Panda et al., 2010) as well as producing around 4 times less emission of greenhouse gases and $CO_2$ than traditional incineration processes (Mauricio et al., 2016). Although, coal gasification is well developed, gasification of biomass has not been widely commercialised due to a number of challenges including high content of volatile matter (75-85 wt%), low energy density (500-800 kW/$m^3$), low bulk density (40-200 kg/$m^3$) and heterogeneity (size, shape and properties) (Ghaly et al., 1999). These challenges can be reduced through physical pre-treatment methods, i.e. milling, grinding, pelleting, briquetting and torrefaction. Pellets and briquettes can transform course ground material into uniform sized feedstock, i.e. 4-10 mm diameter and 20-50 mm length for pellets (García-Maraver et al., 2011) and 10-200 mm diameter and 16-400 mm length for briquettes (Amaya et al., 2007), which is easy to handle, transport and store. Moreover, densification of biomass into briquettes/pellets increases the bulk density of the fuel

(400-800 kg/$m^3$) and improves conveyance efficiency (less dust and wastage), which drives its potential uses in combustion, pyrolysis and gasification and other biomass-based conversions (Adapa et al., 2009). However, production of high quality biomass briquettes/pellets to meet the quality standards (i.e. moisture content, density, durability/impact resistance and compressive strength) is likely to be a limitation to large scale briquette/pellet production, due to the quality of briquettes/pellets being strongly dependent upon compaction pressure and temperature and the nature of the feedstock used (Mitchual et al., 2013). Cubing can be preferred over pelleting/briquetting for biomass (wood in particular) because it can accommodate feedstock with large particle sizes and high moisture content (Tumuluru et al., 2011) which in turn reduces the energy consumption in pre-processing of feedstock by 2-3 times compared to pelleting/briquetting technologies (Mani et al., 2004). The results of this study shows that the uniform particle size distribution of biomass feedstock ($\leq$ 1 $cm^3$ cube) is required to obtain uniform temperature across the gasifier and minimize mass and heat transfer limitations inside the particles, accelerating heterogeneous solid-gas reactions compared when to ground material (< 0.2 $cm^3$ cube) used in industrial scale biomass gasification (Molino et al., 2016). This will consequently reduce 15-20% of energy required for grinding of biomass feedstock, providing economic viability of biomass gasification for industrial use.

As shown in Table 7.1, the majority of biomass gasification plants focus on liquid fuel production for the transportation sector (i.e. diesel, gasoline and jet fuel) to substitute fossil fuels from syngas processed via Fischer-Tropsch synthesis. The Fischer-Tropsch process requires $H_2/CO \geq 2$ and tar content below 0.001 g/$Nm^3$ in the producer gas (de Diego et al., 2016). However, typical biomass gasification plants produce low $H_2/CO$ ratio (0.4-1), low $H_2$ content (40-60 mol%), low process efficiency (70-80%), high tar formation (30-80 g/$Nm^3$) and high $CO_2$ (20-30 mol%) in the gas stream. Therefore, the syngas needs to be cleaned and/or upgraded to meet the requirement ratios and contaminant limits for syngas applications. This study shows that the use of $CO_2$ as a carrier gas in biomass/waste steam gasification is a promising approach for high quality producer gas generation (78 mol% $H_2$; $H_2/CO \geq 2$; < 10 mol% $CO_2$) with high process efficiency (97%) compared to $N_2$/steam or air/steam gasification. The use of $CO_2$ as the gasifying agent contributes significantly to the environmental footprint and sustainability of the process as well as providing an alternative carbon capture, utilization and storage techniques. The producer gas obtained from $CO_2$/steam gasification can potentially be used for synthetic liquid fuels (diesel fuels and gasoline) for the transportation sector and to make valuable chemicals (i.e. methanol, ethanol and alcohol) via a Fischer-Tropsh processes as a substitute for heavy fuel oil. This will consequently reduce the level of greenhouse gas

emissions (~ 36 Gt per year) and health related problems and improve the standards of living of the local population (Sikarwar et al., 2017).

The annual production of hydrogen worldwide is estimated at ~ 55 million tonnes and it expected to increase by 17% per year (Kalamaras and Efstathiou, 2013) since hydrogen is an important material for a wide range of applications such as chemical (57%), petroleum (37%) and agro-based (6%) industries (Ashik et al., 2015). For example, in the petroleum refining industry large quantities of hydrogen (14-71 $Nm^3$ $H_2$/barrel of crude oil) (Baharudin and James Watson, 2017) are required in conjunction with catalytic cracking to remove impurities in crude oil (sulfur, nitrogen, oxygen and metals) and improve product yield before conversion into gasoline, kerosene, jet fuel or diesel oil. Hydrogen is also used in the chemical industry for ammonia and methanol synthesis. Approximately 0.2 tonnes of hydrogen is required to synthesize one tonne of ammonia (which equals more than 850 $Nm^3$ of natural gas) and ~ 0.1 tonnes $H_2$ are required for one tonne of methanol produced (Hewu et al., 2013). Recently, hydrogen is considered as a clean fuel (zero emission of $CO_2$ and air pollutants) and as an energy carrier in fuel cells for generating electricity, powering electric vehicles including in aerospace applications. This is due to the fact that the energy contained in hydrogen on a mass basis (120 MJ/kg) is much higher than coal (35 MJ/kg), fossil fuel (47 MJ/kg) and natural gas (50 MJ/kg) (Møller et al., 2017). Thus, hydrogen will play an important role as an alternative energy vector and a bridge to a sustainable energy future. Nonetheless, hydrogen is currently produced from fossil fuel processing, with raw materials such as natural gas (48%), petroleum (30%) and coal (18%) (Konieczny et al., 2008) which contributes massive greenhouse gas emissions (9-12 tonnes of $CO_2$/tonnes of $H_2$ produced) (Collodi and Wheeler, 2010) with the process efficiency around 70-85% (Kaiwen et al., 2018). This study shows that $H_2$ production from gasification of biomass/waste is competitive with conventional processes in terms of process efficiency (≤ 97%) and environmental (~ 3 tonnes of $CO_2$/tonnes of $H_2$ produced) aspects. In an assessment of hydrogen production technologies, biomass gasification is the most economical process for hydrogen production ($10/GJ or $1.2/kg) compared to other renewable technologies, i.e. biomass pyrolysis ($16/GJ or $1.3/kg), electrolysis ($24/GJ $2.9/kg), photobiological ($31/GJ or $3.8/kg) and solar electrolysis ($36/GJ or $4.3/kg) (Norman, 2007); however its cost is around 3 times higher than that for hydrogen produced from steam reforming of natural gas ($4/GJ or $0.8/kg) (Spath et al., 2003). Therefore, it is very important to keep the focus not only the environmental benefits of biomass gasification but also on the profitability of the process to make implementation of biomass gasification a more commercial prospect.

Table 7.1: Commercial biowaste gasification plants (Watson et al., 2018).

| Organization | Feedstock | Technology | Gasifying agent | Capacity (tonnes/day) | Output (MW) | End-product | Operation year | Status |
|---|---|---|---|---|---|---|---|---|
| West Biofuels (Austria) | Wood chips | Dual Fluidized bed gasifier | Steam | 52 | 12 | Electricity/ Heating/ FT products | 2008 | Operational |
| Tacuarembo CHP Unit (Uruguay) | Wood Residue | Updraft gasifier | Steam | 400 | 60 | | 2010 | Operational |
| Concord Blue Eagar (USA) | Mill waste | Concord Blue Reformer | Steam | 40 | 3 | Electricity | 2017 | Construction |
| Maharashtra Enviro Power (India) | Hazardous Waste | Plasma gasifier | Air | 72 | 8 | | 2009 | Operational |
| Columbia Ridge Facility (USA) | MSW | - | Oxygen | 25 | - | Hydrogen production | 2011 | Operational |
| Fulcrum Sierra Biofuels (USA) | MSW | - | Steam | 600 | 80 | Chemicals | 2017 | Construction |

| | | | | | | | | |
|---|---|---|---|---|---|---|---|---|
| Haldor-Topsoe (USA) | Waste wood | Circulating fluidized bed gasifier | Steam | 20 | - | Gasoline | 2016 | Development |
| Renewable Energy Institute (USA) | Agriculture and Forest residues | - | Steam | 25 | - | Diesel Fuel | 2017 | |
| Solena Fuels, Green Sky (UK) | MSW | Velocys reactor | - | - | 52 | Jet fuel | 2015 | |
| Rentech-ClearFuels (USA) | Waste wood and Bagasse | - | Steam | 16 | - | Diesel/ Jet fuel | 2016 | |
| SYNDIESE (USA) | Forest and agricultural residues | - | Oxygen | 205 | - | Liquid fuel | 2015 | |
| AssetGen Partner (UK) | Refuse-derived Fuel | - | - | - | 42 | | 2017 | |
| Red RockBiofuels (USA) | Forest and Sawmill waste | - | Steam | 460 | - | | | |

This study also explores the use of red mud (waste product of bauxite processing) as a cracking catalyst in biomass gasification for the first time. Red mud proved to be a successful catalyst for cracking/reforming of naphthalene constituents (58%), the main component in tar, compared to only 50% reduction for the commercial catalysts available. These findings will open up a potential new research paths on the utilisation of waste/cheap materials as catalysts to enhance the economics and sustainability of the process. Moreover, the results of this study will help the bauxite industry avoid the disposal of over 70 million tonnes/year of red mud in landfill, thereby reducing capital costs of ~ $210 million per year and their environmental issues (Vangelatos et al., 2009). However, the findings of this study show that the major problem of using red mud as a catalyst is the deactivation of catalyst after two consecutive cycles in an $N_2$/steam gasification process caused by coke deposition and crystallite agglomeration during gasification. These challenges can be overcome by using $CO_2$ as a carrier gas, since $CO_2$ reacts with tar and carbon residues (coke) on the surface of the spent catalyst, enhancing the recovery of catalyst activity comparable to that of the fresh catalyst.

Modification of a gasifier is one of the approaches to minimize tar formation as well as improving and developing the biomass gasification process in terms of process efficiency and syngas quality (Han et al., 2017). Recently, Computational Fluid Dynamics (CFD) modelling is considered as an efficient design tool to predict the behaviour of biomass gasification to optimize operating conditions of an existing gasifier or design and optimize a new gasifier (Meenaroch et al., 2015). Fixed-bed gasifiers are the most common technology for small and medium scale biomass gasification (150 kW to 10 MW) due to their simplicity construction and low investment costs compared to fluidized bed and entrained flow gasifiers (Kumar, 2015). The optimising of the design of air-blown throat downdraft gasifier for hydrogen production is preferable in this study because it is known to produce relatively high quality syngas and low tar concentration (~ 1 g/$Nm^3$) compared to that in a fluidized bed (~ 10 g/$Nm^3$) and an updraft gasifier (~ 50 g/$Nm^3$) (Basu, 2010a). A throat to gasifier diameter ratio of 0.4 and the position of the air inlet nozzles at 10 cm above the throat provided the highest $H_2$ production (31.2 mol% $H_2$ and $H_2$/CO of 1.3) as well as high and uniform temperature across the oxidation zone (> 1500 K), which could help to minimize tar formation in the gas stream (Zhao et al., 2013). A good agreement between experimental and modelling data (with less than 5% difference) in terms of gas composition and temperature distribution was observed. This confirms that the numerical approaches in this study are valid and can be used to predict scale-up behaviour of the gasification process therefore reduce engineering cost and process development time from laboratory to pilot/industrial scales.

## 7.2 Conclusions from chapters 4 to 6

- The pyrolysis temperature has a strong effect on char morphology and the volatiles produced, which in turn affect the syngas properties. Increasing pyrolysis temperature increased the surface area and total pore size of char up to 2-3 times from 38.6 $m^2/g$ (600 $^oC$) to 98.4 $m^2/g$ (900 $^oC$), accelerating the heterogeneous solid-gas reactions. Pyrolysis temperatures above 700 $^oC$ fully decomposed unstable compounds, i.e. levoglucosan and their derivatives in the liquid fraction, but promoted the formation of phenolic compounds which are precursors for multi-ring aromatic species in the later stages of processing.
- When using $CO_2$ as a carrier gas in pyrolysis the gas yield increased by 60% (from 30 wt% to 49 wt%) at the expense of liquid (from 47 wt% to 35 wt%) and char (22 wt% to 16 wt%) fractions compared to that in an $N_2$ atmosphere at a temperature of 900 $^oC$. Moreover, $CO_2$ improved the properties of the liquid in terms of calorific value (21.7 MJ/kg) and composition to be closer to that needed for conversion to transportation fuel.
- $CO_2$ enhances the pyrolysis product properties, i.e. char with high porosity (618.6 $m^2/g$), high CO concentration (55.4 mol%) in the gas stream and low phenolic compounds in the liquid product (11.7 wt%) that are required for high quality syngas/hydrogen production via a gasification process.
- Increasing the pyrolysis temperature from 600 $^oC$ to 900 $^oC$ resulted in an increase in $H_2$ (from 54 mol% to 66 mol%) and CO (from 5 mol% to 10 mol%) and a reduction in $CO_2$ (from 37 mol% to 22 mol%), $CH_4$ (from 5 mol% to 2 mol%) and tar content (from 39 $g/Nm^3$ to 24 $g/Nm^3$) in the gas stream after gasification at a temperature of 1000 $^oC$ and steam to carbon in feedstock (S/C) molar ratio of 3.4.
- Around 67 mol% $H_2$ together with high carbon conversion (94%) and process efficiency (84%) were observed under $N_2$/steam gasification at a pyrolysis temperature of 900 $^oC$ and gasification temperature of 1000 $^oC$ with a S/C molar ratio of 5.7. More than 50% of tar in the gas stream (from 43 $g/Nm^3$ to 21 $g/Nm^3$) was removed when increasing the gasification temperature from 600 $^oC$ to 1000 $^oC$ at a S/C molar ratio of 5.7 in the $N_2$/steam gasification.
- Combining $CO_2$ and steam produced up to 78 mol% $H_2$ and a low tar content (9 $g/Nm^3$), with carbon conversion and process efficiency ~ 97% achieved at pyrolysis temperature of 900 $^oC$ and gasification temperature of 1000 $^oC$ and S/C molar ratio of 3.4.

- Less than 10 mol% $CO_2$ resulted from $CO_2$/steam gasification compared to 20-30 mol% in $N_2$/steam gasification. When 100% $CO_2$ was used as a gasifying agent and a S/C molar ratio of 1.0 at pyrolysis temperature of 900 $^oC$ and gasification temperature of 1000 $^oC$, there was no $CO_2$ in the syngas produced.
- Adding a Ni-based catalyst in the gasification process had no effect on the syngas properties and $H_2$ production, but reduced by 2-3 times, the amount of tar; particularly heavy PAH compounds (97% reduction), which can not be removed by changing the operating conditions, i.e. temperatures and S/C molar ratio.
- A Ni/MRM catalyst (waste product of bauxite processing) proved to be a successful/alternative catalyst for removal of naphthalene constituents (58%), the main component in tar compared to only 50% reduction for the commercial Ni-based catalysts ($Ni/Al_2O_3$ and Ni/HZSM-5).
- The modelling results of a small-scale air-blown throat downdraft gasifier showed the highest concentration of $H_2$ (31 mol%) and $H_2$/CO ratio (1.3) with low $CH_4$ concentration (3 mol%) was obtained at a throat to gasifier diameter ratio of 0.4 and the position of the air inlet nozzles at 10 cm above the throat. A very good agreement between experiment and modelling data in term of gas composition and temperature distribution was observed with less than 5% difference.

### 7.3 Recommendations for future work

- Waste wood showed promising results for $H_2$/syngas production that can be directly used for heat and electricity generation or converted further into synthetic liquid fuels and valuable chemicals; further experimental investigation of different lignocellulosic materials or other waste residues (i.e. multiple solid waste, glass and plastics) would be beneficial.
- Two-stage gasification provides an operating window for developing a simple, highly efficient and robust gasification unit that can be used for green hydrogen production. A continuous system needs to be examined to compare its performance with the batch conditions investigated here before it can be considered for use at an industrial scale.
- Combining $CO_2$ and steam shows favourable results in terms of $H_2$/syngas production and minimizes tar formation as well as increases process efficiency compared to $N_2$/steam gasification. A further investigation using raw flue gas produced from an industrial plant as gasifying agent in the gasification process

and/or a combined with $CO_2$-looping would be a promising approach to utilise waste $CO_2$ for energy production and could increase the sustainability in terms of both environmental and economical drivers for an industrial process.

- The use of red mud proved to be successful catalyst for cracking/reforming of tar in biomass gasification, however there is still a small amount of tar remaining in the gas stream. Therefore, more research on developing different types of catalyst or other downstream gas cleaning techniques that promote complete destruction of tar is still required. This would make implementation of biomass gasification a more commercial prospect.
- Life-cycle assessment and total energy requirement of the whole biomass gasification process needs to be fully assessed, not only the energy required to generate steam and to heat biomass feedstock as in this work. This will help in assessing the environment and economic viability of biomass gasification for industrial use.

# References


Abdel-Fattah, T., E. Mahmoud, M., B. Ahmed, S., Huff, M., Lee, J. and Kumar, S. (2015) 'Biochar from woody biomass for removing metal contaminants and carbon sequestration', Journal of Industrial and Engineering Chemistry, 22(25), pp. 103-109.

Abu El-Rub, Z., Bramer, E.A. and Brem, G. (2004) 'Review of Catalysts for Tar Elimination in Biomass Gasification Processes', Industrial & Engineering Chemistry Research, 43(22), pp. 6911-6919.

Abuadala, A. and Dincer, I. (2010) 'Investigation of a multi-generation system using a hybrid steam biomass gasification for hydrogen, power and heat', International Journal of Hydrogen Energy, 35(24), pp. 13146-13157.

Acharya, B., Sule, I. and Dutta, A. (2012) 'A review on advances of torrefaction technologies for biomass processing', Biomass Conversion and Biorefinery, 2(4), pp. 349-369.

Acıkgoz, C., Onay, O. and Kockar, O.M. (2004) 'Fast pyrolysis of linseed: product yields and compositions', Journal of Analytical and Applied Pyrolysis, 71(2), pp. 417-429.

Adams, P., Bridgwater, T., Lea-Langton, A., Ross, A. and Watson, I. (2018) 'Chapter 8 - Biomass Conversion Technologies', in Thornley, P. and Adams, P. (eds.) Greenhouse Gas Balances of Bioenergy Systems. Academic Press, pp. 107-139.

Adapa, P., Tabil, L. and Schoenau, G. (2009) 'Compaction characteristics of barley, canola, oat and wheat straw', Biosystems Engineering, 104(3), pp. 335-344.

Ahmad, M., Lee, S.S., Dou, X., Mohan, D., Sung, J.-K., Yang, J.E. and Ok, Y.S. (2012) 'Effects of pyrolysis temperature on soybean stover- and peanut shell-derived biochar properties and TCE adsorption in water', Bioresource Technology, 118, pp. 536-544.

Ahmed, T.Y., Ahmad, M.M., Yusup, S., Inayat, A. and Khan, Z. (2012) 'Mathematical and computational approaches for design of biomass gasification for hydrogen production: A review', Renewable and Sustainable Energy Reviews, 16(4), pp. 2304-2315.

Akhtar, J. and Saidina Amin, N. (2012) 'A review on operating parameters for optimum liquid oil yield in biomass pyrolysis', Renewable and Sustainable Energy Reviews, 16(7), pp. 5101-5109.

Akhtari, S., Sowlati, T. and Day, K. (2014) 'Economic feasibility of utilizing forest biomass in district energy systems – A review', Renewable and Sustainable Energy Reviews, 33, pp. 117-127.

Alén, R., Kuoppala, E. and Oesch, P. (1996) 'Formation of the main degradation compound groups from wood and its components during pyrolysis', Journal of Analytical and Applied Pyrolysis, 36(2), pp. 137-148.

Alipour Moghadam Esfahani, R., Osmieri, L., Specchia, S., Yusup, S., Tavasoli, A. and Zamaniyan, A. (2017) '$H_2$-rich syngas production through mixed residual biomass and HDPE waste via integrated catalytic gasification and tar cracking plus bio-char upgrading', Chemical Engineering Journal, 308, pp. 578-587.

Alvarez, J., Lopez, G., Amutio, M., Bilbao, J. and Olazar, M. (2014) 'Bio-oil production from rice husk fast pyrolysis in a conical spouted bed reactor', Fuel, 128, pp. 162-169.

Amaya, A., Medero, N., Tancredi, N., Silva, H. and Deiana, C. (2007) 'Activated carbon briquettes from biomass materials', Bioresource Technology, 98(8), pp. 1635-1641.

Ammendola, P., Piriou, B., Lisi, L., Ruoppolo, G., Chirone, R. and Russo, G. (2010) 'Dual bed reactor for the study of catalytic biomass tars conversion', Experimental Thermal and Fluid Science, 34(3), pp. 269-274.

Anis, S. and Zainal, Z.A. (2011) 'Tar reduction in biomass producer gas via mechanical, catalytic and thermal methods: A review', Renewable and Sustainable Energy Reviews, 15(5), pp. 2355-2377.

Arena, U. (2012) 'Process and technological aspects of municipal solid waste gasification. A review', Waste Management, 32(4), pp. 625-639.

Arenas, E. and Chejne, F. (2004) 'The effect of the activating agent and temperature on the porosity development of physically activated coal chars', Carbon, 42(12), pp. 2451-2455.

Asadullah, M. (2014) 'Barriers of commercial power generation using biomass gasification gas: A review', Renewable and Sustainable Energy Reviews, 29, pp. 201-215.

Ashik, U.P.M., Wan Daud, W.M.A. and Abbas, H.F. (2015) 'Production of greenhouse gas free hydrogen by thermocatalytic decomposition of methane – A review', Renewable and Sustainable Energy Reviews, 44, pp. 221-256.

Ashok, J., Wai, M.H. and Kawi, S. (2018) 'Nickel-based Catalysts for High-temperature Water Gas Shift Reaction-Methane Suppression', ChemCatChem, 10(18), pp. 3927-3942.

Atnaw, S.M., Sulaiman, S.A. and Yusup, S. (2013) 'Syngas production from downdraft gasification of oil palm fronds', Energy, 61, pp. 491-501.

Aubin, H. and Roy, C. (1990) 'Study on the corrosiveness of wood pyrolysis oils', Fuel Science and Technology International, 8(1), pp. 77-86.

Aysu, T. and Küçük, M.M. (2014) 'Biomass pyrolysis in a fixed-bed reactor: Effects of pyrolysis parameters on product yields and characterization of products', Energy, 64, pp. 1002-1025.

Baharudin, L. and James Watson, M. (2017) 'Hydrogen applications and research activities in its production routes through catalytic hydrocarbon conversion', Reviews in Chemical Engineering, 34(1), pp. 43-72.

Bai, X., Johnston, P., Sadula, S. and Brown, R.C. (2013) 'Role of levoglucosan physiochemistry in cellulose pyrolysis', Journal of Analytical and Applied Pyrolysis, 99, pp. 58-65.

Bajpai, P. (2016) 'Structure of Lignocellulosic Biomass', in Pretreatment of Lignocellulosic Biomass for Biofuel Production. Singapore: Springer Singapore, pp. 7-12.

Baker, E.G., Mudge, L.K. and Brown, M.D. (1987) 'Steam gasification of biomass with nickel secondary catalysts', Industrial & Engineering Chemistry Research, 26(7), pp. 1335-1339.

Baktash, E., Littlewood, P., Schomäcker, R., Thomas, A. and Stair, P.C. (2015) 'Alumina coated nickel nanoparticles as a highly active catalyst for dry reforming of methane', Applied Catalysis B: Environmental, 179, pp. 122-127.

Balakrishnan, M., Batra, V.S., Hargreaves, J.S.J., Monaghan, A., Pulford, I.D., Rico, J.L. and Sushil, S. (2009) 'Hydrogen production from methane in the presence of red mud –making mud magnetic', Green Chemistry, 11(1), pp. 42-47.

Balat, M., Balat, M., Kırtay, E. and Balat, H. (2009a) 'Main routes for the thermo-conversion of biomass into fuels and chemicals. Part 1: Pyrolysis systems', Energy Conversion and Management, 50(12), pp. 3147-3157.

Balat, M., Balat, M., Kırtay, E. and Balat, H. (2009b) 'Main routes for the thermo-conversion of biomass into fuels and chemicals. Part 2: Gasification systems', Energy Conversion and Management, 50(12), pp. 3158-3168.

Bambang, S., Abdul, G., Arif Rahman, S., Bambang Arip, D. and Sampurno (2018) 'The effect of two stage gasifying agent on biomass downdraft gasification to the gasifier performance', AIP Conference Proceedings, 1983(1), pp. 20-37.

Basu, P. (2010a) 'Chapter 5 - Gasification Theory and Modeling of Gasifiers', in Basu, P. (ed.) Biomass Gasification and Pyrolysis. Boston: Academic Press, pp. 117-165.

Basu, P. (2010b) 'Chapter 6 - Design of Biomass Gasifiers', in Basu, P. (ed.) Biomass Gasification and Pyrolysis. Boston: Academic Press, pp. 167-228.

Basu, P. (2018) 'Chapter 8 - Design of Biomass Gasifiers', in Basu, P. (ed.) Biomass Gasification, Pyrolysis and Torrefaction (Third Edition). Boston: Academic Press, pp. 263-329.

Begum, S., Rasul, M., Akbar, D. and Ramzan, N. (2013) 'Performance Analysis of an Integrated Fixed Bed Gasifier Model for Different Biomass Feedstocks', Energies, 6(12), pp. 6508-6524.

Beis, S.H., Onay, Ö. and Koçkar, Ö.M. (2002) 'Fixed-bed pyrolysis of safflower seed: influence of pyrolysis parameters on product yields and compositions', Renewable Energy, 26(1), pp. 21-32.

Belgiorno, V., De Feo, G., Della Rocca, C. and Napoli, R.M.A. (2003) 'Energy from gasification of solid wastes', Waste Management, 23(1), pp. 1-15.

Benedetti, V., Patuzzi, F. and Baratieri, M. (2018) 'Characterization of char from biomass gasification and its similarities with activated carbon in adsorption applications', Applied Energy, 227(1), pp. 92-99.

Benguerba, Y., Dehimi, L., Virginie, M., Dumas, C. and Ernst, B. (2015) 'Modelling of methane dry reforming over $Ni/Al_2O_3$ catalyst in a fixed-bed catalytic reactor', Reaction Kinetics, Mechanisms and Catalysis, 114(1), pp. 109-119.

Bennadji, H., Smith, K., Serapiglia, M.J. and Fisher, E.M. (2014) 'Effect of Particle Size on Low-Temperature Pyrolysis of Woody Biomass', Energy & Fuels, 28(12), pp. 7527-7537.

Beurskens LWM, H.M.a.V.P. (2018) Renewable Energy Projections as Published in the National Renewable Energy Action Plans of the European Member States. Petten, NL.

Bhavanam, A. and Sastry, R.C. (2011) 'Biomass Gasification Processes in Downdraft Fixed Bed Reactors: A Review', IJCEA, 2(6), pp. 425-433.

Bhavanam, D.A. (2011) 'Biomass Gasification Processes in Downdraft Fixed Bed Reactors: A Review', International Journal of Chemical Engineering and Applications, 2(6), pp. 425-433.

Bhutani, G., Brito-Parada, P.R. and Cilliers, J.J. (2016) 'Polydispersed flow modelling using population balances in an adaptive mesh finite element framework', Computers & Chemical Engineering, 87, pp. 208-225.

Biba, V., Macák, J., Klose, E. and Malecha, J. (1978) 'Mathematical Model for the Gasification of Coal under Pressure', Industrial and Engineering Chemistry Process Design and Development, 17(1), pp. 92-98.

Blasi, C.D. (2000) 'Dynamic behaviour of stratified downdraft gasifiers', Chemical Engineering Science, 55(15), pp. 2931-2944.

Borrego, A.G., Garavaglia, L. and Kalkreuth, W.D. (2009) 'Characteristics of high heating rate biomass chars prepared under $N_2$ and $CO_2$ atmospheres', International Journal of Coal Geology, 77(3), pp. 409-415.

Brage, C., Yu, Q., Chen, G. and Sjöström, K. (2000) 'Tar evolution profiles obtained from gasification of biomass and coal', Biomass and Bioenergy, 18(1), pp. 87-91.

Branca, C., Giudicianni, P. and Di Blasi, C. (2003) 'GC/MS Characterization of Liquids Generated from Low-Temperature Pyrolysis of Wood', Industrial & Engineering Chemistry Research, 42(14), pp. 3190-3202.

Brandt, P., Larsen, E. and Henriksen, U. (2000) 'High Tar Reduction in a Two-Stage Gasifier', Energy & Fuels, 14(4), pp. 816-819.

Brendova, K., Tlustos, P., Szakova, J. and Habart, J. (2012) 'Biochar properties from different materials of plant origin', European Chemical Bulletin, 1(12), pp. 535-539.

Bridgwater, A.V. (1994) 'Catalysis in thermal biomass conversion', Applied Catalysis A: General, 116(1), pp. 5-47.

Bridgwater, A.V. (1995) 'The technical and economic feasibility of biomass gasification for power generation', Fuel, 74(5), pp. 631-653.

Bridgwater, A.V. (2003) 'Renewable fuels and chemicals by thermal processing of biomass', Chemical Engineering Journal, 91(2), pp. 87-102.

Bridgwater, A.V. (2012) 'Review of fast pyrolysis of biomass and product upgrading', Biomass and Bioenergy, 38, pp. 68-94.

Bridgwater, T. (2018) 'Challenges and Opportunities in Fast Pyrolysis of Biomass: Part I', Johnson Matthey Technology Review, 62(1), pp. 118-130.

Bryden, K.M. and Ragland, K.W. (1996) 'Numerical Modeling of a Deep, Fixed Bed Combustor', Energy & Fuels, 10(2), pp. 269-275.

Buchireddy, P.R., Bricka, R.M., Rodriguez, J. and Holmes, W. (2010) 'Biomass Gasification: Catalytic Removal of Tars over Zeolites and Nickel Supported Zeolites', Energy & Fuels, 24(4), pp. 2707-2715.

Buragohain, B., Mahanta, P. and Moholkar, V.S. (2010) 'Biomass gasification for decentralized power generation: The Indian perspective', Renewable and Sustainable Energy Reviews, 14(1), pp. 73-92.

Bustamante, F., Enick, R., Rothenberger, K., Howard, B., Cugini, A. and Ciocco, M. (2002) 'Kinetic study of the reverse water gas shift reaction in high-temperature, high-pressure homogeneous systems', Fuel Chemistry Division Preprints, 47(1), pp. 663-664.

Cao, J.-L., Yan, Z.-L., Deng, Q.-F., Wang, Y., Yuan, Z.-Y., Sun, G., Jia, T.-K., Wang, X.-D., Bala, H. and Zhang, Z.-Y. (2014) 'Mesoporous modified-red-mud supported Ni catalysts for ammonia decomposition to hydrogen', International Journal of Hydrogen Energy, 39(11), pp. 5747-5755.

Cao, Y., Gao, Z., Jin, J., Zhou, H., Cohron, M., Zhao, H., Liu, H. and Pan, w.-p. (2008) 'Synthesis Gas Production with an Adjustable $H_2$/CO Ratio through the Coal Gasification Process: Effects of Coal Ranks And Methane Addition', Energy & Fuels, 22(3), pp. 1720-1730.

Cazenave, A. and Cozannet, G.L. (2014) 'Sea level rise and its coastal impacts', Earth's Future, 2(2), pp. 15-34.

Chaiwatanodom, P., Vivanpatarakij, S. and Assabumrungrat, S. (2014) 'Thermodynamic analysis of biomass gasification with $CO_2$ recycle for synthesis gas production', Applied Energy, 114, pp. 10-17.

Chakraborty, S., Aggarwal, V., Mukherjee, D. and Andras, K. (2012) 'Biomass to biofuel: a review on production technology', Asia-Pacific Journal of Chemical Engineering, 7(3), pp. 254-262.

Chan, F.L. and Tanksale, A. (2014) 'Review of recent developments in Ni-based catalysts for biomass gasification', Renewable and Sustainable Energy Reviews, 38, pp. 428-438.

Chaudhari, S.T., Bej, S.K., Bakhshi, N.N. and Dalai, A.K. (2001) 'Steam Gasification of Biomass-Derived Char for the Production of Carbon Monoxide-Rich Synthesis Gas', Energy & Fuels, 15(3), pp. 736-742.

Chaurasia, A. (2016) 'Modeling, simulation and optimization of downdraft gasifier: Studies on chemical kinetics and operating conditions on the performance of the biomass gasification process', Energy, 116, pp. 1065-1076.

Chawdhury, M.A. and Mahkamov, K. (2010) 'Development of a Small Downdraft Biomass Gasifier for Developing Countries', Journal of Scientific Research, 3(1), pp. 51-64.

Chen, C., Wang, J., Liu, W., Zhang, S., Yin, J., Luo, G. and Yao, H. (2013) 'Effect of pyrolysis conditions on the char gasification with mixtures of $CO_2$ and $H_2O$', Proceedings of the Combustion Institute, 34(2), pp. 2453-2460.

Chen, D., Chen, X., Sun, J., Zheng, Z. and Fu, K. (2016a) 'Pyrolysis polygeneration of pine nut shell: Quality of pyrolysis products and study on the preparation of activated carbon from biochar', Bioresource Technology, 216, pp. 629-636.

Chen, D., Li, Y., Cen, K., Luo, M., Li, H. and Lu, B. (2016b) 'Pyrolysis polygeneration of poplar wood: Effect of heating rate and pyrolysis temperature', Bioresource Technology, 218, pp. 780-788.

Chen, D., Zhou, J. and Zhang, Q. (2014) 'Effects of heating rate on slow pyrolysis behavior, kinetic parameters and products properties of moso bamboo', Bioresource Technology, 169, pp. 313-319.

Chen, W., Shi, S., Nguyen, T., Chen, M. and Zhou, X. (2016c) 'Effect of Temperature on the Evolution of Physical Structure and Chemical Properties of Bio-char Derived from Co-pyrolysis of Lignin with High-Density Polyethylene', Bioresources, 11(2), pp. 3923-3936.

Chen, Y., Yang, H., Wang, X., Zhang, S. and Chen, H. (2012) 'Biomass-based pyrolytic polygeneration system on cotton stalk pyrolysis: Influence of temperature', Bioresource Technology, 107, pp. 411-418.

Cheng, J. (2017) Biomass to Renewable Energy Processes. Abingdon: Taylor & Francis.

Chew, J.J. and Doshi, V. (2011) 'Recent advances in biomass pretreatment – Torrefaction fundamentals and technology', Renewable and Sustainable Energy Reviews, 15(8), pp. 4212-4222.

Cho, D.-W., Kwon, E.E. and Song, H. (2016) 'Use of carbon dioxide as a reaction medium in the thermo-chemical process for the enhanced generation of syngas and tuning adsorption ability of biochar', Energy Conversion and Management, 117, pp. 106-114.

Choi, Y. and Stenger, H.G. (2003) 'Water gas shift reaction kinetics and reactor modeling for fuel cell grade hydrogen', Journal of Power Sources, 124(2), pp. 432-439.

Choudhury, N.D., Chutia, R.S., Bhaskar, T. and Kataki, R. (2014) 'Pyrolysis of jute dust: effect of reaction parameters and analysis of products', Journal of Material Cycles and Waste Management, 16(3), pp. 449-459.

Collodi, G. and Wheeler, F. (2010) 'Hydrogen Production via Steam Reforming with $CO_2$ Capture', Chemical Engineering Transactions, 19, pp. 37-42.

Corma, A., Huber, G.W., Sauvanaud, L. and O'Connor, P. (2007) 'Processing biomass-derived oxygenates in the oil refinery: Catalytic cracking (FCC) reaction pathways and role of catalyst', Journal of Catalysis, 247(2), pp. 307-327.

Couto, N., Silva, V., Monteiro, E., Brito, P. and Rouboa, A. (2015) 'Using an Eulerian-granular 2-D multiphase CFD model to simulate oxygen air enriched gasification of agroindustrial residues', Renewable Energy, 77, pp. 174-181.

Cui, H. and Grace, J.R. (2007) 'Fluidization of biomass particles: A review of experimental multiphase flow aspects', Chemical Engineering Science, 62(1), pp. 45-55.

Cypres, R. (1987) 'Aromatic hydrocarbons formation during coal pyrolysis', Fuel Processing Technology, 15, pp. 1-15.

de Diego, L.F., García-Labiano, F., Gayán, P., Abad, A., Mendiara, T., Adánez, J., Nacken, M. and Heidenreich, S. (2016) 'Tar abatement for clean syngas production during biomass gasification in a dual fluidized bed', Fuel Processing Technology, 152, pp. 116-123.

de Lasa, H., Salaices, E., Mazumder, J. and Lucky, R. (2011) 'Catalytic Steam Gasification of Biomass: Catalysts, Thermodynamics and Kinetics', Chemical Reviews, 111(9), pp. 5404-5433.

Dejtrakulwong, C. and Patumsawad, S. (2014) 'Four Zones Modeling of the Downdraft Biomass Gasification Process: Effects of Moisture Content and Air to Fuel Ratio', Energy Procedia, 52, pp. 142-149.

Demiral, İ., Eryazıcı, A. and Şensöz, S. (2012) 'Bio-oil production from pyrolysis of corncob (Zea mays L.)', Biomass and Bioenergy, 36, pp. 43-49.

Demiral, İ. and Şensöz, S. (2006) 'Fixed-Bed Pyrolysis of Hazelnut (Corylus Avellana L.) Bagasse: Influence of Pyrolysis Parameters on Product Yields', Energy Sources, Part A: Recovery, Utilization, and Environmental Effects, 28(12), pp. 1149-1158.

Demirbas, A. (2007) 'Effect of Temperature on Pyrolysis Products from Biomass', Energy Sources, Part A: Recovery, Utilization, and Environmental Effects, 29(4), pp. 329-336.

Demirbaş, A. (2001) 'Biomass resource facilities and biomass conversion processing for fuels and chemicals', Energy Conversion and Management, 42(11), pp. 1357-1378.

Demırbas, A. (2016) 'Future energy systems', Energy Sources, Part A: Recovery, Utilization, and Environmental Effects, 38(12), pp. 1721-1729.

Demirbas, M.F. (2006) 'Hydrogen from Various Biomass Species via Pyrolysis and Steam Gasification Processes', Energy Sources, Part A: Recovery, Utilization, and Environmental Effects, 28(3), pp. 245-252.

Demirel, E. and Ayas, N. (2017) 'Thermodynamic modeling of the water-gas shift reaction in supercritical water for hydrogen production', Theoretical Foundations of Chemical Engineering, 51(1), pp. 76-87.

Desroches-Ducarne, E., Dolignier, J.C., Marty, E., Martin, G. and Delfosse, L. (1998) 'Modelling of gaseous pollutants emissions in circulating fluidized bed combustion of municipal refuse', Fuel, 77(13), pp. 1399-1410.

Detchusananard, T., Im-orb, K., Ponpesh, P. and Arpornwichanop, A. (2018) 'Biomass gasification integrated with $CO_2$ capture processes for high-purity hydrogen production: Process performance and energy analysis', Energy Conversion and Management, 171, pp. 1560-1572.

Devi, L., Nair, S.A., Pemen, A.J.M., Yan, K., Heesch, E.J.M., Ptasinski, K.J. and Janssen, F.J.J.G. (2006) 'Tar removal from biomass gasification processes', in Brenes, M.D. (ed.) Biomass and bioenergy : new research. New York: NOVA Science Publishers, pp. 249-274.

Devi, L., Ptasinski, K.J. and Janssen, F.J.J.G. (2003) 'A review of the primary measures for tar elimination in biomass gasification processes', Biomass and Bioenergy, 24(2), pp. 125-140.

Devi, L., Ptasinski, K.J., Janssen, F.J.J.G., van Paasen, S.V.B., Bergman, P.C.A. and Kiel, J.H.A. (2005) 'Catalytic decomposition of biomass tars: use of dolomite and untreated olivine', Renewable Energy, 30(4), pp. 565-587.

Di Blasi, C. (2008) 'Modeling chemical and physical processes of wood and biomass pyrolysis', Progress in Energy and Combustion Science, 34(1), pp. 47-90.

Di Blasi, C. (2009) 'Combustion and gasification rates of lignocellulosic chars', Progress in Energy and Combustion Science, 35(2), pp. 121-140.

Diebold, J.P. and Bridgwater, A.V. (1997) 'Overview of Fast Pyrolysis of Biomass for the Production of Liquid Fuels', in Bridgwater, A.V. and Boocock, D.G.B. (eds.) Developments in Thermochemical Biomass Conversion: Volume 1 / Volume 2. Dordrecht: Springer Netherlands, pp. 5-23.

Dogru, M., Midilli, A. and Howarth, C.R. (2002) 'Gasification of sewage sludge using a throated downdraft gasifier and uncertainty analysis', Fuel Processing Technology, 75(1), pp. 55-82.

Dou, B., Gao, J., Sha, X. and Baek, S.W. (2003) 'Catalytic cracking of tar component from high-temperature fuel gas', Applied Thermal Engineering, 23(17), pp. 2229-2239.

Dunens, O.M., MacKenzie, K.J. and Harris, A.T. (2010) 'Synthesis of multi-walled carbon nanotubes on 'red mud' catalysts', Carbon, 48(8), pp. 2375-2377.

Dzulfansyah, D., Nelwan, L. and Wulandani, D. (2014) 'Computational Fluid Dynamics Analysis for Designing Downdraft-Rice Husk Gasifier', Jurnal Keteknikan Pertanian, 2(2), pp. 133-140.

Elliott, D.C. (1988) 'Relation of Reaction Time and Temperature to Chemical Composition of Pyrolysis Oils', in Pyrolysis Oils from Biomass. American Chemical Society, pp. 55-65.

Elmay, Y., Le Brech, Y., Delmotte, L., Dufour, A., Brosse, N. and Gadiou, R. (2015) 'Characterisation of Miscanthus pyrolysis by DRIFTs, UV Raman spectroscopy and Mass Spectrometry', Journal of Analytical and Applied Pyrolysis, 113, pp. 402-411.

Elshahed, M.S. (2010) 'Microbiological aspects of biofuel production: Current status and future directions', Journal of Advanced Research, 1(2), pp. 103-111.

Emami Taba, L., Irfan, M.F., Wan Daud, W.A.M. and Chakrabarti, M.H. (2012) 'The effect of temperature on various parameters in coal, biomass and CO-gasification: A review', Renewable and Sustainable Energy Reviews, 16(8), pp. 5584-5596.

Encinar, J.M., González, J.F. and González, J. (2000) 'Fixed-bed pyrolysis of Cynara cardunculus L. Product yields and compositions', Fuel Processing Technology, 68(3), pp. 209-222.

Enders, A., Hanley, K., Whitman, T., Joseph, S. and Lehmann, J. (2012) 'Characterization of biochars to evaluate recalcitrance and agronomic performance', Bioresource Technology, 114, pp. 644-653.

Ertaş, M. and Hakkı Alma, M. (2010) 'Pyrolysis of laurel (Laurus nobilis L.) extraction residues in a fixed-bed reactor: Characterization of bio-oil and bio-char', Journal of Analytical and Applied Pyrolysis, 88(1), pp. 22-29.

Evans, K. (2016) 'The History, Challenges, and New Developments in the Management and Use of Bauxite Residue', Journal of Sustainable Metallurgy, 2(4), pp. 316-331.

Fabry, F., Rehmet, C., Rohani, V. and Fulcheri, L. (2013) 'Waste Gasification by Thermal Plasma: A Review', Waste and Biomass Valorization, 4(3), pp. 421-439.

Fan, H., Mei, D., Tian, F., Cui, X. and Zhang, M. (2016) 'DEM simulation of different particle ejection mechanisms in a fluidized bed with and without cohesive interparticle forces', Powder Technology, 288, pp. 228-240.

Fang, X., Liu, Q., Li, P., Li, H., Li, F. and Huang, G. (2016) 'A Nanomesoporous Catalyst from Modified Red Mud and Its Application for Methane Decomposition to Hydrogen Production', Journal of Nanomaterials, 1, pp. 1-8.

Farrow, T.S., Sun, C. and Snape, C.E. (2015) 'Impact of $CO_2$ on biomass pyrolysis, nitrogen partitioning, and char combustion in a drop tube furnace', Journal of Analytical and Applied Pyrolysis, 113, pp. 323-331.

Farzad, S., Mandegari, M.A. and Görgens, J.F. (2016) 'A critical review on biomass gasification, co-gasification, and their environmental assessments', Biofuel Research Journal, 3(4), pp. 483-495.

Feng, D., Zhao, Y., Zhang, Y. and Sun, S. (2017) 'Effects of $H_2O$ and $CO_2$ on the homogeneous conversion and heterogeneous reforming of biomass tar over biochar', International Journal of Hydrogen Energy, 42(18), pp. 13070-13084.

Feng, Y., Swenser-Smith, T., Witt, P.J., Doblin, C., Lim, S. and Schwarz, M.P. (2012) 'CFD modeling of gas–solid flow in an internally circulating fluidized bed', Powder Technology, 219, pp. 78-85.

Fernando, N., Amin, M., Narayana, M., Jayawickrama, T., Asadumllah and Jayasena, S. (2015) 2015 Moratuwa Engineering Research Conference (MERCon). 7-8 April 2015.

Fernando, N. and Narayana, M. (2016) 'A comprehensive two dimensional Computational Fluid Dynamics model for an updraft biomass gasifier', Renewable Energy, 99, pp. 698-710.

Figueredo, N.A.d., Costa, L.M.d., Melo, L.C.A., Siebeneichlerd, E.A. and Tronto, J. (2017) 'Characterization of biochars from different sources and evaluation of release of nutrients and contaminants', Revista Ciência Agronômica, 48(3), pp. 3-403.

Fryda, L., Panopoulos, K.D. and Kakaras, E. (2008a) 'Integrated CHP with autothermal biomass gasification and SOFC–MGT', Energy Conversion and Management, 49(2), pp. 281-290.

Fryda, L.E., Panopoulos, K.D. and Kakaras, E. (2008b) 'Agglomeration in fluidised bed gasification of biomass', Powder Technology, 181(3), pp. 307-320.

Fu, P., Yi, W., Bai, X., Li, Z., Hu, S. and Xiang, J. (2011) 'Effect of temperature on gas composition and char structural features of pyrolyzed agricultural residues', Bioresource Technology, 102(17), pp. 8211-8219.

Furusawa, T. and Tsutsumi, A. (2005) 'Development of cobalt catalysts for the steam reforming of naphthalene as a model compound of tar derived from biomass gasification', Applied Catalysis A: General, 278(2), pp. 195-205.

Fushimi, C., Katayama, S. and Tsutsumi, A. (2009) 'Elucidation of interaction among cellulose, lignin and xylan during tar and gas evolution in steam gasification', Journal of Analytical and Applied Pyrolysis, 86(1), pp. 82-89.

Gabra, M., Pettersson, E., Backman, R. and Kjellström, B. (2001) 'Evaluation of cyclone gasifier performance for gasification of sugar cane residue—Part 1: gasification of bagasse', Biomass and Bioenergy, 21(5), pp. 351-369.

Gai, C., Guo, Y., Liu, T., Peng, N. and Liu, Z. (2016) 'Hydrogen-rich gas production by steam gasification of hydrochar derived from sewage sludge', International Journal of Hydrogen Energy, 41(5), pp. 3363-3372.

Gai, X., Wang, H., Liu, J., Zhai, L., Liu, S., Ren, T. and Liu, H. (2014) 'Effects of Feedstock and Pyrolysis Temperature on Biochar Adsorption of Ammonium and Nitrate', PLoS ONE, 9(12), pp. 1-19.

Galindo, A.L., Lora, E.S., Andrade, R.V., Giraldo, S.Y., Jaén, R.L. and Cobas, V.M. (2014) 'Biomass gasification in a downdraft gasifier with a two-stage air supply: Effect of operating conditions on gas quality', Biomass and Bioenergy, 61, pp. 236-244.

Gani, A. and Naruse, I. (2007) 'Effect of cellulose and lignin content on pyrolysis and combustion characteristics for several types of biomass', Renewable Energy, 32(4), pp. 649-661.

Gao, X., Zhang, Y., Li, B., Zhao, Y. and Jiang, B. (2016a) 'Determination of the intrinsic reactivities for carbon dioxide gasification of rice husk chars through using random pore model', Bioresource Technology, 218, pp. 1073-1081.

Gao, Y., Yang, Y., Qin, Z. and Sun, Y. (2016b) 'Factors affecting the yield of bio-oil from the pyrolysis of coconut shell', SpringerPlus, 5, pp. 1-8.

García-Maraver, A., Popov, V. and Zamorano, M. (2011) 'A review of European standards for pellet quality', Renewable Energy, 36(12), pp. 3537-3540.

Gaurav, N., Sivasankari, S., Kiran, G.S., Ninawe, A. and Selvin, J. (2017) 'Utilization of bioresources for sustainable biofuels: A Review', Renewable and Sustainable Energy Reviews, 73, pp. 205-214.

Ge, H., Guo, W., Shen, L., Song, T. and Xiao, J. (2016) 'Experimental investigation on biomass gasification using chemical looping in a batch reactor and a continuous dual reactor', Chemical Engineering Journal, 286, pp. 689-700.

Gerber, S., Behrendt, F. and Oevermann, M. (2010) 'An Eulerian modeling approach of wood gasification in a bubbling fluidized bed reactor using char as bed material', Fuel, 89(10), pp. 2903-2917.

Gerçel, H.F. (2002) 'Production and characterization of pyrolysis liquids from sunflower-pressed bagasse', Bioresource Technology, 85(2), pp. 113-117.

Gerun, L., Paraschiv, M., Vîjeu, R., Bellettre, J., Tazerout, M., Gøbel, B. and Henriksen, U. (2008) 'Numerical investigation of the partial oxidation in a two-stage downdraft gasifier', Fuel, 87(7), pp. 1383-1393.

Ghaly, R.A., Pyke, J.B., Ghaly, A.E. and Ugursal, V.I. (1999) 'Physical and Thermochemical Properties of Uncontaminated and Diesel-Contaminated Peat', Energy Sources, 21(5), pp. 433-451.

GIB (2014) The UK residual waste market.

Gil, J., Aznar, M.P., Caballero, M.A., Francés, E. and Corella, J. (1997) 'Biomass Gasification in Fluidized Bed at Pilot Scale with Steam−Oxygen Mixtures. Product Distribution for Very Different Operating Conditions', Energy & Fuels, 11(6), pp. 1109-1118.

Gil, J., Corella, J., Aznar, M.a.P. and Caballero, M.A. (1999) 'Biomass gasification in atmospheric and bubbling fluidized bed: Effect of the type of gasifying agent on the product distribution', Biomass and Bioenergy, 17(5), pp. 389-403.

Gilbert, P., Ryu, C., Sharifi, V. and Swithenbank, J. (2009) 'Tar reduction in pyrolysis vapours from biomass over a hot char bed', Bioresource Technology, 100(23), pp. 6045-6051.

Gómez-Barea, A., Leckner, B., Villanueva Perales, A., Nilsson, S. and Fuentes Cano, D. (2013a) 'Improving the performance of fluidized bed biomass/waste gasifiers for distributed electricity: A new three-stage gasification system', Applied Thermal Engineering, 50(2), pp. 1453-1462.

Gómez-Barea, A., Ollero, P. and Leckner, B. (2013b) 'Optimization of char and tar conversion in fluidized bed biomass gasifiers', Fuel, 103, pp. 42-52.

Gomez, L.D., Steele-King, C.G. and McQueen-Mason, S.J. (2008) 'Sustainable liquid biofuels from biomass: the writing's on the walls', New Phytologist, 178(3), pp. 473-485.

González, J.F., Román, S., González-García, C.M., Nabais, J.M.V. and Ortiz, A.L. (2009) 'Porosity Development in Activated Carbons Prepared from Walnut Shells by Carbon Dioxide or Steam Activation', Industrial & Engineering Chemistry Research, 48(16), pp. 7474-7481.

Göransson, K., Söderlind, U., He, J. and Zhang, W. (2011) 'Review of syngas production via biomass DFBGs', Renewable and Sustainable Energy Reviews, 15(1), pp. 482-492.

Gordillo, G., Annamalai, K. and Carlin, N. (2009) 'Adiabatic fixed-bed gasification of coal, dairy biomass, and feedlot biomass using an air–steam mixture as an oxidizing agent', Renewable Energy, 34(12), pp. 2789-2797.

Goyal, H.B., Seal, D. and Saxena, R.C. (2008) 'Bio-fuels from thermochemical conversion of renewable resources: A review', Renewable and Sustainable Energy Reviews, 12(2), pp. 504-517.

Gräfe, M., Power, G. and Klauber, C. (2011) 'Bauxite residue issues: III. Alkalinity and associated chemistry', Hydrometallurgy, 108(1), pp. 60-79.

Groeneveld, M.J. and van Swaaij, W.P.M. (1980) '39 Gasification of char particles with $CO_2$ AND $H_2O$', Chemical Engineering Science, 35(1), pp. 307-313.

Gu, H., Hargreaves, J.S.J., McFarlane, A.R. and MacKinnon, G. (2016) 'The carbon deposits formed by reaction of a series of red mud samples with methanol', RSC Advances, 6(52), pp. 46421-46426.

Guan, G., Kaewpanha, M., Hao, X. and Abudula, A. (2016) 'Catalytic steam reforming of biomass tar: Prospects and challenges', Renewable and Sustainable Energy Reviews, 58, pp. 450-461.

Guan, Y., Luo, S., Liu, S., Xiao, B. and Cai, L. (2009) 'Steam catalytic gasification of municipal solid waste for producing tar-free fuel gas', International Journal of Hydrogen Energy, 34(23), pp. 9341-9346.

Guizani, C., Escudero Sanz, F.J. and Salvador, S. (2013) 'The gasification reactivity of high-heating-rate chars in single and mixed atmospheres of $H_2O$ and $CO_2$', Fuel, 108, pp. 812-823.

Guizani, C., Escudero Sanz, F.J. and Salvador, S. (2014) 'Effects of $CO_2$ on biomass fast pyrolysis: Reaction rate, gas yields and char reactive properties', Fuel, 116, pp. 310-320.

Guizani, C., Escudero Sanz, F.J. and Salvador, S. (2015a) 'Influence of temperature and particle size on the single and mixed atmosphere gasification of biomass char with $H_2O$ and $CO_2$', Fuel Processing Technology, 134, pp. 175-188.

Guizani, C., Jeguirim, M., Gadiou, R., Escudero Sanz, F.J. and Salvador, S. (2016) 'Biomass char gasification by $H_2O$, $CO_2$ and their mixture: Evolution of chemical, textural and structural properties of the chars', Energy, 112, pp. 133-145.

Guizani, C., Louisnard, O., Sanz, F.J.E. and Salvador, S. (2015b) 'Gasification of woody biomass under high heating rate conditions in pure $CO_2$: Experiments and modelling', Biomass and Bioenergy, 83, pp. 169-182.

Gunarathne, D., Jatunarachchi, S.S., Senanayake, N.S. and Wei, B. (2013) 'The Effect of Throat Diameter on the Performance a Downdraft Biomass Gasifier', International Journal of Energy Engineering, 3(3), pp. 171-175.

Halász, J., Hodos, M., Hannus, I., Tasi, G. and Kiricsi, I. (2005) 'Catalytic detoxification of $C_2$-chlorohydrocarbons over iron-containing oxide and zeolite catalysts', Colloids and Surfaces A: Physicochemical and Engineering Aspects, 265(1), pp. 171-177.

Hamelinck, C.N., Faaij, A.P.C., den Uil, H. and Boerrigter, H. (2004) 'Production of FT transportation fuels from biomass; technical options, process analysis and optimisation, and development potential', Energy, 29(11), pp. 1743-1771.

Han, J. and Kim, H. (2008) 'The reduction and control technology of tar during biomass gasification/pyrolysis: An overview', Renewable and Sustainable Energy Reviews, 12(2), pp. 397-416.

Han, J., Liang, Y., Hu, J., Qin, L., Street, J., Lu, Y. and Yu, F. (2017) 'Modeling downdraft biomass gasification process by restricting chemical reaction equilibrium with Aspen Plus', Energy Conversion and Management, 153, pp. 641-648.

Hanson, S., Patrick, J.W. and Walker, A. (2002) 'The effect of coal particle size on pyrolysis and steam gasification', Fuel, 81(5), pp. 531-537.

Hasler, P. and Nussbaumer, T. (1999) 'Gas cleaning for IC engine applications from fixed bed biomass gasification', Biomass and Bioenergy, 16(6), pp. 385-395.

Hassan, M.H. and Kalam, M.A. (2013) 'An Overview of Biofuel as a Renewable Energy Source: Development and Challenges', Procedia Engineering, 56, pp. 39-53.

Hautman, D.J., Dryer, F.L., Schug, K.P. and Glassman, I. (1981) 'A Multiple-step Overall Kinetic Mechanism for the Oxidation of Hydrocarbons', Combustion Science and Technology, 25(5-6), pp. 219-235.

He, M., Hu, Z., Xiao, B., Li, J., Guo, X., Luo, S., Yang, F., Feng, Y., Yang, G. and Liu, S. (2009) 'Hydrogen-rich gas from catalytic steam gasification of municipal solid waste (MSW): Influence of catalyst and temperature on yield and product composition', International Journal of Hydrogen Energy, 34(1), pp. 195-203.

Heidenreich, S. and Foscolo, P.U. (2015) 'New concepts in biomass gasification', Progress in Energy and Combustion Science, 46, pp. 72-95.

Henriksen, U., Ahrenfeldt, J., Jensen, T.K., Gøbel, B., Bentzen, J.D., Hindsgaul, C. and Sørensen, L.H. (2006) 'The design, construction and operation of a 75kW two-stage gasifier', Energy, 31(10), pp. 1542-1553.

Heo, H.S., Park, H.J., Yim, J.-H., Sohn, J.M., Park, J., Kim, S.-S., Ryu, C., Jeon, J.-K. and Park, Y.-K. (2010) 'Influence of operation variables on fast pyrolysis of Miscanthus sinensis var. purpurascens', Bioresource Technology, 101(10), pp. 3672-3677.

Herguido, J., Corella, J. and Gonzalez-Saiz, J. (1992) 'Steam gasification of lignocellulosic residues in a fluidized bed at a small pilot scale. Effect of the type of feedstock', Industrial & Engineering Chemistry Research, 31(5), pp. 1274-1282.

Hernández, J.J., Aranda-Almansa, G. and Bula, A. (2010) 'Gasification of biomass wastes in an entrained flow gasifier: Effect of the particle size and the residence time', Fuel Processing Technology, 91(6), pp. 681-692.

Hernández, J.J., Aranda, G., Barba, J. and Mendoza, J.M. (2012) 'Effect of steam content in the air–steam flow on biomass entrained flow gasification', Fuel Processing Technology, 99, pp. 43-55.

Hewu, W., Haiyan, H., Xue, D. and Minggao, O. (2013) 'Hydrogen and Fuel-Cell Vehicle Technology', in Sustainable Automotive Energy System in China. Berlin, Heidelberg: Springer Berlin Heidelberg, pp. 301-333.

Hobbs, M.L., Radulovic, P.T. and Smoot, L.D. (1993) 'Combustion and gasification of coals in fixed-beds', Progress in Energy and Combustion Science, 19(6), pp. 505-586.

Hochman, G., Traux, M. and Zilberman, D. (2017) 'US Biofuel Policies and Markets', in Khanna, M. and Zilberman, D. (eds.) Handbook of Bioenergy Economics and Policy: Volume II: Modeling Land Use and Greenhouse Gas Implications. New York, NY: Springer New York, pp. 15-38.

Hosoya, T., Kawamoto, H. and Saka, S. (2007) 'Pyrolysis behaviors of wood and its constituent polymers at gasification temperature', Journal of Analytical and Applied Pyrolysis, 78(2), pp. 328-336.

Hosoya, T., Kawamoto, H. and Saka, S. (2008) 'Pyrolysis gasification reactivities of primary tar and char fractions from cellulose and lignin as studied with a closed ampoule reactor', Journal of Analytical and Applied Pyrolysis, 83(1), pp. 71-77.

Hosseini Koupaie, E., Johnson, T. and Eskicioglu, C. (2018) 'Comparison of Different Electricity-Based Thermal Pretreatment Methods for Enhanced Bioenergy Production from Municipal Sludge', Molecules, 23(8), pp. 1-15.

Hosseini, M., Dincer, I. and Rosen, M.A. (2012) 'Steam and air fed biomass gasification: Comparisons based on energy and exergy', International Journal of Hydrogen Energy, 37(21), pp. 16446-16452.

Hulteberg, P.C. and Karlsson, H.T. (2009) 'A study of combined biomass gasification and electrolysis for hydrogen production', International Journal of Hydrogen Energy, 34(2), pp. 772-782.

Huynh, T.M., Armbruster, U. and Martin, A. (2016) 'Deoxygenation of Liquid and Liquefied Biomass', in Chemicals and Fuels from Bio-Based Building Blocks. Wiley-VCH Verlag GmbH & Co. KGaA, pp. 403-430.

International Energy, A. (2018) World Energy Outlook 2018.

Isahak, W.N.R.W., Hisham, M.W.M., Yarmo, M.A. and Yun Hin, T.-y. (2012) 'A review on bio-oil production from biomass by using pyrolysis method', Renewable and Sustainable Energy Reviews, 16(8), pp. 5910-5923.

Isikgor, F.H. and Becer, C.R. (2015) 'Lignocellulosic biomass: a sustainable platform for the production of bio-based chemicals and polymers', Polymer Chemistry, 6(25), pp. 4497-4559.

James, A.K., Helle, S.S., Thring, R.W., Rutherford, P.M. and Masnadi, M.S. (2014) 'Investigation of air and air-steam gasification of high carbon wood ash in a fluidized bed reactor', Energy and Environment Research, 4(1), pp. 15-24.

Janajreh, I. and Al Shrah, M. (2013) 'Numerical and experimental investigation of downdraft gasification of wood chips', Energy Conversion and Management, 65, pp. 783-792.

Janajreh, I., Raza, S.S. and Valmundsson, A.S. (2013) 'Plasma gasification process: Modeling, simulation and comparison with conventional air gasification', Energy Conversion and Management, 65, pp. 801-809.

Jaojaruek, K., Jarungthammachote, S., Gratuito, M.K.B., Wongsuwan, H. and Homhual, S. (2011) 'Experimental study of wood downdraft gasification for an improved producer gas quality through an innovative two-stage air and premixed air/gas supply approach', Bioresource Technology, 102(7), pp. 4834-4840.

Jaya Shakar, T., Shahab, S. and Christopher, T.W. (2010) Biomass Torrefaction Process Review and Moving Bed Torrefaction System Model Development (INL/EXT-10-19569; TRN: US20102267 United States 10.2172/991885 TRN: US20102267 INL English). Idaho National Laboratory (INL).

Jayah, T.H., Aye, L., Fuller, R.J. and Stewart, D.F. (2003) 'Computer simulation of a downdraft wood gasifier for tea drying', Biomass and Bioenergy, 25(4), pp. 459-469.

Jenkins, B.M., Baxter, L.L., Miles, T.R. and Miles, T.R. (1998) 'Combustion properties of biomass', Fuel Processing Technology, 54(1), pp. 17-46.

Jiang, G., Nowakowski, D.J. and Bridgwater, A.V. (2010) 'Effect of the Temperature on the Composition of Lignin Pyrolysis Products', Energy & Fuels, 24(8), pp. 4470-4475.

Jianjun, D., Jean, S., John, R.G. and Naoko, E. (2015) 'Gasification of Woody Biomass', Annual Review of Chemical and Biomolecular Engineering, 6(1), pp. 77-99.

Jindo, K., Mizumoto, H., Sawada, Y., Sánchez-Monedero, M. and Sonoki, T. (2014) 'Physical and chemical characterizations of biochars derived from different agricultural residues', Biogeosciences, 11, pp. 6613-6621.

Kaiwen, L., Bin, Y. and Tao, Z. (2018) 'Economic analysis of hydrogen production from steam reforming process: A literature review', Energy Sources, Part B: Economics, Planning, and Policy, 13(2), pp. 109-115.

Kalamaras, C.M. and Efstathiou, A.M. (2013) 'Hydrogen Production Technologies: Current State and Future Developments', Conference Papers in Energy, 1(1), pp. 1-9.

Kalinci, Y., Hepbasli, A. and Dincer, I. (2009) 'Biomass-based hydrogen production: A review and analysis', International Journal of Hydrogen Energy, 34(21), pp. 8799-8817.

Kan, T., Strezov, V. and Evans, T.J. (2016) 'Lignocellulosic biomass pyrolysis: A review of product properties and effects of pyrolysis parameters', Renewable and Sustainable Energy Reviews, 57, pp. 1126-1140.

Karimi, E., Teixeira, I.F., Ribeiro, L.P., Gomez, A., Lago, R.M., Penner, G., Kycia, S.W. and Schlaf, M. (2012) 'Ketonization and deoxygenation of alkanoic acids and conversion of levulinic acid to hydrocarbons using a Red Mud bauxite mining waste as the catalyst', Catalysis Today, 190(1), pp. 73-88.

Kashiwagi, T. and Nambu, H. (1992) 'Global kinetic constants for thermal oxidative degradation of a cellulosic paper', Combustion and Flame, 88(3), pp. 345-368.

Kastner, J.R., Hilten, R., Weber, J., McFarlane, A.R., Hargreaves, J.S.J. and Batra, V.S. (2015) 'Continuous catalytic upgrading of fast pyrolysis oil using iron oxides in red mud', RSC Advances, 5(37), pp. 29375-29385.

Kaza, S., Yao, L.C., Bhada-Tata, P. and Van Woerden, F. (2018) What a Waste 2.0 : A Global Snapshot of Solid Waste Management to 2050. Washington, D.C.: World Bank Group.

Kim, W.-K., Shim, T., Kim, Y.-S., Hyun, S., Ryu, C., Park, Y.-K. and Jung, J. (2013a) 'Characterization of cadmium removal from aqueous solution by biochar produced from a giant Miscanthus at different pyrolytic temperatures', Bioresource Technology, 138, pp. 266-270.

Kim, Y.D., Yang, C.W., Kim, B.J., Kim, K.S., Lee, J.W., Moon, J.H., Yang, W., Yu, T.U. and Lee, U.D. (2013b) 'Air-blown gasification of woody biomass in a bubbling fluidized bed gasifier', Applied Energy, 112, pp. 414-420.

Kimura, T., Miyazawa, T., Nishikawa, J., Kado, S., Okumura, K., Miyao, T., Naito, S., Kunimori, K. and Tomishige, K. (2006) 'Development of Ni catalysts for tar removal by steam gasification of biomass', Applied Catalysis B: Environmental, 68(3), pp. 160-170.

Kinoshita, C.M., Wang, Y. and Zhou, J. (1994) 'Tar formation under different biomass gasification conditions', Journal of Analytical and Applied Pyrolysis, 29(2), pp. 169-181.

Kirkels, A.F. and Verbong, G.P.J. (2011) 'Biomass gasification: Still promising? A 30-year global overview', Renewable and Sustainable Energy Reviews, 15(1), pp. 471-481.

Klinghoffer, N.B., Castaldi, M.J. and Nzihou, A. (2012) 'Catalyst Properties and Catalytic Performance of Char from Biomass Gasification', Industrial & Engineering Chemistry Research, 51(40), pp. 13113-13122.

Klopries, B., Hodek, W. and Bandermann, F. (1990) 'Catalytic hydroliquefaction of biomass with red mud and $CoO/MoO_3$ catalysts', Fuel, 69(4), pp. 448-455.

Konieczny, A., Mondal, K., Wiltowski, T. and Dydo, P. (2008) 'Catalyst development for thermocatalytic decomposition of methane to hydrogen', International Journal of Hydrogen Energy, 33(1), pp. 264-272.

Kosov, V.V. and Zaichenko, V.M. (2016) 'Development and optimization of a two-stage gasifier for heat and power production', Journal of Physics: Conference Series, 774(1), pp. 1-6.

Ku, X., Li, T. and Løvås, T. (2015) 'CFD–DEM simulation of biomass gasification with steam in a fluidized bed reactor', Chemical Engineering Science, 122, pp. 270-283.

Kumar, A., Jones, D.D. and Hanna, M.A. (2009) 'Thermochemical Biomass Gasification: A Review of the Current Status of the Technology', Energies, 2(3), pp. 556-581.

Kumar, Y. (2015) 'Biomass gasification - A Review', IJESTA, 1, pp. 12-27.

Kumararaja, L. and Sethumadhavan, R. (2013) 'Experimental Studies on Biomass Bed Height and Certain Process Parameters in a Fully Co-current Flow Biomass Gasifier', Energy Sources, Part A: Recovery, Utilization, and Environmental Effects, 35(10), pp. 945-954.

Kuo, P.-C. and Wu, W. (2015) 'Design, Optimization and Energetic Efficiency of Producing Hydrogen-Rich Gas from Biomass Steam Gasification', Energies, 8(1), pp. 94-110.

Kwiatkowski, K., Dudyński, M. and Bajer, K. (2013) 'Combustion of Low-Calorific Waste Biomass Syngas', Flow, Turbulence and Combustion, 91(4), pp. 749-772.

Kwon, E.E. and Castaldi, M.J. (2012) 'Urban energy mining from municipal solid waste (MSW) via the enhanced thermo-chemical process by carbon dioxide ($CO_2$) as a reaction medium', Bioresource Technology, 125, pp. 23-29.

Kwon, E.E., Cho, S.-H. and Kim, S. (2015) 'Synergetic Sustainability Enhancement via Utilization of Carbon Dioxide as Carbon Neutral Chemical Feedstock in the Thermo-Chemical Processing of Biomass', Environmental Science & Technology, 49(8), pp. 5028-5034.

Kwon, E.E., Jeon, Y.J. and Yi, H. (2012) 'New candidate for biofuel feedstock beyond terrestrial biomass for thermo-chemical process (pyrolysis/gasification) enhanced by carbon dioxide ($CO_2$)', Bioresource Technology, 123, pp. 673-677.

La Villetta, M., Costa, M. and Massarotti, N. (2017) 'Modelling approaches to biomass gasification: A review with emphasis on the stoichiometric method', Renewable and Sustainable Energy Reviews, 74, pp. 71-88.

Ladji, R., Yassaa, N., Balducci, C. and Cecinato, A. (2014) 'Particle size distribution of n-alkanes and polycyclic aromatic hydrocarbons (PAHS) in urban and industrial aerosol of Algiers, Algeria', Environmental Science and Pollution Research, 21(3), pp. 1819-1832.

Lan, X., Zhong, H. and Gao, J. (2014) 'CFD simulation on the gasification of asphalt water slurry in an entrained flow gasifier', Petroleum Science, 11(2), pp. 308-317.

Leal, A.M.M., Kulik, D.A. and Kosakowski, G. (2016) 'Computational methods for reactive transport modeling: A Gibbs energy minimization approach for multiphase equilibrium calculations', Advances in Water Resources, 88, pp. 231-240.

Ledesma, E.B., Kalish, M.A., Nelson, P.F., Wornat, M.J. and Mackie, J.C. (2000) 'Formation and fate of PAH during the pyrolysis and fuel-rich combustion of coal primary tar', Fuel, 79(14), pp. 1801-1814.

Lee, A.C., Mitchell, R.E. and Gür, T.M. (2009) 'Thermodynamic analysis of gasification-driven direct carbon fuel cells', Journal of Power Sources, 194(2), pp. 774-785.

Lee, J.-Y., Keener, T. and Yang, Y.J. (2008) Air and Waste Management Association - 7th Power Plant Air Pollutant Control 'Mega' Symposium 2008. Baltimore, MD.

Lee, J., Yang, X., Cho, S.-H., Kim, J.-K., Lee, S.S., Tsang, D.C.W., Ok, Y.S. and Kwon, E.E. (2017) 'Pyrolysis process of agricultural waste using $CO_2$ for waste management, energy recovery, and biochar fabrication', Applied Energy, 185, pp. 214-222.

Lehto, J., Oasmaa, A., Solantausta, Y., Kytö, M. and Chiaramonti, D. (2013) Fuel oil quality and combustion of fast pyrolysis bio-oils. Finland: VTT Technical Research Centre of Finland.

Leibbrandt, N.H., Aboyade, A.O., Knoetze, J.H. and Görgens, J.F. (2013) 'Process efficiency of biofuel production via gasification and Fischer–Tropsch synthesis', Fuel, 109, pp. 484-492.

Leibold, H., Hornung, A. and Seifert, H. (2008) 'HTHP syngas cleaning concept of two stage biomass gasification for FT synthesis', Powder Technology, 180(1), pp. 265-270.

Li, C. and Suzuki, K. (2009) 'Tar property, analysis, reforming mechanism and model for biomass gasification—An overview', Renewable and Sustainable Energy Reviews, 13(3), pp. 594-604.

Li, L.Y. (2001) 'A study of iron mineral transformation to reduce red mud tailings', Waste Management, 21(6), pp. 525-534.

Li, W., Arshad, A., Haydar, Z., Yaqoob, N. and Hussain, S. (2018) 'Evaluating removal of tar contents in syngas produced from downdraft biomass gasification system AU - Awais, Muhammad', International Journal of Green Energy, 15(12), pp. 724-731.

Lin, Y. and Tanaka, S. (2006) 'Ethanol fermentation from biomass resources: current state and prospects', Applied Microbiology and Biotechnology, 69(6), pp. 627-642.

Liu, H., Elkamel, A., Lohi, A. and Biglari, M. (2013) 'Computational Fluid Dynamics Modeling of Biomass Gasification in Circulating Fluidized-Bed Reactor Using the Eulerian–Eulerian Approach', Industrial & Engineering Chemistry Research, 52(51), pp. 18162-18174.

Liu, H., Ul Hai, I., Zhang, W., Schröder, P., Neubauer, Y., Seilkopf, A., Oldenburg, H. and Kölling, A. (2012) 'Gas cleaning strategies for biomass gasification product gas', International Journal of Low-Carbon Technologies, 7(2), pp. 69-74.

Liu, J., He, Y., Ma, X., Liu, G., Yao, Y., Liu, H., Chen, H., Huang, Y., Chen, C. and Wang, W. (2016) 'Catalytic Pyrolysis of Tar Model Compound with Various Bio-Char Catalysts to Recycle Char from Biomass Pyrolysis', Bioresources, 11(2), pp. 3752-3768.

Liu, Q., Li, H., Fang, X., Zhang, J., Zhang, C., Ma, M., Li, F. and Huang, G. (2017) 'Preparation of Modified Red Mud-Supported Fe Catalysts for Hydrogen Production by Catalytic Methane Decomposition', Journal of Nanomaterials, 1, pp. 1-11.

Liu, W.-J., Jiang, H. and Yu, H.-Q. (2015) 'Development of Biochar-Based Functional Materials: Toward a Sustainable Platform Carbon Material', Chemical Reviews, 115(22), pp. 12251-12285.

Liu, X. and Zhang, N. (2011) 'Utilization of red mud in cement production: a review', Waste Management & Research, 29(10), pp. 1053-1063.

Liu, Z., Zhang, F., Liu, H., Ba, F., Yan, S. and Hu, J. (2018) 'Pyrolysis/gasification of pine sawdust biomass briquettes under carbon dioxide atmosphere: Study on carbon dioxide reduction (utilization) and biochar briquettes physicochemical properties', Bioresource Technology, 249, pp. 983-991.

Loha, C., Chatterjee, P.K. and Chattopadhyay, H. (2011) 'Performance of fluidized bed steam gasification of biomass – Modeling and experiment', Energy Conversion and Management, 52(3), pp. 1583-1588.

Lu, L., Ismail, T.M., Jin, Y., Abd El-Salam, M. and Yoshikawa, K. (2016) 'Numerical and experimental investigation on co-combustion characteristics of hydrothermally treated municipal solid waste with coal in a fluidized bed', Fuel Processing Technology, 154, pp. 52-65.

Luo, S., Xiao, B., Hu, Z., Liu, S., Guo, X. and He, M. (2009) 'Hydrogen-rich gas from catalytic steam gasification of biomass in a fixed bed reactor: Influence of temperature and steam on gasification performance', International Journal of Hydrogen Energy, 34(5), pp. 2191-2194.

Luo, S., Zhou, Y. and Yi, C. (2012) 'Syngas production by catalytic steam gasification of municipal solid waste in fixed-bed reactor', Energy, 44(1), pp. 391-395.

Luo, Z., Wang, S., Liao, Y., Zhou, J., Gu, Y. and Cen, K. (2004) 'Research on biomass fast pyrolysis for liquid fuel', Biomass and Bioenergy, 26(5), pp. 455-462.

Lv, D., Xu, M., Liu, X., Zhan, Z., Li, Z. and Yao, H. (2010) 'Effect of cellulose, lignin, alkali and alkaline earth metallic species on biomass pyrolysis and gasification', Fuel Processing Technology, 91(8), pp. 903-909.

Lv, P.M., Xiong, Z.H., Chang, J., Wu, C.Z., Chen, Y. and Zhu, J.X. (2004) 'An experimental study on biomass air–steam gasification in a fluidized bed', Bioresource Technology, 95(1), pp. 95-101.

Ly, H.V., Kim, S.-S., Choi, J.H., Woo, H.C. and Kim, J. (2016) 'Fast pyrolysis of Saccharina japonica alga in a fixed-bed reactor for bio-oil production', Energy Conversion and Management, 122, pp. 526-534.

Ma, Z., Zhang, Y., Zhang, Q., Qu, Y., Zhou, J. and Qin, H. (2012) 'Design and experimental investigation of a 190 kWe biomass fixed bed gasification and polygeneration pilot plant using a double air stage downdraft approach', Energy, 46(1), pp. 140-147.

Madadkhani, S. (2016) Red mud as an iron-based catalyst for catalytic cracking of naphthalene. The University of British Columbia.

Mahamulkar, S., Yin, K., Agrawal, P.K., Davis, R.J., Jones, C.W., Malek, A. and Shibata, H. (2016) 'Formation and Oxidation/Gasification of Carbonaceous Deposits: A Review', Industrial & Engineering Chemistry Research, 55(37), pp. 9760-9818.

Mahishi, M.R. and Goswami, D.Y. (2007) 'Thermodynamic optimization of biomass gasifier for hydrogen production', International Journal of Hydrogen Energy, 32(16), pp. 3831-3840.

Mani, S., Tabil, L.G. and Sokhansanj, S. (2004) 'Grinding performance and physical properties of wheat and barley straws, corn stover and switchgrass', Biomass and Bioenergy, 27(4), pp. 339-352.

Matas Güell, B., Sandquist, J. and Sørum, L. (2012) 'Gasification of Biomass to Second Generation Biofuels: A Review', Journal of Energy Resources Technology, 135(1), pp. 1-9.

Materazzi, M., Lettieri, P., Mazzei, L., Taylor, R. and Chapman, C. (2013) 'Thermodynamic modelling and evaluation of a two-stage thermal process for waste gasification', Fuel, 108, pp. 356-369.

Mauricio, D., Maya, Y., Lizeth, A., Sarmiento, E., Aparecida, C. and Bôas De Sales Oliveira, V. (2016) 'Gasification of municipal solid waste for power generation in brazil, a review of available technologies and their environmental benefits', Journal of Chemistry and Chemical Engineering, 10(1), pp. 249-255.

Mayerhofer, M., Mitsakis, P., Meng, X., de Jong, W., Spliethoff, H. and Gaderer, M. (2012) 'Influence of pressure, temperature and steam on tar and gas in allothermal fluidized bed gasification', Fuel, 99, pp. 204-209.

McKendry, P. (2002) 'Energy production from biomass (part 3): gasification technologies', Bioresource Technology, 83(1), pp. 55-63.

Md Isa, K., Osman, K., Abdullah, N.R., Mukhtar, A. and Othman, N.F. (2015) 'CFD Modelling of a Fluidized Bed Gasifier; Effects of Drag Model and Bed Heights', Applied Mechanics and Materials, 699, pp. 730-735.

Meenaroch, P., Kerdsuwan, S. and Laohalidanond, K. (2015) 'Development of Kinetics Models in Each Zone of a 10kg/hr Downdraft Gasifier using Computational Fluid Dynamics', Energy Procedia, 79, pp. 278-283.

Menéndez, J.A., Domínguez, A., Fernández, Y. and Pis, J.J. (2007) 'Evidence of Self-Gasification during the Microwave-Induced Pyrolysis of Coffee Hulls', Energy & Fuels, 21(1), pp. 373-378.

Milne, T.A., Evans, R.J. and Abatzaglou, N. (1998) Biomass Gasifier "Tars": Their Nature, Formation, and Conversion (NREL/TP-570-25357; ON: DE00003726; Other: ON: DE00003726; TRN: US200305983 United States 10.2172/3726 Other: ON: DE00003726; TRN: US200305983 NREL English). ; National Renewable Energy Laboratory, Golden, CO (US).

Mitchual, S.J., Frimpong-Mensah, K. and Darkwa, N.A. (2013) 'Effect of species, particle size and compacting pressure on relaxed density and compressive strength of fuel briquettes', International Journal of Energy and Environmental Engineering, 4(1), pp. 4-30.

Mojtahedi, W., Ylitalo, M., Maunula, T. and Abbasian, J. (1995) 'Catalytic decomposition of ammonia in fuel gas produced in pilot-scale pressurized fluidized-bed gasifier', Fuel Processing Technology, 45(3), pp. 221-236.

Molino, A., Chianese, S. and Musmarra, D. (2016) 'Biomass gasification technology: The state of the art overview', Journal of Energy Chemistry, 25(1), pp. 10-25.

Møller, K.T., Jensen, T.R., Akiba, E. and Li, H.-w. (2017) 'Hydrogen - A sustainable energy carrier', Progress in Natural Science: Materials International, 27(1), pp. 34-40.

Monarca, D., Colantoni, A., Cecchini, M., Longo, L., Vecchione, L., Carlini, M. and Manzo, A. (2012) 'Energy Characterization and Gasification of Biomass Derived by Hazelnut Cultivation: Analysis of Produced Syngas by Gas Chromatography', Mathematical Problems in Engineering, 1, pp. 1-9.

Moralı, U. and Şensöz, S. (2015) 'Pyrolysis of hornbeam shell (Carpinus betulus L.) in a fixed bed reactor: Characterization of bio-oil and bio-char', Fuel, 150, pp. 672-678.

Moralı, U., Yavuzel, N. and Şensöz, S. (2016) 'Pyrolysis of hornbeam (Carpinus betulus L.) sawdust: Characterization of bio-oil and bio-char', Bioresource Technology, 221, pp. 682-685.

Morf, P., Hasler, P. and Nussbaumer, T. (2002) 'Mechanisms and kinetics of homogeneous secondary reactions of tar from continuous pyrolysis of wood chips', Fuel, 81(7), pp. 843-853.

Myrén, C., Hörnell, C., Björnbom, E. and Sjöström, K. (2002) 'Catalytic tar decomposition of biomass pyrolysis gas with a combination of dolomite and silica', Biomass and Bioenergy, 23(3), pp. 217-227.

Navarro, R.M., Peña, M.A. and Fierro, J.L.G. (2007) 'Hydrogen Production Reactions from Carbon Feedstocks: Fossil Fuels and Biomass', Chemical Reviews, 107(10), pp. 3952-3991.

Ni, M., Leung, D.Y.C., Leung, M.K.H. and Sumathy, K. (2006) 'An overview of hydrogen production from biomass', Fuel Processing Technology, 87(5), pp. 461-472.

Nikoo, M.K. and Amin, N.A.S. (2011) 'Thermodynamic analysis of carbon dioxide reforming of methane in view of solid carbon formation', Fuel Processing Technology, 92(3), pp. 678-691.

Nilsson, S., Gómez-Barea, A., Fuentes-Cano, D. and Campoy, M. (2014) 'Gasification kinetics of char from olive tree pruning in fluidized bed', Fuel, 125, pp. 192-199.

Nipattummakul, N., Ahmed, I.I., Kerdsuwan, S. and Gupta, A.K. (2010) 'Hydrogen and syngas production from sewage sludge via steam gasification', International Journal of Hydrogen Energy, 35(21), pp. 11738-11745.

Niu, M., Huang, Y., Jin, B. and Wang, X. (2014) 'Oxygen Gasification of Municipal Solid Waste in a Fixed-bed Gasifier', Chinese Journal of Chemical Engineering, 22(9), pp. 1021-1026.

Niu, Y., Han, F., Chen, Y., Lyu, Y. and Wang, L. (2017) 'Experimental study on steam gasification of pine particles for hydrogen-rich gas', Journal of the Energy Institute, 90(5), pp. 715-724.

Norman, K. (2007) Interim report:feasibility of microscale glucose reforming for renewable hydrogen (SAND2007-1713; TRN: US200717494 United States 10.2172/902223 TRN: US200717494 SNL English). Sandia National Laboratories.

Oasmaa, A. and Czernik, S. (1999) 'Fuel Oil Quality of Biomass Pyrolysis OilsState of the Art for the End Users', Energy & Fuels, 13(4), pp. 914-921.

Oasmaa, A., Leppämäki, E., Koponen, P., Levander, J. and Tapola, E. (1997) Physical characterisation of biomass-based pyrolysis liquids Application of standard fuel oil analyses. Finland, V.T.R.C.o.

Oliveira, A.A.S., Tristão, J.C., Ardisson, J.D., Dias, A. and Lago, R.M. (2011) 'Production of nanostructured magnetic composites based on $Fe^0$ nuclei coated with carbon nanofibers and nanotubes from red mud waste and ethanol', Applied Catalysis B: Environmental, 105(1), pp. 163-170.

Ordóñez, S., Sastre, H. and Díez, F.V. (2001) 'Characterisation and deactivation studies of sulfided red mud used as catalyst for the hydrodechlorination of tetrachloroethylene', Applied Catalysis B: Environmental, 29(4), pp. 263-273.

Paethanom, A. and Yoshikawa, K. (2012) 'Influence of Pyrolysis Temperature on Rice Husk Char Characteristics and Its Tar Adsorption Capability', Energies, 5(12), pp. 4941-4951.

Panda, A.K., Singh, R.K. and Mishra, D.K. (2010) 'Thermolysis of waste plastics to liquid fuel: A suitable method for plastic waste management and manufacture of value added products—A world prospective', Renewable and Sustainable Energy Reviews, 14(1), pp. 233-248.

Pandey, S., Baral, B. and Lohani, S.P. (2012) 2nd International Conference on the Developments in Renewable Energy Technology (ICDRET 2012). 5-7 Jan. 2012.

Paredes, J.R., Ordóñez, S., Vega, A. and Díez, F.V. (2004) 'Catalytic combustion of methane over red mud-based catalysts', Applied Catalysis B: Environmental, 47(1), pp. 37-45.

Paula. G. Peres, A., Lunelli, B. and Filho, R. (2013) 'Application of Biomass to Hydrogen and Syngas Production', Chemical Engineering Transactions, 32, pp. 589-594.

Pei, H., Wang, X., Dai, X., Jin, B. and Huang, Y. (2018) 'A novel two-stage biomass gasification concept: Design and operation of a 1.5 MWth demonstration plant', Bioresource Technology, 267, pp. 102-109.

Peralta-Yahya, P.P., Zhang, F., del Cardayre, S.B. and Keasling, J.D. (2012) 'Microbial engineering for the production of advanced biofuels', Nature, 488, pp. 320-328.

Pereira, E.G., da Silva, J.N., de Oliveira, J.L. and Machado, C.S. (2012) 'Sustainable energy: A review of gasification technologies', Renewable and Sustainable Energy Reviews, 16(7), pp. 4753-4762.

Pérez, J., Muñoz-Dorado, J., de la Rubia, T. and Martínez, J. (2002) 'Biodegradation and biological treatments of cellulose, hemicellulose and lignin: an overview', International Microbiology, 5(2), pp. 53-63.

Pfeifer, C. and Hofbauer, H. (2008) 'Development of catalytic tar decomposition downstream from a dual fluidized bed biomass steam gasifier', Powder Technology, 180(1), pp. 9-16.

Pfeifer, C., Rauch, R. and Hofbauer, H. (2004) 'In-Bed Catalytic Tar Reduction in a Dual Fluidized Bed Biomass Steam Gasifier', Industrial & Engineering Chemistry Research, 43(7), pp. 1634-1640.

Plis, P. and Wilk, R.K. (2011) 'Theoretical and experimental investigation of biomass gasification process in a fixed bed gasifier', Energy, 36(6), pp. 3838-3845.

Pohořelý, M., Jeremiáš, M., Svoboda, K., Kameníková, P., Skoblia, S. and Beňo, Z. (2014) '$CO_2$ as moderator for biomass gasification', Fuel, 117, pp. 198-205.

Prabowo, B., Susanto, H., Umeki, K., Yan, M. and Yoshikawa, K. (2015) 'Pilot scale autothermal gasification of coconut shell with $CO_2$-$O_2$ mixture', Frontiers in Energy, 9(3), pp. 362-370.

Pradhan, D., Singh, R.K., Bendu, H. and Mund, R. (2016) 'Pyrolysis of Mahua seed (Madhuca indica) – Production of biofuel and its characterization', Energy Conversion and Management, 108, pp. 529-538.

Prasertcharoensuk, P., Bull, S.J. and Phan, A.N. (2019) 'Gasification of waste biomass for hydrogen production: Effects of pyrolysis parameters', Renewable Energy, 143, pp. 112-120.

Ptasinski, K.J., Prins, M.J. and Pierik, A. (2007) 'Exergetic evaluation of biomass gasification', Energy, 32(4), pp. 568-574.

Puig-Arnavat, M., Bruno, J.C. and Coronas, A. (2010) 'Review and analysis of biomass gasification models', Renewable and Sustainable Energy Reviews, 14(9), pp. 2841-2851.

Pütün, A.E., Apaydın, E. and Pütün, E. (2004) 'Rice straw as a bio-oil source via pyrolysis and steam pyrolysis', Energy, 29(12), pp. 2171-2180.

Qin, Y., Campen, A., Wiltowski, T., Feng, J. and Li, W. (2015) 'The influence of different chemical compositions in biomass on gasification tar formation', Biomass and Bioenergy, 83, pp. 77-84.

Quaak, P., Knoef, H. and Stassen, H. (1999) Energy from biomass : a review of combustion and gasification technologies (No. WTP 422). Washington, D.C.: Bank, T.W.

Radwan, A.M. (2012) 'An overview on gasification of biomass for production of hydrogen rich gas ', Der Chemica Sinica, 3(2), pp. 323-335.

Rafiq, M.K., Bachmann, R.T., Rafiq, M.T., Shang, Z., Joseph, S. and Long, R. (2016) 'Influence of Pyrolysis Temperature on Physico-Chemical Properties of Corn Stover (Zea mays L.) Biochar and Feasibility for Carbon Capture and Energy Balance', PLoS ONE, 11(6), pp. 1-17.

Ran, J. and Li, C. (2012) 'High temperature gasification of woody biomass using regenerative gasifier', Fuel Processing Technology, 99, pp. 90-96.

Rapagnà, S., Jand, N., Kiennemann, A. and Foscolo, P.U. (2000) 'Steam-gasification of biomass in a fluidised-bed of olivine particles', Biomass and Bioenergy, 19(3), pp. 187-197.

Ratnadhariya, J.K. and Channiwala, S.A. (2009) 'Three zone equilibrium and kinetic free modeling of biomass gasifier – a novel approach', Renewable Energy, 34(4), pp. 1050-1058.

Rauch, R., Hrbek, J. and Hofbauer, H. (2014) 'Biomass gasification for synthesis gas production and applications of the syngas', Wiley Interdisciplinary Reviews: Energy and Environment, 3(4), pp. 343-362.

Ravi Kumar, R., Narendhar Baba, M., Suresh Kumar, K. and Vishnu, A. (2016) 'CFD Simulation of Down Drought Biomass Gasifier', International Journal of Advance Engineering and Research Development, 3(1), pp. 58-64.

Ravi, M.R. and Kohli, S. (2018) 'Thermodynamics and Kinetics of Gasification', in De, S., Agarwal, A.K., Moholkar, V.S. and Thallada, B. (eds.) Coal and Biomass Gasification: Recent Advances and Future Challenges. Singapore: Springer Singapore, pp. 37-62.

Rehrah, D., Bansode, R.R., Hassan, O. and Ahmedna, M. (2016) 'Physico-chemical characterization of biochars from solid municipal waste for use in soil amendment', Journal of Analytical and Applied Pyrolysis, 118, pp. 42-53.

Ren, S., Lei, H., Wang, L., Bu, Q., Chen, S. and Wu, J. (2014) 'Hydrocarbon and hydrogen-rich syngas production by biomass catalytic pyrolysis and bio-oil upgrading over biochar catalysts', RSC Advances, 4(21), pp. 10731-10737.

Renganathan, T., Yadav, M.V., Pushpavanam, S., Voolapalli, R.K. and Cho, Y.S. (2012) '$CO_2$ utilization for gasification of carbonaceous feedstocks: A thermodynamic analysis', Chemical Engineering Science, 83, pp. 159-170.

Richardson, Y., Blin, J., Volle, G., Motuzas, J. and Julbe, A. (2010) 'In situ generation of Ni metal nanoparticles as catalyst for $H_2$-rich syngas production from biomass gasification', Applied Catalysis A: General, 382(2), pp. 220-230.

Roberts, A.F. (1970) 'A review of kinetics data for the pyrolysis of wood and related substances', Combustion and Flame, 14(2), pp. 261-272.

Rodriguez, C., Alaswad, A., Benyounis, K. and Olabi, A.G. (2017) 'Pretreatment techniques used in biogas production from grass', Renewable and Sustainable Energy Reviews, 68, pp. 1193-1204.

Rogel, A. and Aguillón, J. (2006) 'The 2D Eulerian Approach of Entrained Flow and Temperature in a Biomass Stratified Downdraft Gasifier', American Journal of Applied Sciences, 3(10), pp. 2068-2075.

Ronsse, F., van Hecke, S., Dickinson, D. and Prins, W. (2013) 'Production and characterization of slow pyrolysis biochar: influence of feedstock type and pyrolysis conditions', GCB Bioenergy, 5(2), pp. 104-115.

Rosmaninho, M.G., Moura, F.C.C., Souza, L.R., Nogueira, R.K., Gomes, G.M., Nascimento, J.S., Pereira, M.C., Fabris, J.D., Ardisson, J.D., Nazzarro, M.S., Sapag, K., Araújo, M.H. and Lago, R.M. (2012) 'Investigation of iron oxide reduction by ethanol as a potential route to produce hydrogen', Applied Catalysis B: Environmental, 115-116, pp. 45-52.

Ruiz, J.A., Juárez, M.C., Morales, M.P., Muñoz, P. and Mendívil, M.A. (2013) 'Biomass gasification for electricity generation: Review of current technology barriers', Renewable and Sustainable Energy Reviews, 18, pp. 174-183.

Sadhwani, N., Adhikari, S. and Eden, M.R. (2016) 'Biomass Gasification Using Carbon Dioxide: Effect of Temperature, $CO_2$/C Ratio, and the Study of Reactions Influencing the Process', Industrial & Engineering Chemistry Research, 55(10), pp. 2883-2891.

Saleh, A.R., Sudarmanta, B. and Ependi, D.R. (2018) 'Numerical study of gasification pelletized municipal solid waste using multi-stage air inlet downdraft gasifier', 3rd Annual Applied Science and Engineering Conference. 2018/12/03. IOP Publishing, pp. 1-9.

Sanchez-Hernandez, A.M., Martin-Sanchez, N., Sanchez-Montero, M.J., Izquierdo, C. and Salvador, F. (2018) 'Effect of pressure on the gasification of dodecane with steam and supercritical water and consequences for $H_2$ production', Journal of Materials Chemistry A, 6(4), pp. 1671-1681.

Sass, B., Monzyk, B., Ricci, S., Gupta, A., Hindin, B. and Gupta, N. (2005) 'Chapter 17 - Impact of $SO_x$ and $NO_x$ in Flue Gas on $CO_2$ Separation, Compression, and Pipeline Transmission', in Thomas, D.C. (ed.) Carbon Dioxide Capture for Storage in Deep Geologic Formations. Amsterdam: Elsevier Science, pp. 955-981.

Saxena, R.C., Seal, D., Kumar, S. and Goyal, H.B. (2008) 'Thermo-chemical routes for hydrogen rich gas from biomass: A review', Renewable and Sustainable Energy Reviews, 12(7), pp. 1909-1927.

Sehested, J. (2006) 'Four challenges for nickel steam-reforming catalysts', Catalysis Today, 111(1), pp. 103-110.

Şensöz, S. and Angın, D. (2008) 'Pyrolysis of safflower (Charthamus tinctorius L.) seed press cake: Part 1. The effects of pyrolysis parameters on the product yields', Bioresource Technology, 99(13), pp. 5492-5497.

Şensöz, S. and Can, M. (2002) 'Pyrolysis of Pine ( Pinus Brutia Ten.) Chips: 1. Effect of Pyrolysis Temperature and Heating Rate on the Product Yields', Energy Sources, 24(4), pp. 347-355.

Şensöz, S., Demiral, İ. and Ferdi Gerçel, H. (2006) 'Olive bagasse (Olea europea L.) pyrolysis', Bioresource Technology, 97(3), pp. 429-436.

Seo, D.K., Park, S.S., Hwang, J. and Yu, T.-U. (2010) 'Study of the pyrolysis of biomass using thermo-gravimetric analysis (TGA) and concentration measurements of the evolved species', Journal of Analytical and Applied Pyrolysis, 89(1), pp. 66-73.

Septien, S., Valin, S., Dupont, C., Peyrot, M. and Salvador, S. (2012) 'Effect of particle size and temperature on woody biomass fast pyrolysis at high temperature (1000–1400°C)', Fuel, 97, pp. 202-210.

Serrano, D.P., Aguado, J. and Escola, J.M. (2012) 'Developing Advanced Catalysts for the Conversion of Polyolefinic Waste Plastics into Fuels and Chemicals', ACS Catalysis, 2(9), pp. 1924-1941.

Shafie, S.M., Mahlia, T.M.I., Masjuki, H.H. and Ahmad-Yazid, A. (2012) 'A review on electricity generation based on biomass residue in Malaysia', Renewable and Sustainable Energy Reviews, 16(8), pp. 5879-5889.

Shahkarami, P. and Fatemi, S. (2015) 'Mathematical Modeling and Optimization of Combined Steam and Dry Reforming of Methane Process in Catalytic Fluidized Bed Membrane Reactor', Chemical Engineering Communications, 202(6), pp. 774-786.

Sharma, A.K. (2011) 'Modeling and simulation of a downdraft biomass gasifier 1. Model development and validation', Energy Conversion and Management, 52(2), pp. 1386-1396.

Sharma, S. and Sheth, P.N. (2016) 'Air–steam biomass gasification: Experiments, modeling and simulation', Energy Conversion and Management, 110, pp. 307-318.

Sharma, T., Yepes Maya, D.M., M. Nascimento, F.R., Shi, Y., Ratner, A., Silva Lora, E.E., Mendes Neto, L.J., Escobar Palacios, J.C. and Vieira Andrade, R. (2018) 'An Experimental and Theoretical Study of the Gasification of Miscanthus Briquettes in a Double-Stage Downdraft Gasifier: Syngas, Tar, and Biochar Characterization', Energies, 11, pp. 1-23.

Shayan, E., Zare, V. and Mirzaee, I. (2018) 'Hydrogen production from biomass gasification; a theoretical comparison of using different gasification agents', Energy Conversion and Management, 159, pp. 30-41.

Shen, Y. (2015) 'Chars as carbonaceous adsorbents/catalysts for tar elimination during biomass pyrolysis or gasification', Renewable and Sustainable Energy Reviews, 43, pp. 281-295.

Shen, Y. and Fu, Y. (2018) 'Advances in in situ and ex situ tar reforming with biochar catalysts for clean energy production', Sustainable Energy & Fuels, 2(2), pp. 326-344.

Shen, Y., Ma, D. and Ge, X. (2017) '$CO_2$-looping in biomass pyrolysis or gasification', Sustainable Energy & Fuels, 1(8), pp. 1700-1729.

Sikarwar, V.S., Zhao, M., Clough, P., Yao, J., Zhong, X., Memon, M.Z., Shah, N., Anthony, E.J. and Fennell, P.S. (2016) 'An overview of advances in biomass gasification', Energy & Environmental Science, 9(10), pp. 2939-2977.

Sikarwar, V.S., Zhao, M., Fennell, P.S., Shah, N. and Anthony, E.J. (2017) 'Progress in biofuel production from gasification', Progress in Energy and Combustion Science, 61, pp. 189-248.

Simell, P., Kurkela, E., Ståhlberg, P. and Hepola, J. (1996) 'Catalytic hot gas cleaning of gasification gas', Catalysis Today, 27(1), pp. 55-62.

Simell, P.A. and Bredenberg, J.B.s. (1990) 'Catalytic purification of tarry fuel gas', Fuel, 69(10), pp. 1219-1225.

Simone, M., Nicolella, C. and Tognotti, L. (2013) 'Numerical and experimental investigation of downdraft gasification of woody residues', Bioresource Technology, 133, pp. 92-101.

Singhvi, M.S., Chaudhari, S. and Gokhale, D.V. (2014) 'Lignocellulose processing: a current challenge', RSC Advances, 4(16), pp. 8271-8277.

Sircar, I., Sane, A., Wang, W. and Gore, J.P. (2014) 'Experimental and modeling study of pinewood char gasification with $CO_2$', Fuel, 119, pp. 38-46.

Siva Kumar, S., Pitchandi, K. and Natarajan, E. (2008) 'Modeling and Simulation of Down Draft Wood Gasifier', Journal of Applied Sciences, 8(2), pp. 271-279.

Snoeck, J.W., Froment, G.F. and Fowles, M. (2002) 'Steam/$CO_2$ Reforming of Methane. Carbon Filament Formation by the Boudouard Reaction and Gasification by $CO_2$, by $H_2$, and by Steam: Kinetic Study', Industrial & Engineering Chemistry Research, 41(17), pp. 4252-4265.

Sohaib, Q., Muhammad, A. and Younas, M. (2017) 'Fast pyrolysis of sugarcane bagasse: Effect of pyrolysis conditions on final product distribution and properties', Energy Sources, Part A: Recovery, Utilization, and Environmental Effects, 39(2), pp. 184-190.

Song, T., Wu, J., Shen, L. and Xiao, J. (2012) 'Experimental investigation on hydrogen production from biomass gasification in interconnected fluidized beds', Biomass and Bioenergy, 36, pp. 258-267.

Song, W. and Guo, M. (2012) 'Quality variations of poultry litter biochar generated at different pyrolysis temperatures', Journal of Analytical and Applied Pyrolysis, 94, pp. 138-145.

Songolzadeh, M., Soleimani, M., Takht Ravanchi, M. and Songolzadeh, R. (2014) 'Carbon Dioxide Separation from Flue Gases: A Technological Review Emphasizing Reduction in Greenhouse Gas Emissions', The Scientific World Journal, 1, pp. 1-34.

Sonwane, P., Ban, H. and Gale, T.K. (2006) 'Speciation of Chlorine and Alkali Metals in Biomass Combustion and Gasification', ASME Proceedings, 1, pp. 259-265.

Spath, P.L., Mann, M.K. and Amos, W.A. (2003) Update of Hydrogen from Biomass -- Determination of the Delivered Cost of Hydrogen. National Renewable Energy Lab., Golden, CO. (US).

Srinakruang, J., Sato, K., Vitidsant, T. and Fujimoto, K. (2006) 'Highly efficient sulfur and coking resistance catalysts for tar gasification with steam', Fuel, 85(17), pp. 2419-2426.

Stephanopoulos, G. (2007) 'Challenges in Engineering Microbes for Biofuels Production', Science, 315, pp. 801-804.

Šulc, J., Štojdl, J., Richter, M., Popelka, J., Svoboda, K., Smetana, J., Vacek, J., Skoblja, S. and Buryan, P. (2012) 'Biomass waste gasification – Can be the two stage process suitable for tar reduction and power generation?', Waste Management, 32(4), pp. 692-700.

Suliman, W., Harsh, J.B., Abu-Lail, N.I., Fortuna, A.-M., Dallmeyer, I. and Garcia-Perez, M. (2016) 'Influence of feedstock source and pyrolysis temperature on biochar bulk and surface properties', Biomass and Bioenergy, 84, pp. 37-48.

Sun, Y., Li, R., Yang, T., Kai, X. and He, Y. (2013) 'Gasification of biomass to hydrogen-rich gas in fluidized beds using porous medium as bed material', International Journal of Hydrogen Energy, 38(33), pp. 14208-14213.

Sutton, D., Kelleher, B. and Ross, J.R.H. (2001) 'Review of literature on catalysts for biomass gasification', Fuel Processing Technology, 73(3), pp. 155-173.

Tan, Y.L., Abdullah, A.Z. and Hameed, B.H. (2017) 'Fast pyrolysis of durian (Durio zibethinus L) shell in a drop-type fixed bed reactor: Pyrolysis behavior and product analyses', Bioresource Technology, 243, pp. 85-92.

Tanger, P., Field, J., Jahn, C., DeFoort, M. and Leach, J. (2013) 'Biomass for thermochemical conversion: targets and challenges', Frontiers in Plant Science, 4(218), pp. 1-20.

Thamavithya, M. and Dutta, A. (2008) 'An investigation of MSW gasification in a spout-fluid bed reactor', Fuel Processing Technology, 89(10), pp. 949-957.

Tijmensen, M.J.A., Faaij, A.P.C., Hamelinck, C.N. and van Hardeveld, M.R.M. (2002) 'Exploration of the possibilities for production of Fischer Tropsch liquids and power via biomass gasification', Biomass and Bioenergy, 23(2), pp. 129-152.

Tinaut, F.V., Melgar, A., Pérez, J.F. and Horrillo, A. (2008) 'Effect of biomass particle size and air superficial velocity on the gasification process in a downdraft fixed bed gasifier. An experimental and modelling study', Fuel Processing Technology, 89(11), pp. 1076-1089.

Torres, W., Pansare, S.S. and Goodwin, J.G. (2007) 'Hot Gas Removal of Tars, Ammonia, and Hydrogen Sulfide from Biomass Gasification Gas', Catalysis Reviews, 49(4), pp. 407-456.

Trippe, F., Fröhling, M., Schultmann, F., Stahl, R. and Henrich, E. (2011) 'Techno-economic assessment of gasification as a process step within biomass-to-liquid (BtL) fuel and chemicals production', Fuel Processing Technology, 92(11), pp. 2169-2184.

Trubetskaya, A., Broström, M., Kling, J., Brown, A., T. Timko, M., Tompsett, G. and Umeki, K. (2017) 'Effects of Lignocellulosic Compounds on the Yield, Nanostructure and Reactivity of Soot from Fast Pyrolysis at High Temperatures', Nordic Flame Days. KTH - The Royal Institute of Technology, 10/10/2017-11/10/2017. pp. 1-5.

Tumuluru, J.S., Wright, C.T., Hess, J.R. and Kenney, K.L. (2011) 'A review of biomass densification systems to develop uniform feedstock commodities for bioenergy application', Biofuels, Bioproducts and Biorefining, 5(6), pp. 683-707.

Tursun, Y., Xu, S., Wang, C., Xiao, Y. and Wang, G. (2016) 'Steam co-gasification of biomass and coal in decoupled reactors', Fuel Processing Technology, 141, pp. 61-67.

Ud Din, Z. and Zainal, Z.A. (2016) 'Biomass integrated gasification–SOFC systems: Technology overview', Renewable and Sustainable Energy Reviews, 53, pp. 1356-1376.

Udomsirichakorn, J. and Salam, P.A. (2014) 'Review of hydrogen-enriched gas production from steam gasification of biomass: The prospect of CaO-based chemical looping gasification', Renewable and Sustainable Energy Reviews, 30, pp. 565-579.

Valderrama Rios, M.L., González, A.M., Lora, E.E.S. and Almazán del Olmo, O.A. (2018) 'Reduction of tar generated during biomass gasification: A review', Biomass and Bioenergy, 108, pp. 345-370.

Valin, S., Bedel, L., Guillaudeau, J., Thiery, S. and Ravel, S. (2016) '$CO_2$ as a substitute of steam or inert transport gas in a fluidised bed for biomass gasification', Fuel, 177, pp. 288-295.

Van de steene, L., Tagutchou, J.P., Escudero Sanz, F.J. and Salvador, S. (2011) 'Gasification of woodchip particles: Experimental and numerical study of char–$H_2O$, char–$CO_2$, and char–$O_2$ reactions', Chemical Engineering Science, 66(20), pp. 4499-4509.

Van de Velden, M., Baeyens, J., Brems, A., Janssens, B. and Dewil, R. (2010) 'Fundamentals, kinetics and endothermicity of the biomass pyrolysis reaction', Renewable Energy, 35(1), pp. 232-242.

Van Soest, P.J., Robertson, J.B. and Lewis, B.A. (1991) 'Methods for Dietary Fiber, Neutral Detergent Fiber, and Nonstarch Polysaccharides in Relation to Animal Nutrition', Journal of Dairy Science, 74(10), pp. 3583-3597.

Vangelatos, I., Angelopoulos, G.N. and Boufounos, D. (2009) 'Utilization of ferroalumina as raw material in the production of Ordinary Portland Cement', Journal of Hazardous Materials, 168(1), pp. 473-478.

Varma, A.K. and Mondal, P. (2017) 'Pyrolysis of sugarcane bagasse in semi batch reactor: Effects of process parameters on product yields and characterization of products', Industrial Crops and Products, 95, pp. 704-717.

Vassilev, S.V., Baxter, D., Andersen, L.K. and Vassileva, C.G. (2013) 'An overview of the composition and application of biomass ash. Part 1. Phase–mineral and chemical composition and classification', Fuel, 105, pp. 40-76.

Vassilev, S.V., Baxter, D., Andersen, L.K., Vassileva, C.G. and Morgan, T.J. (2012) 'An overview of the organic and inorganic phase composition of biomass', Fuel, 94, pp. 1-33.

Velegol, D., Gautam, M. and Shamsi, A. (1997) 'Catalytic cracking of a coal tar in a fluid bed reactor', Powder Technology, 93(2), pp. 93-100.

Voloshin, R.A., Rodionova, M.V., Zharmukhamedov, S.K., Nejat Veziroglu, T. and Allakhverdiev, S.I. (2016) 'Review: Biofuel production from plant and algal biomass', International Journal of Hydrogen Energy, 41(39), pp. 17257-17273.

Wang, D., Czernik, S. and Chornet, E. (1998) 'Production of Hydrogen from Biomass by Catalytic Steam Reforming of Fast Pyrolysis Oils', Energy & Fuels, 12(1), pp. 19-24.

Wang, F.-J., Zhang, S., Chen, Z.-D., Liu, C. and Wang, Y.-G. (2014) 'Tar reforming using char as catalyst during pyrolysis and gasification of Shengli brown coal', Journal of Analytical and Applied Pyrolysis, 105, pp. 269-275.

Wang, L., Weller, C.L., Jones, D.D. and Hanna, M.A. (2008) 'Contemporary issues in thermal gasification of biomass and its application to electricity and fuel production', Biomass and Bioenergy, 32(7), pp. 573-581.

Wang, X., Jin, B. and Zhong, W. (2009) 'Three-dimensional simulation of fluidized bed coal gasification', Chemical Engineering and Processing: Process Intensification, 48(2), pp. 695-705.

Warnecke, R. (2000) 'Gasification of biomass: comparison of fixed bed and fluidized bed gasifier', Biomass and Bioenergy, 18(6), pp. 489-497.

Watson, J., Zhang, Y., Si, B., Chen, W.-T. and de Souza, R. (2018) 'Gasification of biowaste: A critical review and outlooks', Renewable and Sustainable Energy Reviews, 83, pp. 1-17.

Wei, L., Xu, S., Zhang, L., Liu, C., Zhu, H. and Liu, S. (2007) 'Steam gasification of biomass for hydrogen-rich gas in a free-fall reactor', International Journal of Hydrogen Energy, 32(1), pp. 24-31.

Wei, X., Schnell, U. and Hein, K.R.G. (2005) 'Behaviour of gaseous chlorine and alkali metals during biomass thermal utilisation', Fuel, 84(7), pp. 841-848.

Werkelin, J., Skrifvars, B.-J., Zevenhoven, M., Holmbom, B. and Hupa, M. (2010) 'Chemical forms of ash-forming elements in woody biomass fuels', Fuel, 89(2), pp. 481-493.

Weston, P.M., Sharifi, V. and Swithenbank, J. (2014) 'Destruction of Tar in a Novel Coandă Tar Cracking System', Energy & Fuels, 28(2), pp. 1059-1065.

Wolfesberger-Schwabl, U., Aigner, I. and Hofbauer, H. (2012) 'Mechanism of Tar Generation during Fluidized Bed Gasification and Low Temperature Pyrolysis', Industrial & Engineering Chemistry Research, 51(40), pp. 13001-13007.

Wolfesberger, U., Aigner, I. and Hofbauer, H. (2009) 'Tar Content and Composition in Producer Gas of Fluidized Bed Gasification of Wood-Influence of Temperature and Pressure', Environmental Progress & Sustainable Energy, 28(3), pp. 372-379.

Woolcock, P.J. and Brown, R.C. (2013) 'A review of cleaning technologies for biomass-derived syngas', Biomass and Bioenergy, 52, pp. 54-84.

Wu, C.-z., Yin, X.-l., Ma, L.-l., Zhou, Z.-q. and Chen, H.-p. (2009) 'Operational characteristics of a 1.2-MW biomass gasification and power generation plant', Biotechnology Advances, 27(5), pp. 588-592.

Wu, S.P., Tao, S. and Liu, W.X. (2006a) 'Particle size distributions of polycyclic aromatic hydrocarbons in rural and urban atmosphere of Tianjin, China', Chemosphere, 62(3), pp. 357-367.

Wu, W., Kawamoto, K. and Kuramochi, H. (2006b) 'Hydrogen-rich synthesis gas production from waste wood via gasification and reforming technology for fuel cell application', Journal of Material Cycles and Waste Management, 8(1), pp. 70-77.

Wu, Y., Zhang, Q., Yang, W. and Blasiak, W. (2013) 'Two-Dimensional Computational Fluid Dynamics Simulation of Biomass Gasification in a Downdraft Fixed-Bed Gasifier with Highly Preheated Air and Steam', Energy & Fuels, 27(6), pp. 3274-3282.

Xie, Q., Kong, S., Liu, Y. and Zeng, H. (2012) 'Syngas production by two-stage method of biomass catalytic pyrolysis and gasification', Bioresource Technology, 110, pp. 603-609.

Yaliwal, V.S., Banapurmath, N.R., Gireesh, N.M. and Tewari, P.G. (2014) 'Production and utilization of renewable and sustainable gaseous fuel for power generation applications: A review of literature', Renewable and Sustainable Energy Reviews, 34, pp. 608-627.

Yan, F., Luo, S.-y., Hu, Z.-q., Xiao, B. and Cheng, G. (2010) 'Hydrogen-rich gas production by steam gasification of char from biomass fast pyrolysis in a fixed-bed reactor: Influence of temperature and steam on hydrogen yield and syngas composition', Bioresource Technology, 101(14), pp. 5633-5637.

Yang, H.-H., Chien, S.-M., Chao, M.-R. and Lin, C.-C. (2005) 'Particle size distribution of polycyclic aromatic hydrocarbons in motorcycle exhaust emissions', Journal of Hazardous Materials, 125(1), pp. 154-159.

Yang, H., Yan, R., Chen, H., Lee, D.H. and Zheng, C. (2007) 'Characteristics of hemicellulose, cellulose and lignin pyrolysis', Fuel, 86(12), pp. 1781-1788.

Yang, H.M., Liu, J.G., Zhang, H., Han, X.X. and Jiang, X.M. (2019) 'Experimental research for biomass steam gasification in a fluidized bed', Energy Sources, Part A: Recovery, Utilization, and Environmental Effects, 41(16), pp. 1993-2006.

Yokoyama, S., Yamamoto, M., Maekawa, Y. and Kotanigawa, T. (1989) 'Catalytic activity of sulphate for hydroliquefaction of coal by using diphenylether and diphenylmethane', Fuel, 68(4), pp. 531-533.

Yoon, H., Wei, J. and Denn, M.M. (1978) 'A model for moving-bed coal gasification reactors', AIChE Journal, 24(5), pp. 885-903.

Yorgun, S. (2003) 'Fixed-Bed Pyrolysis of Miscanthus x giganteus: Product Yields and Bio-Oil Characterization', Energy Sources, 25(8), pp. 779-790.

Yorgun, S. and Yıldız, D. (2015) 'Slow pyrolysis of paulownia wood: Effects of pyrolysis parameters on product yields and bio-oil characterization', Journal of Analytical and Applied Pyrolysis, 114, pp. 68-78.

Yu, H., Zhang, Z., Li, Z. and Chen, D. (2014) 'Characteristics of tar formation during cellulose, hemicellulose and lignin gasification', Fuel, 118, pp. 250-256.

Yu, Q., Brage, C., Chen, G. and Sjöström, K. (1997) 'Temperature impact on the formation of tar from biomass pyrolysis in a free-fall reactor', Journal of Analytical and Applied Pyrolysis, 40-41, pp. 481-489.

Yucel, O. and Hastaoglu, M.A. (2016) 'Kinetic modeling and simulation of throated downdraft gasifier', Fuel Processing Technology, 144, pp. 145-154.

Yung, M.M., Jablonski, W.S. and Magrini-Bair, K.A. (2009) 'Review of Catalytic Conditioning of Biomass-Derived Syngas', Energy & Fuels, 23(4), pp. 1874-1887.

Zainal, Z.A., Rifau, A., Quadir, G.A. and Seetharamu, K.N. (2002) 'Experimental investigation of a downdraft biomass gasifier', Biomass and Bioenergy, 23(4), pp. 283-289.

Zeng, J., Xiao, R., Zeng, D., Zhao, Y., Zhang, H. and Shen, D. (2016) 'High $H_2$/CO Ratio Syngas Production from Chemical Looping Gasification of Sawdust in a Dual Fluidized Bed Gasifier', Energy & Fuels, 30(3), pp. 1764-1770.

Zhai, M., Liu, J., Wang, Z., Guo, L., Wang, X., Zhang, Y., Dong, P. and Sun, J. (2017) 'Gasification characteristics of sawdust char at a high-temperature steam atmosphere', Energy, 128, pp. 509-518.

Zhang, J., Liu, J. and Liu, R. (2015) 'Effects of pyrolysis temperature and heating time on biochar obtained from the pyrolysis of straw and lignosulfonate', Bioresource Technology, 176, pp. 288-291.

Zhang, L., Liu, R., Yin, R. and Mei, Y. (2013) 'Upgrading of bio-oil from biomass fast pyrolysis in China: A review', Renewable and Sustainable Energy Reviews, 24, pp. 66-72.

Zhang, L., Xu, C. and Champagne, P. (2010) 'Overview of recent advances in thermo-chemical conversion of biomass', Energy Conversion and Management, 51(5), pp. 969-982.

Zhang, R., Brown, R.C., Suby, A. and Cummer, K. (2004) 'Catalytic destruction of tar in biomass derived producer gas', Energy Conversion and Management, 45(7), pp. 995-1014.

Zhao, S.-X., Ta, N. and Wang, X.-D. (2017) 'Effect of Temperature on the Structural and Physicochemical Properties of Biochar with Apple Tree Branches as Feedstock Material', Energies, 10(9), pp. 1-15.

Zhao, S., Su, Y., Wu, W., Zhang, Y., Wang, Y. and Luo, Y. (2013) 'Numerical Simulation of Partial Combustion for Biomass Tar Elimination in Two-Stage Gasifier', Journal of Sustainable Bioenergy Systems, 3(1), pp. 86-92.

Zhao, Y., Sun, S., Zhou, H., Sun, R., Tian, H., Luan, J. and Qian, J. (2010) 'Experimental study on sawdust air gasification in an entrained-flow reactor', Fuel Processing Technology, 91(8), pp. 910-914.

Zhou, J., Chen, Q., Zhao, H., Cao, X., Mei, Q., Luo, Z. and Cen, K. (2009) 'Biomass–oxygen gasification in a high-temperature entrained-flow gasifier', Biotechnology Advances, 27(5), pp. 606-611.

# Appendix A Analytical standards

## A.1 Proximate analysis (BS ISO 11722:2013)

### Moisture content

- Weight an empty crucible. Gradually add about 1 g of sample (nearest 0.1 mg) and record the weight of the crucible and contents.
- Tap the crucible gently to spread the sample evenly over the bottom of the crucible.
- Place the crucible in an oven at a temperature of 105 $^{o}$C to 110 $^{o}$C for one hour.
- Cool the crucible in a desiccator and reweight. The percentage moisture is calculated:

$$\%\text{Moisture} = \frac{\text{Mass of water removed}}{\text{Mass of original sample}} = \frac{M_2 - M_3}{M_2 - M_1} \times 100\%$$

Where:

$M_1$ is the mass of empty crucible;

$M_2$ is the mass of crucible plus sample before heating;

$M_3$ is the mass of crucible plus sample after heating.

### Volatile content

- Weight an empty crucible plus lid.
- Gradually add about 1 g of sample (nearest 0.1 mg) and record the weight of the crucible (plus lid) and contents.
- Place the covered crucible into a high temperature furnace of 925 $^{o}$C for exactly seven minutes in the absence of air.
- Remove the crucible from the furnace. Let it cool for about one minute in the laboratory and then place it in a desiccator.
- Reweight the sample. The volatiles content is given:

$$\%\text{Volatile} = \frac{\text{Mass of residue after heating}}{\text{Mass of original sample}} = \frac{M_2 - M_3}{M_2 - M_1} \times 100\% - \%\text{Moisture}$$

Where:

$M_1$ is the mass of empty crucible and lid;

$M_2$ is the mass of crucible, lid and sample before heating;

$M_3$ is the mass of crucible, lid and residue after heating.

**Ash content**

- Weigh an empty crucible. Gradually add about 1 g of sample (nearest 0.1 mg) and record the weight of the crucible and contents.
- Tap the crucible gently to spread the sample evenly over the bottom of the crucible.
- Place the crucible in a high temperature furnace of 750 $^oC$ for one hour.
- Remove the crucible from the furnace. Let it cool for about one minute in the laboratory and then place it in a desiccator until it has cooled to room temperature.
- Reweight the sample. The percentage ash is given:

$$\%\text{Ash} = \frac{\text{Mass of residue after combustion}}{\text{Mass of original sample}} = \frac{M_3 - M_1}{M_2 - M_1} \times 100\%$$

Where:

$M_1$ is the mass of empty crucible;

$M_2$ is the mass of crucible and sample before heating;

$M_3$ is the mass of crucible and residue after heating.

**Fixed carbon content**

Fixed carbon is determined by difference as expressed by:

$$\%\text{Fixed carbon} = 100 - (\%\text{Moisture} + \%\text{volatiles} + \%\text{Ash})$$

**A.2 Acid digestion (BS EN ISO 16967:2015)**

- Approximately 500 mg of sample (nearest 0.1 mg) was weighed into the digestion vessel.
- 8 ml of $HNO_3$ (65%), 1 ml of HF (40%) and 3 ml of $H_2O_2$ (30%) were added to digestion vessel and closed the digestion vessel.

- Place the digestion vessel in a microwave heating at a rate of 12 $^{o}$C/min to a temperature of 190 $^{o}$C and held for 15 minutes.
- Remove the digestion vessel from the microwave. Let it cooled to room temperature.
- 10 ml $H_3BO_4$ (4%) was added to the digestion vessel for neutralisation of HF.
- Reheat the sample in a microwave at temperature of 150 $^{o}$C and held for 15 minutes.
- Remove the sample from the microwave. Let it cooled to room temperature.
- Transfer the digest sample to a 100 ml volumetric flask and made up to volume with deionised water (18 Mohmwater).

**A.3 Lignocellulose composition (AOAC 2002.04:2002)**

**Solution preparation**

**The neutral detergent solution (NDS)**

| | |
|---|---|
| Sodium lauryl sulfate | 30 g/L |
| Ethylene diamine tetra-acetic acid (EDTA) anhydrous | 18.6 g/L |
| Borate decahydrate sodium | 6.8 g/L |
| Disodium hydrogen phosphate anhydrous | 4.6 g/L |
| 2-Ethoxyethanol | 10 ml |
| Distilled water | Up to 1000 ml |

- Mix sodium borate and EDTA in a beaker of 2 L.
- Add distilled water, heat to dissolve and then add the lauryl sulfate.
- Weigh disodium phosphate and add distilled water in another flask, heat the solution until it is completely dissolved.
- Mix the solution and then add 2-ethoxyethanol to limit foaming.
- Check the pH value is between 6.9 and 7.1.

**Acid detergent solution (ADS)**

| | |
|---|---|
| Cetyl trimethyl ammonium bromide | 20 g/L |
| Sulfuric acid 1 mol/L | 1 L |
| Dissolve 20 g of cetyl trimethyl ammonium bromide in the sulfuric acid | 1 mol/L |
| Amylase solution | |
| Alpha-amylase (density: 1.13 g/ml) | 2 g |
| Ethoxyethanol | 10 ml |
| Distilled water | To fulfill 1 L |

- Dissolve 2 g of amylase in distilled water and adjust with ethoxyethanol. Keep the solution at 5 $^{o}$C.
- Dilute 750 ml of acid (96% concentration) in water slowly to make 1 l of solution.

**Analytical procedures**

- Sample preparation: Remove the solubles of the sample using ethanol and then sample was dry in an oven at 60 $^{o}$C for 18 h and determine the moisture of the sample.
- Crucible preparation: Wash and let the crucible submerged in a sulfochromic solution for 8 h, then rinse and dry. Weigh the dried crucible with a smaller difference of 0.1% (weight=P0).
- Weigh 1 g of the sample (S) in the crucible with a minor difference of 0.1% (taking weight as E).
- Add 50 ml of neutral detergent solution (NDS) at the top of the columns, turn the equipment on and set the temperature of the heater. Once boiling point is reached, count 30 min.
- After 30 min, add another 50 ml of detergent solution (NDS) with 2 ml of alpha-amylase to solubilize the starch content in the sample and then boil for additional 30 min.
- Heat the sample on the stove at 105 $^{o}$C for 8 h or until constant weight. Then, cool the crucible with the sample in a desiccator for 20 min and weigh with a weight difference less than 0.1% (P1).

- Add 50 ml of acid detergent solution (ADS) at the top of the columns, heat to boiling point, and count 1 h when boiling point is reached.
- Remove the crucible. Dry in the oven at 100 $^{o}$C for 8 h or until constant weight. Then, place the sample in the desiccator for 20 min and weigh for a weight difference of less than 0.1% (P2).
- After that, place the crucible in a glass container and add sulfuric acid (72% v/v) to the sample to cover it. Shake and leave for 3 h then, rinse with hot distilled water to remove sulfuric acid.
- Heat the crucible with the sample at 100 $^{o}$C in an oven for 8 h or until constant weight, followed by placing it in the desiccator for 20 min and weigh to obtain weight P3 with a minor difference of 0.1%.
- In order to mineralize the sample, the crucible is carried muffle at 550 $^{o}$C for 4 h followed by an hour in the oven at 100 $^{o}$C.
- Finally, cool the sample down in the desiccator for 20 min and weigh to obtain the weight P4 with a minor difference of 0.1%. The composition of lignocellulose was subsequently determined by:

$$\mathrm{NDF} = \frac{\mathrm{P1} - \mathrm{P4}}{\mathrm{S}} \times 100$$

$$\mathrm{ADF} = \frac{\mathrm{P2} - \mathrm{P4}}{\mathrm{S}} \times 100$$

$$\%\mathrm{Hemicellulose} = \frac{\mathrm{P1} - \mathrm{P2}}{\mathrm{S}} \times 100$$

$$\%\mathrm{Cellulose} = \frac{\mathrm{P2} - \mathrm{P3}}{\mathrm{S}} \times 100$$

$$\%\mathrm{Lignin} = \frac{\mathrm{P3} - \mathrm{P4}}{\mathrm{S}} \times 100$$

# Appendix B Standard chemicals

The lists of standard chemical used to quantify the amount of a component in the liquid products derived from pyrolysis and gasification processes.

| No. | Chemical | Purity (%) | Formula | MW* |
|---|---|---|---|---|
| 1 | Benzene | 99.99 | $C_6H_6$ | 78.11 |
| 2 | Toluene | 99.50 | $C_7H_8$ | 92.14 |
| 3 | p-xylene | 99.70 | $C_8H_{10}$ | 106.17 |
| 4 | o/m-xylene | 99.98 | $C_8H_{10}$ | 106.17 |
| 5 | Ethylbenzene | 99.90 | $C_8H_{10}$ | 106.17 |
| 6 | Indene | 99.50 | $C_9H_8$ | 116.16 |
| 7 | Naphthalene | 99.90 | $C_{10}H_8$ | 128.17 |
| 8 | Decahydronaphthalene | 99.00 | $C_{10}H_{18}$ | 138.25 |
| 9 | Naphthalene, 2-methyl | 99.90 | $C_{11}H_{10}$ | 142.20 |
| 10 | Naphthalene, 1-methyl | 99.90 | $C_{11}H_{10}$ | 142.20 |
| 11 | Acenaphthylene | 91.70 | $C_{12}H_8$ | 152.19 |
| 12 | Biphenyl | 99.99 | $C_{12}H_{10}$ | 154.21 |
| 13 | Fluorene | 98.20 | $C_{13}H_{10}$ | 166.21 |
| 14 | 1,1'-Biphenyl, 3-methyl | 97.90 | $C_{13}H_{12}$ | 168.23 |
| 15 | Phenanthrene | 99.50 | $C_{14}H_{10}$ | 178.23 |
| 16 | Anthracene | 98.60 | $C_{14}H_{10}$ | 178.23 |
| 17 | 4H-Cyclopenta[def]phenanthrene | 98.90 | $C_{15}H_{10}$ | 190.24 |
| 18 | Anthracene, 2-methyl | 98.60 | $C_{15}H_{12}$ | 192.26 |
| 19 | Phenanthrene, 4-methyl | 99.50 | $C_{15}H_{12}$ | 192.26 |
| 20 | Fluoranthene | 98.20 | $C_{16}H_{10}$ | 202.25 |

| | | | | |
|---|---|---|---|---|
| 21 | Pyrene | 98.20 | $C_{16}H_{10}$ | 202.25 |
| 22 | Acephenanthrylene | 98.00 | $C_{16}H_{10}$ | 202.25 |
| 23 | 11H-Benzo[b]fluorene | 98.20 | $C_{17}H_{12}$ | 216.28 |
| 24 | Fluoranthene, 2-methyl | 98.20 | $C_{17}H_{12}$ | 216.28 |
| 25 | Pyrene, 1-methyl | 98.20 | $C_{17}H_{12}$ | 216.28 |
| 26 | Cyclopenta[cd]pyrene | 97.70 | $C_{18}H_{10}$ | 226.27 |
| 27 | Chrysene | 97.40 | $C_{18}H_{12}$ | 228.29 |
| 28 | Benz[a]anthracene | 99.98 | $C_{18}H_{12}$ | 228.29 |
| 29 | Benzo[a]pyrene | 96.00 | $C_{20}H_{12}$ | 252.31 |
| 30 | Methanol | 99.99 | $CH_4O$ | 32.04 |
| 31 | Acetaldehyde | 99.97 | $C_2H_4O$ | 44.05 |
| 32 | Propanal | 99.60 | $C_3H_6O$ | 58.08 |
| 33 | 2-cyclopenten-1-one | 98.60 | $C_5H_6O$ | 82.10 |
| 34 | Phenol | 99.80 | $C_6H_6O$ | 94.11 |
| 35 | Hexanal | 98.00 | $C_6H_{12}O$ | 100.16 |
| 36 | Benzaldehyde | 99.50 | $C_7H_6O$ | 106.12 |
| 37 | Methoxybenzene | 99.90 | $C_7H_8O$ | 108.14 |
| 38 | p-cresol | 99.98 | $C_7H_8O$ | 108.14 |
| 39 | o/m-cresol | 99.99 | $C_7H_8O$ | 108.14 |
| 40 | Benzofuran | 99.90 | $C_8H_6O$ | 118.13 |
| 41 | 2,3-dihydrobenzofuran | 99.90 | $C_8H_8O$ | 120.15 |
| 42 | 1-methoxy-4-methylbenzene | 99.80 | $C_8H_{10}O$ | 122.16 |
| 43 | 2,4-xylenol | 98.00 | $C_8H_{10}O$ | 122.16 |
| 44 | 2,6-dimethylphenol | 99.82 | $C_8H_{10}O$ | 122.16 |
| 45 | 2,4-dimethylphenol | 99.99 | $C_8H_{10}O$ | 122.16 |

| | | | | |
|---|---|---|---|---|
| 46 | 4-methylmethoxybenzene | 99.40 | $C_8H_{10}O$ | 122.16 |
| 47 | 2-methoxytoluene | 98.99 | $C_8H_{10}O$ | 122.16 |
| 48 | 2,5-dimethylphenol | 99.99 | $C_8H_{10}O$ | 122.16 |
| 49 | Isoamyl ether | 99.00 | $C_{10}H_{22}O$ | 158.28 |
| 50 | Dibenzofuran | 99.99 | $C_{12}H_8O$ | 168.19 |
| 51 | Dibenzofuran, 4-methyl | 99.99 | $C_{13}H_{10}O$ | 182.22 |
| 52 | Formic acid | 97.90 | $CH_2O_2$ | 46.03 |
| 52 | Acetic acid | 99.79 | $C_2H_4O_2$ | 60.05 |
| 54 | Glycolaldehyde | 95.00 | $C_2H_4O_2$ | 60.05 |
| 55 | Propanoic acid | 99.50 | $C_3H_6O_2$ | 74.08 |
| 56 | Acetol | 99.00 | $C_3H_6O_2$ | 74.08 |
| 57 | 2(5H)-Furanone | 98.70 | $C_4H_4O_2$ | 84.07 |
| 58 | Butanoic acid | 99.99 | $C_4H_8O_2$ | 88.11 |
| 59 | Furfural | 99.60 | $C_5H_4O_2$ | 96.08 |
| 60 | Furfural alcohol | 99.10 | $C_5H_6O_2$ | 98.10 |
| 61 | Catechol | 99.80 | $C_6H_6O_2$ | 110.11 |
| 62 | 5-methylfurfural | 97.70 | $C_6H_6O_2$ | 110.11 |
| 63 | Hydroquinone | 99.90 | $C_6H_6O_2$ | 110.11 |
| 64 | 2,5-Hexadione | 99.70 | $C_6H_{10}O_2$ | 114.14 |
| 65 | 1,3-benzodioxole | 99.90 | $C_7H_6O_2$ | 122.12 |
| 66 | 4-methylcatechol | 99.80 | $C_7H_8O_2$ | 124.14 |
| 67 | Guaiacol | 99.10 | $C_7H_8O_2$ | 124.14 |
| 68 | 4-methylguaiacol | 99.50 | $C_8H_{10}O_2$ | 138.16 |
| 69 | 1,2-dimethoxybenzene | 99.98 | $C_8H_{10}O_2$ | 138.16 |
| 70 | 2-methoxy-5-methylphenol | 98.00 | $C_8H_{10}O_2$ | 138.16 |

| | | | | |
|---|---|---|---|---|
| 71 | 2-methoxy-4-vinylphenol | 99.60 | $C_9H_{10}O_2$ | 150.17 |
| 72 | 4-ethylguaiacol | 98.00 | $C_9H_{12}O_2$ | 152.19 |
| 73 | Eugenol | 99.00 | $C_{10}H_{12}O_2$ | 164.20 |
| 74 | Methyl laurate | 99.50 | $C_{13}H_{26}O_2$ | 214.34 |
| 75 | Maltol | 99.90 | $C_6H_6O_3$ | 126.11 |
| 76 | 5-hydroxymethylfurfural | 99.90 | $C_6H_6O_3$ | 126.11 |
| 77 | Vanillin | 99.70 | $C_8H_8O_3$ | 152.15 |
| 78 | 2,6-dimethoxyphenol | 99.10 | $C_8H_{10}O_3$ | 154.16 |
| 79 | Apocynin | 97.70 | $C_9H_{10}O_3$ | 166.17 |
| 80 | 2′,4′-Dimethoxyacetophenone | 97.00 | $C_{10}H_{12}O_3$ | 180.20 |
| 81 | Glycolaldehyde dimer | 99.10 | $C_4H_8O_4$ | 120.10 |
| 82 | 3-hydroxy-2-butanone | 95.00 | $C_8H_{16}O_4$ | 176.22 |
| 83 | Syringylaldehyde | 99.90 | $C_9H_{10}O_4$ | 182.17 |
| 84 | Acetosyringone | 97.00 | $C_{10}H_{12}O_4$ | 196.20 |
| 85 | Levoglucosan | 99.95 | $C_6H_{10}O_5$ | 162.14 |
| 86 | Pyrazine | 99.99 | $C_4H_4N_2$ | 80.09 |

* MW: Molecular weight

**Procedure of preparation of internal standard solution, standard solutions and liquid sample for gas chromatography**

**Preparation of internal standard solution**

- Weigh approximately 1.2 mg of 1-octanol into a 1.0 ml volumetric flask.
- Fill the volumetric flask to the graduation mark with acetonitrile.
- Invert flask a minimum of three times to mix and pour solution into a labelled 250 ml bottles. The solution should be stored in a freezer when not in use.

**Procedure of stock mixed standard**

- Weigh each of the standard compounds into a 25 ml volumetric flask.
- Fill the volumetric flask to the graduation mark with acetonitrile then close with stopper.
- Place the solution in ultrasonic bath at 25 $^{o}$C and sonicate for 5 minutes or until all compounds are fully dissolved.
- Invert a minimum of three times to mix and transfer solution to a labelled 30 ml jar. The solution should be stored in a freezer when not in use.

**Preparation of calibration standards**

- Using gas-tight syringes add the following volumes of the stock mixed standard, internal standard solution, and acetonitrile into pre-labeled GC vials. Weight and record amount of each solution loaded into the vials.

| Curve Point | 1 | 2 | 3 | 4 | 5 | 6 | 7 | 8 |
|---|---|---|---|---|---|---|---|---|
| Stock Standard, µL | 25 | 50 | 75 | 100 | 250 | 500 | 750 | 1000 |
| Internal Standard, µL | 100 | 100 | 100 | 100 | 100 | 100 | 100 | 100 |
| Acetonitrile, µL | 975 | 950 | 925 | 900 | 750 | 500 | 250 | 0 |

- After adding each solution and capping vials, shake each vial to mix.

**Preparation of liquid samples**

- Weigh approximately 400 mg of sample into a labelled 8 ml vial.
- Using a gas-tight syring add 0.5 ml of internal standard solution and record the weight.
- Add 5 ml acetonitrile using a Class A volumetric pipet and record the weight.
- Shake thoroughly to dissolve liquid sample.
- Place diluted samples into ultrasonic bath to sonicate at 30 $^{o}$C for 20 minutes to dissolve.
- Transfer 1 ml of diluted sample to a labelled 1.5 ml GC vial. If a precipitate is present, filter the sample with a 0.45 µm syringe filter using a 5 ml disposable syringe and transfer filtered sample into GC vial.

# Appendix C Laboratory scale air-blown throat downdraft gasifier

All details of a laboratory scale air-blown throat downdraft gasifier.

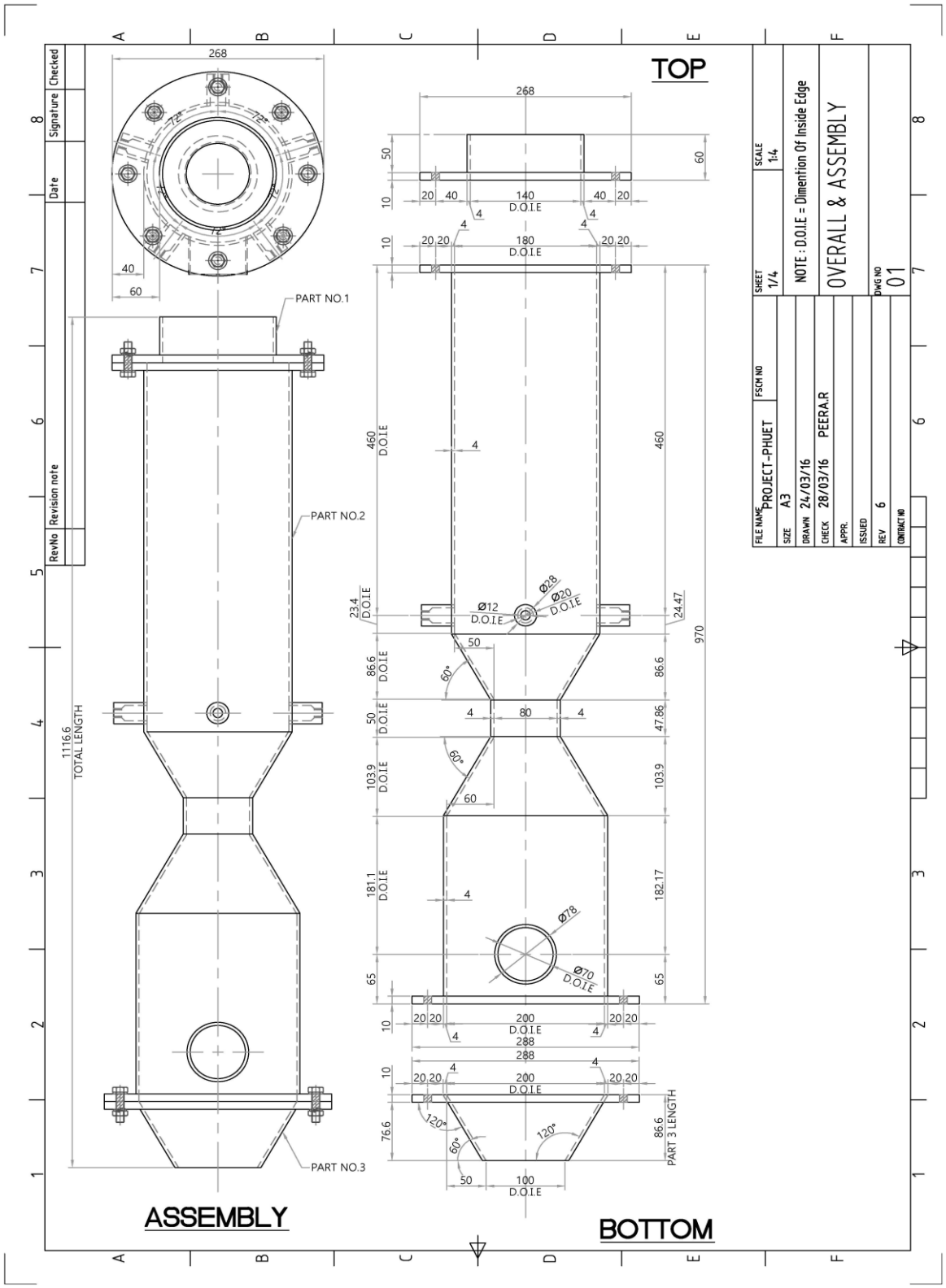


The overview of laboratory scale air-blown throat downdraft gasifier.

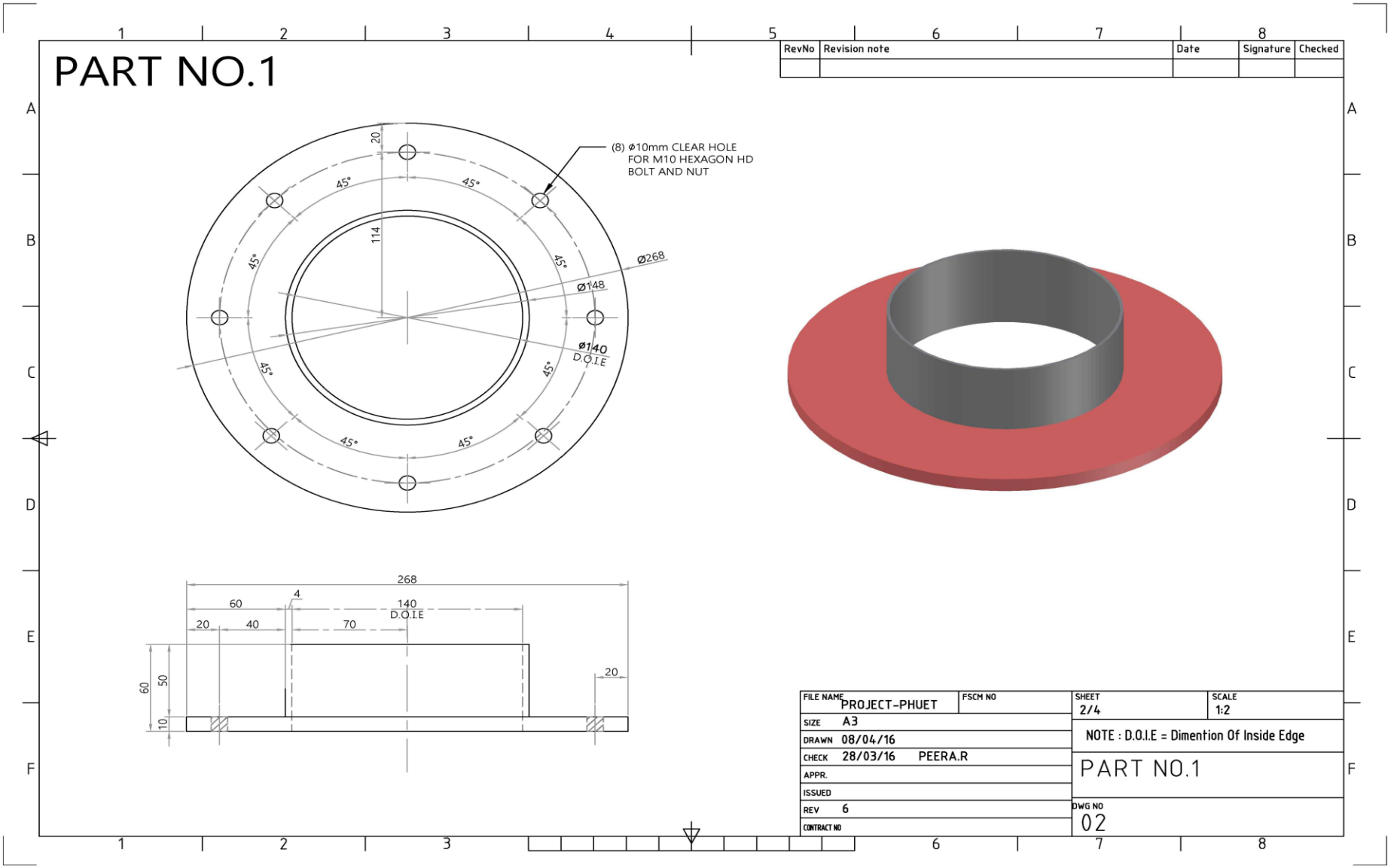


The top part of laboratory scale air-blown throat downdraft gasifier.

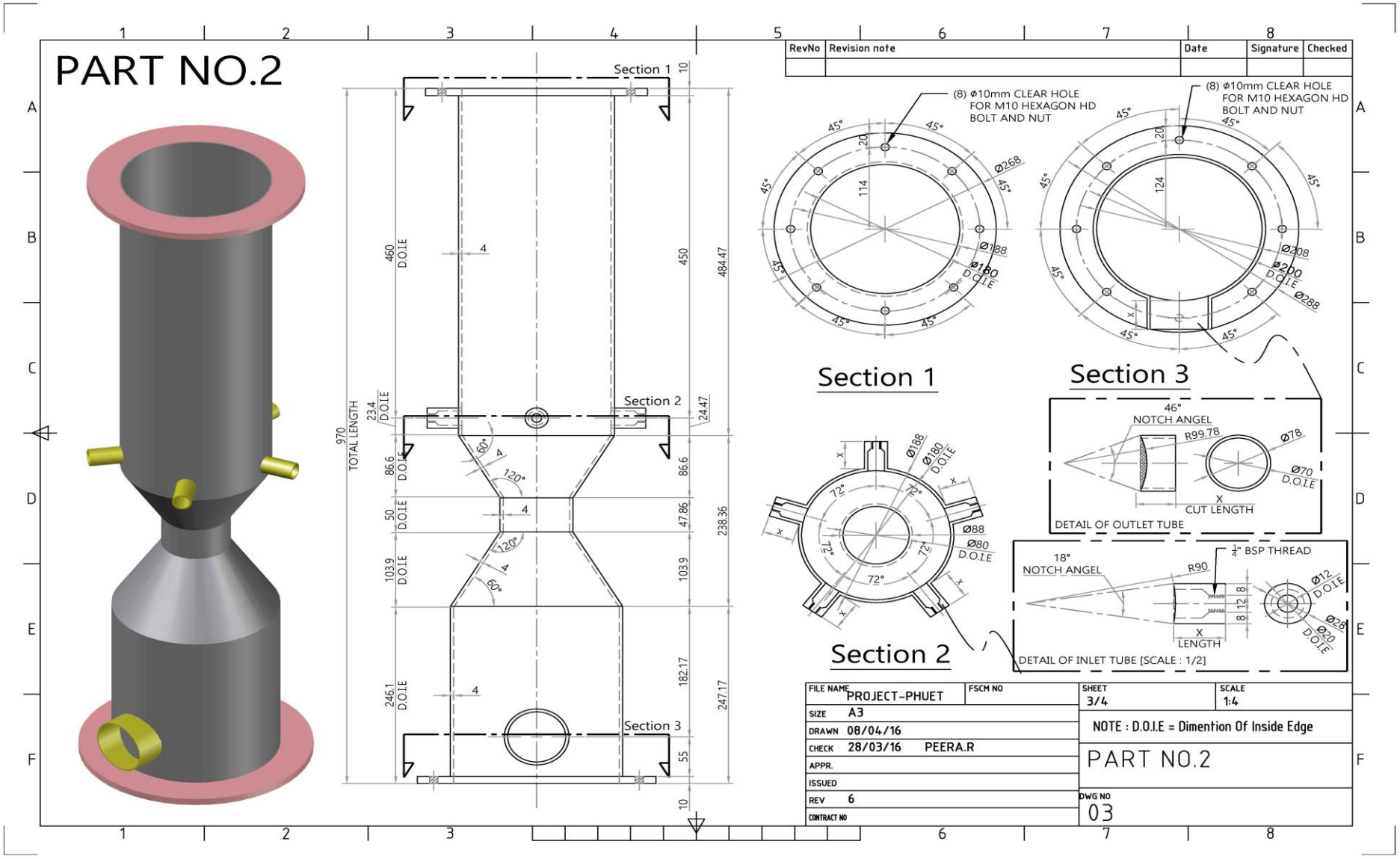


The main body of laboratory scale air-blown throat downdraft gasifier.

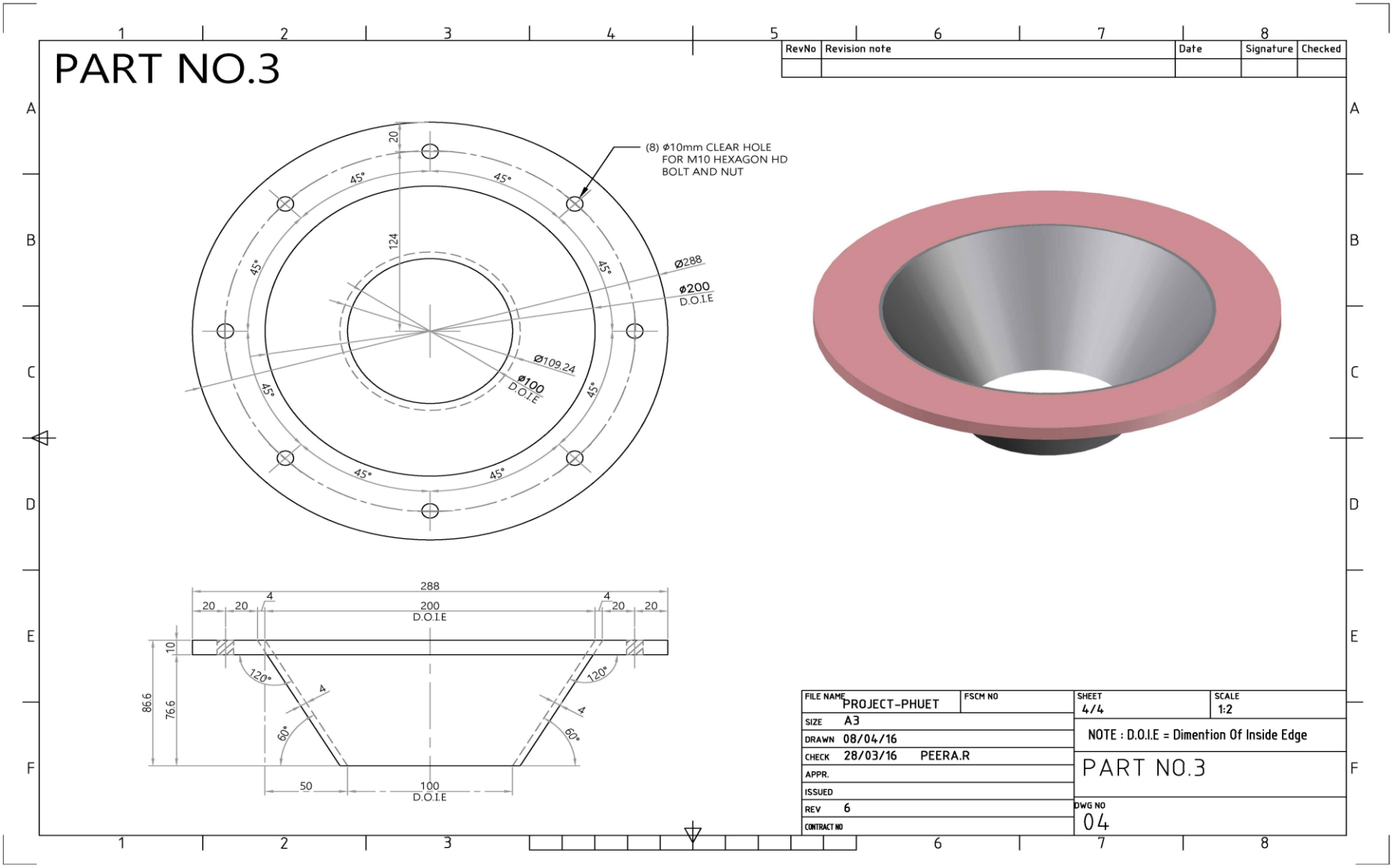


The bottom part of laboratory scale air-blown throat downdraft gasifier.